Transfer of twin-screw granulation processes and predictions of barrel fill

Inaugural-Dissertation

zur Erlangung des Doktorgrades
der Mathematisch-Naturwissenschaftlichen Fakultät
der Heinrich-Heine-Universität Düsseldorf

vorgelegt von

Sebastian Pohl
aus Großenhain

Düsseldorf, April 2022

aus dem Institut für Pharmazeutische Technologie und Biopharmazie
der Heinrich-Heine-Universität Düsseldorf

Gedruckt mit der Genehmigung der
Mathematisch-Naturwissenschaftlichen Fakultät der
Heinrich-Heine-Universität Düsseldorf

Berichterstatter:

1. Prof. Dr. Dr. h. c. Peter Kleinebudde

2. Prof. Dr. Jörg Breitkreutz

Tag der mündlichen Prüfung: 07.07.2022

Table of contents

List of publications and contributions

Original manuscripts

Review

S. Pohl, P. Kleinebudde, *A review of regime maps for granulation.* International Journal of Pharmaceutics, 587 (2020) 119660.

DOI: https://doi.org/10.1016/j.ijpharm.2020.119660

The idea of writing a review dealing with regime maps for granulation processes had already been defined in the beginning of the PhD thesis. Keywords for literature research had been prepared by Sebastian Pohl and revised according to the discussion with Peter Kleinebudde. Literature research was performed using Scopus, ScienceDirect, PubMed and Web of Science and was done by Sebastian Pohl. Structuring and writing the manuscript were mainly done by Sebastian Pohl and optimised based on the advices and revisions of Peter Kleinebudde.

Evaluation of the authorship

Author/ co-author	Idea [%]	Study design [%]	Literature research [%]	Manuscript [%]
Sebastian Pohl	0	80	100	80
Peter Kleinebudde	100	20	0	20

Research paper

C. Köster, S. Pohl, P. Kleinebudde, *Evaluation of Binders in Twin-Screw Wet Granulation,* Pharmaceutics, 13 (2021) 241.

DOI: https://doi.org/10.3390/pharmaceutics13020241

The topic of the paper is based on the Diploma thesis of Claudia Köster, who was technically supervised by Sebastian Pohl during her time as Diploma student. Sebastian Pohl mainly supported the thesis of Claudia Köster with regards to specified process parameters and screw configuration, offered solutions if problems had been arisen and set the characterisation methods. Peter Kleinebudde gave input throughout all steps of this study. Experiments, characterisation and data analysis were mostly performed by Claudia Köster herself. The idea of writing the paper was encouraged by Peter Kleinebudde. The manuscript was prepared by Claudia Köster and reviewed by Sebastian Pohl and Peter Kleinebudde.

Evaluation of the authorship

Author/ co-author	Idea [%]	Study design [%]	Experimental [%]	Evaluation [%]	Manuscript [%]
Claudia Köster	0	20	100	80	80
Sebastian Pohl	0	50	0	10	10
Peter Kleinebudde	100	30	0	10	10

Conference contributions

Oral presentations

S. Pohl, P. Kleinebudde, *Transfer of twin-screw granulation process using a shear stress description of configuration*, 3rd Symposium of Young Researchers on Pharmaceutical Technology, Biotechnology and Regulatory Science, 2021, Online.

S. Pohl, P. Kleinebudde, *Zweischneckengranulierung: Prozesstransfer mittels numerischer Beschreibung der Schneckenkonfiguration*, Jahrestreffen der ProcessNet-Fachgruppe Agglomeration und Schüttguttechnik, 2021, Online.

Poster presentations

S. Pohl, P. Kleinebudde, *Use of mixer torque rheometry to predict optimal L/S ratio for twin-screw granulation*, 3rd European Conference on Pharmaceutics, 2019, Bologna, Italy.

S. Pohl, P. Kleinebudde, *Dimensionsanalyse eines Doppelschneckengranulierprozesses*, 15. Herbst-kolloquium Prozessanalytik, 2019, Marl, Germany.

S. Pohl, P. Kleinebudde, *Twin-screw granulation: An attempt for a quantitative description of screw configuration*, 12th World Meeting on Pharmaceutics, Biopharmaceutics and Pharmaceutical Technology, 2021, Online.

S. Pohl, P. Kleinebudde, *Estimation of material hold-up in twin-screw granulation*, 12th World Meeting on Pharmaceutics, Biopharmaceutics and Pharmaceutical Technology, 2021, Online.

Other contributions

Oral presentations within the scope of the 1st, 2nd, 3rd, 6th and 10th Technical Committee Meeting of the Drug Delivery Innovation Center (DDIC) of the INVITE GmbH in Leverkusen, Germany.

List of abbreviations

Greek symbols

Symbol	Meaning
α	offset angle of kneading elements or helix angle of conveying elements
β	deformation value
ε	porosity
η_v	volumetric efficiency

Symbol	Meaning
ρ_{bulk}	bulk density
ρ_{tapped}	tapped density
ρ_{true}	true density
τ	shear stress
φ	barrel fill level (dimensionless)

Latin symbols

Symbol	Meaning
$A_{contact,element}$	contact area between screw element and barrel wall
$A_{overlap}$	overlapping area of the two barrel cylinders
API	active pharmaceutical ingredient
BCG	Bohle Continuous Granulation
BFD	barrel fill density (surrogate for barrel fill level)
CE	conveying element
cGMP	current Good Manufacturing Practice
CM	continuous manufacturing
CQA	critical quality attributes
CV	coefficient of variation
d_{barrel}	barrel diameter
$d_{element}$	diameter of a screw element (outer diameter)
d_{inner}	inner diameter of a conveying element
DCP	dicalcium phosphate anhydrous
DE	distributive element
DFS	distributive feed screw
DME	distributive mixing element
DoE	design of experiments
EMD	Earth Mover's Distance
ff_c	flow function coefficient
Fr	Froude number
g	gravitational force
GSD	granule size distribution
HF	Hausner factor
ICH	International Council for Harmonization of Technical Requirements for Pharmaceuticals for Human Use

Symbol	Meaning
IP	inflection point
KB	kneading block
KE	kneading element
$L_{C1\text{-}C2}$	distance between the centres of each barrel cylinder
L/D	length-to-diameter
L/S	liquid-to-solid
l_{barrel}	barrel length
l_{crest}	length of the crest of a conveying element
l_{eff}	effective length
$l_{element}$	length of a screw element
$l_{KB,tot}$	total kneading block length
l_{lead}	lead length of a conveying element
l_{rev}	distance per revolution
l_{screw}	screw length
LOD	loss on drying
LPCE	long pitch conveying element
Max	maximum
MCC	microcrystalline cellulose
MCS	Manufacturing Classification System
Min	minimum
MPCE	medium pitch conveying element
MTR	mixer torque rheometer
MU	mass uniformity
m_H	material hold-up
$\dot{m}_p$	powder throughput
m_{theo}	theoretical mass hold-up
$\dot{m}_{tot}$	total material throughput
n	screw speed
PAT	process analytical technology

Symbol	Meaning
PCM	paracetamol
PFN	powder feed number
PFR	powder feed rate
Ph.Eur.	European Pharmacopoeia
PM	Parteck M (mannitol)
PMMA	polymethyl methacrylate
PSD	particle size distribution
PVP	polyvinylpyrrolidone
QbD	Quality by Design
r_{barrel}	barrel radius
RTD	residence time distribution
SFL	specific feed load (surrogate for barrel fill level)
SME	specific mechanical energy
SPCE	short pitch conveying element
T	drying air temperature
t_1	time after which the tracer can be detected (lag-time)
$t_{1,theo}$	theoretical t_1 value
TM	theophylline monohydrate
TME	tooth-mixing element
t_{mean}	mean residence time
t_{out}	time at which tracer is washed out
t_{peak}	time point of highest tracer concentration
TSG	twin-screw granulation
t_{turn}	circulation time
$V_{empty\ barrel}$	maximum free volume of the barrel (empty, without screws)
V_{free}	free, available volume of the entire screw configuration
$V_{free,element}$	free, available volume of a single screw element
$\bar{v}_{harmonic}$	harmonic mean transportation velocity
$V_{overlap}$	overlapping volume of the two barrel cylinders
v_t	theoretical velocity
v_{tip}	circumferential speed
$\dot{V}_{tot}$	total volumetric throughput
w_{barrel}	total horizontal width across the two barrel cylinders
w_{crest}	width of the crest of a conveying element
w_{pitch}	width of the pitch of a conveying element
w_{tip}	width of the rectangular on the tip of a kneading disc
$x_{element}$	number of a specific element used within the screw setup
$\%_{KB}$	percentage of kneading blocks in screw configuration

1 Introduction

1.1 Manufacturing of tablets as solid oral dosage forms

Due to their simple oral administration, tablets are one of the most preferred dosage forms by patients. They can be mass produced at relatively low costs by compacting uniform volumes of powders or granules at high compression pressures. As they contain a single dose of one or more active pharmaceutical ingredients (APIs), precise dosing is possible. Tablets can be easily packaged, transported and stored [1-3].

The manufacturing process of tablets strongly depends on the type and specific properties of the APIs and excipients added. Each compound as well as the powder blends must meet requirements such as good flowability, without adhering to surfaces, to facilitate the filling into high-speed tablet presses and thus enable the large-production production of tablets that comply with the previously defined specifications [1, 4]. Depending on the intended functions of the tablets and their form of administration, the tablet composition has to be chosen carefully. According to the monograph on tablets of the European Pharmacopoeia (Ph.Eur.), the addition of diluents, binders, glidants, lubricants, disintegrating agents, release modifiers, colouring and flavouring agents is possible [3]. If necessary, the excipients should ensure a certain powder blend volume, improve their flow characteristics, ease the compression step by preventing the adhesion of the tablets to the punch surfaces and enhancing its expulsion from the die, influence the tablet characteristics and appearance or can have a taste-masking effect. Coating agents may be applied after compression and can further influence tablet properties, e.g. appearance, swallowability, protection of the API from gastric juices or achievement of specific release behaviours [1-3].

Common processing steps are either the direct compression of powder blends or the compression of intermediate products, such as granules. However, all production routes require a homogeneous blend for further processing. This is one of the most critical unit operations in the production of tablets and is influenced by particle properties (size distribution, density, cohesiveness, shape), moisture, electrostatics and flow behaviour [1, 2, 5].

Direct compression is usually economical and not labour-intensive, but suitable excipients can be expensive. Depending on the characteristics of the API and its crystal structure, the tableting pressure may vary to ensure sufficient mechanical tablet stability. The mechanical stability may be challenging as the compaction properties of the dry powder particles are often poor compared to granules, which can reduce the mechanical resistance of the tablet. Since the dies of a tablet press are filled volumetrically, good flowability of the powder blend is mandatory to enable uniform die filling and thus low mass variation and high content uniformity. Differences in particle sizes, particle shapes and densities of the several compounds can lead to segregation tendencies of the blends. This is particularly important in batch production, where the individual steps are carried out one after the other and blend homogeneity has to be guaranteed during the various steps [1, 2, 5, 6].

Due to the challenges of direct compaction, it is often necessary to perform granulation prior to the tableting step. According to Ennis et al. [7], granulation is a size enlargement technique in which small particles are converted into larger, relatively persistent agglomerates. Granulation is a fundamental step in the manufacturing of solids in numerous industries, e.g. food, chemicals and agriculture. It received special attention in the 60s and 70s of the last century due to environmental requirements in the chemical industry and the development of high-speed tablet presses and capsule filling machines. Generally, granule formation enables improvements in particle and bulk characteristics. By enlarging the primary particles to granules, a reduction in specific surface area, bulk volume and dust content is achieved, resulting in lower adhesion forces between the particles and thus improving flow properties, uniform die filling and dosing accuracy. The granule porosity enables the deformation during the tableting process and allows for the production of tablets with sufficient mechanical strength. Furthermore, the granulation process lowers segregation tendencies by immobilising the API in the composition. However, since granules can also be administered directly, appropriate granule characteristics may also be required regarding packaging, transport and consumer handling. Nevertheless, granulation processes are often energy- and cost-intensive as well as time-consuming [2, 5, 8-15].

Standard equipment used for granulation in the pharmaceutical industry includes roll compactors, rotating drums, fluidised bed apparatuses, high-shear and twin-screw granulators. Different techniques can be used for granulation: dry, wet and melt granulation, with wet granulation being the preferred choice of pharmaceutical manufacturers and the most commonly used technique for the production of solid oral dosage forms [4, 7, 11, 16-20]. During wet granulation, a liquid is added to the solid material that penetrates the powder bed. Constant agitation and the capillary pressure, viscous forces and surface tension of the liquid induce the cohesion of the particles and the formation of aggregates [12, 13, 21, 22]. Wetting and nucleation, consolidation and coalescence as well as attrition and breakage are mechanisms that have been identified playing a vital role in granule formation and granule characteristics [7]. Wetting depends on the properties of the formulation and granulation liquid but also on the method of liquid addition. Granule growth is impacted by the extent of agitation and particle collision among each other and with the equipment surfaces. This further affects consolidation and thus granule porosities and strength. The strength of moist granules is essential for granule growth and is determined by liquid bridges and capillary forces, whereas the strength of granules produced by dry granulation is mainly determined by van der Waals forces. Drying of wet granules leads to solid bonds [7, 13, 18, 21, 23].

Depending on the wet granulation process conducted as well as on the composition and properties of the formulation, different liquid contents could result. For the description of granulation processes, the degree of liquid saturation (S) has proven to be suitable [23]. It describes the proportion of the pore volume that is filled by the liquid. It is advantageous that it is standardised and ranges between 0 and 1 as it enables the comparison of different wet granulation processes. Several saturation degrees have been described by Newitt and Conway-

Jones [24]. The pendular state (S < 0.25) is reached at low liquid contents. Here, the liquid bridges only attach the particles to each other at their contact points, while an additional decrease in granule porosity or increase in liquid content shifts the system to the funicular state (0.25 < S < 0.8). A coherent fluid network is formed due to increased saturation of intragranular voids. Capillary state (0.8 < S < 1) is achieved when the intragranular voids are almost filled by further liquid addition or by lowering the granule porosity. If the amount of liquid rises further, the overall system enters the droplet state (S > 1) [21, 23, 24]. The transition area from the pendular to the funicular state has been reported to be suitable for high-shear wet granulation processes [25].

1.2 Traditional manufacturing of medicinal products

The production of medicinal products is traditionally subject to a regulatory framework that ensures the quality of the finished products and requires the testing of starting and in-process materials, the characteristics of the final products and the specified process conditions of batch-based operations. Although continuous manufacturing of food and chemical goods has been well-established for large-throughput productions in the respective industries for decades, the manufacturing of medicinal products in the pharmaceutical industry is mostly still based on batch-wise production. In batch production, the different unit operations are predominantly executed one after the other. The starting materials are added at the beginning of a unit operation and the intermediates are removed after the process step is completed and transferred to the next production step. However, depending on the number and types of unit operations as well as the durations of intermediate storage, batch production could take several days or even weeks until the finished product is produced. The focus is mainly on the quality control of the final product (end-of-line testing), which results in rejection or acceptance of the entire batch if it either does not meet or does match the specifications, which makes this type of production very convenient [6, 26-30].

1.3 A different approach of manufacturing medicinal products

In the past, the decision about the manufacturing process of a medicinal product was based on empirical knowledge, the availability of equipment and individual preferences, whereas currently rationale considerations and systematic, science-driven approaches dominate [1, 4, 20]. The change has been fostered as costs for healthcare were constantly rising which increased public pressure for cost reductions. A study from 2008 on the manufacturing expenses in pharmaceutical companies further revealed that the material and production costs of pharmaceutical products was 26 % on average for branded products and doubled for generic products. In addition, repeated recalls due to quality problems of medicinal products were responsible for calling the current quality and risk management processes into question. All these factors were driving forces for a change in thinking in the pharmaceutical industry about the production principles, to make it

more efficient and cost-effective, while maintaining the product quality by applying process control engineering methods to continuously improve the process [31, 32].

The change in thinking has led to using process analytical technologies (PAT) to create a system for designing, analysing and monitoring the production process, assessing the critical quality attributes and performance parameters of raw materials, intermediates and processes in real-time to ensure the quality of the final product. All this should lead to the real-time release of the medicinal products. The implementation of PAT tools and principles in the development and manufacturing of medicinal products was promoted by the Food and Drug Administration (FDA) and the provision of several guidelines. The guidelines aim to ensure that enough information on physical, chemical, and biological attributes are obtained to increase the scientific understanding of the process, to aid its design and subsequently control and optimise it. Furthermore, the application of innovative technologies is expected to improve efficiency, shorten production time, increase yield and safety while reducing costs [1, 2, 30].

In extension to the PAT approach, the Quality by Design (QbD) concept was introduced to provide a framework for risk- and science-based product and process development by designing a space in which the process can be freely operated and controlled by in-line measurements. In doing so, thorough process understanding has become even more important [1, 2]. A process can be considered to be thoroughly understood if: "(1) all critical sources of variability are identified and explained, (2) the variability encountered is managed by the process according to control strategies, and (3) the quality characteristics of the product can be accurately and reliably predicted" over the design space [1, 30]. Several quality-related guidelines on pharmaceutical development (Q8(R2)), risk management (Q9) and pharmaceutical quality systems (Q10) provided by the International Council for Harmonization of Technical Requirements for Pharmaceuticals for Human Use (ICH) [33-35] should ensure an intelligent design of processes as well as its reliable operation, the prospective definition of critical quality characteristics of materials and processes and their timely measurements [2, 36].

1.4 Continuous Manufacturing

1.4.1 General

To improve the quality of medicinal products and the efficiency of pharmaceutical manufacturing processes, continuous production has been identified as the next step [36]. In a continuous process, both starting materials and the respective product are continuously added to or removed from the process, whereas in batch production, materials are added at the beginning of a process and intermediate or end products are removed after the end of the process [6]. From a regulatory perspective, the traditional batch definition has to be called into question and redefined based on the current regulations [36]. According to the current good manufacturing practice (cGMP), a batch is a defined drug quantity or quantity of material possessing uniform characteristics and quality that are within predetermined specifications which is manufactured according to a single

production order during the same production cycle [37]. However, in continuous manufacturing (CM), a batch can be defined on the basis of the production period, the amount of material processed or produced or on variations that affect the production, e.g. varying batches of raw materials. Continuous processing enables the manufacturing at different scales, e.g. longer processing times and/or increasing mass throughputs, which allows for the production of a flexible batch size to meet market demands [38]. A new ICH guideline currently under public consultation and endorsement by the members of the ICH Assembly is the guideline Q13. It focuses on continuous production of drug substances and drug products and facilitates the implementation of CM in the pharmaceutical industry. ICH guideline Q13 expands on already existing quality-related guidelines and specifically describes regulatory and scientific considerations for the development, implementation, operation and life cycle management of CM [39, 40].

Next to the batch definition, several other factors differentiate CM from batch-wise operation. In comparison to the batch mode, CM operates continuously without interruptions, requiring constant supply of starting materials at given supply rates, appropriate rate-controlled feeders and liquid pumps of high precision throughout the process. Smooth operation of the equipment over a longer period of time must be ensured by applying preventive or partially predictive maintenance and requires continuous condition monitoring. Compared to batch production, there are no stopping points during a CM process to take samples, analyse them and make quality decisions between unit operations. As the materials are permanently in motion, analyses and decisions have to be made in real time, so tighter and excellent control of the processes is required. Although the CM equipment is not as proven and well-established as for batch processes, it enables the linkage of much smaller scale equipment to a CM line which can achieve similar quantities to a batch line [29].

1.4.2 Authorised medicinal products manufactured by applying CM

According to Badman et al. [41], multiple medicinal products have already been authorised by the regulatory authorities where CM is used, which shows that change is underway:

- *Orkambi*™, a fixed combination of lumacaftor and ivacaftor, and *Symdeko*®, a fixed combination of tezacaftor and ivacaftor, of Vertex Pharmaceuticals for the treatment of cystic fibrosis
- *Prezista*® of Janssen-Cilag contains darunavir for the treatment of HIV-1 infections
- *Verzenios*® of Eli Lilly contains abemaciclib to treat breast neoplasms
- *Tramcet*™, a fixed combination of tramadol hydrochloride and acetaminophen, of Janssen to treat chronic non-cancer pain
- *Daurismo*® of Pfizer contains glasdegib to treat acute myeloid leukaemia

1.4.3 Benefits of continuous manufacturing and hurdles to be overcome

Despite the availability of respective guidelines of regulatory authorities and the ICH, the implementation of CM is slower than expected and it has not yet become standard in the pharmaceutical industry. However, next to the medicinal products that have already been authorised, the establishment of special working groups in the research and development units of companies that deal with this topic and are responsible for its implementation proves the change in thinking even more [36, 41].

Moreover, CM offers tangible benefits in general, such as much shorter manufacturing times due to integrated process steps as well as smaller equipment size than that needed for batch-wise operation. This leads to cost reductions, more flexibility and less space needed in production and good manufacturing process (GMP) areas. The transition from lab to launch scale can be done more economically and much faster as the higher degree of automation of the CM can ensure stable product quality. The higher automation rate, an increased throughput and thus yield combined with the reduced employee number to run the CM line will lower labour costs. As several process steps and unit operations are linked to each other, a lower probability of open manual handling of the active ingredients increases the safety of the process and thus the employees. Due to greater flexibility of CM reacting to demands from the market, stockpiling of medicinal products could be lowered to avoid unnecessary disposal at expiry date. A reduction of supply bottlenecks could lead to less medicinal shortages. Furthermore, the application of PAT principles allows for real-time release of the medicinal products due to the consistent process monitoring, control and assessment in real time [29, 41-45].

Although the benefits for the implementation of CM are promising, there are some obstacles to be overcome first. Roberge et al. [42] analysed how many synthesis processes in the fine chemistry would benefit from CM and determined a share of about 50 %. Even though costs can be reduced when using CM lines, initial investments into multi-purpose plant equipment were found to be major and as high or even higher as for the equipment used in batch production [36, 42]. Despite the fact that PAT tools are an essential benefit, sufficient strategies must be developed to cope with sensor and probe fouling during the continuous process. Therefore, cleaning cycles must be considered as a part of the entire manufacturing process [46].

Furthermore, variabilities in raw materials (API and excipients) of medicinal products can occur due to their unique development processes. Since excipients have a share of < 1 to > 99 % of the total formulation mass, their properties and functionalities essentially impact the CQAs and performance of the final product [47]. Kushner et al. [48] examined the impact of variabilities of material properties of commonly used excipients on the manufacturability and performance of immediate-release tablets. Variabilities in particle size caused a change in size of the granules resulted from roll compaction. The tensile strength of the ribbons and tablet hardness statistically significantly increased with decreasing particle sizes of the excipients. Fonteyne et al. [49] investigated the impact of variabilities of microcrystalline cellulose (MCC) on twin-screw wet granulation and revealed an effect of the different water binding capacities of the MCC samples,

due to varying crystallinities, on granule size distribution. It was reported, for lower water binding capacity, that more granulation liquid is available for granulation, which resulted in more oversized granules. The results of the research groups particularly emphasized the necessity to investigate the effects of excipient variability to determine a sound design and control strategy of new medicinal products. As variabilities cannot be entirely avoided, both formulation and process should be designed robustly to compensate for these variabilities without compromising the performance of the final product. Therefore, the consideration of potential variabilities of excipients is recommended at an early stage of process and formulation development [47, 50, 51].

As backmixing of material is common in CM and can lead to re-blending with material added later, a profound understanding of the process dynamics also facilitates the definition of process conditions and specifications. It can help to isolate material when it was out-of-specification. Therefore, the traceability of the material is essential to assess its flow through the CM line. Residence time distribution (RTD) measurements in combination with other measurements can be used to gain in-depth knowledge of the materials residence times for each unit operation and equipment and to better assess the impact of disturbances [52, 53].

1.4.4 CM lines available on the market

Typical equipment for unit operations used in the continuous production of solid oral dosage forms are tablet presses, roll compactors, spray-driers, high-shear, low-shear, fluid bed and twin-screw granulators. Since twin-screw granulation (TSG) offers the opportunity to conduct wet granulation, the preferred choice of manufacturers in the production of solid oral dosage forms [4], this type of granulation technology is even more important in the context of CM. The design of a twin-screw granulator offers great flexibility and makes it suitable for continuous production as it allows for an easy infeed of different compounds, the processing of a wide range of powder and liquid feed rates, sufficient mixing of the different ingredients, operation at high throughputs, individual settings of screw configurations that can be easily changed, and the development and production on the same machine [28, 45, 54]. Therefore, several companies have already developed CM lines for the production of tablets with twin-screw wet granulation as integral part, such as QbCon® from L.B. Bohle Maschinen + Verfahren, Germany, ConsiGma™ from GEA, Germany, Granuformer® from Freund, Japan [55] or MODCOS from Glatt, Germany.

1.5 Twin-screw granulation

1.5.1 Construction of a twin-screw granulator

The twin-screw extruder has originally been used in the plastic industry since the 1950s [56] but also in the rubber and food industry. It consists of a stationary cylindrical barrel, where two co- or counter-rotating, intermeshing screws are embedded. A motor serves as the drive unit and enables the rotation of the screws at a predefined speed [57]. Barrel and screws are adjusted so that the screws fit tightly and thus create a confined space for the material to be transported. This

allows for similar shear history for all powder particles along the barrel in TSG. A barrel consists of several zones of equal length that can be heated to enable individual temperature settings, tailored to the formulation and its properties as well as to the final granule characteristics. The overall number of zones can vary from granulator to granulator [58, 59].

Applications for pharmaceutical purposes of wet twin-screw granulation were first described by Gamlen and Eardley [60] and Lindberg et al. [61-63] in the 1980s. Increased interest of the pharmaceutical industry to use the extrusion equipment for wet granulation has occurred especially within the last two decades. Here, the co-rotating type has commonly been used for investigations [64]. Various types of twin-screw granulators with different barrel diameters and processing capacities exist on the market [65-68]. The screw length used related to the barrel diameter is a common dimensionless descriptor of twin-screw granulators and well-known as length-to-diameter ratio (L/D) [59, 64]. In the thesis, different twin-screw granulators from different manufacturers with different diameters (16 mm to 27 mm) and L/D ratios (25 to 40) were used and investigated for their effects on granule properties. An exemplary photograph of a twin-screw granulator is given in Figure 1.

Figure 1. BCG 25 twin-screw granulator (with courtesy of L.B. Bohle Maschinen + Verfahren).

During a twin-screw wet granulation process, the powder blend and granulation liquid are fed directly into the barrel using a feeder and pump, respectively. The wet mass is conveyed along the screw length whilst the mechanical energy needed for granule formation and homogeneous liquid distribution is imparted. Due to the intermeshing setup of the two screws, the flight of one screw will wipe material adhesions from the surface of the other screw. Differing from the extrusion process, no die plate is attached at the barrel end, which is why the wet granules can freely fall out when exiting the barrel [59, 64, 69].

Next to twin-screw wet granulation, the same equipment can be used in a dry and melt version of twin-screw granulation. In dry TSG, the physical powder mixture is fed into the barrel, while the temperature settings of the barrel remain below the glass transition temperature or melting point of the binder used. The overall mass inside remains in a dry, non-molten state, but softens and is well distributed by a suitable screw configuration, allowing granule formation. In melt TSG, a binder with low melting point is required that acts as liquid binder after melting. The temperature settings cause the mass to heat up near or above the melting point of the binder. Granule formation can then occur after homogeneous distribution by the screw configuration [28, 58, 70, 71].

Investigations of lactose monohydrate on a twin-screw and high-shear granulator revealed that TSG produced granules with lower friability compared to the traditionally used high-shear granulation technique. TSG also provided a higher yield fraction, was more efficient and required much less granulation liquid than the high-shear granulation process. This is why TSG was seen to have a key benefit for wet granulation. Superior results were also described for tablets consisting of granules produced with TSG in comparison to direct compression [68, 72, 73].

Since numerous parameters influence TSG processes and the outcomes, the main effects will be outlined briefly in the following.

1.5.2 Screw configuration

Several elements with different impact on granule formation are available which can be chosen to produce granules with specific, pre-defined properties. Screw setup is often modular and the elements are assembled on a shaft that is connected to the engine. Since the barrel consists of a series of multiple short zones [59], it enables the usage of different barrel lengths, and thus screw lengths, as the infeed of powder and granulation fluid can occur along the entire length of the barrel, provided that infeed ports can be installed [67]. In consequence of the modular construction of barrel and screw as well as of the variety of different screw elements available, multiple different screw designs can be set in TSG [19, 74, 75]. In addition to that, the screws themselves can either end with the barrel or protrude slightly from the barrel to ease the discharge of the wet mass and avoid undesired adhesion and densification of material at the exit. In the studies conducted within the frame of the thesis, screws were usually longer than the barrel.

It should be noted that the choice of screw configuration is closely linked to the granulation performance of a twin-screw granulator and therefore to granule formation and the production of agglomerates with suitable characteristics. Although there are numerous elements, three types are commonly used in TSG, namely conveying elements, kneading elements as well as, if assembled to a larger unit, kneading blocks and mixing elements [76-79].

Conveying elements

Conveying elements (CE, Figure 2) possess a helical shape and are known for their transport capability. They are used in the infeed area of the solid and liquid to convey the material towards the barrel exit. Mostly, the double-winged CEs are used where the two flights have an offset of 180°, resulting in a cross-sectional geometry that has two lobes, also known as bilobal. The distance a flight traverses per revolution (axial displacement) is the flight lead, whereas the axial distance between two adjacent flights is the flight pitch. It mainly determines the conveying capacity. Therefore, long-pitch CEs possess a higher transport capacity (mass conveyed per revolution) than CEs with shorter pitches. Typically, CEs only apply low shear forces and impart low mechanical energy to the material [54, 59, 64, 76, 80].

Figure 2. Exemplary photograph of conveying elements with different pitches.

Kneading elements and kneading blocks

Kneading blocks (KB, Figure 3), a type of mixing zone, are composed of several kneading discs, assembled to a greater unit. The discs themselves have, similarly to the CEs, a bilobal appearance, a defined thickness and belong to the minimal- or non-conveying elements. The choice of offset angle of each kneading element (KE) affects the conveying capacity of the resulting kneading block. Typical offset angles are 30, 60 and 90°, which can be set in forward or reversed direction to generate flow obstacles of different extent. In the studies performed in the thesis, only forward-orientated KBs were used, which is why the focus in the following part is on this type of KB. While angles of 30 and 60° possess some conveying capacity and slightly resemble CEs, the conveying capacity decrease with greater angles and resulted in neutral one at 90° stagger angle [74, 75, 81, 82]. KBs provide densification and agglomeration of the wet material. The disc width is relevant for the extent of dispersive mixing. Broader discs possess more pronounced dispersive effects and the material is likely to be pushed into the gap between the tip of the discs and the barrel wall, where shearing takes place. Distributive effects dominate for narrower discs. The input of shear energy is much higher in the kneading zones than in conveying zones and increases with increasing offset angles and length of both disc thickness and kneading zones [54, 58, 76, 80, 83].

Figure 3. Exemplary photograph of kneading blocks at various offset angles.

Mixing elements

Distributive feed screws (DFSs, Figure 4), also called comb mixer elements, are similar to CEs but have longitudinal slots to offer more space for the wet material. They enable a more homogeneous filling of the barrel and a partial backflow of product into the upstream channel and therefore have both conveying and mixing functions. DFSs do not apply high shear stresses as they have a positive conveying capacity in comparison to kneading zones. This leads to low and stable torque values throughout the process. Another type of mixing elements are the tooth-mixing elements (TMEs, Figure 5). They are made of cylindrical discs and have evenly distributed notches cut into the flank of the disc to create blades. Their shape and orientation are determined by the shape and cutting direction relative to the screw channel. Due to the short, disc-like element length and the open geometry they possess neutral conveying capacity. The TMEs can be further distinguished in narrow and wide TMEs. Compared to DFSs, TMEs possess no conveying character [58, 80, 84].

Figure 4. Exemplary photograph of distributive feed screw (kindly provided by K. Kiricenko).

Figure 5. Exemplary photograph of tooth-mixing element [80]. (Reprinted with permission of Carl Hanser Verlag).

Impact of the screw elements on product quality

Typically, a screw configuration consists of more than one type of element, so the properties of the final product are determined by all of the elements used. Therefore, in the following, the effects of the screw configuration on the product quality are considered by increasing the complexity of the screw configuration, starting with only CEs, through the inclusion of KBs and ending with the additional use of the other mixing elements.

A study conducted by Dhenge et al. [85] proved that the CEs alone are capable of producing granules from a mixture of lactose monohydrate, MCC and croscarmellose sodium (80-18.5-1.5 % w/w). Granule size distributions (GSDs) were bimodal, independently of the binder fluid used and its viscosity. Granulation with water produced a lower proportion of fines and small granules but a higher fraction of big granules than with the aqueous solutions of higher viscosities. The manufacturing of less fines was assumed to be a consequence of the better wettability and a shorter penetration time of water into the powder. When applying the viscous solution, some material remained un-granulated while some big granules were obtained, indicating that the shear stresses applied by the CEs were too low to sufficiently distribute the viscous liquids. Thus, a necessity of higher shear application was concluded when using high viscous liquids. Similar conclusions were drawn by Djuric and Kleinebudde [75, 86], who investigated different CEs with different pitches (15, 20, 30, 40 mm). However, they further found an impact of pitch on granule properties. Less fines but larger yield fraction, slightly lower granule porosity and lower granule friability were obtained when using CEs with larger pitch. Djuric and Kleinebudde assumed that the larger volumes available in CEs with larger pitches caused a simple passage of the wet material with sufficient interaction to lower the amount of fines. A counter-effect was assumed for CEs with smallest pitch. However, granule characteristics were worst in all cases compared to screw configurations with kneading and mixing elements, which considerably improved granule characteristics and highlighted the necessity of additional elements within the screw setup.

As a screw configuration often consists of kneading blocks separated by a conveying zone [69, 87], an additional impact of KBs and the various stagger angles on granule properties occurs.

Although Vercruysse et al. [83] found no significant impact for the offset angle on granule attributes under the examined process conditions, a significant effect was revealed for the number of KEs. The mass was more intensively mixed with the binder liquid when more KEs were incorporated in the kneading zone, resulting in less fines, more oversized and less friable granules. In addition, granules of higher densities were described. Other research groups reported similar results for the number of KEs [75, 88] but also revealed an influence of the stagger angle. The lowest yield fraction and the most oversized granules but most dense and least friable granules were manufactured when the KBs with neutral conveying character (90°) were used. The KBs retain the material and squeeze the liquid out of the granular voids. A higher degree of liquid saturation is achieved and causes the manufacturing of bigger granules. Van Melkebeke et al. [88] additionally reported an influence of the offset angle and kneading disc thickness on the manner of mixing (distributive or dispersive) that occurs in the barrel. The authors described dispersive mixing (size reduction of droplets and granules) for thicker discs and smaller angles, while distributive mixing (homogeneous distribution without size change) occurs for thinner discs with greater offset angles. According to van Melkebeke et al. [88], the usage of thinner discs caused the production of less robust granules with negligible effect on other granule characteristics. However, one should be aware that the number of kneading discs and stagger angle cannot be considered solely as studies revealed an interaction, partially with screw speed settings, on relevant granule and process characteristics, e.g. torque, residence times and residence time distributions [81, 89]. Although kneading zones are speculated to operate entirely filled [76], Lee et al. [74] investigated different screw configurations with different offset angles in the kneading zones at varying material throughputs and revealed otherwise. In addition, apart from the necessity of KB incorporation, CEs provide a positive effect on the yield and width of granule size distributions when located downstream of a KB [77, 78].

The incorporation of DFSs led to a higher yield fraction but less friable and porous granules compared to configurations consisting of CEs only. As the material in the DFS-section experienced a decreased conveying velocity, the local filling degree and thus compaction was higher, resulting in less abrasion. However, in comparison to the different KB setups, the granules produced with DFSs exhibited higher porosity and friability [75]. In addition to that, Sayin et al. [90] reported that the solid-liquid distribution quality of DFSs was less homogeneous compared to a KB made up of seven KEs at 90° offset angle. Although the GSD was bimodal for both configurations, DFSs produced much bigger granules and thus much broader distributions, which was even more pronounced at the expense of the yield fraction when the higher liquid-to-solid (L/S) ratio was applied. The more efficient breakage of bigger granules caused by the KBs was held responsible. Nevertheless, granule porosities were also found to be higher for granules produced with DFSs at all examined liquid contents. Vercruysse et al. [84] described positive effects when two or four DFSs were additionally incorporated next to kneading blocks. The additional DFSs lowered the oversized granule fraction and increased the process yield. GSD was generally narrower and the median granule size was lower.

Vercruysse et al. [84] also investigated the impact of TMEs on granule formation. It was reported that both types of TMEs lowered the amount of fines to similar extent when incorporated in a screw configuration, while their effects on the oversized fraction was opponent. Whereas narrow TMEs reduced the oversized fraction from 23 to 10 %, an increase was noticeable (from 23 to 26 %) when the wide TME was used. In contrast to DFSs, the combination of narrow TMEs with KBs only had partially positive effects. The implementation of one narrow TME lowered the oversized granule fraction (from 37.9 to 29.3 %). Although the incorporation of a second narrow TME caused further reduction of oversized granules (to 20.4 %), the fine fraction increased compared to the usage of a conveying section (30.8 % vs. 20.2 %) [84].

Currently, screw configurations in literature are usually presented by mentioning different screw sections, e.g. conveying zone and kneading zone, with specific information on the number of kneading elements and kneading blocks, the offset angle and other types of elements used [81, 88, 89, 91, 92]. To the best of my knowledge, no quantification approach exists that depicts various screw configurations as a single number to ease comparability, especially for screw configurations used on different granulators but also between different research groups and experiments.

1.5.3 Barrel fill level

One of the key factors in TSG is the barrel fill level, which is the occupied volume related to the available volume provided by the screw configuration [93]. Since the screw configuration and thus free volume is a fixed parameter in TSG, barrel fill can mainly be controlled by material throughput and screw speed. Barrel length and properties of powder blend and granulation liquid have further impact on the barrel filling degree [81, 94-96].

Lowering the screw speed or increasing the material throughput causes a rise in barrel fill with direct impact on granule characteristics due to increased material accumulation in the barrel and the resulting densification and compaction. In starved condition the material may lack of sufficient interaction and rather faces particle separation with consequences for granule formation and mixing efficiency [89]. The material does not experience sufficient friction at low fill level, which is why only few abrasions of fines occur and (very) big granules survive [85, 97, 98]. In contrast, the granulation liquid is likely squeezed out of the solid phase at a high fill level due to densification processes and additionally distributed by the screw geometry, which enhances granule growth [86, 99]. In addition to this, mixing quality was described to be different at varying fill levels. Axial mixing dominates at low levels while plug flow prevails at high fill levels [89]. In process upscaling, the knowledge of the fill level is essential to produce a final product with similar properties, especially with change of the granulator and its dimension [64].

An appropriate indicator for estimating actual barrel fill level during TSG processes is the specific mechanical energy (SME), a depiction of the mechanical energy imparted into each mass unit conveyed, that allows for a direct comparison of different twin-screw granulators [96, 100].

However, the SME is a parameter reflecting actual conditions and cannot be predicted and thus actively set on other granulators. Therefore, the quantification and prediction of the barrel fill is a major need in TSG to facilitate further process understanding [59], allow comparison of twin-screw granulators and will support scale-up and process characterisation [64]. For this purpose, several attempts have been made to quantify barrel fill during TSG processes. The dimensional specific feed load (SFL) was introduced as surrogate for volumetric barrel occupancy that considers the amount of mass conveyed per revolution [101]. It revealed limited validity to the formulation, screw geometry and twin-screw granulator used for the examination only [93]. In contrast, other research groups have proposed dimensionless attempts. Although these attempts are scale-independent [102, 103], they lack applicability tests on twin-screw granulators other than those on which they were first tested and described [66, 95].

The prediction of the barrel fill level is still an unsolved problem of TSG which needs to be solved with a suitable validated model that allows for the consideration of the actual screw elements in the screw setups and process settings chosen on the different granulators. Of course, the same equipment can be used in CM for the process development and manufacturing, but an increase in throughput, as a scale-up principle, should still lead to granules with the predefined and desired properties.

Seem et al. [64] assumed that even though a sound fill level quantification could allow for the direct comparison of various granulators, without considering energy input and the materials residence time in the different barrels, the overall approach remained incomplete.

1.5.4 Barrel residence time

Residence time distributions can be defined as the probability distribution of time that a material remains within one or more unit operations. It is commonly determined in industries for chemicals, polymers, food, plastics, catalysts and pharmaceutical products. Its measurement increases the understanding of the materials flow pattern as well as transport phenomena inside the unit operations and marks a crucial step towards design, improvement, successful troubleshooting and upscaling of production processes [38, 104].

In TSG, the residence times of the wet masses in the barrel are usually in the range of a few seconds and are thus very short [98, 99, 105-107]. This is why sufficient solid-liquid distribution is vital to facilitate appropriate granule formation [81]. The shape of the distribution mirrors the extent of both axial dispersion and back mixing and is influenced by various factors, e.g. material properties, throughput, process settings (material throughput, screw speed, barrel fill) and geometry of screws and barrel [108, 109].

Dhenge et al. [98] described a decrease in mean residence time with both increasing screw speed and material throughput in consequence of the increased conveying velocity of the screws and high throughput force. In addition to that, the distribution width was also affected. Similar

observations have been made by Kumar et al. [89], who additionally found that the impact of material throughput on mean residence times was less dominant than a change in screw speed.

Therefore, the RTD measurements should be an integral part of the experimental plan in TSG as it allows the interpretation of flow behaviours and process dynamics.

1.5.5 Liquid content required

In comparison to the rather conventional granulation techniques high shear or fluid bed granulation, TSG requires much less liquid [73, 97] and produced granules of higher yield fraction with both lower porosity and friability due to increased shear forces and densification provoked by the kneading zones in the screw configuration [78, 84]. In consequence, tablets produced with granules produced on a twin-screw granulator were more resistant against external forces in comparison to tablets produced on a high shear granulator [68]. It has been described that an increase in liquid content caused an increase in granule sizes at the expense of fines while the GSD changed from a broad and bimodal towards a narrower and monomodal appearance [105, 110, 111]. Typically, the granules obtained also showed higher strengths and lower porosities when liquid contents were increased [82, 105].

2 Aims and outline of the thesis

Although numerous interesting investigations have essentially contributed to the understanding of TSG in the last two decades and new study results are still being regularly published, some of the puzzle elements of the knowledge gained so far cannot be put together to form an overall picture.

TSG processes are mainly influenced by the screw configuration, barrel fill level, screw speed, residence times, properties of powder and granulation liquid as well as liquid content. In consequence of the modular setup, infinite options are available to set the screws for granulation processes. The various elements enable individual screw setups to achieve granules of defined properties, which are suitable for tableting. Keeping all influencing factors on TSG processes in mind, it is even more difficult to compare the numerous study results of the different research groups with each other.

Aim of the thesis at hand was therefore to contribute to TSG by predicting:

- optimal liquid content using a mixer torque rheometer (MTR),
- suitable process parameters based on a numerical description of screw configurations to enable successful process transfers between differently sized granulators and
- material hold-ups and lag times in the barrel as an initial step in predicting barrel fill levels at defined process settings.

The first working package dealt with the investigation of different formulations regarding their rheological behaviour using mixer torque rheometry and its change with the addition of liquid. Optimal L/S ratios should mathematically be determined based on the torque curve obtained on the MTR and subsequently be assessed on the twin-screw granulator. As this procedure was successfully described for high shear wet granulation processes, a successful implementation in TSG was striven for. As the liquid content has already been described as being crucial for achieving granules with specific properties, the prediction of optimal L/S ratios for TSG would speed up process development of new formulations.

Development and implementation of a quantification approach for various screw configurations were the focus in the second working package. This approach should be critically assessed in transfer experiments of processes onto twin-screw granulators of different dimensions.

In the third part of the thesis, a model should be developed that predicts material hold-up in the barrel for various screw configurations at given process settings as an essential step towards the determination of the real filling conditions within the barrel. The model should consider the different conveying capacities and flow restrictions induced by different screw elements. In addition, the model should be able to estimate the materials lag-time in the barrel.

3 Results and Discussion

3.1 Usage of mixer torque rheometry to predict optimal L/S ratio for twin-screw wet granulation processes

3.1.1 Introduction

Quality variations of batches or between vendors of excipients are common but may lead to issues if they behave differently. Applying mixer torque rheometry enables an easy and quick pre-assessment of excipients and formulations regarding their rheological behaviours as well as wet mass cohesiveness and their functionalities [112-114]. The torque recorded during the investigation of a wet mass was proposed to be in accordance with the states of liquid saturation [114, 115] defined by Newitt and Conway-Jones [24], which in turn is decisive for a subsequent granulation, extrusion and spheronisation process [21, 114]. Control of granule formation is highly important since uncontrolled processes may lead to final products with suboptimal characteristics. This is particularly necessary if the optimum of liquid amount is located within a narrow span, which emphasises the striving for an approach for determining optimal liquid quantities as well as their predictions for granulation processes [116-118].

Based on this ambition, prediction of suitable L/S ratios using mixer torque rheometry was described for subsequent pelletisation processes (extrusion, spheronisation) [112, 119] and high-shear granulation processes [118]. Chitu et al. [25] investigated pure lactose monohydrate and MCC as well as their mixtures (70-30% and 30-70%) on a MTR and on a high-shear granulator with ultra-pure water. Granulation revealed to be reproducible within the area of transition from pendular to funicular saturation state, which was observed to be a plateau phase on the online-recorded torque curve of the high-shear granulator. In this phase, interparticle voids become steadily saturated by the granulation liquid [23, 120]. Optimal results were achieved at 38 % and 68 % liquid content for the respective lactose-MCC mixtures at the end of the plateau, which enabled a sufficient decrease of fines while over-wetting could still be prevented. These optimal liquid contents corresponded to L/S ratios, where stronger upward movements of the offline-measured torques were noticeable on the MTR if further liquid addition occurred. This indicated a change from pendular to rather funicular state at the optimal L/S ratio and its further transition to capillary state with stronger capillary forces after additional liquid administration [25, 118, 121]. Similar observations could be made in a previous study of Chitu et al. [122]. Santomaso et al. [118] continued this approach and assumed the L/S ratio at the inflection point of the torque curve being optimal for the production of granules on a high-shear granulator. Mean granule sizes obtained at previously determined L/S ratio were within the targeted range, which demonstrated the suitability of the MTR for determining appropriate liquid quantities of given formulations for subsequent high shear granulation processes.

Aim of this working package was to apply this approach for twin-screw granulation (TSG). Similarly to Santomaso et al. [118], the inflection point of the torque curve obtained on the MTR was assumed to be optimal for subsequently performed TSG. To assess this assumption

sufficiently, eight L/S ratios were investigated for each formulation, covering a broad range of liquid contents, starting below the L/S ratio at the inflection point and ending at a L/S ratio above the L/S ratio at the maximum on the torque curve.

3.1.2 Determination procedure of optimal L/S ratio

Prior to the experiments to determine the optimal L/S ratios, preliminary test runs had to be conducted with the respective material. Based on that, the final water addition scheme was specified. If the torque changes were highly sensitive to each liquid addition, depicted by considerable changes in the torque profile, and by this only few data points displayed the torque increase up to its maximum, the quantity of the liquid added was lowered to increase the density of data in this critical phase. A change to the previous quantity of liquid added was made after the torque had passed its maximum and thus decreased again.

In Figure 6A, the torque recorded during the investigation of one run of theophylline monohydrate (TM) is exemplarily depicted. The torque started at a low level. Since the system lacked sufficient liquid at the beginning, interparticle friction as well as interaction of the particles with the kneading blades and wall of the kneading chamber of the MTR might cause these torque values [121]. At approximately 5 min, the torque started to increase. The liquid content seemed to be enough to form interparticle, lens-shaped liquid bridges at the contact points of the primary particles leading to an increase in cohesive forces. The system reached the pendular state of liquid saturation. Further increase in torque was noticed with further liquid addition. The liquid formed a coherent network with air inclusions that caused higher cohesive forces. The system entered the funicular state. At approximately 16 min, capillary state was reached as the torque reached its maximum. All interparticle voids were completely saturated. Strong forces had to be overcome [121], which were mainly driven by negative capillary pressures of the liquid due to concave meniscus at the surface [23]. Further water addition (above 16 min) caused a shift in phases - water became the external one, in which the powder particles were dispersed. Droplet state of liquid saturation was reached and a suspension was formed. The torque steadily decreased until it approximated 0 Nm [21, 114, 115, 121].

For data analysis the first half of each minute was generally considered as mixing time while the (wet) material was assumed to be thoroughly and homogeneously mixed in the second part. The torque values recorded in the respective second part of a minute were averaged to one value and finally normalised by relating it to the investigated mass. The liquid amount at each time point could be specified accurately due to the verification of the precision pipettes as described in section 5.2.2.3. The mean value of the starting moisture was added to the amount of liquid added during the experiment. Liquid content was related to the solid mass investigated and depicted as L/S ratio (Figure 6B).

Due to the fluctuations of the originally recorded torque curve (Figure 6A), the normalised torque curve also showed partial ups and downs in its progression, which would have made further

analysis difficult. A smoothing of the curve was therefore necessary. Thus, the moving average was applied to the torque curve two times (based on personal communication with R. Baggio on 20 June 2018, co-author of [118]). The first application was done from time point zero towards the end which caused a left shift of the curve and would result in incorrect calculations of the L/S ratio. The second one was performed in reverse order with the values of the first moving average to correct the location of the smoothed curve (exemplarily depicted in Figure 41 in the appendix). The final smoothed curve is the dotted one depicted in Figure 6B. The number of values used for the determination of the moving average was an individual decision for each formulation investigated and was considerably influenced by the data density of the overall curve. For materials that were less sensitive to the liquid addition and thus enabled a greater data density, more values were included for the determination than for materials that responded more sensitively. In the TM example, four values were used for the moving average.

Further analysis occurred with the curve that resulted from the second application of the moving average (Figure 6B). The first (Figure 6C) and second derivatives (Figure 6D) were used to determine the L/S ratio at maximum and, if existing, minimum as well as at the inflection point, respectively. The presentation of the normalised values in Figure 6C and D is for the sake of completeness to show that the determined extreme values as well as the inflection point are close to the corresponding points on the original curve.

Table 1 compiles the investigated materials, their starting moisture content, the water addition schemes and the mean volume pipetted per minute. The L/S ratios determined are also depicted. Some further materials and formulations were examined on the MTR. The results were used in other working packages. The results of the respective systems can be found in Table 34 in the appendix.

Table 1. Investigated materials and calculated L/S ratios (*n=10x10, **n=6, ***n=3, mean ± s).

Material	**Water addition**		**Mean volume***	**Starting Moisture****	**L/S ratio at**	
					IP***	**Max*****
[% w/w]	**[min]**	**[µL]**	**[µL]**	**[%]**	**[-]**	**[-]**
TM	0-end	1000	0.9786	0.11 ± 0.02	0.359 ± 0.031	0.464 ± 0.008
PM200, 3 % PVP K30	0-8 9-end	500 200	0.4939 0.1990	0.35 ± 0.06	0.184 ± 0.008	0.222 ± 0.002
DCP A150, 3 % PVP K30	0-12 13-50 51-end	500 200 500	0.4939 0.1990	0.90 ± 0.03	0.246 ± 0.012	0.318 ± 0.002

Legend:
TM: theophylline monohydrate, PM: Parteck M (mannitol), PVP: polyvinylpyrrolidone, DCP: dicalcium phosphate anhydrous, IP: inflection point, Max: maximum

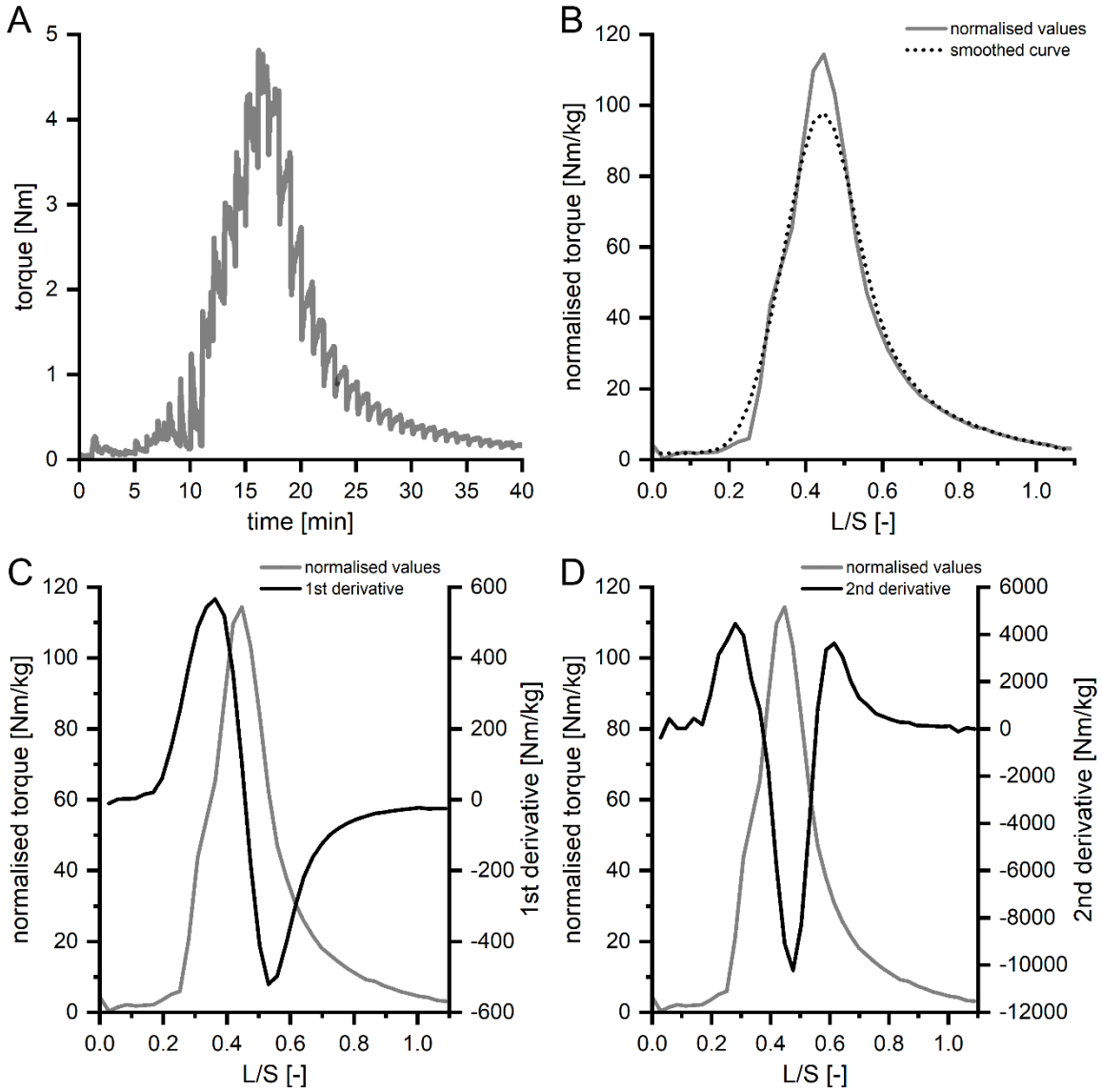

Figure 6. Determination procedure of the optimal L/S ratio with one experiment of TM: A) originally torque recorded during experiment, B) normalised values and smoothed curve in relation to the actual liquid amount inside, C) the 1st and D) the 2nd derivative of the smoothed normalised torque curve. L/S ratios at maxima and inflection points were these values, where the derivatives became zero.

3.1.3 Accuracy of defined liquid contents

Although the L/S ratio at the inflection point (IP) was assumed to be the optimal one, further seven L/S ratios were decided to be tested covering a broad range of defined liquid contents. The L/S ratios investigated ranged from far below the L/S ratio at the IP and to a L/S ratio far above the L/S ratio at torque maximum (Max) as described in section 5.2.3.6 and depicted in Table 26.

First, the accuracy of the liquid infeed during TSG had to be thoroughly tested whether targeted liquid contents were actually achieved. Further details on this procedure are given in section 5.2.3.6. As it can be seen in Figure 7A, the measured liquid contents at the different times fluctuated only slightly around the target, except for those related to L/S ratio of 0.289 and 0.359, which showed higher fluctuations. However, fluctuations can be affected by variations in liquid

and powder infeed itself as well as by the choice of feeding equipment [81, 123, 124]. Nevertheless, target and achieved L/S ratios were linearly well correlated as depicted in Figure 7B and a strong positive linear relationship was revealed (R= 0.9996). An accurate feeding was feasible. However, fluctuations must presumably be accepted due to the process dynamics but can be regarded as negligibly small.

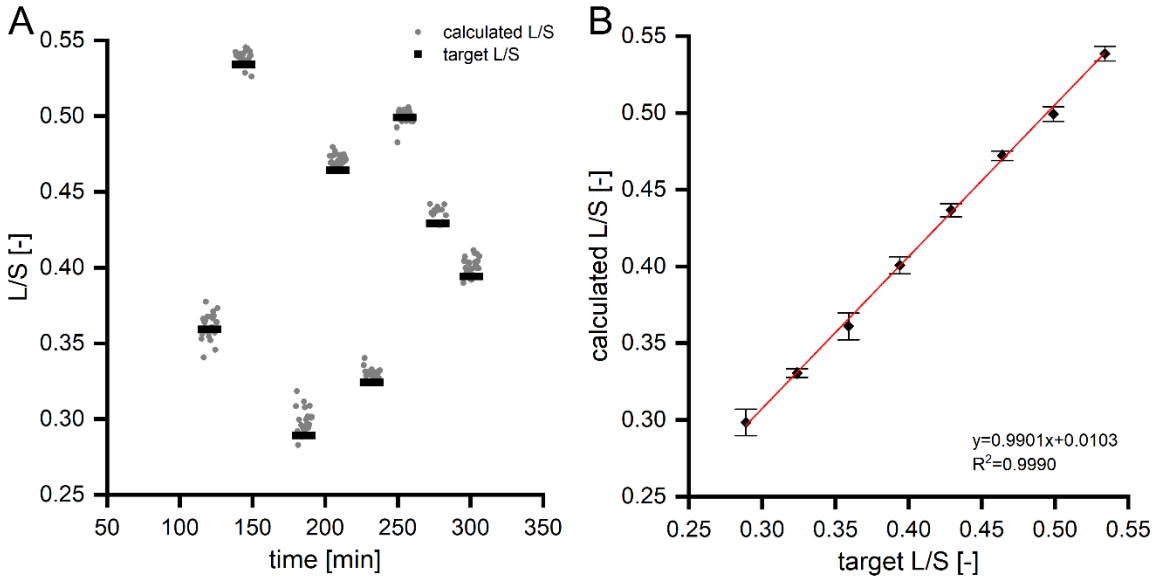

Figure 7. Test on achieving target liquid contents with TM: A) comparison of target L/S ratios and each ratio determined at the different times throughout the test (n=1) and B) linear correlation of target and determined ratios (n=3, mean ± s).

3.1.4 Check of determined optimal L/S ratio on twin-screw granulator

Results obtained from the accuracy test of liquid infeed were promising to perform in-depth investigation on the previously defined L/S ratios and its impact on granule formation, granule size and granule size distribution (GSD).

GSD of TM (Figure 8A) indicated slight bimodal distributions at lower liquid contents up to a L/S ratio at IP and more pronounced bimodal appearance for L/S ratios at Max -1 and Max, which changed to monomodal distributions at even higher liquid contents. The GSD curves of the lowest L/S ratios (at IP -2 and IP -1) were very similar in shape and position; thus, similar x-values (x_{10}, x_{50}, x_{90}) were obtained. At slightly higher L/S ratio (at IP), liquid content seemed to be enough to increase the proportion of bigger granules on the extent of the finer fraction (increase of x_{50} and x_{90}), whereas this was accelerated at the next L/S ratio (at IP +1). However, with change to L/S ratio at Max -1, a threshold might be exceeded as the granule sizes sharply rocketed onto noticeably greater sizes. Further liquid addition caused further right-shifts of the curves [78], associated with the production of granules up to approximately 15000 µm. The effect of the amount of liquid on granule growth can be seen well in Figure 9, using x_{50} as an example. While TM was less sensitive to changes in liquid content at low L/S ratios (IP -2 to IP) and x_{50} increased almost negligibly from 530 µm to 680 µm, it increased when the L/S ratio was changed to IP +1

(950 µm) and grew extremely considerably at even higher L/S ratios (2400 µm at Max -1 to 4160 µm at Max +1). In addition, with transition of liquid content at IP -2 to Max +2, the GSD became constantly narrower resulting in a steady decrease of spans from almost 2.7 for the curve obtained at IP -2 to almost 1.4 obtained at Max +2. The effects of liquid content on both width and appearance of GSDs curves are in accordance with the reportings of Vercruysse et al. [84].

When this working package was conducted at the beginning of the PhD period, only the Camsizer XT was available, which could only measure granules up to about 3000 µm. Bigger granules had to be sieved resulting in the removal of large amounts of granules; a sieve with 2000 µm mesh widths was used. Thus, the resulted GSD curves reflected only a part of the total spectrum of granules produced at the different L/S ratios. The respective curves as well as the percentages of removal can be found in Figure 42A in the appendix. The curves themselves will not be discussed further, but the amount of removals might still be interesting. Whereas the percentage proportions of granules greater 2000 µm were quite small at L/S ratios ranging from the IP -2 (0.04 %) to IP +1 (3.65 %), considerable growth of granules was observed with change of liquid content at Max -1 that resulted also in a considerable increase of granules greater 2000 µm (15.12 %) with further rise to 54.36% at the highest L/S ratio (at Max +2). As shown in Figure 42B, the granule fraction larger than 2000 µm increases essentially with increasing liquid content, proving that liquid proportions in wet granulation are important. Due to the oversized granules, additional process steps would have to be taken, especially for high L/S ratios, e.g. milling, in order to obtain suitable granule size fractions for further processing, e.g. tableting. Nevertheless, with the availability of the CPA 2-1, all batches with their entire spectrum of granule sizes were measured again. The GSDs from these measurements are depicted in Figure 8A. However, the bimodal appearing distributions obtained at L/S ratios at Max -1 and Max (Figure 8A) could be a result of the storage in closed plastic bags in a carton until remeasurement, where bigger granules may have broken into smaller subunits.

The GSDs of mixtures of mannitol and PVP (PM200-PVP) as well as anhydrous dicalcium phosphate and PVP (DCP A150-PVP) obtained at the different liquid contents are depicted in Figure 8C and E, respectively. All distribution curves obtained with PM200-PVP were monomodal, independently of the liquid content, but showed a steady right-shift with increasing L/S ratio. As expected, the lowest liquid content (at IP -2) produced the smallest granules with highest fine proportion. Considerable granule growth could be noticed at next higher L/S ratio (at IP), the fine fraction completely disappeared (x_{10} of 723 µm) and caused essential growth in oversized granules (x_{50} of 1523 µm, x_{90} of 2414 µm), which was even more pronounced at higher liquid levels with the production of granules up to 7000 µm at Max +2. The change of x_{50} (Figure 9) makes the impact of L/S ratio on granule growth clearer. Whereas x_{50} was approximately 630 µm at IP -2, it was about a factor of 5.5 larger (3530 µm) at Max +2. Similarly to TM, an increase in liquid content resulted in narrower distribution widths [84]. The span decreased from 1.6 to 1.0 (Figure 8C).

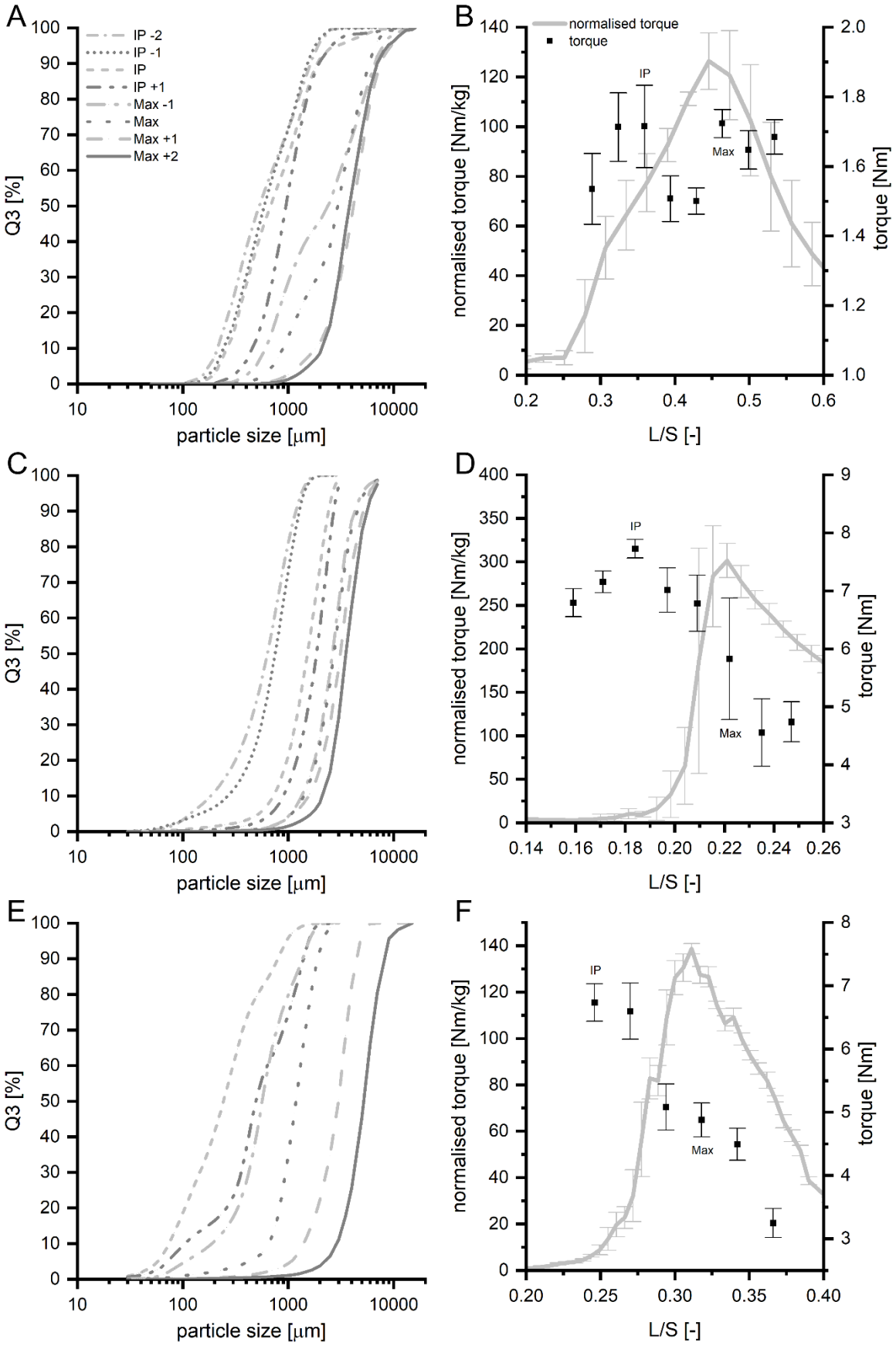

Figure 8. GSD (left diagrams) and comparison of normalised torque obtained on MTR and torque obtained during TSG (right diagrams) for TM (A, B), PM200-PVP (C, D) and DCP A150-PVP (E, F) (GSD: n=3, mean, normalised torque: n=3, mean ± s, torque: n=660 (TM), n= 480 (PM200-PVP and DCP A150-PVP), mean ± s).

The influence of liquid content on the curve position in the diagram was also noticeable for the DCP A150-PVP system. However, in contrast to TM and PM200-PVP, monomodal distribution curves were only observed for the investigations at L/S ratios at Max and onwards. The L/S ratio at the IP was the lowest that could be investigated. Investigations at lower liquid levels were not feasible to perform because of deafening noises of the granulator. It can only be conjectured whether the liquid content was possibly too low to ensure sufficient lubrication for the screw elements and/or whether the dicalcium phosphate anhydrous particles can be held responsible for this when they got into the gap between the screw elements and barrel wall. Nevertheless, with change of liquid content from those at the IP to that at Max +2, the impact of liquid addition on granule formation became overproportionately stronger and resulted in biggest granules at Max +2. This was also highlighted by the change of x_{50} (Figure 9), which indicates less sensitivity when changing the L/S ratio from IP to Max -1, while changing the L/S ratio to Max and higher liquid contents resulted in a massive increase in size. In addition, span decreased again with increasing water content (from almost 3.0 at IP to 1.0 at Max +2) (Figure 8E).

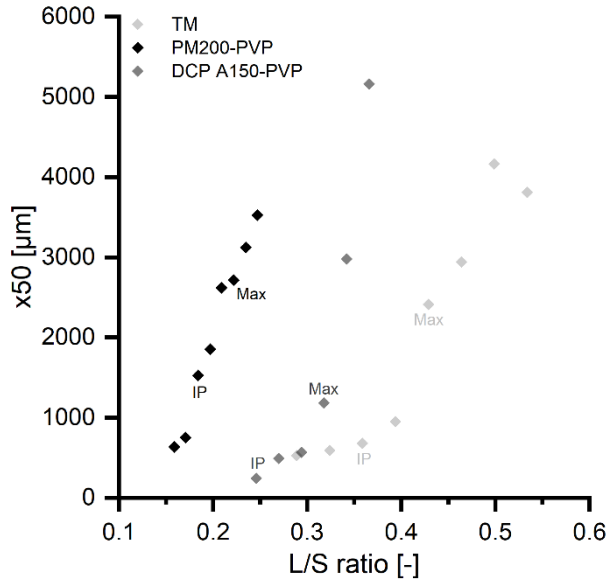

Figure 9. Change of x_{50} as a function of L/S ratio (n=3, mean).

Comparing the granule sizes of PM200-PVP and DCP A150-PVP (Figure 8C and E) revealed granules made of DCP A150-PVP being essentially smaller up to the L/S ratio at Max, even though the liquid contents started at higher levels compared to PM200-PVP. However, since both dicalcium phosphate anhydrous and mannitol represented each the same proportion (each 97%) of the formulations, the reason might be found in the material properties themselves. Compactability studies of various mannitol grades revealed particularly good compactability for spray-dried grades [125, 126], e.g. Parteck M200 [127] as utilised in this study, since they showed bigger surface areas and higher plasticity than other mannitol qualities, which allowed the formation of larger bonding areas during compression [125, 126] and could, therefore, be assumed

to further encourage granule formation in addition to the function of PVP as binder. It was also assumed that the freely soluble characteristic of mannitol in water [128] played an additional role in granule formation as the dissolved part of mannitol probably increased both the viscosity and stickiness of the wet mass locally and thus further promoted granule growth [99]. In contrast to that, dicalcium phosphate anhydrous reacts rather insensitive to external forces due to its brittleness [129, 130]. Consequently, only the binder provided any type of contribution to granule formation in the latter case, which is why the liquid content was of particular importance for proper granulation. The fluid was assumed to be absorbed by the PVP leading to increased stickiness of the wet mass which in turn fostered further particle adhesion and finally granule growth [99]. A comparing assessment to TM cannot be made since investigations occurred without PVP addition as well as at other process settings.

Based on the results described above, agitation intensity on the materials on the granulator was most likely higher than on the MTR. A better liquid distribution and more densification on the granulator was assumed, mainly induced by the shear and compaction forces of the kneading discs incorporated in the screw geometry [78, 84], which would have lowered granule porosities and thus provide more granulation liquid available on the granule surfaces and in interparticle spaces. Further adhesion of ungranulated material would be encouraged and could even lead to uncontrolled agglomeration and very large sizes [13, 23, 131, 132]. Assuming that the torques resulted on the twin-screw granulator at the different L/S ratios is similarly in accordance with the liquid saturation degrees as stated by Rowe and Sadeghnejad [114] as well as Hancock et al. [115], Figure 8D and F showed higher torque values during TSG at the L/S ratio at the IP than at the Max, indicating that the capillary state was already achieved at L/S ratio at IP and thus above the initially targeted liquid saturation degree (funicular state). Similar observations were made in a study recently published by Kyttä et al. [133] who postulated similar assumptions. However, the torque recordings for TM (Figure 8B) lacked a clear trend as for the other formulations, which was assumed to be a consequence of the low material throughput. Densification within the kneading blocks was probably insufficient. Higher material throughputs would potentially have revealed clearer observations.

Considering all observations and results, it must be said, that the MTR is an appropriate tool to get an understanding for the formulation of interest, its behaviour under agitation by tracking the changes in torque and relating it to liquid saturations [114] during liquid addition and giving valuable insights into binder-substrate interactions [118]. However it definitely lacks of transferability to a twin-screw granulator [133] without any adjustments of the liquid contents. Since the highest torques were achieved at the L/S ratios at the IPs, liquid levels below these are more advisable for most formulations in TSG.

3.1.5 Summary

Aim of this study was the investigation of materials on the MTR and its potential for predicting optimal L/S ratios for subsequent TSG processes, based on the torque development on the MTR. Mixer torque rheometry appeared to be suitable to examine materials with respect to their behaviour during liquid addition as well as their binder-fluid-interplay and its impact on torque development. Since Rowe and Sadeghnejad [114] found the torque obtained on MTR in accordance with the different liquid saturation degrees of a granule, the L/S ratio at the IP was found to be in the funicular state, whereas capillary state was reached at the maximum of the torque curve [121]. As the L/S ratio at the IP of the torque curve was already described being suitable for high-hear granulation processes [118], this was the working hypothesis in this study for the examination of different systems on the Brabender MTR and twin-screw granulator.

GSDs obtained during TSG revealed no superiority of a specific L/S ratio, neither at the previously assumed optimal liquid content at the IP nor at any other L/S ratio. Lower liquid levels were supposed to be more effective for TSG in general. Considerable granule growth was observed when a crucial liquid content was exceeded which was in accordance with literature reports [92]. Since all systems showed a distinct onset in granule growth below the liquid content at Max, stronger external forces acting on the primary particles during TSG were hypothesized that led to the achievement of capillary state much earlier than previously predicted on the MTR. If the torque obtained on the granulator is also relatable to the states of liquid saturation, the highest torque achieved corresponded to the L/S ratio at the IP, which would reflect capillary state and by this emphasizing the assumption of stronger agitation during TSG. As a result, the primary particles were brought closer together on the twin-screw granulator than on the MTR which causes an increase in liquid saturation.

3.2 Process Transfer: Attempt for a quantitative description of screw configuration and its impact on granule and tablet characteristics

3.2.1 Introduction

If a formulation has been developed at the laboratory scale, it is usually transferred onto production scale afterwards [66, 67, 94]. For TSG, it was reported that formulations cannot be easily interchanged between granulators of different dimensions [65] and that the manufacturing of granules with similar properties, without further adjustments of process condition, was not feasible [86]. Similar critical quality attributes of granules and tablets are generally striven for when production occurs at different scales and/or on different granulators [134]. The difficulty in TSG is based on several facts:

1. There are numerous options for setting up a screw configuration for TSG because of the modular form of construction [74, 75, 135, 136].
2. Screw elements of different types and profiles, e.g. pitches, free volumes, lengths and stagger angles (single kneading elements or ready-to-use KBs) can be implemented in the screw setup [88, 109, 137].
3. There is no uniform quantification approach of screw configurations so far. Typically, the number of KBs and kneading discs at given offset angles is given [81, 88, 89, 91, 92].
4. A fully validated predictive model for barrel filling degrees at defined process settings is still lacking which is applicable to granulators of different dimensions and ensures equal manufacturing conditions and thus equal characteristics of the final product.

In addition, it should be taken into consideration that the screw elements of the various manufacturers for twin-screw granulators, despite performing the same function, also differ in their dimensions, which increases the uncertainties for achieving complete screw similarity on different granulators. The aim in this part of the thesis was therefore to develop a numerical description of screw configurations for TSG using the shear stress as target quantity, which should, among others, take these differences into account. An equation was developed that contained various parameters which influence the shear stress. The equation was finally tested for its usability.

Since a constant impeller speed was described as suitable for process scaling and granulator change in high shear wet granulation, as it indicates a kinematic process similarity as well as a similar maximum shear rate [138, 139], a similar tip speed on the granulators was also aimed for in the experiments in this working package.

Thus, process transfers were performed at tip speeds similar to those achieved during the basic experiment on a QbCon®1 or a QbCon®25 and the respective shear stresses were calculated according to the newly developed equation and were critically evaluated. Two screw configurational setups were investigated for the comparative examinations on the Pharma 16 twin-screw granulator, where either the percentage proportion or the total length of the kneading blocks in the screw setup were kept as similar as possible to identify a suitable screw design for

process transfers. The applicability of the approach was additionally controlled using a Leistritz Micro 27 GL-28D. An in-depth investigation was performed to further assess the impact of process transfer on granule (size, size distribution, friability, porosity, strength, flowability) and tablet characteristics (tensile strength, tabletability, porosity, friability, disintegration time, mass uniformity).

3.2.2 Theoretical Development

3.2.2.1 General

Among the manufacturers of twin-screw granulators, numerous screw elements can be used for the modular setup of a screw configuration. Depending on the operators' targets for granule properties, millions of combinations are available of setting up a screw configuration. This, together with the manner of specifying the screw configurations in literature, makes it difficult to compare the results of different research groups. Usually only the different screw sections, e.g. conveying and kneading section, or particularities, e.g. screw length, the number and offset angles of kneading elements used in the setup or other element types, are given [81, 88, 89, 91, 92]. As far as I am aware, there is no approach to quantify screw configurations as single values to allow for a better comparison of published data obtained on different granulators at different process parameters and with different formulations. Therefore, the aim was to find a suitable quantification approach that would make the various results on TSG more comparable and thus easier to assess.

The shear stress was chosen as the target value because it was assumed that due to the numerous options of setting a screw, the areas of the various elements where shear can occur can be better represented in this way. All variables that might have a crucial impact and which had been considered are given in Table 2. The dimensions of the variables comprise mass, *M*, length, *L*, and time, *T*. Since the final equation should reflect a shear stress, τ, the variables were grouped according to this objective. The result is depicted in Eq. (1)

$$\tau = \frac{\dot{m}_{tot} \cdot n \cdot \pi \cdot d_{element}}{L/S} \cdot \sum \left(\left(\frac{A_{contact,element}}{V_{free,element}} \right)^2 \cdot \frac{l_{element}}{d_{element}} \cdot \sin(\alpha) \right) \qquad (1)$$

where $n\pi d_{element}$ is the tip speed, which was deemed necessary when different granulator dimensions have to be considered. The first term of the equation ($\dot{m}_{tot} n\pi d_{element} (L/S)^{-1}$) mirrors actual process parameters, whereas the second part was supposed to describe the screw configurational setup and its particularities. It was assumed that the L/S ratio can reflect gliding effects. The gliding effect should not be overestimated as previous experiments on the MTR (see section 3.1) had shown that the torque initially increased due to the effects of swelling or incorporation of liquid into the pores of the primary particles of the starting material, which reduced the liquid available for gliding. Only when a critical amount of liquid was exceeded were there sufficient gliding effects, which also caused a decrease in torque. Similar phenomena should

be expected in the barrel, as the development of the torque values in section 3.1 have indicated. It is therefore to be expected that higher L/S ratios lead to more gliding effects after exceeding a certain point that reduces friction forces and shear stresses at given process settings. The area of contact, $A_{contact,element}$, between a screw element and the barrel wall was meant to be the two tip areas of a kneading element as well as each crest of a screw elements thread.

Transferring the measuring units of the variables into their dimensions showed that the proposed equation reflects a shear stress as depicted in Eq. (2)

$$ML^{-1}T^{-2} = M \cdot L \cdot T^{-2} \cdot \sum L^4 \cdot L^{-6} = ML^{-1}T^{-2} \tag{2}$$

Table 2. Considered parameters for equation setup.

Variable	Symbol	Measuring unit	Dimension
shear stress	τ	$N \cdot m^{-2} = kg \cdot m \cdot s^{-2} \cdot m^{-2}$	$ML^{-1}T^{-2}$
total material throughput	$\dot{m}_{tot}$	$kg \cdot s^{-1}$	$M \cdot T^{-1}$
screw speed	n	s^{-1}	T^{-1}
liquid-to-solid ratio	L/S	-	-
contact area between screw element and barrel wall	$A_{contact,element}$	m^2	L^2
free element volume	$V_{free,element}$	m^3	L^3
screw element length	$l_{element}$	m	L
screw element diameter	$d_{element}$	m	L
stagger angle for kneading elements or helix angle of conveying elements	α	-	-

3.2.2.2 Parameter approximations

3.2.2.2.1 Empty barrel volume

Calculating the free volume of a screw configuration requires the knowledge about the total, empty volume of the barrel itself. The overlap of the two barrel cylinders have to be subtracted, when the barrel volume is calculated. Figure 10 schematically illustrates a barrel cross-section and how the calculation of the empty barrel volume was done.

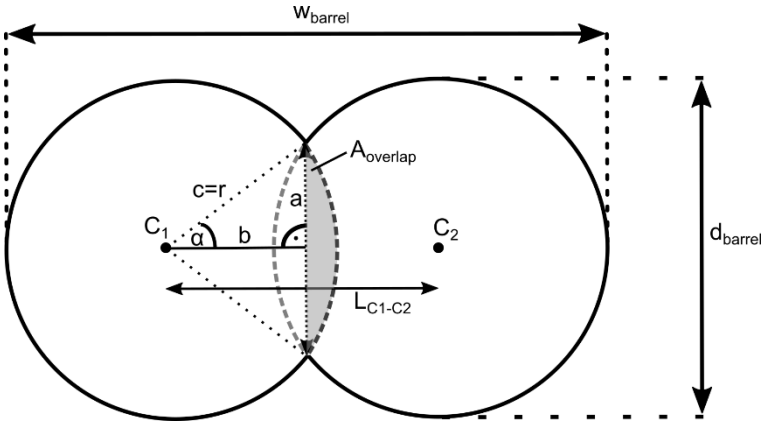

Figure 10. Approximation of empty barrel volume.

As a first step, the distance between the centres of each barrel cylinder ($L_{C1\text{-}C2}$) was determined by Eq. (3)

$$L_{C1-C2} = w_{barrel} - 2 \cdot \frac{d_{barrel}}{2} \tag{3}$$

where w_{barrel} is the total horizontal width across the two barrel cylinders and d_{barrel} is the diameter of one cylinder.

A right-angled triangle, enclosing half the distance of $L_{C1\text{-}C2}$ (b in Figure 10), half the distance between the contact points of the two barrel cylinders (a) and the barrel radius ($d_{barrel}/2 = r_{barrel} = c$) was assumed. Side length a was calculated according to the Pythagorean theorem as given in Eq. (4)

$$a = \sqrt{c^2 - b^2} = \sqrt{{r_{barrel}}^2 - \left(\frac{L_{C1-C2}}{2}\right)^2} \tag{4}$$

Angle α was calculated using Eq. (5)

$$\alpha = sin^{-1}\left(\frac{a}{c}\right) \tag{5}$$

The overlapping area, $A_{overlap}$, assumed as circle segments, was calculated according to Eq. (6)

$$A_{overlap} = \frac{{r_{barrel}}^2}{2} \cdot \left(\frac{\pi \cdot 2\alpha}{180} - sin\,2\alpha\right) \tag{6}$$

Multiplied with *2* and the barrel length used, l_{barrel}, the overlapping volume, $V_{overlap}$, of both barrel cylinders can be approximated as given in Eq. (7)

$$V_{overlap} = 2 \cdot A_{overlap} \cdot l_{barrel} \tag{7}$$

The total, empty volume, $V_{empty\ barrel}$, was finally calculated according to Eq. (8)

$$V_{empty\ barrel} = 2 \cdot \pi \cdot r^2 \cdot l_{barrel} - V_{overlap} \tag{8}$$

where $2\pi r^2 l_{barrel}$ was the calculated empty barrel volume including the overlapping parts of the two cylinders.

3.2.2.2.2 Contact areas of the screw elements

In Figure 11, a conveying element (Figure 11A) and a kneading element (Figure 11B) are exemplarily depicted to ease the understanding of the description of the calculation of the contact areas of the single screw elements.

For the determination of the contact areas of kneading discs, only the rectangular areas at their tips (Figure 11B) were considered and calculated as given in Eq. (9)

$$A_{contact,KE} = 2 \cdot w_{tip} \cdot l_{element} \tag{9}$$

where w_{tip} is the width of the rectangular and $l_{element}$ is the length of the kneading disc.

Similarly to the tip area of kneading discs, the crest area of the conveying elements was also considered to be rectangular and calculated according to Eq. (10)

$$A_{contact,CE} = 2 \cdot w_{crest} \cdot k \cdot \sqrt{\left(\frac{l_{element}}{k}\right)^2 + (\pi \cdot d_{element})^2} \tag{10}$$

where w_{crest} is the width of the elements crest, k is the number of turns of the helix of a CE. The term in the root represents the length of a single helix turn, which multiplied by k reflects the total length of the crest, l_{crest} (Figure 11A).

An overview of the contact areas of the screw elements used can be found in Table 3.

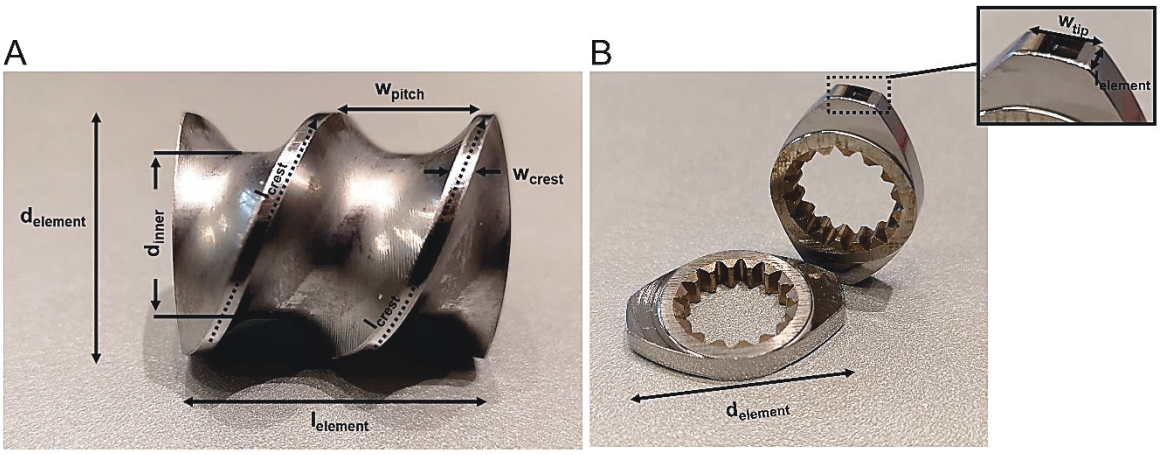

Figure 11. Measured parameters of the screw elements: A) conveying and B) kneading element. Exemplary photographs of screw elements of the granulators (QbCon®1 and BCG 25) at L.B. Bohle.

3.2.2.2.3 Helix angles of conveying element

The helix angle, α, is the angle between the helix and the axis of a conveying element that can be determined by theoretically unwinding the helix from the screw and imagining that as a right-angled triangle. The angle was then calculated as given in Eq. (11)

$$\alpha = \tan^{-1}\left(\frac{\pi \cdot d_m}{l_{lead}}\right) \tag{11}$$

where l_{lead} is the lead length, the axial distance covered by the screw in one complete revolution (360°), and d_m is the mean diameter of a CE. For the CE in Figure 11A, l_{lead} would be equal to $l_{element}$ since the helix winds once along the length of the element.

The mean diameter, d_m, is a compromise between the inner and outer diameter of a CE and was calculated according to Eq. (12)

$$d_m = \sqrt{0.5 \cdot \left({d_{element}}^2 + {d_{inner}}^2\right)} \quad (12)$$

where d_{inner} is the inner diameter of a CE (Figure 11A).

In Table 3, the helix angles of the screw elements can be found.

3.2.2.3 Measuring screw elements

Before the shear stresses in the frame of the transfer studies could be calculated, the single screw elements of each granulator had to be measured. For this, varying parameters needed to be determined for Eq. (1) by applying volume displacement measurements as well as using a calliper or ruler as specified in section 5.2.3.5.

Exemplary photographs and an overview of the different screw elements and relevant parameters determined for each screw element used can be found in Figure 12 and Table 3.

Figure 12. Screw elements used for screw configurational setup: A)-D) on the QbCon®1 and the QbCon®25, E)-G) on Pharma 16 and H)-M) on Leistritz Micro 27 GL-28D.

Table 3. Information on and parameters determined for relevant screw elements used within the screw designs on the different twin-screw granulators (mean).

Granulator type	Screw element	Meaning	Displayed	L/D ratios	$l_{element}$ [mm]	$d_{element}$ [mm]	l_{crest} [mm]	w_{pitch} [mm]	$A_{contact}$ [cm²]	$V_{free,element}$ [cm³]	α [°]
					n=6	n=6	-	n=6	n=6	n=10	-
QbCon®1 and QbCon®25	LPCE	Long pitch conveying element	Figure 12A	L = 1.25D[a,c]; Helix 1 L/D[a]	31.25[c]	25.05	84.68	12.54	3.05	5.44	79.51[d]
	MPCE	Medium pitch conveying element	Figure 12B	L = 1D[a,c]; Helix 1 L/D	25.00[c]	25.03	82.52	10.25	2.05	4.38	69.69[d]
	SPCE	Short pitch conveying element	Figure 12C	L = 0.75D[a,c]; Helix 1 L/D[a]	18.75[c]	25.05	80.91	7.63	2.01	3.29	74.49[d]
	KE	Kneading element	Figure 12D	L = 0.15D[a,c]	3.74	25.07	-	-	0.30	0.68	-
Pharma 16	LPCE	Long pitch conveying element	Figure 12E	L = 2D[a]; Helix 1.44 L/D[a] Helix 3/2 L/D[b]	31.98	15.53	77.20	10.14	1.51	3.05	60.84[d]
	SPCE	Short pitch conveying element	Figure 12F	L = 1D[a] or 0.5D[a]; (0.5D is not depicted) Helix 1 L/D[a,b]	15.99	15.52	51.32	7.20	0.58	1.53	68.13[d]
	KE	Kneading element	Figure 12G	L = 0.25D[a,b] and L=0.125D[a,b] (the latter is not depicted)	3.99	15.55	-	-	0.12	0.38	-
Leistritz Micro 27 GL-28D	LPCE	Long pitch conveying element	Figure 12H	L = 3.35D[a]; Helix 1.43 L/D[a]	90.00	26.91	217.30	17.24	8.68	18.35	62.02[d]
	MPCE long	Medium pitch conveying element, long	Figure 12I	L = 3.35D[a]; Helix 1.08 L/D[a]	90.00	26.83	276.40	13.06	7.68	18.60	68.17[d]
	MPCE intermediate	Medium pitch conveying element, intermediate length	Figure 12J	L = 2.23D[a]; Helix 1.08 L/D[a]	60.00	26.88	183.99	13.02	5.62	11.64	68.08[d]
	MPCE short	Medium pitch conveying element, short	Figure 12K	L = 1.12D[a]; Helix 1.09 L/D[a]	30.05	26.81	89.43	13.36	2.18	6.78	68.05[d]
	SPCE	Short pitch conveying element	Figure 12L	L = 3.34D[a]; Helix 0.72 L/D[a]	90.03	26.92	399.24	8.80	7.03	18.04	75.02[d]
	KB 60°	Ready-to-use kneading block of 5 KE at 60° stagger angle	Figure 12M	L = 1.1D[a]	30.00	26.89	-	-	0.51	5.35	60[e]

Legend:
L/D: length-to-diameter ratio, L: length, D: diameter, [a]: measured with calliper, [b]: according to Thermo Fisher Scientific [140], [c]: kindly provided by L.B. Bohle, [d]: helix angle of CE, [e]: offset angle of consecutive KE

3.2.3 Granulators and screw configuration used in the various transfer studies

During the studies conducted in the frame of this investigation, several granulators of different dimensions were used. Due to the varying dimensions of the granulators and screw elements (see Table 3 in section 3.2.2.3), the screw configurations varied in specific characteristics which had to be taken into account. An overview of the granulators and screw configurations is given in Table 4. Two screw configurations were used on the twin-screw granulator Pharma 16 (screw setup A and B), while only one was used on the others. More detailed information about the granulation equipment, feeders and liquid pumps used within the thesis at hand can be found in section 5.2.3.2. Information on the composition of the screw configurations as well as details on the TSG processes are provided in section 5.2.3.7.

In the transfer studies, the entire barrel lengths of the different granulators were used in each case by feeding the material into the barrel at the first possible location.

Table 4. Information on the granulators and screw configurations used in the process transfer studies.

Granulator type	Granulator			Screw configuration			
	d_{barrel} [mm]	**l_{barrel} [mm]**	**L/D ratio [-]**	**Screw bearing**	**$l_{KB,tot}$ [mm]**	**%KB [%]**	**V_{free} [cm³]**
QbCon®1* / QbCon®25	25.5	500	20:1	Two-sided	45	8.98	176.03
Pharma 16	16	640	40:1	On one side, at the infeed area	A: 56 B: 46	A: 8.72 B: 7.17	A: 122.80 B: 122.42
Leistritz Micro 27 GL-28D	27	810	30:1#	On one side, at the infeed area	60	7.41	330.13

Legend:
d_{barrel}: barrel diameter, l_{barrel}: barrel length, $l_{KB,tot}$: total kneading block length, $\%_{KB}$: percentage of kneading blocks in screw setup, V_{free}: free volume of entire screw configuration, #: original L/D ratio of 28:1, but extended to 30:1 (see description in section 5.2.3.2)
*Note: The QbCon®1 no longer exists in this form, the barrel diameter has now been reduced from 25.5 mm to 16 mm.

3.2.4 Process transfers with critical assessment of the newly developed shear stress approach

3.2.4.1 Pre-examination of the formulation and test of system sensitivity

Prior to the transfer study, the formulation containing lactose monohydrate, MCC and PVP (80-17-3% w/w) was investigated in order to assess its behaviour under liquid addition and agitation by using the Brabender MTR. A L/S ratio of 0.191 at a shoulder on the normalised torque curve (Figure 13) was found to be of interest since the plateau (constant normalised torque values with increasing liquid content) indicated that the system was less sensitive to liquid addition. As variations in liquid content can affect the granulation process and its outcome (yield fraction) [97], which in turn could disturb process analysis, it was assumed that at L/S 0.191 any change in granule characteristics during subsequent experiments would be related to changes in barrel fill or other not-liquid-content-driven changes, e.g. different energy input during the process. The results obtained from the MTR examination can be found in Table 34 in the appendix.

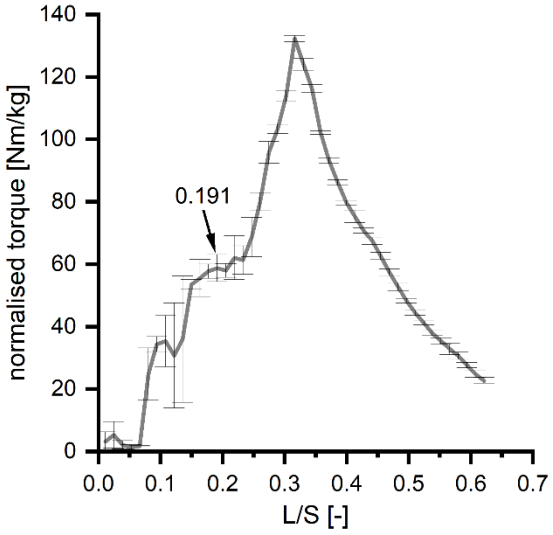

Figure 13. Normalised torque curve obtained on the Brabender MTR (n=3, mean ± s). L/S 0.191 was calculated and chosen to be the target liquid content for upcoming investigations.

A design of experiment (DoE) with L/S ratio and barrel fill density (BFD), a self-developed description of barrel fill level, as factors on 3 levels each was performed on the QbCon®1 twin-screw granulator with focus on granule sizes, GSDs, granule fractions and torque-related parameters for starters. The BFD is an extension of the specific feed load (SFL), a common surrogate for barrel fill level [93, 101] with a dimension of a mass (usually given in g). In order to keep the experimental conditions comparable on the differently dimensioned twin-screw granulators, the SFL value was additionally related to the free volumes, V_{free}, of the respective screw configurations used. Due to the units of *SFL* and V_{free} (g and cm³, respectively), it was denoted as barrel fill density (BFD) (g/cm³). The BFD is calculated as shown in Eq. (13)

$$BFD = \frac{SFL}{V_{free}} = \frac{\dot{m}_{tot}}{n \cdot V_{free}} \tag{13}$$

Enabling an adequate interpretation and comparison of the GSDs obtained at the different process settings, the spectrum of granules produced were divided into different fractions. Since the x_{90}-value of the powder blend was about 123 µm (n=1, distribution curve not depicted), sizes below 125 µm were considered as ungranulated material (fine fraction), whereas granules within 125-1250 µm (from literature [75, 84, 86, 141]) were regarded as yield fraction and agglomerates above 1250 µm as oversized granules. The yield fraction was found to be suitable for downstream processes, e.g. tableting. The percentages of the granule fractions can be found in Table 35 (see appendix).

The GSDs obtained at the different process settings within the DoE can be found in Figure 14A. All distribution curves of the lowest BFD revealed a pronounced bimodality of the GSD curves, whereas those obtained at intermediate and high BFD turned out to be monomodal. Liquid

distribution along the screw length might had been insufficient at low BFD. It can be assumed that overwetted and poorly wetted areas were created at the position of liquid addition, resulting in oversized granules and fines [78]. As screw speed settings were the highest at low BFD, the conveying rate of the screws and consequently the materials wall slippage were high, which usually enabled free movement of powder particles within the channels and resulted in pronounced axial mixing. Additionally, the materials residence times can be expected to be short which increases the challenge of sufficient liquid distribution within the mass [81, 85, 89]. Axial mixing was described as being dominant at low fill levels, which should increase the distribution of the liquid and the solid phase and lower the effects of inhomogeneities of non-optimal pre-blending, fluctuations of liquid pump or powder feeder. It should therefore have favourable consequence on the final product quality [81, 89, 135]. However, the results obtained (Figure 14A) contradicted these postulations of Kumar et al. [81, 89], but their lowest fill level investigated (900 rpm at 10 kg/h) was probably still greater than that in the present study. Usually, the kneading blocks squeeze the material while hampering material flow and cause an increase in liquid saturation. The liquid is forced to the granule surface and leads to granule growth while gaining strength at the same time [86, 142]. It can be assumed that the filling conditions in the actual study were too low and the material was consequently just transported forward with incomplete destruction of overwetted nests and insufficient compaction of the material by the kneading blocks [81, 106]. Additionally, a lack of intergranular friction and collision could be accountable for only little abrasion and the survival of bigger granules [97, 98]. Figure 14A shows that when the liquid content was changed from L/S 0.177 to L/S 0.191, the proportions of oversized granules increased, while no further effect was revealed with further increase of L/S to 0.205.

At high BFD, liquid distribution was assumed to be more homogeneous at all liquid levels due to less fine proportions and a shift of the curves (up to a frequency of about 85 %) to the right (Figure 14A). The curves were generally steeper compared to the other fill levels and mirrored narrower size distributions, which supported the assumption. However, this would contradict the results of research groups that proposed a convective flow regime with tendency to plug flow at high fill levels. In this case, the wet material would experience increased compaction along the screws due to their confined conveying capacity that additionally decreased wall slippage and consequently a reduction of axial mixing [81, 89, 135]. In contrast, Lee et al. [74] found that kneading block sections with 30 and 60° offset angles still have conveying capacity and were never completely filled. The extent of axial mixing was found to be similar, regardless of the screw setup and barrel fill investigated. It was reported that some of the wet material temporarily adhered to the barrel wall or screw surface and created a thin deposition layer. The entire layer moved only slowly towards the barrel outlet provoked by the rotating screws and flow direction of the wet mass [74]. However, based on the findings of the different research groups, it can be suggested that with increasing fill level axial mixing was lowered and convective flow behaviour became dominant, which allowed only restricted movement of individual particles relative to each other [85]. When material compaction increased at higher fill levels, while axial mixing was still possible, more

liquid was probably squeezed out of the material and distributed, with an essential increase in granule sizes, but without an amplified formation of oversized agglomerates [86, 99].

The intermediate fill density also indicated an intermediate position regarding granule formation (Figure 14A). The granule growth appeared equally weak as at the lowest BFD on the one hand but seemed high enough to lower the amount of oversized granules on the other hand. With increasing BFD the attrition of the material on the barrel wall and screws increased [85, 92, 98] but more importantly the intergranular friction and collision rate increased which resulted in more breakdown of granules and thus in a considerable increase of yield fraction at the expense of oversized agglomerates [85, 97, 98]. In comparison to the high BFD, axial mixing and thus liquid distribution seemed best at intermediate BFD as the yield fraction was much higher than at low and slightly higher than at high BFD (Table 35 in appendix). In contrast to the lowest, the intermediate and high BFDs showed no impact of increasing L/S ratios on the granule sizes. Granulation at intermediate fill conditions investigated in this study seemed promising as the balance between throughput and screw speed apparently enabled enough time for both sufficient solid-liquid mixing and sufficient granule formation [81], which is important when considering the short material residence times of a few seconds in TSG [98, 99, 105-107].

The residual moisture of the final products manufactured at the different settings was predominantly below the target value of 2 % (see Table 28), with exception for L/S of 0.205 at 1.25 kg/h and all L/S ratios at 2.5 kg/h. The drying unit of the QbCon®1 probably reached its upper capacity limit and could not ensure uniform drying of the products while passing the chamber. Settings of vibration acceleration, inlet air flow and air temperature had been chosen to enable the slowest transportation through the chamber while considering recommended bed height of 2 mm maximum and ensuring enough hot air flowing through to dry the product. However, the GSD curves of the respective process settings did not show any abnormalities regarding their shapes or locations on the graph. The GSD obtained at L/S of 0.205 and 1.25 kg/h revealed to be like those obtained at the other L/S ratios at the same PFR. No impact of higher residual moisture was observed. Similar conclusions were drawn for the highest material throughput at 2.5 kg/h PFR. The overall circumstance of higher residual moisture was considered negligible. Nevertheless, the experiments revealed the upper limit of the drying chamber that must be taken into account in future experiments on that granulator.

Furthermore, reproducibility was checked thrice at the centre point (intermediate BFD at L/S ratio 0.191) (Figure 14B). GSDs were very similar. The x-values (x_{10}, x_{50} and x_{90}) varied slightly (Table 5), which emphasized the reproducibility of results at the shoulder part.

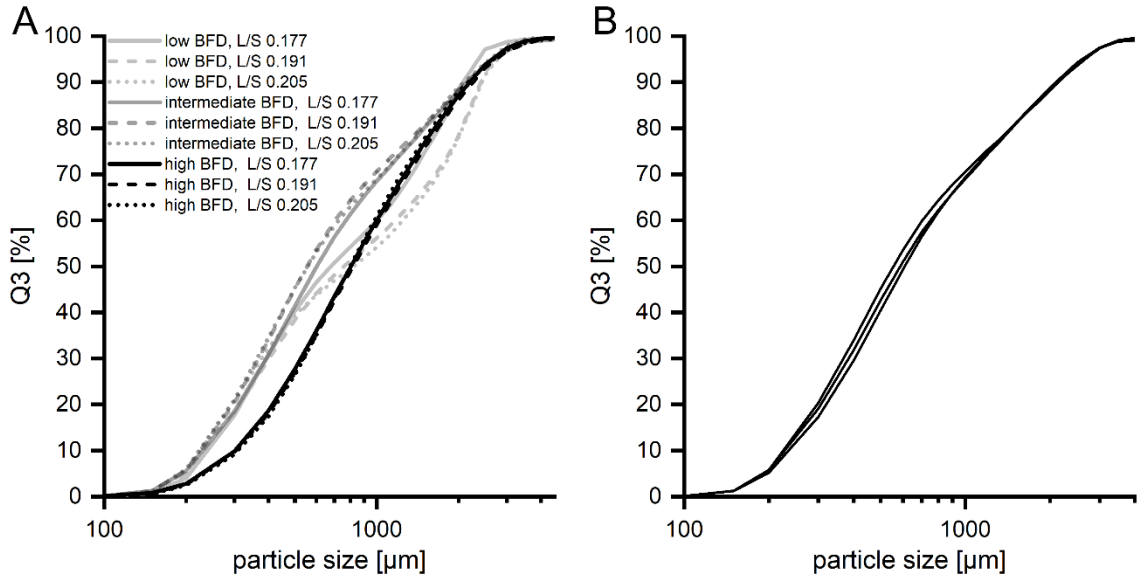

Figure 14. GSDs obtained for A) DoE experiments and B) reproducibility check at the centre points (n=3, mean).

Table 5. x-values of the investigations on repeatability at the centre point.

x-value	run I	run II	run III
x_{10} [µm]	229 ± 2	240 ± 2	232 ± 4
x_{50} [µm]	552 ± 9	606 ± 3	586 ± 30
x_{90} [µm]	2154 ± 105	2124 ± 79	2111 ± 114

Except for the obvious dislocation of the distribution curve obtained at low BFD with change of liquid content from L/S 0.177 to 0.191 (Figure 14A), no impact of liquid content on granule formation and granule properties could be found. This was additionally confirmed by the analysis using the MODDE software. The coefficient plots (Figure 15) indicate predicted changes in granule sizes (mirrored as x-values), the width of the size distribution (span), proportions of granule fractions as well as the process-related measures torque and SME considering the linear and quadratic effects of BFD and L/S ratio on the listed characteristics. The contour plots (Figure 16-Figure 18) reflect the study window in more detail and enable both an additional evaluation of the linear and quadratic effects as well as the determination of an optimal operation window. The direction of the bars for each factor in the coefficient plots, BFD and L/S ratio, indicates the predicted change for each characteristic listed above when only the factor is changed, which can be interpreted as the change of the response when the value of the factor is increased. The direction of the bar reflecting the quadratic effect (BFD*BFD in the present study) shows the predicted change in values when the process is shifted from one of the extremes of the study window (low or high BFD in the DoE study) towards the centre of the DoE. A positive direction of the bar means that the values of the characteristic become smaller and vice versa if the bar has a negative direction.

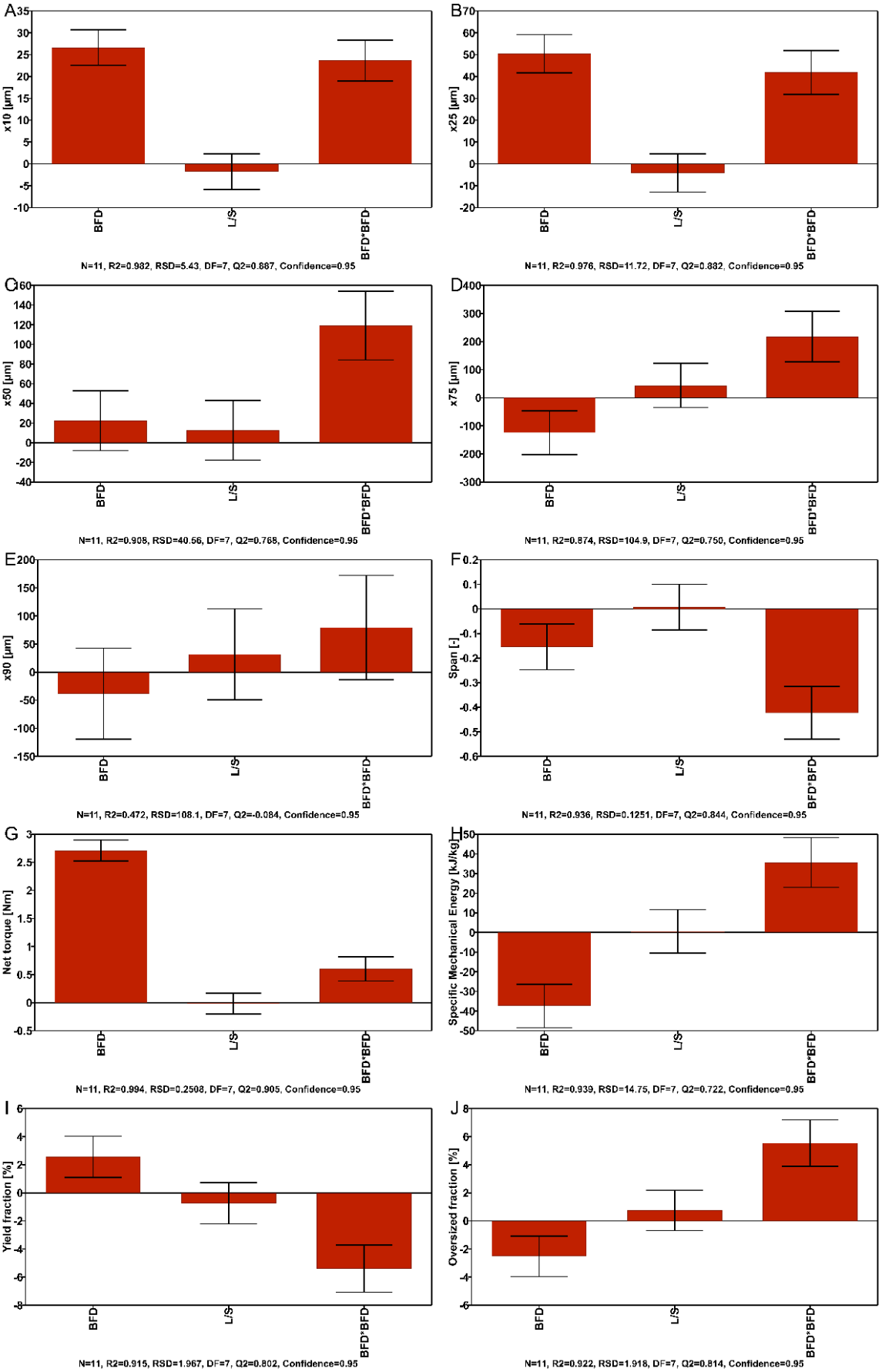

Figure 15. Coefficient plots for granule characteristics: A) x_{10}, B) x_{25}, C) x_{50}, D) x_{75}, E) x_{90}, F) span, G) net torque, H) SME, I) yield fraction (< 125-1250 µm) and J) over-sized fraction (> 1250 µm).

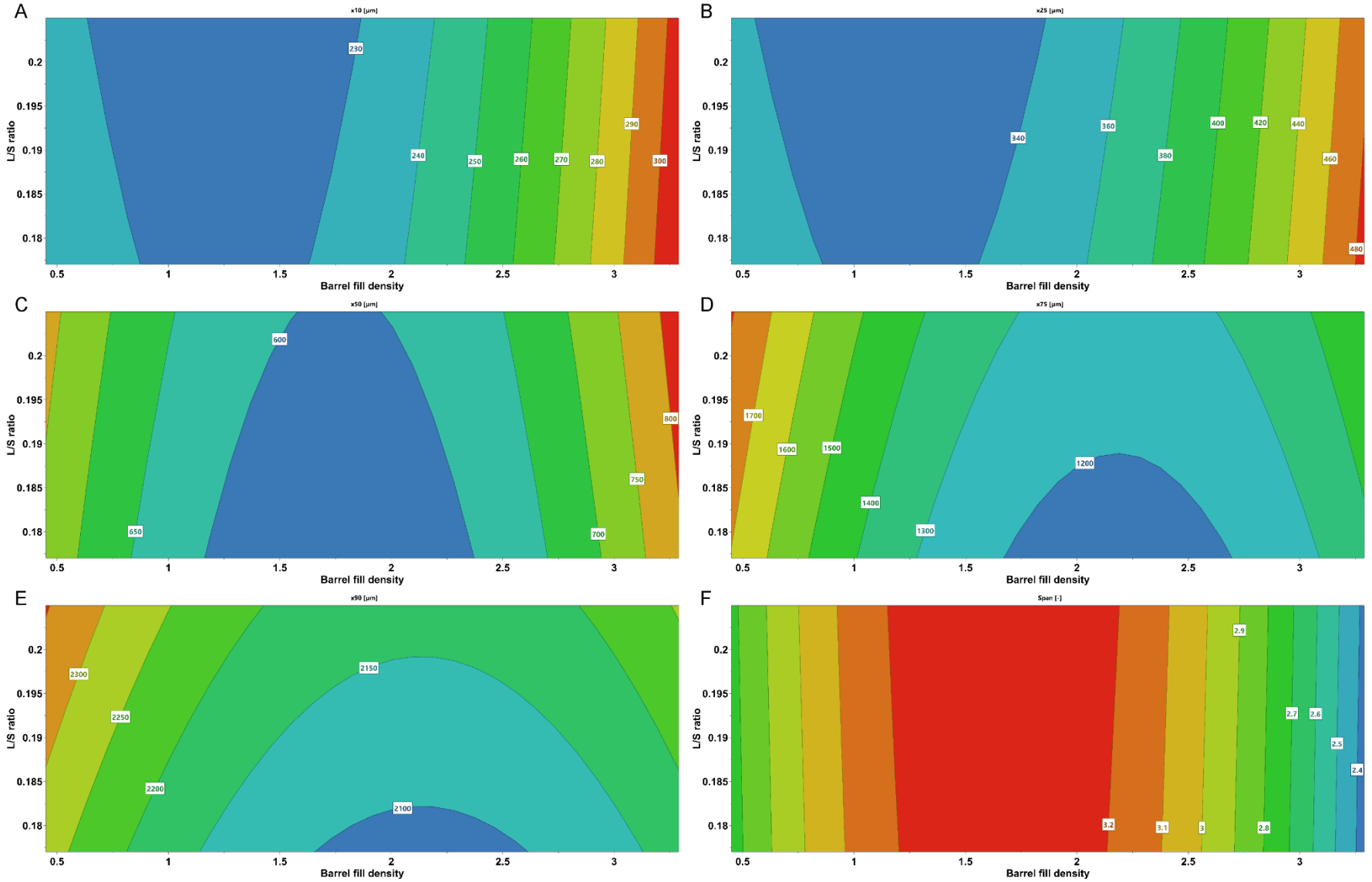

Figure 16. Contour plots for granule characteristics: A) x_{10}, B) x_{25}, C) x_{50}, D) x_{75}, E) x_{90} and F) span.

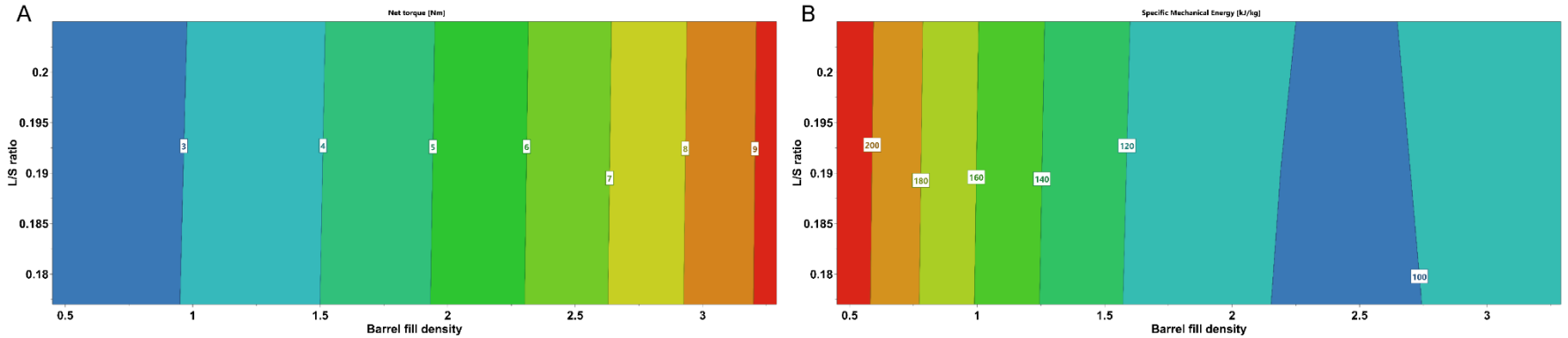

Figure 17. Contour plots for granule characteristics: A) net torque and B) SME.

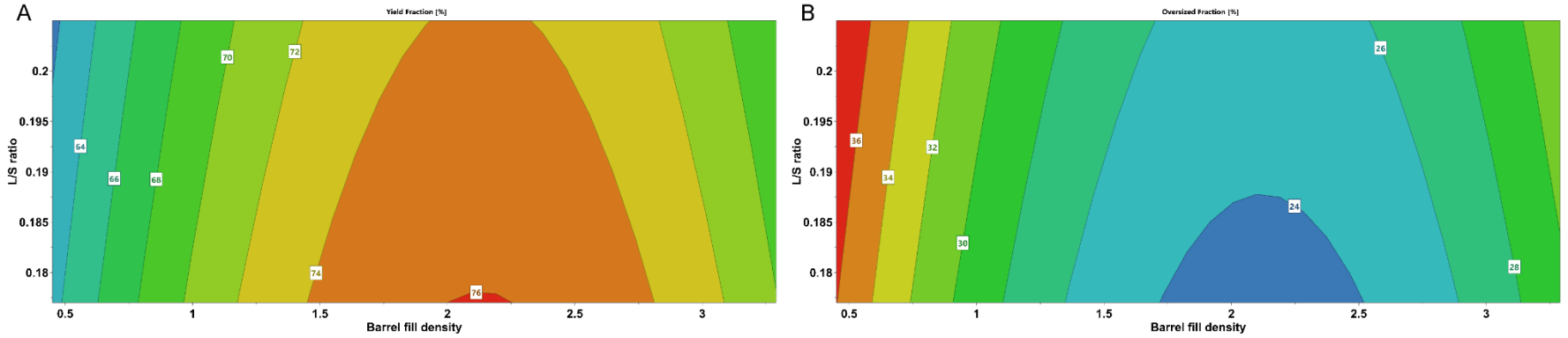

Figure 18. Contour plots for granule characteristics: A) yield fraction (< 125-1250 µm) and B) over-sized fraction (> 1250 µm).

It can be assumed from the GSD curves (Figure 14A) and from the coefficient plots (Figure 15) that the liquid content had no statistical effect on granule formation, whereas filling degree of the barrel was statistically relevant. With increasing barrel fill level, the effect on x_{10} and x_{25} (Figure 15A and B) was positive, whereas bigger granules were reduced ($x_{75,}$ Figure 15D). Since the coefficient for the quadratic effect (Figure 15A and B) was positive and significantly relevant, optimal process settings could be defined. Assuming that less fine would be suitable, higher x_{10} and x_{25} values should be aimed for. Optimal fill level could thus be the intermediate one or higher (Figure 16A and B). The impact of the BFD had even more importance for the yield and oversized fractions (Figure 15I and J) as their proportions increased and decreased, respectively, with increasing barrel fill level. However, the highest yield fraction and lowest oversized fraction were achieved at intermediate BFD (Table 35 in appendix and Figure 18). The optimal process window was also predicted for this area (Figure 18). The L/S ratio revealed no statistical impact as the amount of fines was unaffected. Although a significant effect on the fine fraction was described for the quadratic effect of the BFD and showed an optimum, the amount produced in the study window was generally too low (> 0.4 to < 0.7 %) and can therefore be considered negligible (coefficient and contour plots not shown). Due to the different median granule sizes (x_{50}) at the different BFDs (Figure 14A), no statistically relevant impact could be found for the barrel fill level (Figure 15C). Since similar x_{50} values were obtained in the study at low and high BFD (Figure 14A), implying that increasing barrel fill had no effect, and since the granule sizes obtained at the intermediate filling degree were smaller, the prediction of changes for x_{50} with increasing fill level cannot be described by the linear model. With view at the quadratic effect (BFD*BFD in Figure 15C) as well as the contour plot (Figure 16C), the assumption was confirmed that the optimum is in the centre of the examination window at intermediate BFD. Based on the results in the DoE study, the effect of the barrel fill level on x_{50} can only be described by the quadratic model. In addition, no effect could be found for the L/S ratio (Figure 15C). A similar outcome was obtained for x_{90} (Figure 15E) as the curves approximated to each other. It can be assumed that the free space of the screw elements, which is the available volume in which granules could grow, confined the extent of granule growth. After a critical granule size had been reached, the empty space of the conveying elements might be fully occupied and inhibited further growth as friction and breakage became dominant. The threshold above which further granule growth was hampered might be around 4000 µm on the QbCon®1, which was guessed from the results depicted in Figure 14A. Since the vertical height between the inner and outer diameter of the CEs used was about 3.90 mm, maximum granule sizes in this size range were to be expected. Similar assumptions could be made from the findings of Osorio et al. [66], who found the barrel diameter having a crucial impact on the formation of bigger granules. However, in contrast to x_{50}, x_{90} can neither be described by the linear nor by the quadratic effect as both showed no significance. Although an optimal process window is displayed, the changes were too small to be relevant. Nevertheless, the obtained non-significance of the barrel fill level on x_{90} should not be taken as a general statement, as the statistical analysis is only based on the results of the DoE and thus only applies to the investigated system in the defined window.

Despite the results of the x-values, it is apparent in the contour plots (Figure 16A-E), that the optimum predicted by the software shifted from the left side (for x_{10}) to a location at intermediate BFD and higher (for x_{90}). In contrast, the span decreased statistically with increasing BFD (Figure 15F). The widest distribution, which is usually less favourable, was found in the centre of the examination window and thus also included the intermediate barrel fill (Figure 16F).

The net screw torque (Figure 15G) showed a strong commutated dependency on BFD. If BFD increased, the torque increased as well [98, 106]. Even though a change in BFD was a result of adjustments in material throughput and screw speed in this study and those variables could therefore not considered solely, the effect meets similar observations described in the literature [81] as well as initial expectations. Torque, screw speed and material throughput were additionally used to calculate the SME (Eq. (42), see section 5.2.3.3), a scale-independent measure to assess the mechanical energy input of the granulator into a defined unit of material [100]. The informative character of SME was even more valuable as both screw speed and material throughput had been adjusted for BFD changes and mirrors the energy transferred into the wet mass due to kneading and shear actions from the screws [85]. As depicted in Figure 15H, the granulators energy input per amount of material being granulated significantly decreased with increasing BFD. Both the torque and the SME can be perfectly described by the linear model; the quadratic one might be less relevant (Figure 17). The L/S ratio had also no influence, neither on torque nor on the SME, because of the narrow range in L/S ratio. The overall expectation would be a lowered torque due to more lubrication if the liquid content increased [81] and exceeds a certain threshold.

As yield fraction was one of the highest and reproducibility was good, the L/S ratio of 0.191 was chosen for the upcoming process transfers. Even though the intermediate BFD was indicated as promising for TSG according to the optima in the contour plots (Figure 18), all three BFDs were still considered in the following studies.

3.2.4.2 Test transfer approaches for other differently dimensioned twin-screw granulators

3.2.4.2.1 Determining a suitable screw setup for process transfer

As the various screw configurations could make the transfer of TSG processes difficult, first a suitable screw setup had to be determined. An approach was taken where a similar percentage of the kneading blocks in the screw configuration (screw configuration A) was used on Pharma 16 (see section 5.2.3.7).

For this study part, the results obtained at the different BFDs at L/S 0.191 within the DoE on the QbCon®1 were considered as the basic ones to which the results of the experiments on Pharma 16 were compared. As the diameters of the screws of the granulators were different, the screw speed had to be adapted to achieve similar tip speeds at the different barrel fill levels. The PFRs were also kept similar on the granulators.

For the given screw setup A, the GSDs obtained on Pharma 16 differed considerably from those obtained on the QbCon®1 when tip speeds were kept similar (Figure 19A). Although the curves showed similar curve shapes at the different fill levels, bimodal at low and monomodal at intermediate and high level, the comparative GSDs showed a pronounced shift to bigger granules when they had been produced at low (curve shift below 60 % frequency) and intermediate BFD. It indicated extended densification of the wet material where the granulation liquid was probably sufficiently squeezed and became available for further adherence of fine material and small granules. As the length of screw elements and element sections strongly affects the mixing quality of a wet mass, better liquid distribution due to the longer total KB length in the screw setup on Pharma 16 than on the QbCon®1 (56 mm vs. 45 mm) was likely [109]. Therefore, a reduction of fines and smaller granules was obtained [83, 86]. In addition, the curves of the low and intermediate BFD on Pharma 16 were much steeper and indicated a narrower distribution. It could only be assumed that the fill level in front of and in the longer KB section was higher and axial mixing therefore much lower than on the QbCon®1. In consequence, a setup adjustment (configuration B) with shorter total KB length (46 mm vs. 45 mm) occurred. Similar or even better results were obtained (Figure 19B) than with configuration A, a better fit of the distribution curve of the intermediate BFD could be implied, even though a slight bimodality was observed.

In contrast to the low and intermediate fill level, smaller granules were produced at high BFD with both comparative configurations. However, the focus in this study was mainly at the tip speeds, which is why less attention was paid to the BFD values achieved in the comparative studies (2.60 and 2.62 kg/m^3 on Pharma 16 with configuration A and B, respectively, vs. 3.30 kg/m^3 QbCon®1). Since the fill densities on Pharma 16 ranged between the high and intermediate (1.88 kg/m^3) ones conducted on the QbCon®1, the impact of barrel fill was assumed to be crucially important as it was apparent that the distribution curves of the high BFDs on Pharma 16 approximated to the curve obtained at intermediate BFD on the QbCon®1. In addition, the slopes of the distribution curves were steeper than for the curve related to the intermediate fill density, indicating a different granule formation kinetics on Pharma 16. As already hypothesized in section 3.2.4.1, when the barrel diameter, and with this the available space in the barrel, is lowered, fewer big granules were produced [66].

The shear stresses calculated according to Eq. (1) resulted in higher values for the experiments on Pharma 16 than on the QbCon®1 in all cases. While a shear stress of almost 12.9, 19.6 and 44.6 N/m^2 was applied on the QbCon®1 at low, intermediate and high BFD, respectively, the wet material on Pharma 16 was calculated to be subjected to 33 % higher stresses for configuration A and B. This means that, despite similar shear rates on the two granulators due to similar tip speeds and gaps between the screws and inner barrel wall (QbCon®1: 0.22 µm, Pharma 16: 0.24 µm), higher mechanical forces were exerted on Pharma 16. Since the GSDs obtained on Pharma 16 for the low and intermediate BFD revealed a rightward shift to bigger granules (Figure 15), higher shear stresses acting on the material, leading to improved liquid distribution and thus promoting the agglomeration of fines, would not be implausible, but based on the fact that these values only

reflect a shear stress due to its unit, this might be rather coincidental. However, as only GSDs were investigated so far, other granule characteristics would also be affected, e.g. granule friability and strength, which is why further investigations are needed in order to make a final statement on the usefulness of the newly developed approach.

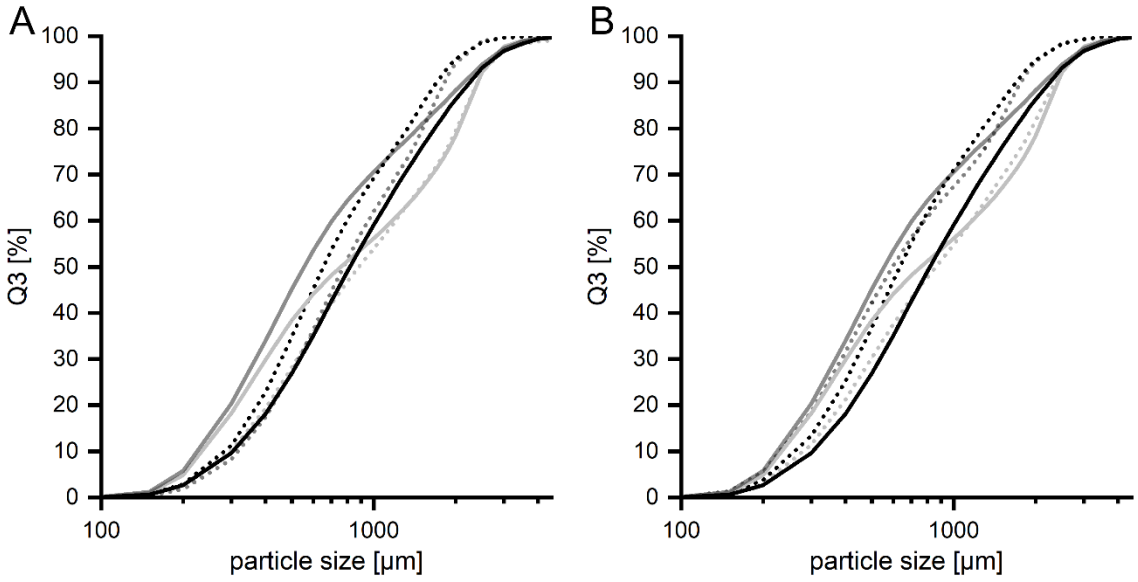

Figure 19. GSDs for low (light grey), intermediate (dark grey) and high BFD (black): A) configuration A and B) configuration B during process transfer from QbCon®1 (straight lines) onto Pharma 16 (dotted lines) by keeping tip speeds nearly constant (n=3, mean).

Based on the results of the preliminary process transfers with configuration A and B, keeping a similar total KB length on the granulators could be advantageous for process transfer as the results obtained with configuration B proved to be promising. However, whether these results really disclosed a superiority of screw setup B to configuration A has to be verified in further experiments, especially since the examinations were only carried out once.

3.2.4.2.2 Impact of barrel fill level on process transfer

In order to assess the influence of the barrel fill level on the success of a process transfer, two processes at intermediate BFDs at L/S of 0.191 were transferred from the QbCon®1 to the Pharma 16 twin-screw granulator with lower or higher tip speeds than on the QbCon®1. The screw speeds were initially deliberately set to ensure a lower or higher tip speed and the PFRs were then adjusted to approach an intermediate BFD.

The results of this study are shown in Figure 20, which depicts, for completeness, all GSDs originally obtained on the QbCon®1 as well as the two comparative experiments at intermediate BFD on Pharma 16, with the light grey dotted curve representing the process at lower tip speed and the black one representing the process at high tip speed. Although the tip speeds applied on Pharma 16 were different (0.081 and 0.140 m/s vs. 0.097 m/s at intermediate BFD on QbCon®1), the distribution curves from Pharma 16 were found to be almost identical to each other and rather

similar to the curve of the intermediate BFD on the QbCon®1, implying that the influence of the barrel fill level on process transfer was more dominant than the tip speeds and that the BFD may play a key role in process transfers. Therefore, the BFD values should be kept constant during process transfers on the different granulators to increase the probability of their success. The discrepancies of GSD curves to entirely match the GSD curve from the QbCon®1 above a frequency of almost 80 % was clearly the result of the confined space on Pharma 16 available for granule growth [66].

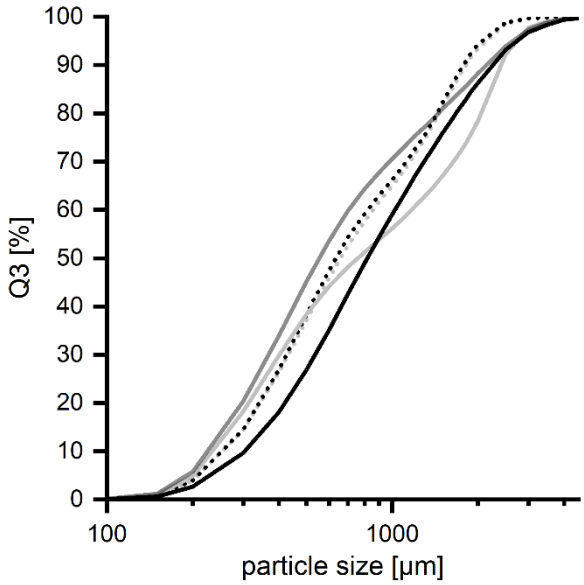

Figure 20. GSDs obtained for process transfers with intermediate BFDs to Pharma 16 (dotted curves) applying lower (light grey) or higher tip speeds (black) than on the QbCon®1 (straight lines). All GSDs obtained on the QbCon®1 at low (light grey), intermediate (dark grey) and high BFD (black) are depicted for the sake of completeness (all n=3, mean).

3.2.4.3 Transfer robustness and reproducibility

Considering the insights from the test transfers regarding the impact of tip speeds and barrel fill level on the outcome of such a process transfer, reproducibility was tested three times with screw setup A and B on Pharma 16. Additionally, the Leistritz Micro 27 GL-28D was used as a third twin-screw granulator to broaden the validity of the proposed equation for quantifying screw configurational setups for TSG processes.

Similarly to the test transfers described above, experiments conducted on the QbCon®1 were the basic ones and their results used as targets to be achieved. However, the basic results will not be discussed again in this section. Similarly to the procedure described before, the screw speed was again initially set to achieve a similar tip speed, while the PFRs were adapted in order to keep the BFD values on the granulators constant. All experiments were conducted at L/S of 0.191.

Figure 21A-C display the investigation on robustness on Pharma 16 for the low, intermediate and high BFD, respectively, while Figure 21D depicts the results obtained at the different BFDs on the Leistritz Micro 27 GL-28D.

As shown in Figure 21A, the GSD curves obtained at low BFD were similar but showed a slight trend to smaller granules in the upper 50 % volume-based fraction, which was not observed in the preliminary studies. An explanation might be the net screw torques achieved during the processes. The net screw torques (Figure 22A-C) obtained on Pharma 16 for screw setup A and B revealed to be higher than on the QbCon®1, indicating more friction between the screw elements and barrel wall. The positioning of the screw bearing could have a crucial effect. The screw bearing on Pharma 16 was localised at one side only (at the infeed area), whereas the screws on the QbCon®1 were additionally supported at the barrel exit. It can be guessed that the screws on Pharma 16 were more likely to oscillate (especially closer to the barrel exit) during the granulation process which increased the stresses acting on the granules. The idle torque could probably not consider this appearance as it was determined in an empty state. However, bigger granules were probably forced to break into smaller subunits and affected granule sizes and their distributions in general. The effect of a smaller barrel diameter on granule growth described by Osorio et al. [66] up to a certain threshold, above which no further growth can take place due to lack of space in the screw channels, could also be a reason for fewer larger granules. It was found that as the barrel diameter decreased, so did the granules, as the pitch space of screw elements through which the granules could flow was important for the survival rate of bigger granules.

Nevertheless, the curve shapes tended to be bimodal just like on the QbCon®1 which indicated the absence of sufficient material densification and liquid distribution in the KB zones due to the starved barrel conditions (Figure 21A, Table 6). The size distributions and elongated granule shapes (Figure 23) obtained supported the assumption of insufficient friction forces within the barrel that usually causes breakage of over-sized granules and rounding of elongated shapes [98, 106, 143]. This was observable among all screw configurations on both granulators.

Bimodal size distributions and elongated granule shapes are typical characteristics of granulation processes with conveying elements only [82]. At the infeed port, the liquid is dropped into the barrel and produces overwetted (granules) and unwetted (fines) material. Since conveying elements have less shear-intensive regions [56], fine material layers around the wet granules and causes further growth during transportation throughout the barrel, which amplifies the bimodality of the final size distribution [82]. El Hagrasy and Litster [82] revealed that the KB setup with 60° stagger angle (forward type) provided the worst liquid distribution among all KB setups investigated (forward and reversed types: 30 and 60°, neutral: 90°). The authors concluded that the conveying capacity was high enough to enable smooth passage while it lacked sufficient mass hold-up, liquid distribution and backmixing. However, it must be emphasized that only KB setups up to seven kneading discs maximum were investigated, which does not fully match the conditions in the present transfer study. Since numerous studies have already proven that a higher number of kneading discs increases mixing quality [74, 81, 88, 89], the usage of two KBs with more discs, as used in this study, was assumed to lower the extent of bimodality. The bimodal distribution and elongated shapes of the granules particularly implied a starved barrel condition, where the material was probably influenced by the CEs rather than by the KB.

In contrast, a broader variability of the GSD curves was received at intermediate BFD (Figure 21B). The distribution curves of configuration A and B were generally similar to those obtained on the QbCon®1, especially up to approximately 1200 µm, but again indicated fewer larger granules above 1200 µm on Pharma 16. Since the net screw torques at intermediate BFD of all experiments on both granulators were in comparable range (Figure 22E-G), more friction of the screw elements and barrel wall due to more screw mobility cannot be held responsible for this. The change in barrel diameter might be the relevant factor in this case [66]. In addition, as both inter-particle friction and attrition of the wet material on the screws and barrel wall increased, the granules were rounded off and appeared to be rather spherical (Figure 23) [98, 106, 143].

It was obvious at high BFD (Figure 21C) that all size distribution curves obtained on Pharma 16 shifted considerably to smaller granules, independently of screw configurational setup which might be forced by the smaller barrel diameter on Pharma 16. Higher friction forces between the granules themselves and with the barrel wall surface could be a consequence of the decreased pitch space that led to higher attrition and breakage. Granule shapes were mainly spherical rather than elongated (Figure 23), as the particles rubbed off each other. Similar observations of granule shapes at high material throughputs have already been described several times in literature [77, 92, 143]. Although the GSD curves of the experiments on Pharma 16 were similar in position and shape, the decreased net screw torques obtained with configuration B (Figure 22K) indicated less load on the screws [81]. Since a similar trend was also received at intermediate fill levels, the shorter total kneading block length of screw setup B was assumed to be responsible as the wet material may have experienced less flow restriction and thus passed the kneading zones much faster [81, 89]. However, in addition to the findings of Osorio et al. [66] it was noticeable that the change of barrel diameter (large to small) caused a considerable increase of granules yield fraction (Table 6) in consequence of the decrease of over-sized granules. This change in the yield fraction was not clearly obvious for the intermediate and low barrel filling degrees, indicating that the high fill level is particularly sensitive to such transfer approaches. Although a trend in yield fractions was noted from the QbCon®1 to the screw setups A and B on Pharma 16, except at high BFD, differences can be regarded as negligible. Nevertheless, screw speed and material throughput generally have crucial impact on granule fractions [81]. Study results obtained on a similar granulator revealed a slight positive influence on fine and yield fraction with increasing screw speed, whereas the amount of over-sized granules was reduced. The material throughput showed an opposite effect [81]. As screw speed and total material throughput had been adjusted simultaneously for BFD settings in the present study, it is difficult to assign a single variable to the differences achieved. In addition, differences in space availability for granule growth in the granulators do not ease the interpretation of the results.

Except at high BFD, process transfers onto the Leistritz Micro 27 GL-28D were successful. GSDs were similar in curve positions and shape at the respective fill densities (Figure 21D). Although bigger barrel diameters can be expected to allow granule growth up to sizes even greater than on the QbCon®1 [66], the differences in barrel diameter (25.5 mm on the QbCon®1 vs 27 mm on the

Leistritz Micro 27 GL-28D) were likely too small to produce measurable differences in greater granules as the x_{90} was always in comparable ranges, which was strongly different to the results obtained on Pharma 16 (Figure 21A-C). As it can be seen in Figure 21D, the process transfer at high BFD revealed a left-shifted distribution curve of slightly bimodal appearance on the Leistritz Micro 27 GL-28D. It was assumed that the total length of the kneading blocks of 60 mm (45 mm on the QbCon®1) with probably better liquid distribution-capability caused a left-shift, while the fluctuations of liquid infeed induced by the piston diaphragm pump caused the bimodality. A similar effect was reported for granulation processes using peristaltic pumps [91]. Unfortunately, such fluctuations cannot easily be compensated by axial mixing processes during the granulation process as the residence times in the barrel are too short [81]. However, the longer kneading blocks probably led to better homogenisation of the over-wetted mass with the under-wetted sections, which presumably levelled the extent of the bimodality and resulted in the production of smaller granules. The over-sized fraction was much smaller and yield fraction higher at high BFD compared to the QbCon®1 (Table 6), whereas the respective fractions at low and intermediate BFD were rather comparable.

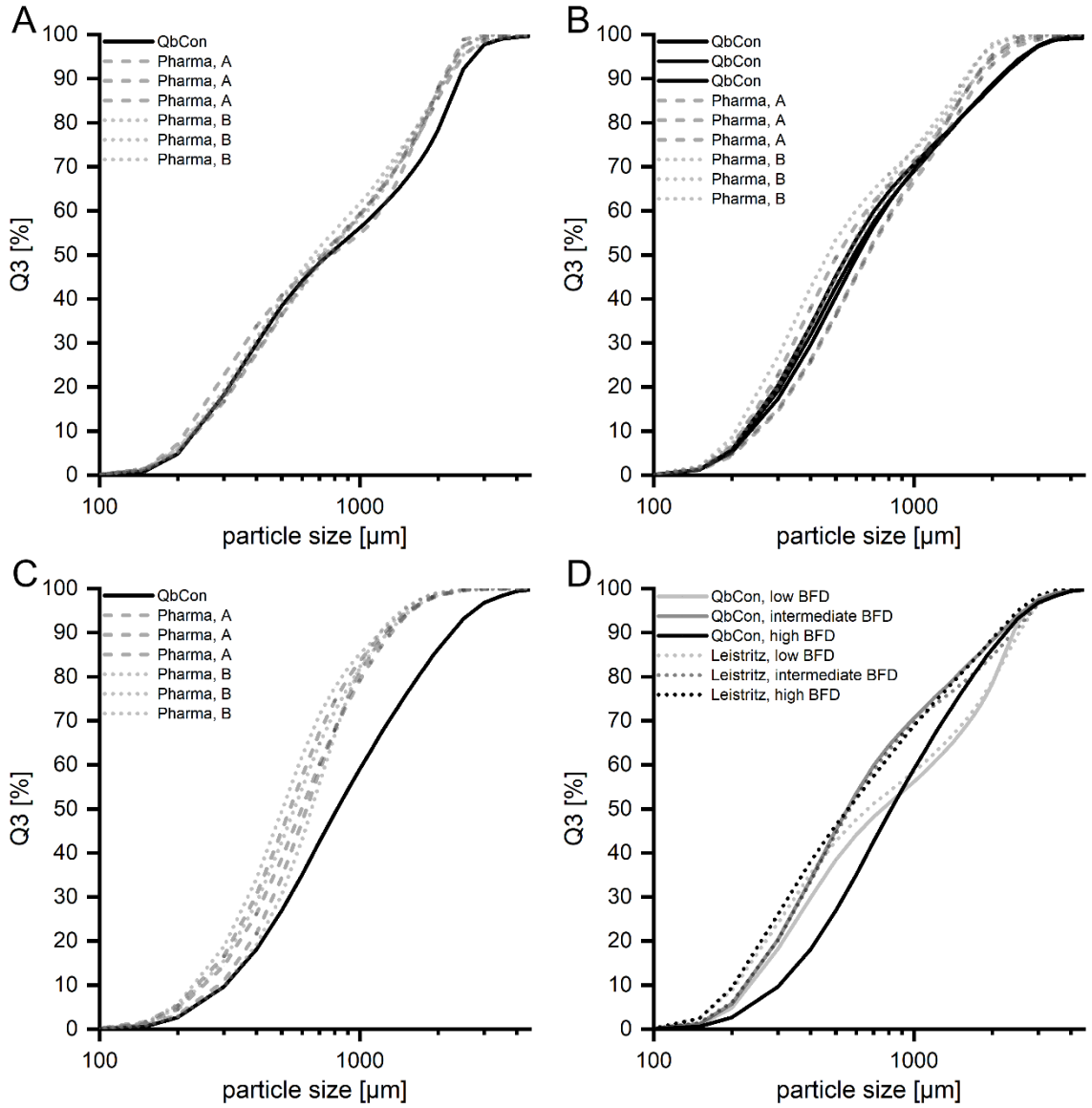

Figure 21. Volume-based GSD of the basic experiments on the QbCon®1, the respective comparative experiments on the Pharma 16 with configuration A and B at the different barrel fill levels at: A) low, B) intermediate and C) high BFD as well as D) on the Leistritz Micro 27 GL-28D at the different fill levels (n=3, mean).

Table 6. Percentage proportion of defined volume fractions calculated from Q3 curves (n=3, mean ± s; *n=1).

Barrel fill level	Screw setup	Fine fraction [%]	Yield fraction [%]	Over-sized fraction [%]
low	QbCon	*0.5	*61.3	*38.2
	Pharma, A	0.8 ± 0.1	63.8 ± 2.6	35.4 ± 2.6
	Pharma, B	0.7 ± 0.1	66.6 ± 1.7	32.7 ± 1.8
	Leistritz	*1.3	*62.4	*36.3
intermediate	QbCon	0.7 ± 0.0	75.2 ± 0.4	24.1 ± 0.4
	Pharma, A	0.8 ± 0.2	76.1 ± 1.4	23.1 ± 1.6
	Pharma, B	1.0 ± 0.1	78.9 ± 1.5	20.0 ± 1.5
	Leistritz	*0.8	*73.6	*25.6
high	QbCon	*0.4	*68.2	*31.4
	Pharma, A	0.7 ± 0.2	88.5 ± 0.9	10.8 ± 1.0
	Pharma, B	0.7 ± 0.2	89.9 ± 1.3	9.4 ± 1.2
	Leistritz	*1.3	*74.2	*24.5

It is obvious from Figure 22, that the net screw torques were the highest among all BFDs on the Leistritz Micro 27 GL-28D. As the screw bearing was at one side only, this could, combined with the much longer barrel, be the reason. At low BFD, net screw torque was higher than on the QbCon®1, but like those obtained on Pharma 16. However, the overall difference to the QbCon®1 was less pronounced but increased with increasing BFD, emphasizing that the load was much higher on the Leistritz Micro 27 GL-28D. This might have been additionally amplified by the considerably bigger areas of contact, $A_{contact}$, compared to the other two granulators (see Table 3 in section 3.2.2.3).

Although the net screw torques revealed an obvious trend, the SMEs (Figure 43, see appendix) displayed that the mechanical energy input into the wet mass on the Leistritz Micro 27 GL-28D was the lowest among all BFDs, which was due to the low screw speeds and higher material throughputs at the different BFDs compared to the respective BFDs on the other granulators. The difference in SMEs was only small to the QbCon®1, while it was rather considerable to Pharma 16 which always displayed the highest SMEs due to the much higher screw speed settings.

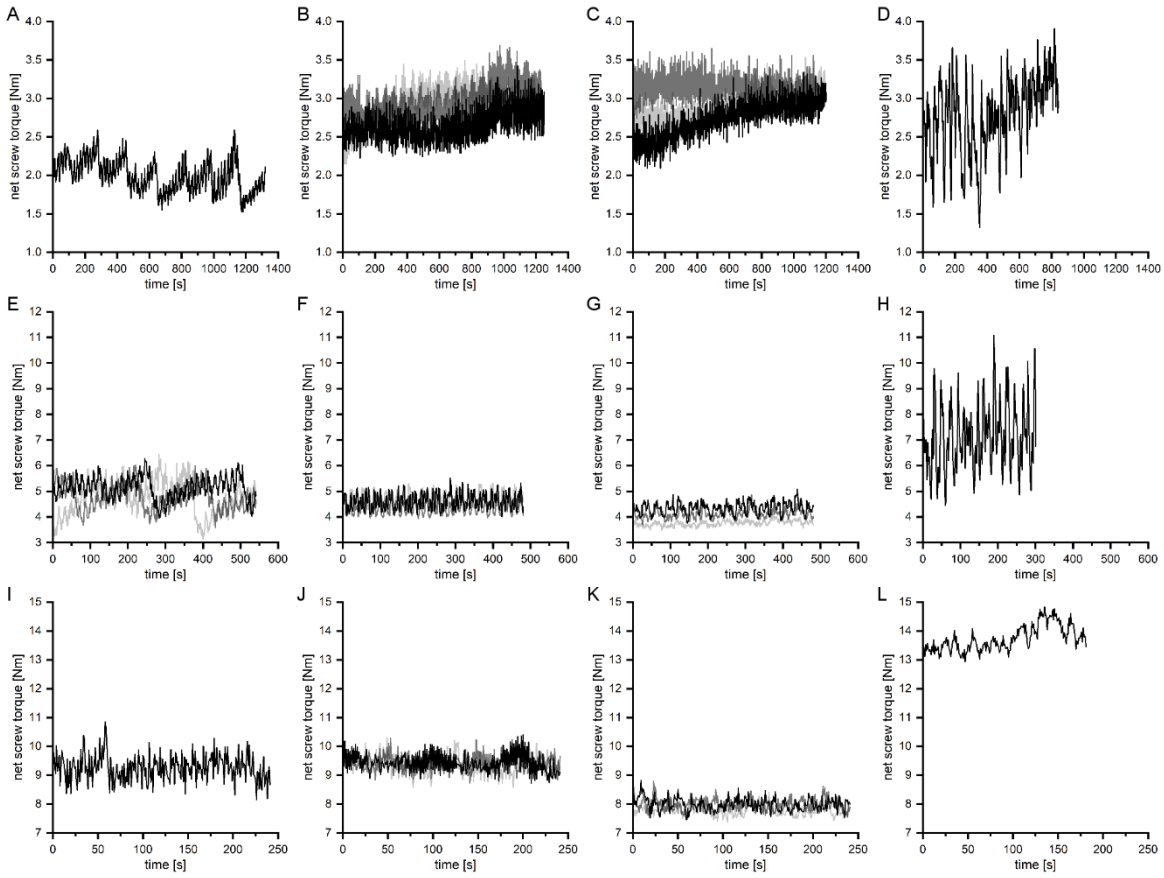

Figure 22. Net screw torques for each run during sampling period on the different twin-screw granulators using screw configuration: A, E, I) on the QbCon®1, B, F, J) A on Pharma 16 , C, G, K) B on Pharma 16 and D, H, L) on the Leistritz Micro 27 GL-28D at the different fill levels: A-D) low, E-H) intermediate and I-L) high BFD (n=1).

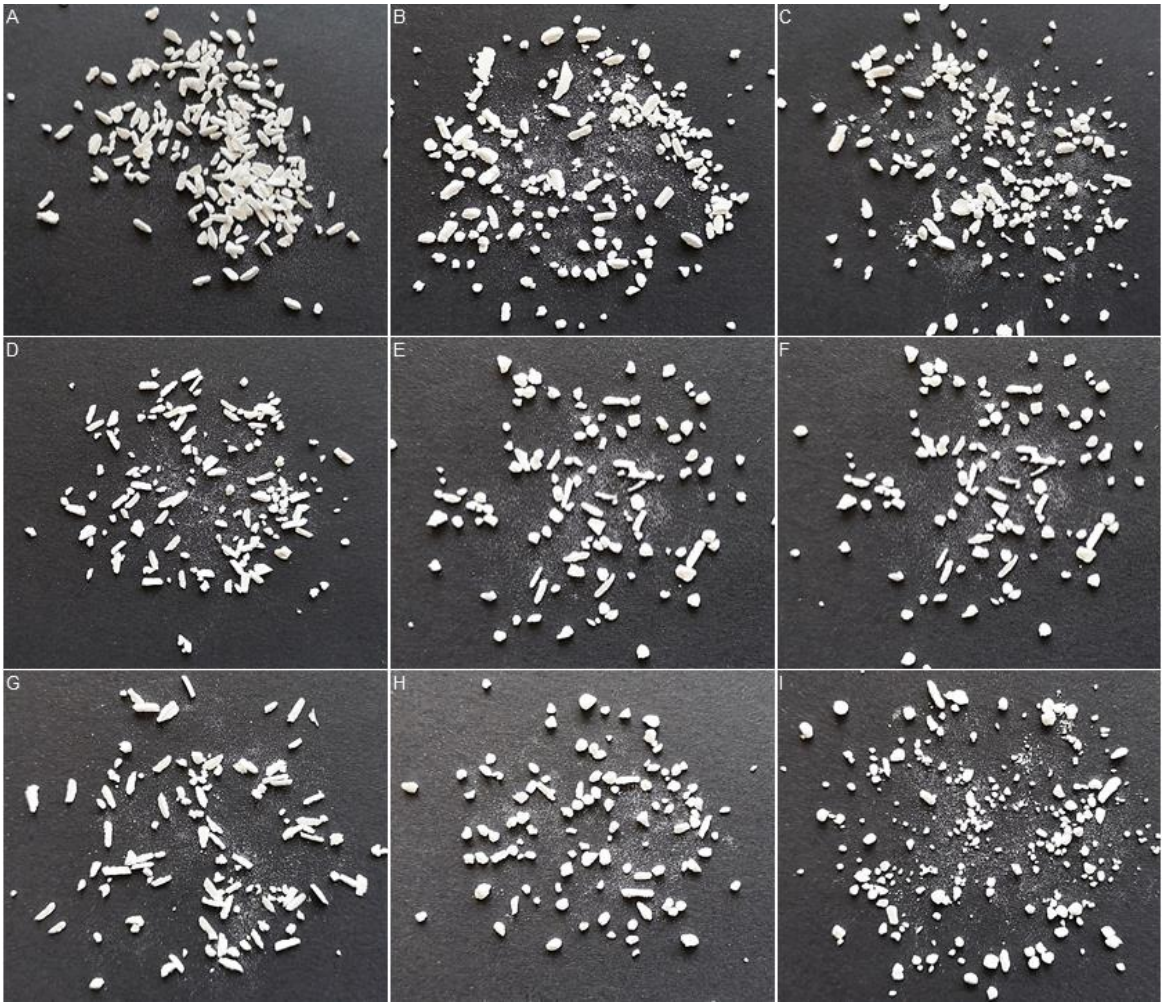

Figure 23. Granule shapes and their changes with increasing barrel fill levels (left to right in each row) applying the different screw configurations: A-C) on the QbCon®1, D-F) setup A on Pharma 16 and G-I) setup B on Pharma 16. Granules depicted were from test 2 for the intermediate BFD (B) on the QbCon®1 and from test1 of the respective BFD for screw setups A (D-F) and B (G-I) on Pharma 16. Note: Figure is of qualitative nature only.

Although characteristic indicators like x_{10}, x_{50}, x_{90} or span are widely used to compare various monomodal size distributions, these are rather less useful for bi- or multimodal distributions as for example x_{50} might be located in the valley between two peaks of a bimodal size distribution. Thus, the application of the Earth Mover's Distance (EMD) was found to be helpful to assess the similarity or dissimilarity of various GSD curves [144], allowing for a more thorough comparison of the numerous GSDs determined in the present study. The EMD is a statistical metric that enables the determination of the discrepancy between size distributions by analysing the entire distribution profile instead of characteristic points. During the analysis of two distributions, the distribution profile of a test sample is compared to a reference and the least amount of work that would be needed to transfer one distribution into the other is calculated. In the literature, this approach is illustrated by comparing two piles of earth, representing the distributions, and determining the minimum amount of work that would have to be expended to move one pile to the other. The work in this case is related to the transport of one unit of earth by one unit of distance (reflects the discrepancy) between the locations of the piles [144]. Thus, the lower the

amount of work necessary, the more similar the distributions are and the smaller the calculated EMD.

Since defining the reference and test sample is crucial and should be kept constant throughout all analyses, GSDs obtained on Pharma 16 and the Leistritz Micro 27 GL-28D were considered as the tests while those obtained on the QbCon®1 were considered as the references. In addition, those experiments that were performed only once at specific process parameters were considered as *n=1*-attempt, although the GSDs depicted in Figure 21 are designated as *n=3* and reflect mean curves from the measurement of three representatively divided sub-samples of the total one. For the calculation of the EMDs only the experiments on Pharma 16 with configurations A and B at each BFD as well as on the QbCon®1 at intermediate BFD were performed three times and can thus considered as *n=3*-approaches.

The EMDs for the GSDs determined in the robustness and reproducibility study are given in Table **7**. With the Python script used (see section 5.2.4.4) several distances were calculated between the individual reference curves and the mean reference curve as well as each test curve and the mean reference curve.

The assumption previously described in the test transfer section 3.2.4.2.1 that screw configuration B (similar total length of kneading zones) could lead to more favourable results in granulation than setup A (similar percentage of kneading zones within the entire setup) was confirmed by the mean averages of the EMD approach. The EMDs of the test curves to mean reference of configuration B revealed to be lower for the GSDs obtained at low and intermediate barrel fill than for screw setup A, implying that those are more similar to their counterparts from the QbCon®1. However, since no defined distances exist so far below which GSDs can be classified as similar, the interpretation of the values in Table 7 only allows their ordering and interpretation as more similar or less similar. As apparent from Figure 21, the curves obtained at high fill level exhibited a decisive leftward shift, their pronounced dissimilarities to the QbCon®1 were also shown by EMDs of approximately 200-220. Considering the EMD from the individual reference curves to the mean reference curve for the intermediate fill level on the QbCon®1 (16 ± 5, coefficient of variance 33.56 %), it was clear on the one hand that the repeated experiments at this fill level yielded similar GSDs, as the EMD was very low, but on the other hand it also showed that all GSDs obtained on the Pharma 16 systematically deviated from those achieved on the QbCon®1 (see Table 7). Nevertheless, the coefficients of variation (CV) for screw setup A and B revealed mostly similarly wide scattering of the results which make the EMDs appear less different. Since the experiments on the Leistritz Micro 27 GL-28D were performed only once, the assessment of the respective EMD is more difficult. According to this, the EMD of the intermediate barrel fill is in the range of those of Pharma 16 when taking the standard deviation into account. In contrast, the distance of the low fill level deviates upwards and is outside the range, which indicates that the intermediate fill level seems to be more suitable to lead to similar results on different granulators during process transfers. The EMD at high fill level also shows a dissimilarity of the GSD to that from the QbCon®1.

The EMD between each reference curve to the mean one is less informative as comparative information for the low and high fill level is missing. However, the CV allows for an assessment of the scatter of the test results. A much larger scatter of the tests would imply that the granulation process is less reproducible and successful. At least for the intermediate fill level it can be said that the obtained test results (if a similar CV was also assumed for the Leistritz Micro 27 GL-28D) might be similarly reproducible as on the QbCon®1.

Table 7. EMD values for test transfer batches (n=3, mean ± s; *n=1, values in parentheses are the coefficients of variation in %). Reference curves from the QbCon®1.

Barrel fill level	Test samples	Test curves to mean reference [-]
low	Pharma, A Pharma, B Leistritz	60 ± 15 (25.16) 52 ± 6 (11.15) *78 (-)
intermediate	Pharma, A Pharma, B Leistritz	76 ± 21 (27.95) 47 ± 15 (32.22) *42.37 (-)
high	Pharma, A Pharma, B Leistritz	205 ± 31 (15.29) 225 ± 42 (18.52) *203 (-)

Similarly to the findings in section 3.2.4.2.1, the shear stresses resulted again in higher values for the experiments on Pharma 16 but also on the Leistritz Micro 27 GL-28D in comparison to the QbCon®1 (see values in Table 29). While on Pharma 16 almost 33 % higher stresses were (mathematically) applied for both configurations, on the Leistritz Micro 27 GL-28D almost 63 % higher stresses were supposedly applied to the wet mass.

Despite the higher values, it must be a coincidence that a change of the twin-screw granulator also caused a considerable change in the envelope densities (Table 8). The material generally appeared to be denser at all barrel fill levels on Pharma 16. Initially, the higher density was assumed to be a consequence of the smaller pitches of the conveying elements and their confined spaces, but surprisingly, the Leistritz Micro 27 GL-28D also produced denser granules compared to the QbCon®1, although more space was available. The contact area of the kneading elements in the screw setup, where shearing mainly occurred, could be a driving force in this case since it was much higher on the Leistritz Micro 27 GL-28D than on the QbCon®1 (5.1 cm^2 vs. 3.6 cm^2). The drying method, continuous vs. tray drying in a drying oven, could also have an influence. While the granules on the QbCon®1 were dried almost immediately after production, the material remained wet for longer times when tray drying was performed and could thus impact the granule densities. However, since both tip speed and BFD were kept the same among the examinations and the BFD was identified as the more decisive parameter in previous studies, the results suggest that they might be due to the insensitivity of the determination method using the envelope density analyser rather than to real differences in granule densities. Besides that, since the GSDs were in a similar range to the QbCon®1, apart from the high barrel fill (see GSD curves in Figure 21 and

EMDs in Table 7), a linkage between the higher shear stresses calculated for Pharma 16 and the Leistritz Micro 27 GL-28D and the higher envelope densities should be questioned even more until further experiments should show otherwise. The examination of other granule properties is still essential for drawing a conclusion.

Table 8. Envelope densities and porosities of the respective granules at the different barrel fill levels received with the different screw configurations (n=3, mean ± s; *n=1).

Barrel fill level	Screw setup	Envelope density [g/cm³]
low	QbCon	*0.615
	Pharma, A	0.733 ± 0.002
	Pharma, B	0.711 ± 0.003
	Leistritz	*0.718
intermediate	QbCon	0.595 ± 0.019
	Pharma, A	0.693 ± 0.005
	Pharma, B	0.692 ± 0.001
	Leistritz	*0.661
high	QbCon	*0.601
	Pharma, A	0.716 ± 0.003
	Pharma, B	0.712 ± 0.004
	Leistritz	*0.716

Barrel residence times of materials were found to be important as the granulation liquid must be distributed homogeneously within a short period of time to produce granules with suitable size distributions for subsequent process steps, e.g. tableting [81]. However, residence times might be even more important for process transfers if similar granule properties are striven for. Although the mean residence time, t_{mean}, is usually of interest in investigations [81, 89, 93], it may be insufficient in process transfers, especially since material throughput, screw speed and screw design were set differently on the granulators. Therefore, the entire spectrum of RTD measurements was used for process analysis. The results are depicted in Table 9. Additionally, some exemplary RTD curves measured on the different granulators at the various barrel fill levels can be found in Figure 24. The times of first tracer detection, t_1, were generally the shortest on the QbCon®1, while no decisive difference was determined for the screw configurations A and B on Pharma 16 proving that small deviations in screw design do not necessarily have a measurable effect. Independently of the screw setup, highest concentrations of tracer, t_{peak}, were achieved on the QbCon®1 and Pharma 16 at similar time points at low and intermediate fill levels, but considerably shorter on the QbCon®1 at high fill level. On Pharma 16, slightly shorter t_{peak} was measured for configuration B than A. In contrast, larger differences were observed for t_{mean} and times at which tracer could no longer be detected, t_{out}. The shortest t_{mean} and t_{out} among all BFDs were detected on the QbCon®1, followed by screw setup B and A on Pharma 16. Although the screw setup on Pharma 16 was only slightly different, it revealed to have a particular effect on those characteristics, suggesting that more kneading elements present in screw setup A slowed down the materials passage and thus prolonged its wash-out phase and broadened the RTD. Nevertheless, residence times were always the longest on the Leistritz Micro 27 GL-28D.

As it can be seen in Figure 24, high fluctuations were recorded during the measurement on the QbCon®1 at low BFD. As a consequence of the insufficiently filled screw channels with wet mass at low fill level, the metal surfaces of the screw elements caused reflections which disturbed the measurement. However, the magnitude of fluctuations lowered with increasing BFDs. In contrast, less disturbances were noticed on the other granulators used within this transfer study.

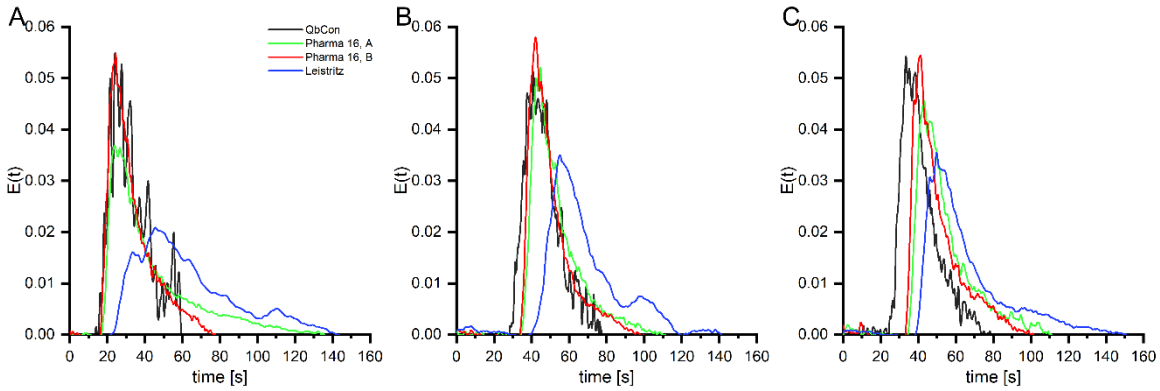

Figure 24. Exemplary RTD profiles of one examination each on the different granulators used during the transfer study at: A) low, B) intermediate and C) high BFD (n=1).

Table 9. Residence times for the different screw configurations on the varying granulators within the transfer study (n=5, mean ± s).

Barrel fill level	Screw setup	t_1 [s]	t_{peak} [s]	t_{mean} [s]	t_{out} [s]
low	QbCon	12.9 ± 1.8	26.1 ± 4.3	29.8 ± 2.6	49.9 ± 7.3
	Pharma, A	16.2 ± 0.3	25.0 ± 1.0	43.6 ± 1.0	129.2 ± 4.3
	Pharma, B	16.0 ± 0.4	24.4 ± 0.8	33.2 ± 1.2	77.2 ± 5.4
	Leistritz	22.2 ± 0.5	47.2 ± 3.3	67.6 ± 3.8	151.2 ± 5.4
intermediate	QbCon	28.7 ± 2.4	42.0 ± 2.8	46.3 ± 1.6	73.3 ± 8.5
	Pharma, A	34.8 ± 0.4	44.6 ± 1.9	52.5 ± 1.3	95.0 ± 8.1
	Pharma, B	34.0 ± 0.4	41.8 ± 0.9	49.4 ± 1.2	89.4 ± 5.3
	Leistritz	35.2 ± 3.1	59.0 ± 4.7	69.3 ± 1.0	140.0 ± 1.4
high	QbCon	24.7 ± 1.4	34.1 ± 2.0	43.8 ± 2.9	87.4 ± 8.2
	Pharma, A	34.3 ± 0.6	44.0 ± 1.8	53.9 ± 0.7	108.3 ± 2.9
	Pharma, B	33.2 ± 0.3	40.2 ± 0.9	50.3 ± 0.2	97.0 ± 3.2
	Leistritz	38.5 ± 0.5	53.3 ± 3.6	68.6 ± 3.6	151.0 ± 8.2

Overall it can be said, that the material generally resided longer with increasing barrel length (from shortest to longest: QbCon®1 < Pharma 16 < Leistritz Micro 27 GL-28D). Narrowest RTD was obtained on the QbCon®1, whereas much broader distributions were obtained on Pharma 16 and broadest on the Leistritz Micro 27 GL-28D (Figure 24). Configuration B on Pharma 16 was in turn narrower than setup A and rather comparable to the processes on the QbCon®1. The impact of screw design together with the respective process conditions is generally essential for TSG, as the materials flow behaviour within the barrel is influenced [81]. This emphasizes the importance of RTD measurements for process transfers. Although residence times and their distributions did not match those determined on the QbCon®1, their general impact on granule formation might be less crucial in this transfer study, as shown by the similar GSDs at the low and intermediate

BFDs (Figure 21). The reasons for the differences in the positions of the GSD curves at high BFD have been discussed previously. An influence of the different residence times is not assumed.

Based on the study results so far (test transfer in section 3.2.4.2 as well as transfer reproducibility), process transfer at high filling degree was less recommendable, as granule formation seemed highly sensitive to changes in process and barrel diameter resulting in clearly different size distributions. However, those processes performed at intermediate or even low filling degrees delivered encouraging results as these fitted fairly those of the QbCon® 1; almost no differences in granule sizes, GSDs, net screw torque and granule shapes were observed for the comparative experiment, even though higher applications of shear stresses were, at least mathematically, applied. The results obtained on Pharma 16 also indicated that differing screw setups might still lead to similar results, although different EMD, mean residence times and RTDs could be determined. Except for different envelope densities and due to the fact that there are no thresholds yet for the EMD approach when the GSDs are similar or not, almost all other investigated granule characteristics were in comparable ranges. Although the BFD might not be able to estimate real filling conditions inside the barrels, the ratio could be an appropriate surrogate and a general improvement to the dimensional specific feed load [93, 101], which did not encourage successful process transfer [145].

The widths of the GSDs obtained were inappropriate for subsequent operations, e.g. tableting, [82] and the study focused on the entire spectrum, which was rather of academic interest with little reference to industry. In further experiments, the application of a milling step should be considered to level any differences in granule sizes and GSDs and to meet the procedure of the industry.

3.2.4.4 In-depth investigation of the impact of process transfer on granule and tablet characteristics and its implication for pharmaceutical industry

As GSDs were only a single characteristic of granules, further ones were analysed. Original (non-milled) and milled granules (high speed cone mill with 1 mm rasp sieve insert) were investigated according to their granule sizes, GSDs, flowability (Hausner factor, *HF*, and flow function coefficient, ff_c), envelope density and granule porosity as well as granule strength. Since the properties were not all determined for the original and milled granules, the respective results are assigned accordingly hereafter. Examination of tablets occurred with regard to tensile strength, friability, disintegration behaviour and mass uniformity.

Due to the change of the formulation (addition of paracetamol and using PVP K25 instead of K30), an initial investigation on the Brabender MTR was conducted to assess its behaviour under liquid addition and agitation. The L/S ratio of 0.195 was determined for the in-depth examination (see Table 34 and Figure 44 in the appendix).

The aim of this part of the study was to further evaluate the transfer performance and to determine whether the differences in granule properties that were observed between the transfer

batches would also lead to differences in tablet properties. To better assess the impact of the shear stress on granule and tablet characteristics and thus the usability of Eq. (1), negative examples have been conducted where the tip speed was intentionally either lower or higher than the usual transfer batches. Consequently, a change in shear stress should influence the properties of the granules and thus also affect tablet properties. Therefore, the following evaluation focuses more on the shear stress in order to be able to make a final statement about the newly developed approach. Furthermore, the QbCon®25, which had the same dimensions as the QbCon®1, was used for this part of the thesis. The same screw setups were used as in the other transfer sub-sections. However, on Pharma 16, only screw configuration B was used to be comparable regarding the total length of the kneading zones. The procedure for setting the tip speeds as well as BFDs is the same as described previously.

The GSDs for the processes with initial PFR of 4 kg/h on the QbCon®25 as well as the comparison experiments on Pharma 16 are depicted in Figure 25. Although the shear stresses were different on the granulators and again much higher on Pharma 16 (see Table 30, QbCon®25: 165.5 N/m^2, Pharma 16: +10 %, +33 % and +59 % at lower, similar or higher tip speed, respectively), granule sizes and their distributions were found similar for the transfer batches (Figure 25A) and all curves revealed slight bimodality. Above a frequency of 50 %, the GSD curve of Pharma 16 obtained at a similar tip speed deviated upwards and revealed smaller granules coinciding with the findings of Osorio et al. [66] as well as own observations in previous studies. The GSDs of the negative experiments conducted at lower and higher tip speeds were also affected by the smaller barrel diameter on Pharma 16. Besides that, the GSD curve obtained at higher tip speed showed higher fine fraction compared to the others. It is plausible that a higher stress was acting on the wet material due to the higher tip speed, which would lead to more attrition and thus more fines. Nevertheless, if the stress was really 59 % higher than on the QbCon®25, it is still questionable but should have had clear effects on other granule properties. However, despite this, the EMDs for the original granules (Table 10) are in the same range as obtained in the previous study, which is why these GSD curves can be regarded as similar. In contrast, the GSD for the process with initially 6 kg/h PFR on the QbCon®25 produced slightly more fines than the experiment on Pharma 16 at similar tip speed (Figure 45 in appendix), which was even more surprising as the calculated shear stress on Pharma 16 was again 33 % higher, suggesting again that the calculation may not reflect reality. Since the EMD for the original granules is 118, the GSD curves are less similar than those batches described above.

As expected, the curves generally shifted to smaller sizes after milling due to the breakage of oversized granules and the creation of more fine material [146]. Both location and shape of the respective GSD curves matched each other well (Figure 25B and Figure 45 in appendix). The EMDs approached zero and therefore indicated increased similarity (Table 10).

A compilation of properties of the original and milled granules can be found in Table 11. Porosity of the original granules manufactured on the QbCon®25 at 4 kg/h was about 58 % while a lower porosity of 51-52 % was observed for all batches produced on Pharma 16, independently of the

applied tip speeds, material throughputs and thus shear stresses. The same trend was also observed for the friabilities. Although different shear stresses had been applied during the granulation process (see Table 30), about 7-9 % of the granules manufactured on Pharma 16 had been abraded after exposure to the air jet, which implied no impact of the shear stress on granule friability. The granules obtained on the QbCon®25 seemed more fragile, as almost 19 % of the granules were abraded. Although the shear stress was lower on the QbCon®25 (165.5 N/m^2), its influence on granule fragility can be considered negligible, as the range of shear stress application on Pharma 16 was, at least mathematically, much broader and still resulted in similar friabilities. Higher resistance to external forces of the Pharma 16-batches was additionally confirmed by their respective granule strength. An averaged force of 0.195 N had to be applied to destroy a granule produced on the QbCon®25, while much higher forces (0.293-0.307 N) were necessary to break the granules obtained on Pharma 16. Scattering of the data was relatively high due to the usage of the total spectrum of the milled granules. Although standard deviations were high, the results still confirmed the differences. Nevertheless, a single sieve fraction should be used in further studies. Flowability of the granular material was improved compared to the initial flow behaviour of powder blend (HF: 1.51, very poor behaviour, ff_c: 3.7, cohesive behaviour). The HF of the granule batches (Table 11) revealed to be similar (fair/passable flow), implying no differences, neither among the batches in general nor between the original and milled granules. However, the ff_c enabled a better view at the respective behaviour revealing an easy flow behaviour [147] for the granules produced on the QbCon®25 and Pharma 16. Despite the pronounced difference in shear stress application on both granulators, the effect of shear stress on the ff_c seemed negligible as the differences were small. The flow behaviour of the batch produced at higher tip speed could not be determined due to functional problems of the ring shear cell.

A similar conclusion could be drawn for the granules produced at 6 and 6.6. kg/h. Granule porosities and friabilities of the original granules as well as flow behaviour (ff_c) of the milled granules were in comparable ranges as those results described above.

Overall, granule characteristics encouraged the assumption of greater densification on Pharma 16. Due to the similar results for friability and strength of the granules, shear stress cannot be assumed to be the cause. The level of occupancies within the limited space in the pitches of CEs and in the KBs were rather a driving force by keeping the material tightly packed and thus enabling an increase in granule density and resistance to external forces. This could be amplified by the fact that the material resided longer on average inside the barrel of Pharma 16 (Table 12). If the thinner kneading discs used in the QbCon®25 setup (see Table 3 in appendix) also had more distributive character and resulted in significantly higher granule friabilities without impact on other granule properties as described by Van Melkebeke et al. [88] cannot be assessed. However, although the absolute difference of 0.25 mm (~6.3 %) between the two types of discs does not seem large, a possible contribution should not be ignored.

One of the commonly used indicators for dynamic similarity of processes in wet granulation is the dimensionless Froude number [148, 149], which is the ratio of the centrifugal force to the gravitational force [150]. The Froude number, *Fr*, was calculated according Eq. (14) [65]

$$Fr = \frac{n^2 \cdot d_{element}}{g} \tag{14}$$

where g is the gravitational acceleration.

As indicated in Table 12, the Froude numbers implied clear differences in process dynamics. All *Fr* of the comparative experiments on Pharma 16 were higher than *Fr* obtained on the QbCon®25, indicating higher centrifugal forces with which the material was pushed against the barrel wall [65, 150]. It might be likely that, similarly to high-shear wet granulation processes, a compaction zone was created that could have caused the production of denser granules [65, 148]. This could also explain the production of less porous and less fragile granules on Pharma 16. Whether the shear stress contributes to the effect on granule friability and density cannot be assessed at this level of insight, but since the *Fr* values indicate a much higher mechanical stress on Pharma 16 (+10 to +59 % than on the QbCon®25), one should expect a potential effect to be more pronounced. It cannot be denied that different shear stresses occurred due to different tip speeds, which could have affected the granule properties, but the actual calculated values seem to be far from reality. Nevertheless, further experiments are recommended.

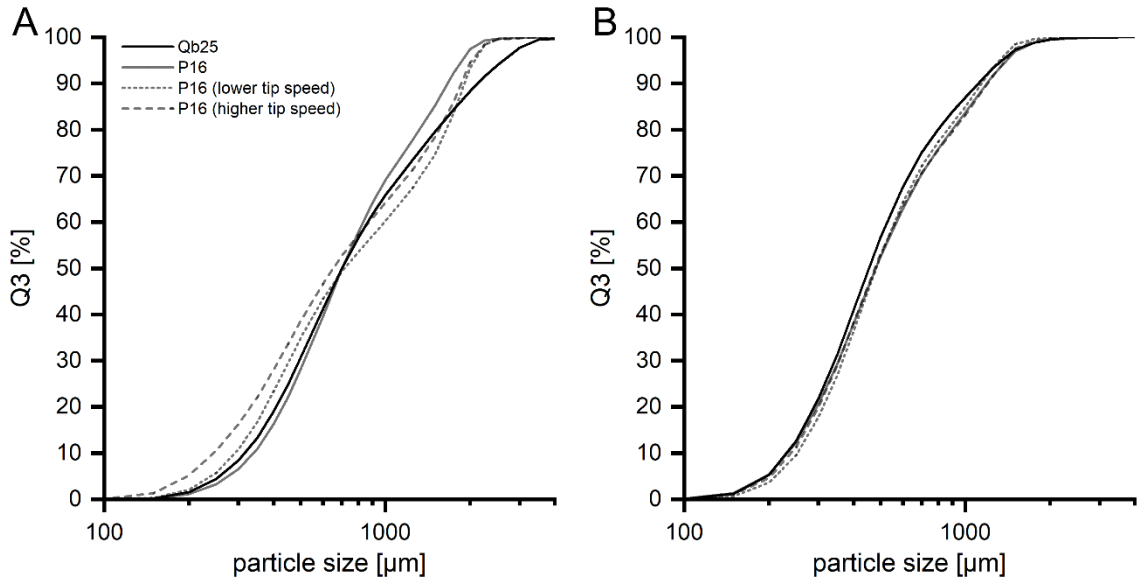

Figure 25. GSDs obtained during process transfer with initial PFR of 4 kg/h on the QbCon®25 and its counterpart on Pharma 16 (similar, lower and higher tip speeds): A) original granules and B) milled granules (n=3, mean). Qb25 and P16 are abbreviations for the granulators used in this study.

Table 10. EMD values (all n=1). Reference curves given in the table.

Granules	Test samples	Test curve to mean reference [-]
Reference: QbCon®25, obtained at PFR of 4 kg/h		
Original	Pharma	48
	Pharma, v_{tip} low	62
	Pharma, v_{tip} high	74
Milled	Pharma	17
	Pharma, v_{tip} low	23
	Pharma, v_{tip} high	17
Reference: QbCon®25, obtained at PFR of 6 kg/h		
Original	Pharma	118
Milled	Pharma	8

Table 11. Characteristics of the granules (mean or mean ± s) (n.d.= not determined due to functional problems of the ring shear cell).

Experiment	PFR	Original granules				Milled granules		
		Envelope density	Porosity	Granule friability	HF	Granule strength	HF	ff_c
	[kg/h]	[g/cm³]	[%]	[%]	[-]	[N]	[-]	[-]
		n=1	n=1	n=3	n=3	n=8	n=3	n=2
QbCon®	4.0	0.621	58.0	18.73 ± 3.29	1.27	0.195 ± 0.037	1.26	9.8
Pharma	4.4	0.721	51.3	7.02 ± 1.72	1.23	0.305 ± 0.055	1.26	9.3
Pharma, v_{tip} low	4.0	0.718	51.5	9.34 ± 2.45	1.19	0.293 ± 0.057	1.24	8.4
Pharma, v_{tip} high	4.8	0.714	51.8	8.89 ± 2.63	1.20	0.307 ± 0.033	1.28	n.d.
QbCon®	6.0	0.611	58.7	16.84 ± 1.30	-	-	-	9.6
Pharma	6.6	0.714	51.7	5.85 ± 0.53	-	-	-	9.5

Table 12. Mean residence time (n=5, mean ± s), Froude number and tip speed of the transfer experiments.

Experiment	PFR [kg/h]	n [min⁻¹]	t_{mean} [s]	Fr [-] ·10³
QbCon®	4.0	200	19.7 ± 1.0	28
Pharma	4.4	321	27.6 ± 1.0	45
Pharma, v_{tip} low	4.0	291	25.6 ± 2.0	37
Pharma, v_{tip} high	4.8	349	23.5 ± 1.6	53
QbCon®	6.0	300	15.0 ± 0.8	64
Pharma	6.6	482	23.6 ± 1.4	102

The impact of differences in granule properties, particularly fragility and porosity, on tablet characteristics was investigated. In the upcoming section the results of the tablets manufactured with the granules obtained at PFR of 4-4.8 kg/h on the QbCon®25 and Pharma 16 will be discussed first.

As depicted in Figure 26A, the tablets made from granules produced at similar tip speeds (Qb25 and P16) showed similar tensile strengths at the different compression pressures, despite the different calculated shear stresses. Although the statistical analysis revealed significant differences of mean values at 100, 150 and 200 MPa (p=0.05, Table 13), both graphs indicated rather little practical relevance within the range of investigation as the slopes of both graphs were quite

comparable (Qb25: 0.0136 MPa/MPa, R^2= 0.9874 vs. P16: 0.0141 MPa/MPa, R^2= 0.9924). The homogeneity of variances was not significantly different. The correlation plot also showed a good batch similarity. Both slope and coefficient of determination tended towards a value of one (Figure 26B). Additionally, the correlation coefficient (R= 0.9966) clearly depicted a strong positive correlation. A similar conclusion could be drawn when comparing the graphs of those tablets produced with granules obtained at lower (R= 0.9998) and higher tip speeds (R= 0.9999) on Pharma 16 but subjected to higher shear stresses in both cases (+10 % and +59 %). A strong positive linear relationship was indicated (Figure 26A, Table 13). Statistical evaluation revealed no significant differences in variance homogeneity and, except for 50 MPa, no difference of the mean values at the different compression pressures. The slopes of both graphs (P16 lower v_{tip}: 0.0122 MPa/MPa, R^2= 0.9903 vs. P16 higher v_{tip}: 0.0119 MPa/MPa, R^2= 0.9909) were also almost equal and suggested no difference in general. In contrast, the correlation plots clearly showed that the batch from the QbCon®25 and the respective batches produced at lower and higher tip speeds on Pharma 16 were not as similar as the batch produced at similar tip speed. Although the correlation coefficient depicted a strong positive linear relationship, the slopes have an essentially lower trend, indicating much lower similarity between the batches.

However, to investigate any distinction between those tablets made up of granules produced at similar tip speeds and those manufactured with granules obtained at lower or higher ones, the respective data at the different compaction pressures were pooled and statistically evaluated (Table 13). The mean values of the tensile strengths were statistically different at 100, 150 and 250 MPa. We are convinced that a statistical difference can also be assumed for 50 and 200 MPa, but the variances were not equal and thus t-tests not conducted. It was surprising that higher tip speeds led to similar tensile strengths as low ones, with significant difference to those tip speeds in the middle of the two extremes. If one takes into account the shear stresses that were supposed to have been applied during the experiments, the results show even more clearly that the values calculated with the newly developed approach do not reflect reality. No satisfying hypothesis could be found to explain these observations.

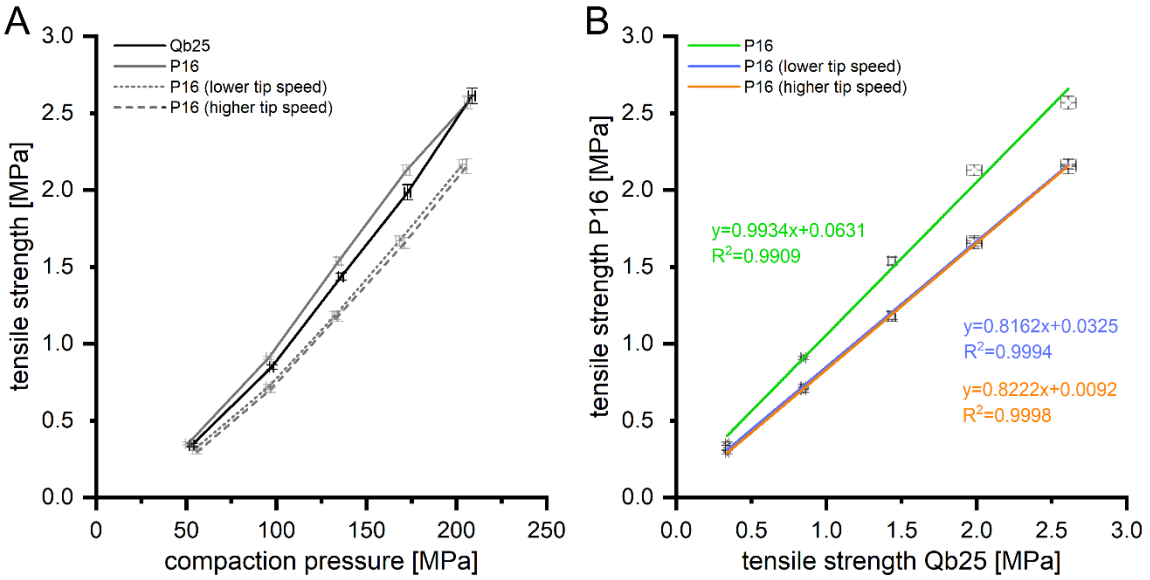

Figure 26. Examination of tablets made up of granules produced at 4 kg/h mass throughput on the QbCon®25 and its counterpart on Pharma 16 (similar, lower and higher tip speeds): (A) tabletability plot and (B) correlation plot (n=20, mean ± CI).

Table 13. p-values of statistical analysis (F- and two-sided t-test) of tablet tensile strengths depicted in Figure 26A manufactured with the granule batches obtained at different process settings. Probability of error, α, was set at 5 %. Asterisk mirrors significant difference.

Compression pressure [MPa]	Qb25 <-> P16		P16 lower v_{tip} <-> P16 higher v_{tip}		Pooled: Qb25/P16 <-> P16 lower/higher v_{tip}	
	F-test	t-test	F-test	t-test	F-test	t-test
50	0.678	0.280	0.442	*0.014	*0.022	-
100	0.185	$*2.122 \cdot 10^{-7}$	0.597	0.104	0.429	$*1.050 \cdot 10^{-30}$
150	0.588	$*1.005 \cdot 10^{-6}$	0.203	0.933	0.500	$*3.214 \cdot 10^{-31}$
200	0.088	$*4.197 \cdot 10^{-5}$	0.875	0.550	*0.006	-
250	0.419	0.187	0.060	0.685	0.279	$*1.286 \cdot 10^{-31}$

Sufficient tensile strength is required as the tablets must withstand external forces in subsequent process steps, e.g. coating or packaging and consumer handling [151]. An official requirement is not available, but a tensile strength of about 2 MPa is described in literature for round flat-faced tablets of similar size to those we used in this study [152]. A sound assessment might be the test on tablet friability, which showed that no tablet batch passed when they had been compressed at 50 and 100 MPa (Table 14). Interestingly, most of the tablets made up of granules produced at lower tip speeds broke when compressed at 100 MPa compression pressure, although higher shear stresses than on the QbCon®25 were applied. The granule strength of the respective granule batch (Table 11) already suggested an insufficient resistance as the average force to be applied for the disaggregation of the granules was lower than for the other batches. This could be a hint that the mechanical stresses acting on the wet material during granulation were lower in reality than calculated, which could have influenced the tablet characteristics. However, although the tablets of the other batches kept integer, the test was also failed in general (Table 14). The batch made up of granules produced on Pharma 16 (PFR 4.4 kg/h) at similar tip speeds than on the QbCon®25 revealed to be most resistant to external forces as two test cycles narrowly passed the test, but

one test failed. All tablets compacted at higher compression pressures (150-250 MPa) passed the test as less than 1 % fines had been abraded and no tablet broke. No superiority of any batch and thus any tip speed during granulation could be identified as the friability was always in comparable ranges. However, based on the tests that had been conducted, the minimum tensile strength to be exceeded to be sufficiently resistant against external forces was assumed to be approximately 1 MPa, at least for the formulation under investigation.

Mass uniformity and requirements on disintegration times were met in each case. All tablets were within the allowed range of ± 5 % for mass uniformity (Table 14) and disintegrated below 900 s (Figure 27).

Overall, a similar conclusion could be drawn for those tablets made up of granules that had been produced at 6 and 6.6. kg/h PFR at similar tip speeds but at different shear stresses (+33 % on Pharma 16). As depicted in Figure 46A (see appendix), the difference between the tensile strengths slightly increased with increasing compaction pressure. The slope of the tablets made up of granules produced on the QbCon®25 was 0.0151 MPa/MPa (R^2= 0.9947) and indicated higher sensitivity to increasing compression pressures, whereas the slope of the Pharma 16-reflecting graph was flatter (0.0139 MPa/MPa, R^2= 0.9980). Additionally, statistical analysis proved their differences at all compression pressures (Table 36 in the appendix). The correlation plot (Figure 46B, appendix) showed both a good linearity and a positive relationship between both batches (R^2= 0.9986, R= 0.9995). The slope (0.8869 MPa/MPa) implied a slightly higher sensitivity towards the QbCon®25-batch, which might be negligible within the examined range. In addition, tablets produced at 50 MPa compression pressure clearly failed the test on friability due to breakages, whereas those manufactured at 100 MPa remained whole and either passed (tablets of Pharma 16-batch) or failed the test (tablets of QbCon®25-batch) (Table 14). However, the amount of attrition was very similar. All other tablet-batches produced at higher compaction pressures passed. Comparable observations could be made for the uniformity of masses and disintegration times. The tablets ranged within the allowed deviation for mass uniformity (Table 14) and disintegrated far below the maximum of 900 s (Figure 47 in the appendix). Although the tensile strengths suggested otherwise, no differences in the disintegration times could be detected, which strongly implied that these differences obtained for the tensile strengths might have less relevance in practice. The results further supported a critical tensile strength of about 1 MPa above which subsequent processing and suitable handling might be possible.

Table 14. Friability and mass uniformity (MU) of tablets at the different compaction pressures. Friability: each value mirrors one test performance, MU: highest deviation in positive and negative direction (maximum deviation allowed: ± 5 %, target tablet mass: 300 mg).

Experiment	PFR [kg/h]	50 [MPa]	100 [MPa]	150 [MPa]	200 [MPa]	250 [MPa]
Friability [%]		n=1	n=3	n=1	n=1	n=1
QbCon®	4.0	breakage	1.23 / 1.23 / 1.22	0.71	0.51	0.42
Pharma	4.4	breakage	0.97 / 1.01 / 0.99	0.63	0.49	0.39
Pharma, v_{tip} low	4.0	breakage	breakage	0.72	0.53	0.46
Pharma, v_{tip} high	4.8	breakage	1.19 / 1.20 / 1.16	0.67	0.50	0.37
QbCon®	6.0	breakage	1.00 / 1.01 / 1.02	0.59	0.42	0.35
Pharma	6.6	breakage	0.94 / 0.98 / 0.95	0.58	0.45	0.35
MU [%]		n=20	n=20	n=20	n=20	n=20
QbCon®	4.0	1.50 / -2.20	1.37 / -4.04	0.95 / -1.47	1.37 / -1.01	2.44 / -1.53
Pharma	4.4	1.04 / -0.73	1.25 / -1.44	1.45 / -1.23	1.49 / -1.45	1.21 / -1.25
Pharma, v_{tip} low	4.0	1.26 / -2.20	1.27 / -1.34	1.66 / -1.37	1.30 / -2.58	1.44 / -1.95
Pharma, v_{tip} high	4.8	1.64 / -1.21	1.96 / -1.31	1.48 / -1.34	1.25 / -1.10	1.43 / -1.05
QbCon®	6.0	0.92 / -1.11	1.83 / -1.55	1.12 / -0.97	1.19 / -1.14	0.73 / -0.94
Pharma	6.6	1.50 / -0.88	2.20 / -1.60	1.46 / -1.85	1.61 / -0.94	1.35 / -1.52

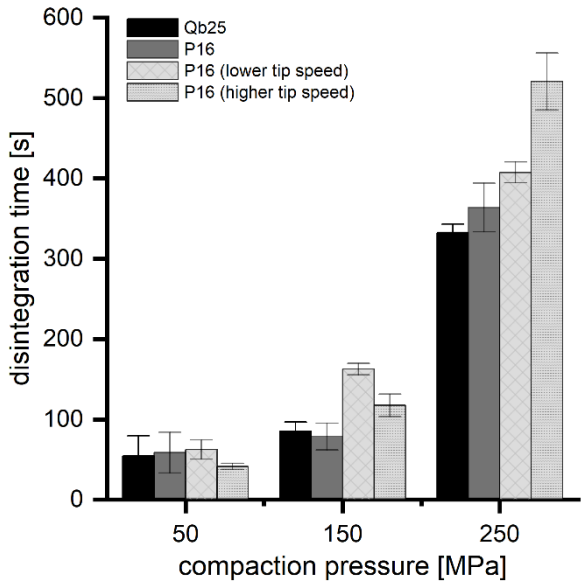

Figure 27. Disintegration times of tablets made up of granules produced at 4 kg/h mass throughput on the QbCon®25 and its counterpart on Pharma 16 (similar, lower and higher tip speeds) (n=6, mean ± s).

All in all, it can be said that the differences in granule characteristics could be mainly ascribed to the different granulators used in this study. It has to be said that the newly developed approach depicted in Eq. (1) clearly failed. Although different shear stresses were applied in the different experiments due to different tip speeds, but also different contact areas of the kneading and conveying elements of the granulators, the calculated values partially indicated a wide range of shear applications which, based on the results of granule and tablet characteristics, are unlikely to reflect reality. It can only be assumed at this stage of research that the formulation containing MCC and lactose possessed sufficient robustness [77, 153-155] and thus levelled bigger differences. A more sensitive formulation with less or even no MCC involvement could display

higher effects when changing tip speeds and thus shear stress application during twin-screw granulation. Since the new approach has failed, further theoretical considerations as well as experimental investigations are needed to improve it and to better reflect reality.

3.2.5 Summary

A newly created approach to quantify a given screw configuration, by considering actual process parameters was created, proposed and checked regarding its suitability in process transfers.

The results of the process transfer studies showed that the approach has failed. According to Eq. (1), constantly higher shear stresses were supposed to be applied on Pharma 16, while the results partially did not display large differences to those granules manufactured on the QbCon®1 or QbCon®25. However, the barrel fill level, quantified as BFD, was found to be a key parameter in process transfers to allow the formation of similar granule sizes and GSDs. The BFD was even found to be more crucial than the applied tip speeds.

The development of a new approach to quantify screw configurations as a single value should continue. In the best case, process and equipment conditions would be better reflected than in the approach presented.

However, due to the usage of a robust formulation containing lactose and MCC, the differences obtained were less pronounced. Formulations without MCC or very low MCC-proportions might most likely be more sensitive. Deviations in process conditions could probably lead to greater differences in granule and tablet properties.

3.3 Assessment of the impact of the KB configuration and varying screw lengths on granule growth

3.3.1 Introduction

Since the screw configuration in general and especially the design of the kneading zone(s) is crucial for granule formation and their characteristics in TSG [78, 81, 89], the impact of the kneading block setup as well as screw length on granule characteristics was considered worth investigating.

The standard experiment for the investigation of the impact of KB was performed with a configurational setup of two kneading blocks with consecutive kneading discs at 60° offset angle (configuration I). The comparative experiments were conducted with either one entire kneading block (configuration II) or three KBs (configuration III), while the number of elements within the screw configuration as well as the offset angle at which the kneading elements were set were kept the same. Experiments were performed at three barrel fill levels, reflected as BFD, at L/S 0.191. As only the KB setup changed, process settings did not have to be changed. Thus, material throughput and screw speed were kept constant to achieve a specific BFD value. Since the process conditions were the same, the tip speeds and therefore the mechanical stresses applied on the wet material at the different BFDs were equal. All experiments were conducted on the QbCon®1.

In the screw length study, the basic experiment was conducted on Pharma 16 using the entire screw length of 640 mm, whereas the comparative experiments used shorter screws (512 and 384 mm). In the latter cases, the screw configuration was adjusted by removing CEs but keeping two, entirely separated kneading blocks at stagger angles of 60°. In this study, the shear stress was calculated according to Eq. (1) and should remain similar for the different screw lengths. Therefore, the shear stresses applied in the basic experiment were considered as target values and the screw speeds were adjusted accordingly to the shorter screw lengths. The PFRs remained unchanged in all experiments. Two BFDs were investigated with each screw length, which were kept similar throughout the experiments. All examinations were carried out at L/S of 0.191.

3.3.2 Examination of kneading block configuration

In Figure 28, the results obtained for the different configurations at varying barrel fill levels are depicted. The results for configuration I have already been discussed intensively in the DoE part of the pre-examination and system sensitivity check in the transfer study (see section 3.2.4.1). The results obtained at L/S 0.191 at the three barrel fill levels were taken as the basic experiment, which is why only the results of the configurations II and III in comparison to configuration I are discussed in the following passage.

It is noticeable that the GSDs obtained with the different kneading block setups were similar to each other in positions and shapes. Independently of the setup, the curves obtained at low filling degrees appeared generally bimodal and turned monomodal with increasing fill levels, indicating similar growth mechanisms inside the barrel at the respective fill levels. However, since the

implications of different barrel fill conditions on granule formation have already been thoroughly discussed previously (see section 3.2.4), this is not repeated in the following. It is apparent that apart from the GSD curve of the intermediate fill level of configuration III, which slightly deviated to bigger granules compared to configuration I, the curves generally fitted well, independently of the barrel fill level. During the experiments at intermediate and high fill level with configuration II and III, the heating of the drying chamber had to be constantly switched off and on again, as the heating permanently exceeded the set point due to a software bug and could not regulate itself independently. Switching the dryer off for a short time allowed the temperature to decrease to values below the setpoint temperature. Afterwards, the drying unit was switched on until the setpoint was exceeded again and the drying unit had to be switched off again. Due to that, the residual moistures of the granules withdrawn in the sampling period exceeded its target value (see Table 31 in the section 5.2.3.8). The residual moisture of configuration III at intermediate fill level exceeded its target the most (actual 4.3 % vs. target 2 %). However, it is not possible to say whether this caused the shift to greater sizes during storage, as more liquid probably remained on the granule surfaces and could bound more fines and small granules. Despite the issue with the heater of the drying unit, the GSDs obtained with configuration II and III at the different barrel fill levels can still be considered as similar compared to those of configuration I as the EMDs are in the same range as in previous studies (Table 15).

Nevertheless, residence times revealed very similar times of first detection as well as mean residence times for the different screw configurations at the same barrel fill (Table 16) which implied the same extent of flow hindrance during granulation, independently of the kneading block design. Due to the higher screw speed at the lowest filling level, the material residence times were the shortest, while the material remained longer in the barrel for the other two filling levels as the screw speed settings were lower. However, since the screw speeds were similar at the intermediate and high fill level, similar residence times were measured.

Although the KB setup normally has a great impact on granule formation and the process itself [81], it can be concluded from the results in this study that the design of the kneading zone(s) investigated does not seem to have a decisive influence on the outcome of the granulation process as long as the number of kneading discs and the offset angle within the screw setup are not changed. However, the conclusion is only based on the examination of the GSD. Other granule characteristics, e.g. friability and porosity, might show differences.

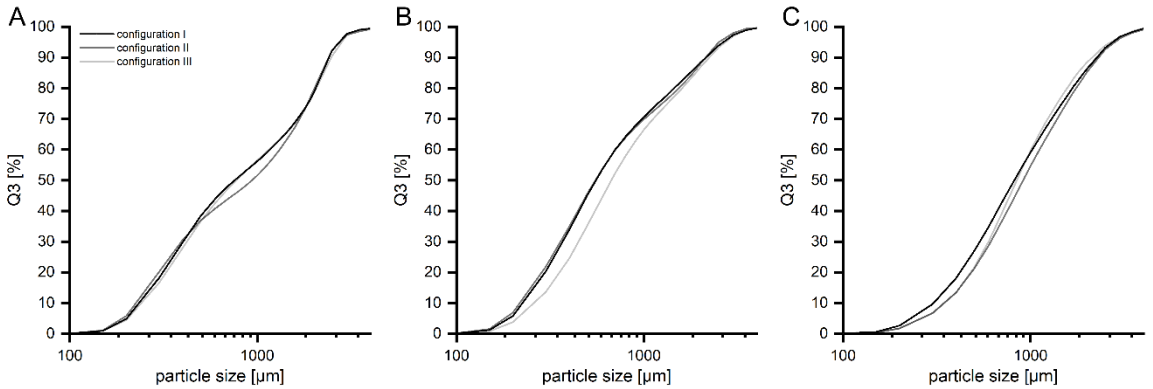

Figure 28. GSDs for varying KB configurations at A) low, B) intermediate and C) high barrel fill level (n=3, mean ± s).

Table 15. EMD values of GSDs of the investigation of KB design on the QbCon®1 (*n=1). EMD value for individual reference curves to the mean reference for screw configuration I containing two KBs:16 ± 5 (n=3, mean ± s) with a coefficient of variation of 33.56 %.

Barrel fill level	Test samples	Individual test curves to mean reference [-]
low	Configuration II Configuration III	*59 *16
intermediate	Configuration II Configuration III	*34 *69
high	Configuration II Configuration III	*70 *48

Table 16. Residence times for the different kneading block configurations (n=5, mean ± s).

Barrel fill level	Screw setup	t_1 [s]	t_{mean} [s]
low	I	12.9 ± 1.8	29.8 ± 2.6
	II	14.6 ± 2.5	35.9 ± 2.8
	III	13.0 ± 1.1	33.4 ± 2.2
intermediate	I	28.7 ± 2.4	46.3 ± 1.6
	II	25.7 ± 2.5	48.5 ± 1.9
	III	24.9 ± 2.8	41.7 ± 2.1
high	I	24.7 ± 1.4	43.8 ± 2.9
	II	25.2 ± 1.6	47.5 ± 0.9
	III	22.8 ± 1.1	41.5 ± 1.2

3.3.3 Examination of varying screw lengths

It could be found that the granules produced at both material throughputs with the 640 and 512 mm screw length were similar regarding their sizes and size distributions (Figure 29), indicating that the conditions for granule growth but also that the distribution of the granulation liquid within the solid material as well as the densification and shearing of the wet mass were similar. The similarity of the GSDs could be confirmed by the low EMD values of 23 and 24, which means that only a small work would be required to transfer the test size distribution into the reference one (Table 17). Interestingly to note was that despite the BFD being regarded as a low fill level, it almost resembled that of the intermediate fill level during the transfer study, but the obtained size distributions were even more bimodal (Figure 29A). The liquid-solid-mixing was

apparently insufficient [82], although the screw configuration with the longer KB was used (configuration A) as in the determination of a suitable screw setup for process transfers (see section 3.2.4.2.1). Therefore, it was initially expected that the usage of the configuration with longer KB would improve mixing efficiency [109]. It can only be guessed that the slightly lower BFD in this study probably indicated an influence of a low fill level, which strongly demands for determining boundaries for different fill levels as well as in-depth investigations on their implications on the final product. Nevertheless, the GSD curves were almost identical regarding their shapes and positions on the graph. At higher material throughput (Figure 29B), the curves proved to be monomodal. Due to the space confinement within the barrel, greater granules broke or were abraded by increased screw pitch fill levels and thus intergranular friction (lower vs. higher BFD: x_{90} 1821 and 1872 µm vs. 1316 and 1474 µm), whereas the fine fraction was unaffected (x_{10} ranged between 208 to 220 µm for both material throughputs) [97]. The median sizes were only slightly lowered (x_{50} 580 and 641 µm vs. 502 and 517 µm). Although the residence times of the material were considerably different for the two screw lengths (Table 18), granule growth was apparently not affected. This was even more surprising as the screw speed had to be increased (150 min^{-1} vs. 185 min^{-1}), and thus the tip speeds and shear rates also increased, when the screw length was shortened to achieve similar shear stresses as in the basic experiment. While the results indicate that the similar shear stresses could be responsible for the formation of the similar granule sizes and GSDs, considering the results of the previous studies, the constant BFDs could be more likely the main reason. However, similar observations have been reported by Van Melkebeke et al. [88], who reported no negative impact on granule and tablet characteristics when the granulation zone was shortened while keeping the same KB setup.

With a further shortening of the screw length, the GSD curves still showed the same curve modalities as the other two screw lengths did (bimodality at lower and monomodality at higher BFD) but revealed an additional right-shifted position as well as a broadening of the distribution. The curve shifted to greater granule sizes at lower BFD (x_{10}: 231 µm, x_{50}: 830 µm and x_{90}: 2173 µm), while only granules above a frequency of 50 % was decisively affected at higher one (x_{10}: 217 µm, x_{50}: 551 µm and x_{90}: 1975 µm). In both cases, the EMDs were larger and much less similar than for 512 mm screw length (Table 17). The findings generally indicated that the granule growth mechanism was different compared to the other screw lengths. The usage of CEs downstream the (second) KB were generally found important for granule properties [77]. Lute et al. [78] investigated granule formation along the barrel length and found less fines and bigger granules, even when only two SPCEs were set after the second KB. Increasing the number of CEs downstream decreased the granule sizes. In addition, GSD became narrower and monomodal and mean granule sizes steadily decreased. It was further hypothesized that the short residence times were not long enough to provide comparable size distributions. Although both the BFD values and shear stresses were kept similar, the shorter residence times (Table 18) could not sufficiently level inhomogeneities in liquid distribution.

Generally, it must be said that experimental repetitions are needed to draw a final conclusion as processes are governed by variabilities due to their dynamic nature. At this stage of insights, it can be said that differences in granule sizes were less pronounced, except for the bigger granules (above 50 % volume-based frequency) produced at higher material throughput using the shortest screw length. The screw speed calculated on the basis of the shear stress might compensate for the shorter screw lengths and residence times until a crucial screw length is achieved. Comparable granule sizes and distributions were achieved by keeping the same curve modalities. Although the shear stresses were kept similar, the influence of the fill level on granule formation might have been stronger.

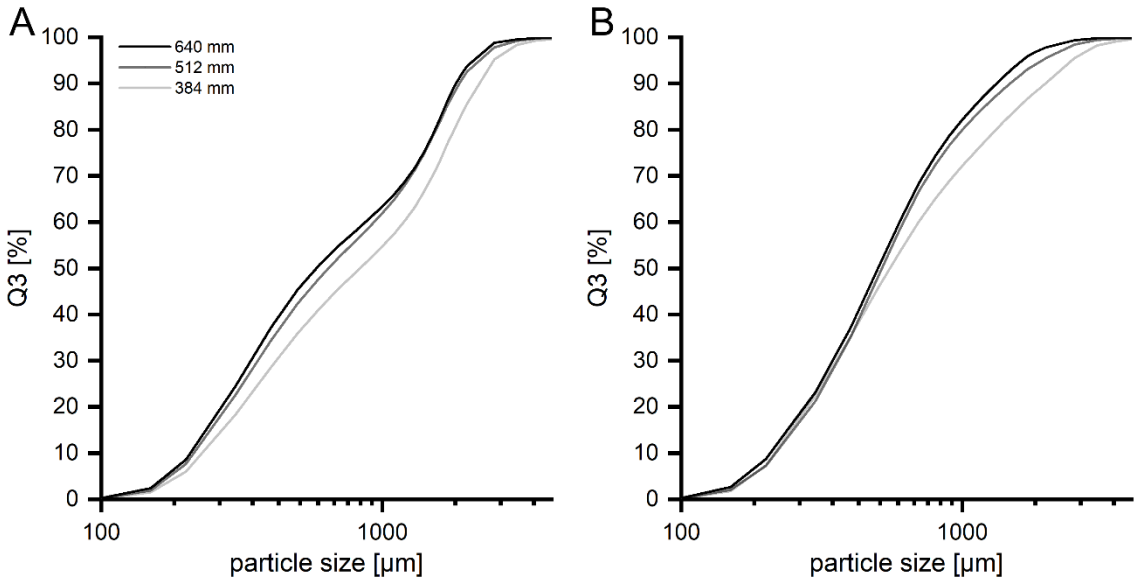

Figure 29. GSDs obtained for the different screw lengths at A) low and B) high BFD (n=3, mean).

Table 17. EMD values of GSDs of the investigation of screw lengths on Pharma 16 (all n=1). Reference curves from screw length of 640 mm.

Barrel fill level	Test samples	Test curve to mean reference [-]
low	512 mm	23
	384 mm	102
high	512 mm	24
	384 mm	70

Table 18. Residence times for the different screw lengths for the two different material throughputs (n=5, mean ± s).

Screw length [mm]	Barrel fill level	t_1 [s]	t_{peak} [s]	t_{mean} [s]	t_{out} [s]
640	low	25.1 ± 1.3	34.3 ± 1.4	41.6 ± 1.6	83.4 ± 3.4
512		17.6 ± 0.5	24.8 ± 0.7	32.4 ± 1.8	69.4 ± 6.0
384		10.0 ± 0.3	17.6 ± 0.8	21.8 ± 0.8	48.2 ± 4.2
640	high	30.2 ± 0.6	38.6 ± 1.2	48.0 ± 0.5	96.8 ± 4.0
512		20.8 ± 0.6	28.3 ± 1.0	38.4 ± 1.8	80.6 ± 5.9
384		11.9 ± 0.4	17.3± 0.6	23.5 ± 0.6	50.5 ± 1.9

3.3.4 Summary

The impact of the design of the kneading zone and screw length on granule growth was investigated by keeping the tip speeds or shear stresses constant compared to the respective basic experiment.

The study in which the kneading zone design was investigated aimed at the question if granule growth changed when the screw configuration contained one, two or three kneading blocks, although the overall number of kneading discs within the entire configuration was kept the same. Investigations occurred at different barrel fill levels. The curves were almost identical regarding their shapes and positions and appeared bimodal at low and monomodal at high filling degrees whereas the intermediate fill level revealed an intermediate shape with characteristics of both low and high fill level. It was concluded that the KB setup itself is less decisive if both the number of kneading discs and the shear stress application is kept constant. However, no effect of the KB design on granule sizes and size distributions was observed, except for configuration III at intermediate fill level, where the GSD was shifted towards larger granules due to functional problems of the heater of the drying unit of the QbCon®1. During the process, the temperature setpoint was always exceeded, resulting in the drying unit having to be switched off regularly for a short time until the temperature fell below the setpoint and the drying unit could be switched on again. As a result, the granules did not experience a uniform drying process and thus higher residual moisture occurred. More liquid was assumed to remain on the granule surfaces after the drying process that could bound further material and caused additional granule growth during storage.

The examination of varying screw lengths was conducted with 640, 512 and 384 mm screw lengths. No difference in GSDs was obtained when the 640 and 512 mm screw lengths were used. Solid-liquid-mixing revealed as insufficient and led to bimodal curves at low BFD, whereas monomodal distributions were obtained at high BFD. Although shorter residence times were measured with lowering the screw length, granule growth and the resulting GSD were similar. Further decrease of screw length caused the production of bigger granules and broader size distributions, indicating different granule formation mechanism. Although the shear stresses remained similar, the barrel fill level was probably the main influence to overcome the shorter granulation zones and still obtain similar granule sizes.

3.4 Attempt of a dimensionless description of the barrel fill level during twin-screw granulation[1]

3.4.1 Introduction

The barrel filling degree of a twin-screw granulator is defined as the volume occupied by the material to be granulated related to the maximum free volume of the screw configuration [93, 95] and reflects an interplay of throughput, screw speed, screw design, barrel length and characteristics of starting material [81, 94-96]. The fill level was identified as a key factor on both the outcome of a granulation process and the granule properties that can be estimated from the actual torque level applied by the granulator [81, 94, 98]. The SME, a scale-independent measure of the energy that is mechanically imparted into the wet mass, is probably a better indicator than the torque only, as it takes throughput, screw speed as well as the actual torque into account (see Eq. (42)) [66, 96, 100] and rather allows for the direct comparison of different granulators [64]. It is a legitimate concern that if the quantification of the fill level remains unclear, further progress in process understanding, especially when differently sized granulators are involved, may remain difficult [59].

The non-dimensionless specific feed load (SFL), a ratio of gravimetric mass to the screw speed and originally introduced for extrusion processes, describes the amount of material on the screws conveyed per rotation [101] and was applied as a surrogate parameter for the volumetric fill level in TSG [93]. Unfortunately, it is only valid for one formulation, screw setup and granulator [93] and failed to provide similar fill levels on differently dimensioned granulators and thus was incapable of producing granules with similar characteristics [145]. However, granulation processes can be regarded as entirely similar when material, geometrical and process-related similarity is given. This can be achieved when the physical relationship of a problem to be worked out, in this case the barrel fill, can be dimensionally homogeneously formulated, meaning dimensionless expressed. The numerical values of the dimensionless terms required for process description are then kept constant [102, 103]. With this, a process can be defined across a broad scale range that helps to set suitable process control strategies, which is particularly attractive for upscaling [94, 96].

Some scale-independent approaches have already been proposed that either consider the ratio of the volumetric flow rate to the volume turnover and net forward velocity of the material [66], the fraction of the element channels filled with powder as well as the volumetric efficiency of the screw [143] or the volumetric flow rate in relation to the forward volumetric transportation rate of the screws [95]. However, although the attempt of Osorio et al. considered particularities in screw design, the net forward velocity of the material could only be estimated, which is why the entire attempt was not applied except for the dimensionless powder feed number. In addition, the cubed barrel diameter was used to reflect a volume, which does not realistically describe the

[1] Some results presented in this section were obtained during an elective practical lab course (dt. “Wahlpflichtfachpraktikum”) with the support of Luna Maschke and Leah Schlüsener.

conditions in TSG. Similarly to Osorio et al., the attempt of Gorringe et al. is based on assumptions for the volumetric efficiency which lowers the applicability considerably [66, 95, 143]. A major improvement had been made with the attempt of Mundozah et al. [95], but comprehensibility was affected by mismatch of symbols in text and tables (*O.D.* vs. D_c), calculation of free volumes not further used and uncertainty regarding the granulation zone.

Another attempt to calculate a dimensionless channel fill level dealt with the volumetric feed rate divided by the maximum free volume of the channels in a screw element with two flights and the screw speed [85] but was only applied for a screw setup made up of conveying elements only. Since the equation does not consider the characteristics of other screw elements, a successful application on other screw designs must be ruled out.

Aim of the working package was therefore the development of a further predictive model for barrel filling degrees in TSG. The model considered the transportation velocity of the wet mass and particularities in screw design that lower the transportation velocity throughout the barrel and caused further material hold-up. The attempt should be tested at varying process settings with different screw designs. A critical evaluation of the proposed models was made and can be found at the end of this section.

3.4.2 Theoretical Development

3.4.2.1 General

As already highlighted, the fill level of a twin-screw granulator barrel is mainly influenced by the material throughput, screw speed, screw configuration and barrel length. Material properties such as density and its deformation behaviour could also be relevant factors on barrel filling degree.

Although some dimensionless descriptions have already been proposed, a new one was created that considered the materials transportation velocity for different screw geometries and further allowed for the estimation of mass hold-up in the barrel and its passage time through the barrel. The new proposal can be found in Eq. (15)

$$\varphi = \frac{\dot{m}_{tot}}{\rho_{true}} \cdot \frac{l_{barrel}}{\bar{v}_{harmonic}} \cdot (1 + sin(\alpha)) \cdot \frac{1}{V_{free}} = \frac{\dot{V}_{tot} \cdot t_{1,theo} \cdot (1 + sin(\alpha))}{V_{free}} \qquad (15)$$

where φ is the dimensionless barrel fill level, $\dot{m}_{tot}$ is the total material throughput (in g/s), ρ_{true} is the materials true density (in g/cm³), l_{barrel} is the barrel length used (in mm), $\bar{v}_{harmonic}$ is the harmonic mean conveying velocity of the material through the barrel, $(1+sin(\alpha))$ the mass hold-up due to the stagger angle (α) of kneading elements within a block, V_{free} is the free volume (in cm³), $\dot{V}_{tot}$ is the total volumetric throughput (in cm³/s) and $t_{1,theo}$ is the theoretical lag-time of the material until it will exit the barrel and thus be detectable for the first time during RTD measurements.

The true density was chosen since the granulation liquid and its proportions in the wet material are easier to calculate than in the bulk or tapped density.

3.4.2.2 Parameter approximations

3.4.2.2.1 Mean conveying distance per revolution

The straight distance covered by the material to be transported per revolution, l_{rev}, appeared to be a more decisive variable in determining the degree of barrel fill. For this, all elements used within a screw setup must be considered as strongly affecting l_{rev}. The manner of mathematical consideration has to be adapted to the different kind of elements (conveying elements) and element sections (kneading blocks) as they provide varying conveying capabilities [74, 81, 89, 109].

The transportation distance per revolution of conveying elements, which length itself was longer than the lead of the respective element, was considered as given in Eq. (16)

$$l_{rev_{CE}} = 2 \cdot \left(w_{crest} + w_{pitch}\right) = l_{lead} \tag{16}$$

where w_{crest} is the crest width of the element, w_{pitch} is width of the element pitch and l_{lead} is the lead length of the double thread conveying element that was meant to be the straight distance the material had covered after one screw turn. If the conveying elements had the same length as the lead, the element length, $l_{element}$, was considered equal to l_{rev}.

Some of the screw element-related variables used for the calculations in Eq. (16) are depicted in Figure 11 in section 3.2.2.2.

3.4.2.2.2 Harmonic mean conveying velocity through the barrel

Next to the mean conveying distance per turn, the harmonic mean velocity, $\bar{v}_{harmonic}$, of the material being transported through the whole barrel was assessed by applying Eq. (17)

$$\bar{v}_{harmonic} = \frac{l_{CE_X} + l_{CE_Y} + l_{CE_Z} + l_{KB_X} + l_{KB_Y}}{\left(\frac{l_{CE_X}}{v_{CE_X}}\right) + \left(\frac{l_{CE_Y}}{v_{CE_Y}}\right) + \left(\frac{l_{CE_Z}}{v_{CE_Z}}\right) + \left(\frac{l_{KB_X}}{v_{KB_X}}\right) + \left(\frac{l_{KB_Y}}{v_{KB_Y}}\right)} \tag{17}$$

where l and v are the length of each conveying or kneading block section and the velocities at which the material is transported through these sections, respectively.

The length (in mm) of a specific type of CEs, l_{CE}, or the lengths of differently designed kneading blocks, l_{KB}, used within the screw setup, where *X, Y, Z* are meant to represent different types of CEs or KBs that could be incorporated into the screw configuration, was calculated according to Eq. (18)

$$l_{CE} = l_{KB} = l_{element} \cdot x_{element} \tag{18}$$

where $x_{element}$ is either the number of elements of a specific CE type used within the screw design or the number of kneading discs within a KB section.

The velocities (in mm/s) of the wet mass through the conveying and kneading block sections, v_{CE} and v_{KB}, are calculated according to the Eqs. (19) and (20)

$$v_{CE} = \frac{l_{rev_{CE}}}{\left(\frac{1}{n}\right)} = \frac{l_{rev_{CE}}}{t_{turn}} \tag{19}$$

$$v_{KB} = \frac{l_{KB}}{\left(\frac{x_{element}}{\left(\frac{360°}{\measuredangle}\right)} \cdot t_{turn}\right)} = \frac{l_{KB}}{k \cdot t_{turn}} \tag{20}$$

where n is the screw speed (in s^{-1}), t_{turn} is the time needed for one turn (circulation time) (in s), $(360°/\measuredangle)$ is the number of kneading elements needed for a complete revolution at a given stagger angle, $x_{element}/(360°/\measuredangle)$ results in the correcting factor, k, for t_{turn} when the KB length is unequal to one turn (longer or shorter). In case of equality, k will have the value of 1.

3.4.2.2.3 Calculated time of first detection and mass hold-up within the barrel during twin-screw granulation

The present dimensionless description of barrel fill level (see Eq. (15)) builds on the ability to predict the time at which the material should theoretically have passed through the barrel and thus be detectable for the first time. Furthermore, the determination of the theoretical mass of material that is in the barrel is also covered in Eq. (15), which is important in quantifying the barrel fill level during a TSG process.

The theoretical time of first detection, $t_{1,theo}$, was considered as given in Eq. (21)

$$t_{1,theo} = \frac{l_{barrel}}{\bar{v}_{harmonic}} \cdot (1 + sin(\alpha)) \tag{21}$$

whereas the theoretical mass hold-up, m_{theo}, was calculated by taking $t_{1,theo}$ into account as shown in Eq. (22)

$$m_{theo} = t_{1,theo} \cdot \dot{m}_{tot} = \frac{l_{barrel}}{\bar{v}_{harmonic}} \cdot (1 + sin(\alpha)) \cdot \dot{m}_{tot} \tag{22}$$

In the following examinations, both predictions were compared to actually measured results. If the predicted data did not correspond to the actual one, the model had to be adjusted.

3.4.3 Review of the proposed attempt to estimate mass hold-up and times of first detection

The results of mass predictions inside the barrel of a twin-screw granulator according to Eq. (22) as well as times of first detections according to Eq. (21) for the different formulations composed of MCC 102 and DCP A12 can be found in Figure 30 and Figure 31. They were examined at

different PFRs and screw speeds to cover a broad range of barrel fill level. The investigated screw setups contained either CE only or one KB of nine kneading elements at 30 or 60° stagger angle, hereinafter denoted as CE only, KB 30° or KB 60°, respectively.

As shown in Figure 30, a change of screw configuration from CE only to KB 30° and finally to KB 60° stagger angle revealed an increase in mass hold-up as these screw configurational changes mark bigger obstacles that lowered the materials throughput speed [74, 81, 89]. It is obvious that the predicting capability of the proposed attempt underestimated the masses for screw setups made up of CE only (Figure 30A, D and G). With increasing PFRs the predictability was clearly lowered; both absolute and relative differences between prediction and reality increased. The predictive power was similar for the formulations containing 20 and 60 % MCC, but a change to pure MCC proved a reduction in predictability. The forecasting correctness improved at higher screw speeds. Although the results met the predictions better, similar conclusions could generally be drawn for the investigations with the screw configuration with 30° stagger angle (Figure 30B, E and H). In contrast, mass hold-up was mainly overestimated if kneading elements (KEs) at 60° stagger angle were incorporated (Figure 30C, F and I). The formulation had an impact on the mass hold-up at the lowest screw speeds (150 and 200 min^{-1}) as an increased MCC proportion increased the remaining material in the barrel. An inversion from an under- to an overestimation was observed in combination with higher PFRs. Contrarily to the screw setup using only CEs, the forecasting correctness tended to be worse at higher screw speeds at higher PFRs. Although no mass hold-up could be determined at 3 kg/h PFR at 450 min^{-1} for formulation containing 20 % MCC (Figure 30C), a lowered predictability can also be assumed.

The measured material hold-ups must generally be considered with caution as these experiments were conducted only once with five measurements each at the defined process settings. The results showed a low variability of the masses measured at specific process settings, but their robustness is not yet given and needs to be examined on different experimental days with newly prepared blends.

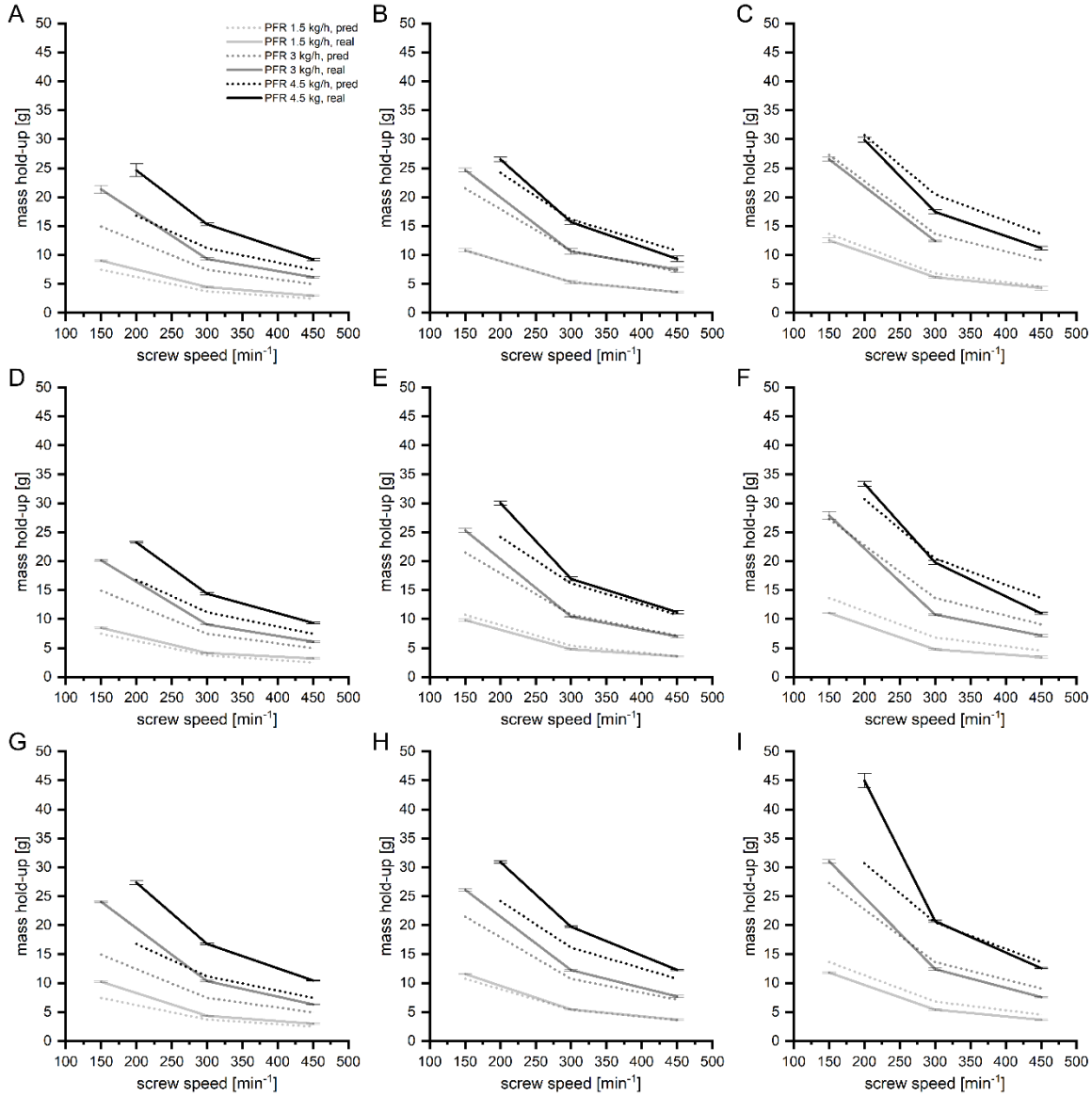

Figure 30. Mass predictions vs. reality of the different formulations A-C) 20:80, D-F) 60:40 and G-I) 100:0 mixture of MCC-DCP (% m/m) using different screw setups: only CE (left), KB of 30° (middle) and 60° stagger angle (right) (n=5, mean ± s).

Similarly to the findings mentioned above, comparable trends could be also observed for the determination of t_1. Independently of the formulation, the times after which the tracer was detected were prolonged from the screw setup made up of CEs only to KB 30° to KB 60° (Figure 31).

For the screw setup made up of CEs only, predictions mostly underestimated the times required for the material to be conveyed through the barrel (Figure 31A, D and G). Increasing the screw speed led to an improvement in predictability. Contrarily, using KB 60° caused an overestimation of the respective times (Figure 31C, F and I). Times measured approached the predicted ones at higher PFRs with increasing proportions of MCC, resulting in a particularly good fit at low screw speeds (150 and 200 min^{-1}) when pure MCC had been used. However, the opposite effect was observed for 1.5 kg/h PFR with increasing MCC content. Predicted and measured times diverged

with increasing screw speeds. A rather good fit was obtained again for the KB 30°. Similarly to the results obtained with KB 60°, the proportions of MCC influenced the times the material needed to pass the barrel (Figure 31B, E and H). Increasing MCC proportions prolonged the passage times, especially at high PFRs, and lowered simultaneously predictability. The results obtained at 1.5 kg/h remained almost unaffected, independent of the formulation.

Interestingly to note is that although predicted times of first detection were equal for the different PFRs at defined screw speeds when examining a particular screw configuration, the differences amid measured t_1 values of the different PFRs increased with increasing proportions of MCC. This trend was visible for each investigated screw setup.

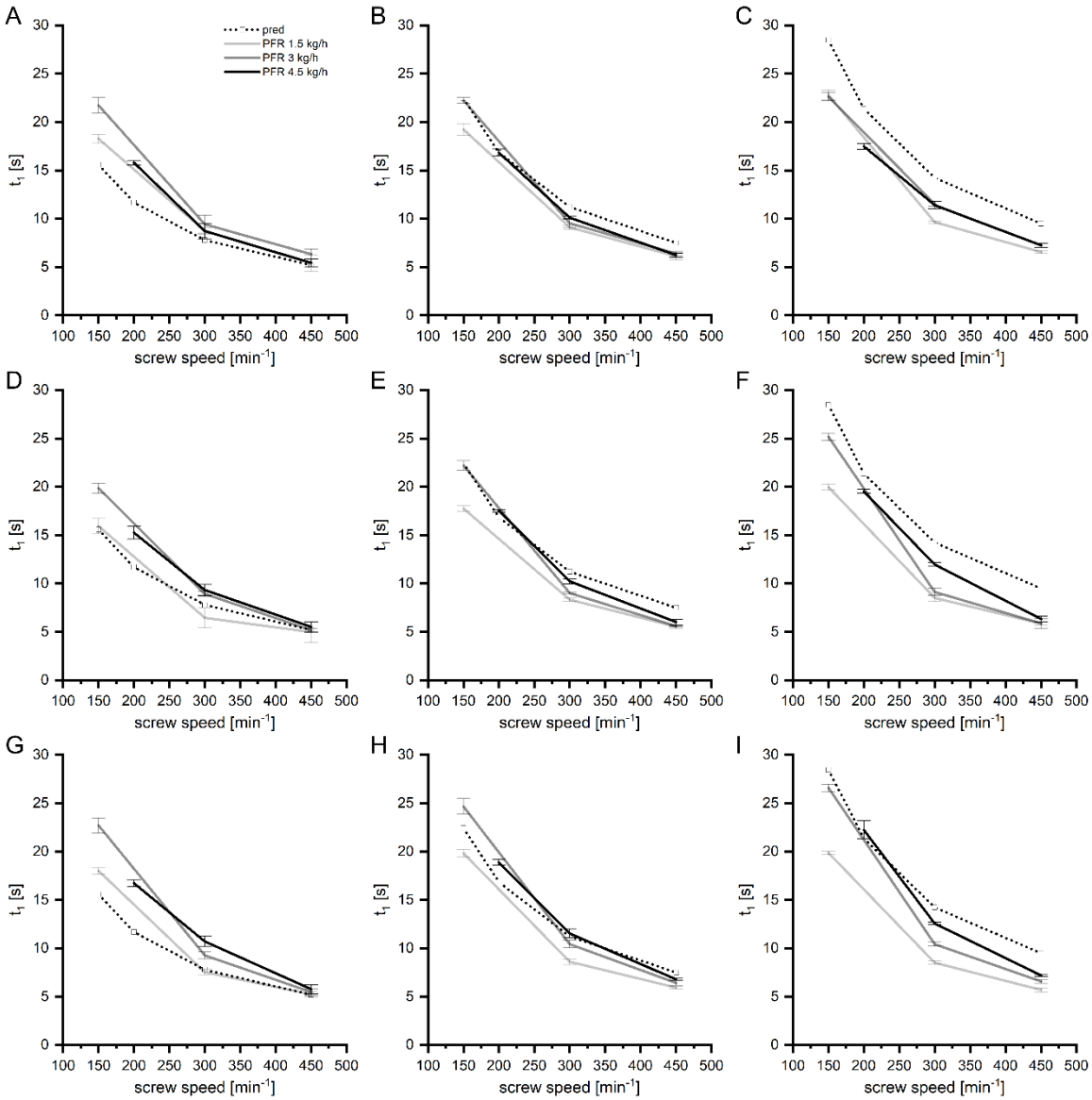

Figure 31. Predictions of first detection vs. reality of the different formulations A-C) 20:80, D-F) 60:40 and G-I) 100:0 mixture of MCC-DCP (% m/m) applying different screw setups: only CE (left), KB of 30° (middle) and 60° stagger angle (right) (n=5, mean ± s).

Although the results generally headed into an encouraging direction, it must be highlighted that the equation for a dimensionless description of barrel fill level needed further theoretical considerations and adjustments. Constant underestimation of masses inside the barrel and times of first detection for screw setup of CEs only was probably caused by intra-material friction and wall slippage. As the materials velocity has already been reported being lower than the tip speed of the screws would lead one to expect [85], this might be also a crucial factor. Since the barrel usually has build-up on its wall [74], friction might take place there when the wet material is conveyed towards the barrel outlet. Thus, friction probably changed the manner of backmixing and might simultaneously increase both mass hold-up and the durations to pass the barrel. In contrast to that, an overestimation with the screw configuration KB 60° might be caused by the way in which the kneading blocks were mathematically described. The *(1+sin(α))*-part should have expressed the mass hold-up and deceleration of throughput speed due to the choice of stagger angle within a kneading block. However, the description might be mathematically insufficient, which the results clearly proved. It is apparent that further time must be invested into this topic to improve the equations predictability.

3.4.4 Improvement and validation of the predictive power of the proposed equation

Based on the results and the conclusion drawn, the consideration of a KB and its respective offset angle by the actual mathematical *(1+sin(α))*-term was fixed at 1.50, rationally justified by the underestimation of CE only (*1+sin(α)*=1.00), the overestimation of KB 60° (*1+sin(α)*=1.87) and the relatively good fit of KB 30° (*1+sin(α)*=1.50). Due to the over- and underestimation, it was assumed that a defined factor, *f*, of 1.50 would lead to better predictions.

Thus, the predictive terms of $t_{1,theo}$ and m_{theo}, were revised as given in Eq. (23)

$$t_{1,theo} = \frac{l_{barrel}}{\bar{v}_{harmonic}} \cdot f \tag{23}$$

and Eq. (24)

$$m_{theo} = \frac{l_{barrel}}{\bar{v}_{harmonic}} \cdot f \cdot \dot{m}_{tot} \tag{24}$$

where *f* is the arbitrarily set factor of 1.50.

As it is depicted in Figure 32, after applying the consideration mentioned above, the predictions enormously changed for the screw configurations containing either only CEs or a KB at 60° stagger angle. Whereas the material hold-up was constantly underestimated for CEs only with the original approach (Figure 31), the predictions met reality much better with the improved version (Figure 32A, D and G). As depicted, results indicated best fit for pure MCC in general, independently of the process settings. Predictability decreased with increasing screw speeds at PFRs of 3.0 and 4.5 kg/h for formulation containing 20 % MCC, while no clear trend could be found for the formulation containing 60 % MCC. However, increased predictability was revealed for PFR

of 1.5 kg/h with increasing screw speed for both formulations, 20 and 60 % MCC proportions. Nevertheless, no clear trend could be extracted from the results that were obtained at the different process settings as well as with the usage of the different powder blends. What is clear is that the predictions slightly overestimated material hold-up with the improved approach, indicating the factor *f* of 1.50 might be too high.

For KB 60° (Figure 32C, F and I), predictions were shifted to lower material hold-ups, leading to low predictability at low screw speeds (150 and 200 min^{-1}) at 3.0 and 4.5 kg/h and an increasing predictive power with increasing screw speeds. Due to the lower factor *f*, an impact of the formulation was even more profound as higher deviations were obtained at higher proportions of MCC. However, a rather good fit of predictions was obtained at PFR of 1.5 kg/h. Applying *f* of 1.50 lowered the predictive power of the model fundamentally, implying that a general factor does not reflect the complex processes that cause material hold-up inside the barrel.

Since the factor *f* of 1.50 was equal to the *(1+sin(α))*-value of the original attempt when the screw setup KB 30° was taken, no changes occurred with the revised version. Thus, Figure 32B, E and H depict the same results. However, although the results matched the predictions well, some slight adjustments might be necessary to make predictions more accurate on average, especially when the same screw setup is used for various formulations of varying properties.

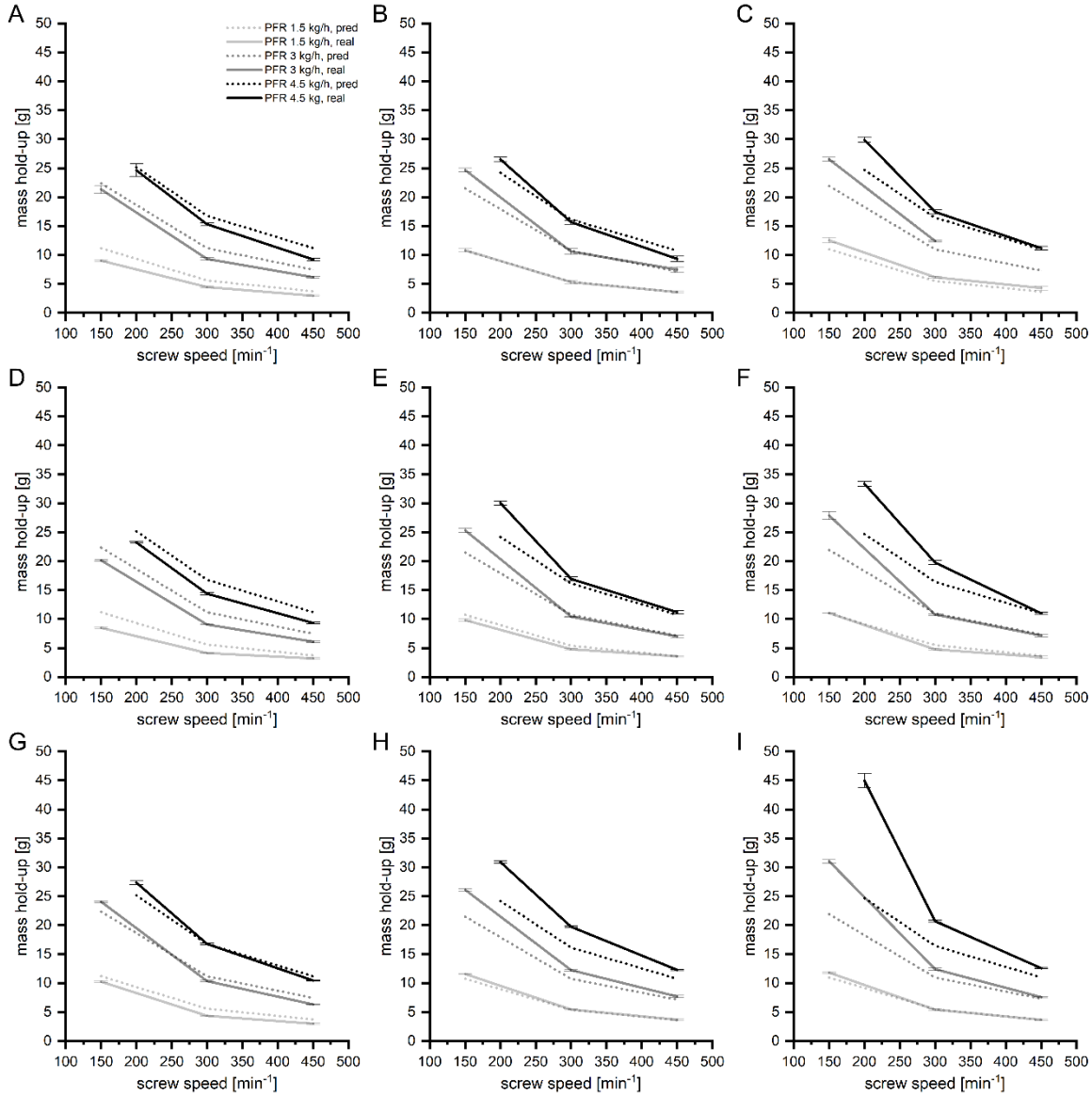

Figure 32. Improved mass predictions vs. reality of the different formulations A-C) 20:80, D-F) 60:40 and G-I) 100:0 mixture of MCC-DCP (% m/m) using different screw setups: only CE (left), KB of 30° (middle) and 60° stagger angle (right) (n=5, mean ± s) by applying the factor *f* of 1.50.

Similarly to the mass hold-ups, the fit of the predicted and measured times of first detection for screw configuration containing CEs only were also enormously impacted with the application of the general factor of 1.50 (Figure 33A, D and G). While the predictive power was, independently of the formulation, good at high screw speeds (300 and 450 min^{-1}), it lacked accuracy at low screw speeds (150 and 200 min^{-1}) at 1.5 kg/h powder throughput. Except for formulation with 60 % MCC, the predictability for the other PFRs was initially very low when using the original attempt but improved essentially with the improved model (Figure 33A, D and G). The predicted times strongly increased and slightly overestimated measured t_1 values. However, predictive power was closer to the results obtained at 3.0 and 4.5 kg/h and low for those obtained at 1.5 kg/h, likewise indicating that the factor of 1.50 should be revised to lower values for such screw setups. A fundamental improvement of the predictability of t_1 was found for screw setup KB 60° among all

process settings and formulations (Figure 33C, F and I). Predictions met the measured values well with the improved approach.

Similar to the mass hold-up prediction, there was no change in the prediction of t_1 for screw setup KB 30° as the value of factor f kept the same (Figure 33B, E and H).

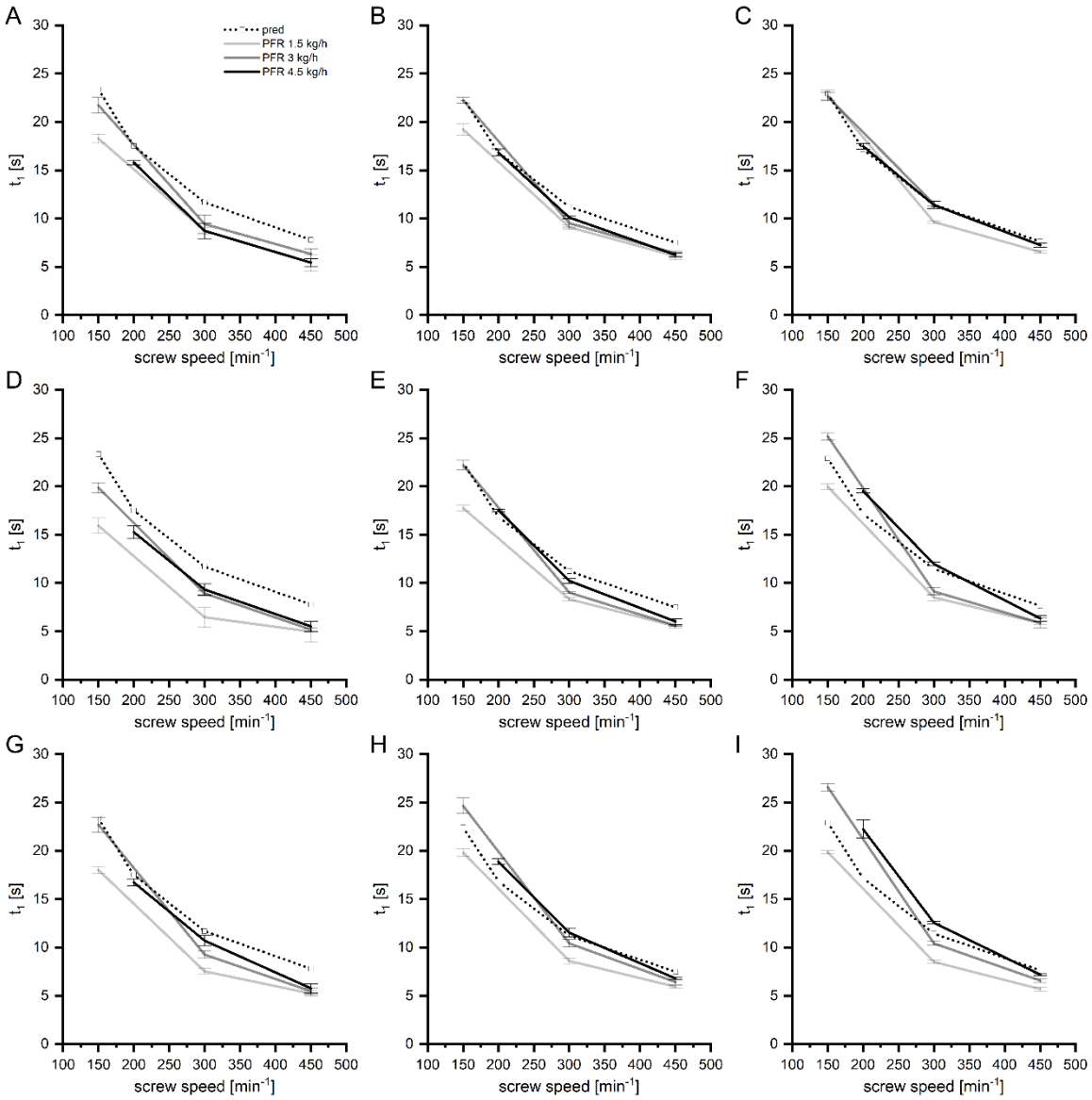

Figure 33. Predictions of first detection vs. reality of the different formulations A-C) 20:80, D-F) 60:40 and G-I) 100:0 mixture of MCC-DCP (% m/m) applying different screw setups: only CE (left), KB of 30° (middle) and 60° stagger angle (right) (n=5, mean ± s) with application of factor f of 1.50.

After the improved version of the model had been applied, the results revealed to be ambiguous and did not allow for clear conclusions on its performance. It can be stated that the new approach influenced the predictability of mass hold-ups positively for screw configurations that had only CEs incorporated as predictions changed from constant underestimations with the original approach to slight overestimations with the new approach. The same could be said for the predictions of times of first detection. The predictions of mass hold-ups and t_1 values for screw

configuration KB 30° kept unaffected by the improved model. In contrast, changes for screw setup KB 60° revealed lower predictability among almost all process settings. Furthermore, an impact of the formulation was even more pronounced compared to the original approach.

All in all, it must be said, that the results indicated that a general factor *f* of 1.50 partially led to insufficient predictions of mass hold-ups among the different screw configurations. Further improvements are clearly needed to increase predictability, independently of process settings and formulations, but depending on screw configurational particularities. The factor *f* was found to be appropriate as it combined all variables with impact on barrel fill that could not specifically be quantified and thus separately included in the model. Once better understanding has been gained, further specification of *f* and inclusion of other variables can be made. Nevertheless, the results showed that using *f* of 1.50 provided, in principle, good predictions of t_1 as well as of mass hold-ups for screw setup KB 30°. Additionally, it revealed a necessity for further adjustments.

Based on the insights gained with the improved version, further editing occurred by the implementation of a variable which objective is the correction of mispredictions for the different screw setups as shown in Eq. (25)

$$m_{theo} = \frac{l_{barrel}}{\bar{v}_{harmonic}} \cdot 1.50 \cdot x \cdot \dot{m}_{tot} = \frac{l_{barrel}}{\bar{v}_{harmonic}} \cdot f_{new} \cdot \dot{m}_{tot} \tag{25}$$

where x is an unspecified variable for correction of mispredictions caused by factor 1.50 that results in f_{new}.

The edited version was integrated into the NLFit application of the OriginPro 2021 software and all numerical values were assigned to the respective parameters. The non-defined variable x was finally determined by non-linear curve fit by applying the Levenberg–Marquardt algorithm for iteration. The averaged results of f_{new}, the product of 1.50 and x, for the different screw configurations can be found in Table 19. The finalised f_{new} values were the overall means of all determined ones for each screw configuration. The results of each non-linear curve fit for the different material compositions, screw configurations and material throughputs are displayed in Table 37 in the appendix for the sake of completeness.

Table 19. Results for f_{new} determined with non-linear curve fit for the given material compositions and screw configurations. The finalised factors f_{new} were the overall means of all determined f_{new} (*n=3, **n=9, mean ± s).

Screw configuration	**Formulation MCC:DCP [% w/w]**	f_{new}* [-]	**Finalised** f_{new}** [-]
Only CE	20:80 60:40 100:0	1.33 ± 0.11 1.26 ± 0.11 1.47 ± 0.14	1.36 ± 0.14
KB 30°	20:80 60:40 100:0	1.57 ± 0.08 1.60 ± 0.20 1.75 ± 0.14	1.64 ± 0.15
KB 60°	20:80 60:40 100:0	1.74 ± 0.04 1.72 ± 0.23 1.98 ± 0.40	1.81 ± 0.26

As already illustrated in Figure 32 and concluded from these results, a defined factor f of 1.50 led to insufficient predictions of mass hold-ups at the different process settings for the different screw configurations, which was particularly highlighted by the determined variables given in Table 19. The factors f_{new} were assumed to consider any particularities concerning screw configurations and additional parameters that could not be specified so far. It is evident that the formulation essentially influenced f_{new}. Whereas f_{new} was very similar for the formulations with 20 and 60 % MCC amid a respective screw configuration, considerably higher ones were obtained for pure MCC. It can be assumed that swelling might have been the reason. Although pure MCC was only of academic interest, all f_{new} values were considered for the calculation of the finalised f_{new}.

Applying the finalised f_{new} revealed a substantial improvement in the prediction (Figure 34), but as it can be seen by the averages and their standard deviation, its application is generally a compromise. Whereas predictions and measurements fitted best only for pure MCC at screw setup CEs only with the previous version, using f_{new} of 1.36 in the edited one led to good match among all formulations. However, due to the described compromise, predictions of 3 and 4.5 kg/h PFR fitted slightly worse for pure MCC than with the previous version but were still sufficient. The other predictions were improved. Using screw configurations KB 30° and KB 60°, predictions matched measured mass hold-ups better than with the previous approach, except for bigger deviations with pure MCC, particularly at 3 and 4.5 kg/h PFR.

Despite everything, a strong positive correlation was found for the determined and predicted mass hold-ups (Figure 35, R=0.9745). It is indicated that the model generally underestimated the mass inside the barrel as the slope is distinctively above 1. It must be emphasized that the plot and thus its informative value is distorted by the results of pure MCC (green symbols). As depicted in Figure 34, much higher masses were determined at low screw speeds, which considerably affected the plot. However, too much importance should not be attached to the results of pure MCC since the investigation of pure MCC was only of academic interest and its exclusion would improve the correlation (y=1.0472x-1.4817, R^2=0.9734, R=0.9869, graph not shown).

The results presented in Figure 34 underlined above all the benefit of the non-linear curve fit as a tool to improve the predictability of mass hold-ups. Contrarily, the times of first detections would have been negatively affected when also applying the different finalised f_{new} values. However, at this stage of research, a conclusion cannot be drawn so far unless something different is proven. Thus, factor f of 1.50 should be kept for predicting t_1. According to that, the predictive terms for t_1 will therefore be revised as given in Eq. (26)

$$t_{1,theo} = \frac{l_{barrel}}{\bar{v}_{harmonic}} \cdot f = \frac{l_{barrel}}{\bar{v}_{harmonic}} \cdot 1.50 \qquad (26)$$

The prediction of mass hold-ups occurred as given in Eq. (25).

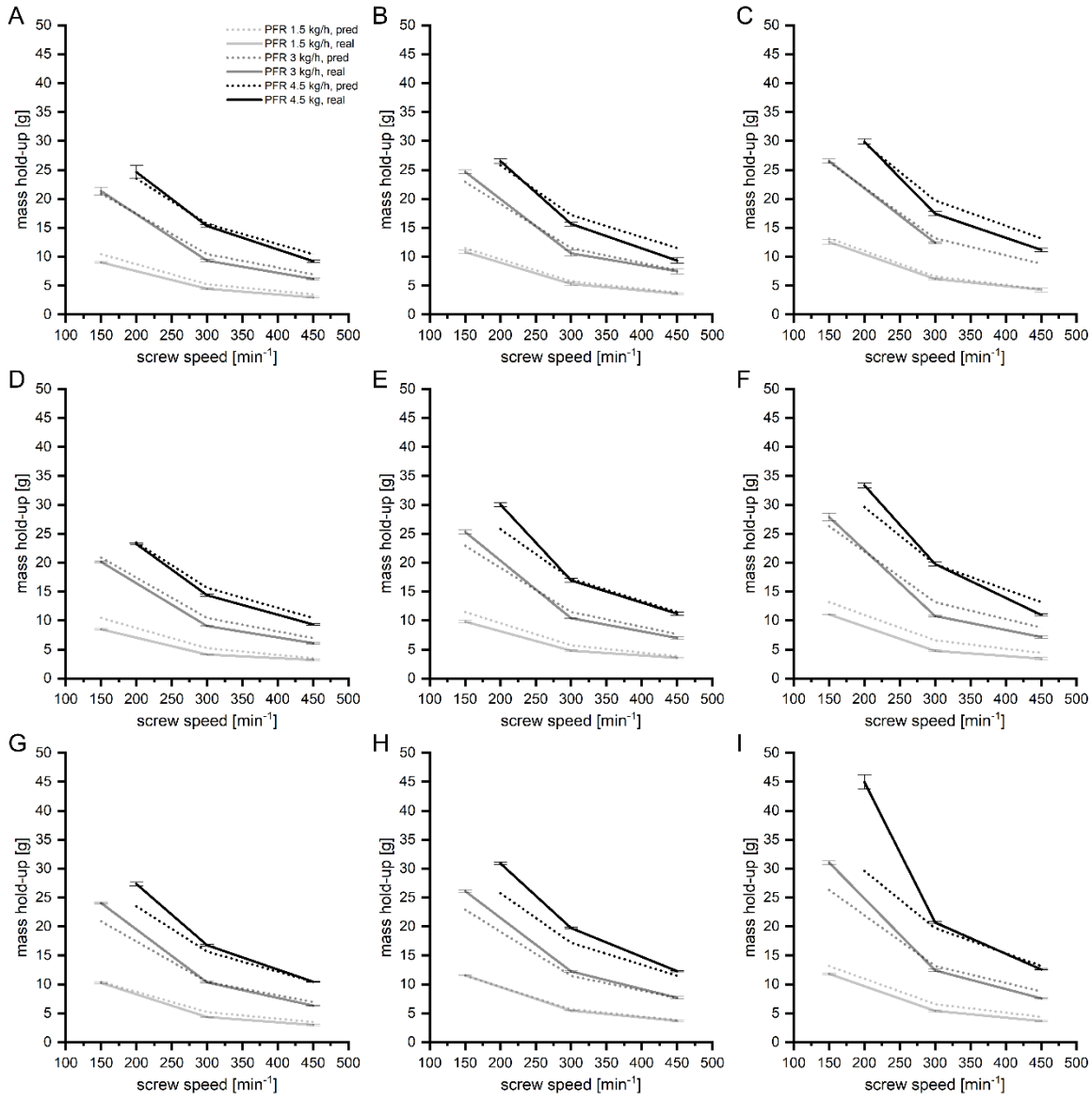

Figure 34. Predictions of mass hold-ups vs. reality of the different formulations A-C) 20:80, D-F) 60:40 and G-I) 100:0 mixture of MCC-DCP (% m/m) applying different screw setups: only CE (left), KB of 30° (middle) and 60° stagger angle (right) (n=5, mean ± s) with application of the finalised f_{new} (see Table 19).

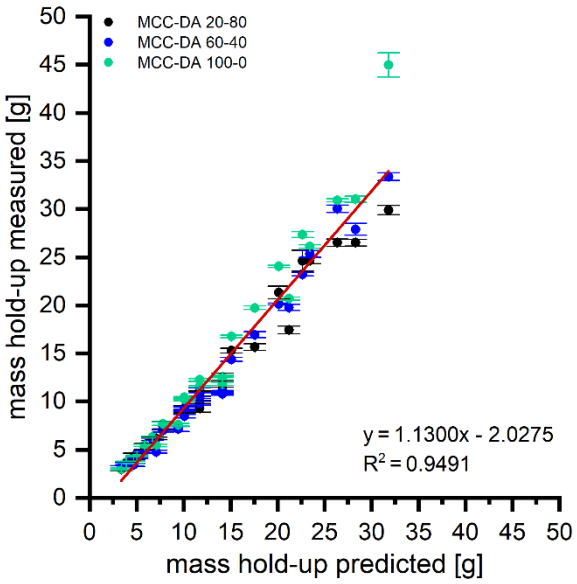

Figure 35. Correlation plot of predicted and measured mass hold-ups of all feed rates and screw setups investigated with the different compositions (n=5, mean ± s).

Additional validation occurred with published data when all required information, e.g. mass hold-ups, screw setups and process settings, was revealed. Sufficient information was provided for experimental studies conducted by Gorringe et al. [143] and Mundozah et al. [95]. A compilation of considered information can be found in Table 20. Fortunately, screw setup A and C of Mundozah et al. were entirely comparable to the screw design with a KB at 60° offset angle and CE only, respectively, used for the study described previously. In contrast to that, screw configuration B of Gorringe et al. was only assumed to be similar due to the presumption of the distributive feed screw (DFS), a small pitch CE (SPCE) with gaps, as KE at 60° offset angle. The DFS element was suspected to have lower conveying capacity than a normal SPCE [84] and probably even less than a KB of KE at 30° stagger angle. The other screw configurations of Gorringe et al. and Mundozah et al. were indeed different for comparison but were analysed for the sake of validation of the proposed model. However, similarly to the procedure described above, a factor f of 1.50 was applied and a non-linear curve fit was performed. Variable x was determined and finally f_{new} calculated.

The analysis of literature data strongly emphasized that a general, fixed factor is inappropriate as the manner of screw setup decisively influenced the transport velocity as well as barrel fill level [74, 81, 89] and thus material hold-up. It was indicated that with increasing complexity of screw design, f_{new} also increased (Table 20): from screw setup C of Mundozah et al. (PMMA and lactose monohydrate) to the screw setups A of Gorringe et al. and Mundozah et al. to screw setup B of Gorringe et al. to screw setup B of Mundozah et al. (lactose monohydrate). Although f_{new} values of screw setup C of Mundozah et al. based only on the examination of one PFR, they revealed lowest numerical values and confirmed the findings of the experiments conducted within our own study. It was guessed that material properties and process settings, e.g. PFR, had less effect on f_{new} for screw designs made up of only CEs, as the results obtained were very similar to the results of

the own experiments. In contrast, if more complex screw setups were used like screw setup B of Mundozah et al., a huge variability of f_{new} with strong likelihood of material dependency (f_{new} of 2.1 vs. 2.6, respectively) was revealed. However, the examination based on one throughput only, which could bias the calculation. Higher variability was also observed for the more complex designs of configuration A of Mundozah et al. and B of Gorringe et al., which was caused by an outlier of f_{new} of one material throughput that distorted the finalised f_{new} value.

Figure 36 depicts the finalised f_{new} values determined for the different formulations in the different studies as a function of the number of KEs at 60° stagger angle. As it can be guessed, f_{new} increased with the incorporation of more KEs into the screw setup and displayed a good correlation. The correlation coefficient R of 0.9726 (Figure 36) revealed a strong, positive linear relationship. Since a broader spectrum of screw setups and formulations were included, the functional equation has a broader validity in general and could therefore be used for the calculation of correction factors for a screw configuration with different numbers of KEs at 60° offset angle. Nevertheless, the validity is limited to the same type of granulator (same barrel diameter, same manufacturer) and to screw setups with KEs at 60° stagger angle. Due to the limited number of studies, a correlation plot for other screw setups was not possible, not to mention a universal one including all screw types which should be aimed.

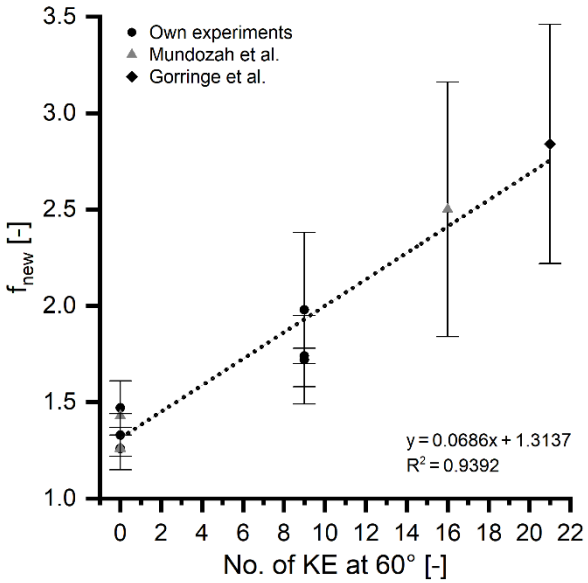

Figure 36. Correlation of the finalised f_{new} values obtained with screw setups of CE only (0 KE) or KEs at 60° stagger angle. No other screw configurations with other offset angles considered. No consideration of results that had been obtained at only one throughput rate. All values are mean values (n= to be taken from Table 20).

For verification of the correlation (Figure 36), mass hold-ups were determined for the process transfer experiments described in section 3.2.4. Determination occurred six times at each process setting, while times of first detections were determined in accordance with section 5.2.1.3. The theoretical values were calculated according to Eqs. (25) and (26). Several further examinations conducted for the thesis at hand were taken into consideration to check the improved model on

its predictability of t_1. Some experiments were not specifically described in this thesis, but were conducted in my PhD. An overview of the experiments taken for verification and the results can be found in Table 21.

The calculated f_{new} and thus the results of predicting mass hold-ups revealed to be promising. Unfortunately, the mass hold-up measured at 0.56 kg/h PFR at 196 min^{-1} (low fill level) was almost 24 % below prediction and showed lack of predictability. Increasing predictive accuracy was observed with increasing fill level resulting in a hold-up of about 5.7 % more than predicted at 2.79 kg/h PFR at 135 min^{-1} (high fill level). Nevertheless, the absolute difference revealed rather good approximations of predictions and reality. In contrast, the measured t_1 values fitted the predictions well for the processes at 0.56 kg/h PFR at 196 min^{-1} and 1.40 kg/h at 118 min^{-1} supporting the assumption of successful application of factor of 1.50 when predicting t_1. However, much shorter run-through times were predicted at high fill level. It can be guessed that a critical threshold of barrel fill was exceeded above which transportation velocity decreased due to increased restrictions in material flow, restricted particle movement and decreased axial mixing [81, 89, 135]. Thus, a delay in t_1 could result, which is also indicated by the results depicted in Figure 33C, F and I, where the measured values were almost always higher at higher PFR and lower screw speed than predicted. In addition, a formulation dependency is likely to affect the results, which is why further examinations should focus on that as well. Almost identical observations could be made for other experiments conducted within the frame of this thesis and discussed previously in detail, independently of the granulator or screw length (Table 21). Interestingly, the absolute difference between the predicted and measured t_1 was again bigger with increasing fill level. However, at higher screw speeds, the extent of the differences generally decreased. Contrarily, experiments performed on the QbCon®1 revealed an opposite trend. At low barrel fill, t_1 determined was smaller than predicted, but predictability increased with increasing fill level. Furthermore, Meier et al. [93] kindly provided data of RTD measurements which were also used for verification. The screw configuration contained amongst others a distributive element (DE) without transport capacity which is why KEs at 90° offset angle were presumed instead (Table 21). RTD measurements were performed in the study at the different process settings, but only once which led to a higher uncertainty. Whereas the model underestimated the t_1 values in the own conducted experiments, no such clear trend could be observed for the data of Meier et al. [93]. The measured values scattered around the predicted ones and the impact of barrel fill level on t_1 values could not be seen. Nevertheless, the matches of prediction and reality were, with some exceptions, quite impressive. The approximation of a DE to be considered as KEs at 90° offset seemed to be applicable at a first glance, but future model development should ideally deal with the probable impact of the real screw elements used in the configuration. However, the suitability of the chosen approximation was convincing.

The results basically emphasized the suitability of 1.50 as factor for the calculation of t_1 as given in Eq. (26), independently of the granulator and screw length used in the different studies. However, the validity of the proposed model is still confined at this level of research.

All in all, it can be said that the analysis of the studies strongly suggested that screw setup is a key factor in mass hold-ups that, on the other hand, cannot be considered solely, but only in combination with the other influencing factors listed in the introduction. The own conducted experiments clearly revealed an increase in mass hold-ups with increasing screw complexity, but to a different extent and depending on the actual throughput. The extent of hold-up was less distinctive at low PFR (1.5 kg/h) whereas more pronounced at higher PFRs (3.0 and 4.5 kg/h) (Figure 32, from CE only to KB 30° to KB 60°). As guessed from Figure 33, a deceleration of a materials throughput speed might be a consequence of higher screw complexity which finally increased the amount of material remaining in the barrel [74, 81, 89, 109]. Nevertheless, such a trend could not explicitly be extracted for the mass hold-ups taken from publications (see Table 38 in the appendix), that either arose from the estimations of mass hold-ups from figures given in the research papers, from less comparable parameters taken for the study performance and/or the shorter barrels used in that respective studies. However, the barrel length itself might influence the remains of material inside the barrel, particularly at higher throughputs, which could become more dominant if longer barrels are used.

An important step towards a (dimensionless) description of a barrel fill level had been achieved with the estimation of mass hold-ups and times of first detection at given process conditions. Although the results were encouraging, further research on other twin-screw granulators of different dimensions is inevitable, which will reveal if the current version in predicting t_1 and mass hold-ups still provide sufficient results. Furthermore, any unspecified parameter that has so far been included unspecified in the preliminary determined factor f of 1.50 for the times of first detection and the variable f_{new} for the mass hold-ups should be uncovered and determined at best. The number of repetitions of the examinations should be at least three, performed at different days with newly prepared formulations for specific screw configurations at defined process settings to determine a usual deviation of results on the one hand as well as to better estimate the fit of predicted values with the measured ones.

Table 20. Compilation of literature data considered for model validation. Factor f_{new} determined with non-linear curve fit for the given materials and respective screw configurations (as well as their approximation). The finalised factors f_{new} were the overall means of all determined factors f_{new} (*n=1; **n=9, mean ± s). The underlined screw speeds were examined in the respective publication, but mass hold-up data were not revealed.

Source	Formulation	Granulator	Screw configuration	Consideration of screw particularities	PFR [kg/h]	$\dot{m}_{tot}$ [kg/h]	n [min^{-1}]	f_{new}* [-]	Finalised f_{new} [-]
Gorringe et al. [143]	Lactose monohydrate, MCC 101, HPMC, croscarmellose sodium	16 mm Prism Euro Lab Twin-Screw Granulator (Thermo Fisher) l_{barrel}: 400 mm (25D)	Screw A: 2x 7x0.25D KE 60°, 1x 3x0.25D KE90°, rest CE	2x 2D LPCE at the beginning (infeed zone) because not disclosed in publication	1.5	1.76	60-150-300-500	2.45	2.50 ± 0.04**
					3.0	8.75	110-200-500	2.52	
					6.0	17.50	300-500	2.53	
			Screw B: 1x 9x0.25D KE 60°, 1x DME (0.25D KE), 3x 1D DFS, rest CE	2x 2D LPCE at the beginning (infeed zone) because not disclosed in publication, 1D DFS (SPCE with gaps) as 4x0.25D KE 60° due to lower transport capacity due to the gaps, DME (probably a single KE) kept unconsidered as it was not revealed at what offset angle this element was set – the impact of non-consideration was assumed to be negligible.	1.5	1.76	55-100-250-300-500	2.34	2.84 ± 0.62**
					3.0	8.75	130-200-500	3.53	
					6.0	17.50	300-400-500	2.66	
Mundozah et al. [95]	Polymethyl methacrylate (PMMA)	16 mm Prism Euro Lab Twin-Screw Granulator (Thermo Fisher) l_{barrel}: 400 mm (25D)	Screw A: 2x 8x0.25D KE 60°, rest CE (2x2D LPCE, rest SPCE)	-	1.0	1.10	100-300-500-900	3.24	2.50 ± 0.66**
					2.0	2.20	100-300-500-900	2.27	
					3.0	3.30	100-300-500-900	1.99	
			Screw B: 1x 4x0.25D KE 60°, 1x 2D LCE, 4x 0.5D nTME, 4x 0.5D wTME, rest CE (2x2D LPCE, rest SPCE)	1x 2D LCE (LPCE with gaps) as 2x 1D SPCE due to lower transport capacity due to the gaps, 4x 0.5D nTME and wTME as 16x 0.25D KE 90°	1.0	1.10	100-300-500-900	2.14	2.14*
			Screw C: Only CE (2x2D LPCE, rest SPCE)	-	1.0	1.10	100-300-500-900	1.26	1.26*

Source	Formulation	Granulator	Screw configuration	Consideration of screw particularities	PFR [kg/h]	$\dot{m}_{tot}$ [kg/h]	n [min^{-1}]	f_{new}* [-]	Finalised f_{new} [-]
Mundozah et al. [95]	Lactose monohydrate	16 mm Prism Euro Lab Twin-Screw Granulator (Thermo Fisher) l_{barrel}: 400 mm (25D)	Screw A: see above	-	1.0	1.10	100-300-500-900	3.88	3.88*
			Screw B: see above	see above	1.0	1.10	100-300-500-900	2.62	2.62*
			Screw C: see above	-	1.0	1.10	100-300-500-900	1.43	1.43*

Table 21. Model verification (n.d.: not determined). Variable f_{new} was calculated using the functional equation given in Figure 36 (*n=6, **n=5, mean ± s; ***n=1).

Source	Formulation	Granulator	Screw configuration	PFR [kg/h]	n [min^{-1}]	f_{new} [-]	Mass hold-up theory [g]	Mass hold-up measured* [g]	Relative deviation [%]	t_1 theory [s]	t_1 measured** [s]
Section 5.2.3.7 Process transfer	Lactose monohydrate, MCC 101, PVP K30	Pharma 16 l_{barrel}: 640 mm (40D)	Screw A: 2x 7x0.25D KE 60°, rest CE	0.56	196	2.27	4.81	3.66 ± 0.35	-23.93	17.3	17.9 ± 0.8
				1.4	118	2.27	19.99	17.70 ± 0.92	-11.45	28.8	33.5 ± 0.5
				2.79	135	2.27	34.83	36.82 ± 1.25	5.73	25.1	32.6 ± 0.5
		QbCon®1 l_{barrel}: 500 mm (20D)	2x 6x0.15D KE 67.5°, rest CE	0.5	123	-	-	n.d.	-	17.6	12.9 ± 1.8
				1.25	74	-	-	n.d.	-	29.2	28.7 ± 2.4
				2.5	85	-	-	n.d.	-	25.4	24.7 ± 1.4
		Leistritz Micro 27 GL-28D l_{barrel}: 810 mm (30D)	2x ready-to-use KB (each 5 KE 60°), rest CE	0.8	106	-	-	n.d.	-	22.3	22.2 ± 0.5
				2.0	64	-	-	n.d.	-	34.8	35.2 ± 3.1
				4.0	74	-	-	n.d.	-	30.5	38.5 ± 0.5
Section 5.2.3.7 Process transfer	PCM, Lactose monohydrate, MCC 101, PVP K30	QbCon®25 l_{barrel}: 500 mm (20D)	2x 6x0.15D KE 67.5°, rest CE	4.0	200	-	-	n.d.	-	10.8	8.8 ± 1.0
				6.0	300	-	-	n.d.	-	7.2	6.4 ± 0.2
		Pharma 16 l_{barrel}: 640 mm (40D)	Screw B: 1x 5.5x0.25D KE 60° and 1x 6x0.25D KE 60°, rest CE	4.0	291	-	-	n.d.	-	11.7	13.0 ± 0.3
				4.4	321	-	-	n.d.	-	10.6	12.2 ± 1.0
				4.8	349	-	-	n.d.	-	9.8	11.3 ± 0.5
				6.6	482	-	-	n.d.	-	7.1	7.9 ± 0.6
-	PCM, lactose monohydrate, MCC 101, PVP K30	Pharma 16 l_{barrel}: 640 mm (40D)	Screw B: 1x 5.5x0.25D KE 60° and 1x 6x0.25D KE 60°, rest CE	2.0	350	-	-	n.d.	-	9.7	8.7 ± 0.5
		QbCon®25 l_{barrel}: 500 mm (20D)	2x 6x0.15D KE 67.5°, rest CE	3.5	182	-	-	n.d.	-	11.9	11.3 ± 0.4
				5.0	151	-	-	n.d.	-	14.3	15.3 ± 0.3
Section 5.2.3.9 Impact of screw	Lactose monohydrate, MCC 101, PVP K30	Pharma 16 l_{barrel}: 640 mm (40D)	2x 7x0.25D KE 60°, rest CE	1.5	150	-	-	n.d.	-	22.63	25.1 ± 1.3
				3.0	150	-	-	n.d.	-	22.63	30.2 ± 0.
		Pharma 16 l_{barrel}: 512 mm (32D)	2x 7x0.25D KE 60°, rest CE	1.5	185	-	-	n.d.	-	17.34	17.6 ± 0.5
				3.0	185	-	-	n.d.	-	17.34	20.8 ± 0.6

Source	Formulation	Granulator	Screw configuration	PFR [kg/h]	n [min^{-1}]	f_{new} [-]	Mass hold-up theory [g]	Mass hold-up measured* [g]	Relative deviation [%]	t_1 theory [s]	t_1 measured** [s]
		Pharma 16 l_{barrel}: 384 mm (24D)	2x 7x0.25D KE 60°, rest CE	1.5 3.0	240 240	- -	- -	n.d. n.d.	- -	8.14 8.14	10.0 ± 0.3 11.9 ± 0.4
Meier et al. [93]	Hydrochlorothiazide, sodium starch glycolate, colloidal silica	Pharma 16 (Thermo Fisher Scientific) l_{barrel}: 640 mm (40D)	1x 5x0.25D KE 60° and 1x 7x0.25D KE 60°, 1x 1D DE, 2x 2D LPCE at the beginning, rest SPCE Consideration of particularities: 2x 0.25D KE used as spacer in front of LPCE kept unconsidered, DE as 4x 0.25D KE 90°	1.62 4.33 4.06 10.81 1.86 8.54 2.05 8.36 5.20 5.20 5.20 1.13 3.79 6.62	200 200 500 500 350 350 138 562 350 350 350 350 350 350	- - - - - - - - - - - - - -	- - - - - - - - - - - - - -	- - - - - - - - - - - - - -	- - - - - - - - - - - - - -	17.03 17.03 6.81 6.81 9.73 9.73 24.69 6.06 9.73 9.73 9.73 9.73 9.73 9.73	13.9*** 18.9*** 5.3*** 8.8*** 7.3*** 4.3*** 26.1*** 6.5*** 9.9*** 9.3*** 9.5*** 7.3*** 9.1*** 10.3***

3.4.5 Critical assessment of already proposed approaches for the prediction of barrel fill levels

In this section, the proposed attempts for predicting barrel fill levels during TSG are critically evaluated, although every attempt marked an important step towards a final predictive model. When the equations are introduced, the variables described in the literature are, if appropriate, converted into the terminology used in the thesis at hand to improve comprehension.

One of the first attempts in dimensionless prediction of barrel fill in twin-screw granulations has been introduced by Osorio et al. [66] and is given in Eq. (27)

$$\varphi_{Osorio} = \frac{1}{F_1 \cdot F_2 \cdot F_3} \cdot PFN = \frac{1}{\frac{A_{element}}{d_{barrel}^{\,2}} \cdot \frac{l_{element}}{d_{barrel}} \cdot \frac{2\pi \cdot v_p}{\omega \cdot l_{element}}} \cdot \frac{\dot{m}_p}{\rho_{bulk} \cdot \omega \cdot d_{barrel}^{\,3}} \qquad (27)$$

where φ_{Osorio} is the barrel fill level, $A_{element}$ is the free cross-sectional area of the element, v_p is the solids net forward velocity, $\dot{m}_p$ is the powder flow rate, ρ_{bulk} is the bulk density of the powder, ω is the angular velocity of the screw shaft, the term $\omega/2\pi$ is the screw speed, F_1-F_3 are screw element-related dimensionless ratios that consider particularities of the screw geometry and *PFN* is the powder feed number which is the ratio of the volumetric flow rate to the volume turnover at given powder feed rate and screw speed. F_1 is a geometric ratio of based on the fraction of the free cross-sectional area of the barrel when the occupied fraction of screw element and shaft were subtracted, F_2 is the length-to-diameter ratio and F_3 is a velocity ratio of the powder to the screw element surface.

The overall equation and its variables appear clear and logical. The intention of F_3 was to meet the circumstances that the powder moves slower than the screw flight due to wall slippages of the powder and thus resulting back mixing processes [66]. However, as the extent of wall slippage could not be quantified, v_p was only estimated and thus set arbitrarily which finally lowered the applicability of the approach as the real filling degree could not be defined at this level of current development. Therefore, focus was laid on the PFN in the study to quantify barrel fill level [66]. Investigations occurred at three PFNs. Unfortunately, the PFN had only a minimal effect on the granule sizes and broadened GSD only slightly with increasing PFN and provided an ambiguous effect on granule porosity.

In addition to that, although d_{barrel}^3 should reflect a volume, in TSG it is rather imprecise as the real dimensions of a barrel are not reflected. Mundozah et al. [95] assumed the consideration of d_{barrel}^3 only for the purpose of creating a dimensionless number. It can be presumed that the usage of the actual empty volume of the screw configurations used on different granulators could facilitate the usability of the powder feed number.

A more practical attempt was provided by Gorringe et al. [143], who calculated the fraction of the channels of conveying elements filled with powder as the ratio of mass flow rate and theoretical maximum screw capacity according to Eq. (28)

$$\varphi_{Gorringe} = \frac{\dot{m}_p}{\eta_v \cdot \bar{\rho}_{bulk} \cdot \left(V_{free} \cdot \frac{l_{lead,screw}}{l_{screw}} \right) \cdot n} \tag{28}$$

where $\varphi_{Gorringe}$ is the barrel fill level, η_v is the volumetric efficiency of the screw to convey the material, $\bar{\rho}_{bulk}$ is the mean bulk density of the material in the screw channels, V_{free} is the conveyor free volume, $l_{lead,screw}$ is the lead length of the elements and l_{screw} is the screw length.

For the mean bulk density, the liquid was assumed to be absorbed into the voids of the powder and thus having an effect on the bulk density. The term $V_{free} \cdot l_{lead,screw}/l_{screw}$ in the denominator of Eq. (28) mirrors the theoretical volume displacement per screw turn. Although not specifically stated, it should be obvious that the variables in the brackets must be related to a screw unit that covers one turn. However, Gorringe et al. [143] as well as the studies applying the same approach (where Gorringe was co-author) [94, 96] always used the term "screw" which might lead to confusion, but since the focus was on volume displacement per rotation, V_{free}, $l_{lead,screw}$ and l_{screw} are assumed to be the same as $V_{free,element}$, l_{lead} and $l_{element}$, respectively, that were used in this thesis. It must be highlighted that V_{free} was determined for a screw configuration consisting of only conveying elements, which appears logical on the one hand if the volumetric efficiency of a screw setup was without flow hindrances and other particularities should be determined. However, it is questionable why V_{free} was not determined for the other screw setups used in the studies [94, 96, 143].

The volumetric screw efficiency for material transport was assumed to be less than 100 %, due to the wall slippage of the material. Although the density was likely to vary along the screw axis, both parameters, η_v and $\bar{\rho}_{bulk}$, were assumed constant when process steady state was achieved [143]. Initially, the process was operated at a mass flow rate and screw speed at which the channel fill was assumed to reach its maximum. Based on this, φ was set 1. The $\eta_v \bar{\rho}_{bulk}$-term was calculated afterwards [94]. Mass hold-ups were determined additionally in numerous experiments at different material throughputs and screw speeds. Strong correlations of mass hold-ups and φ were revealed and the product of η_v and $\bar{\rho}_{bulk}$ was implied to be constant. The y-intercept of the functional equation was related to the additional mass hold-up due to screw particularities, e.g. KBs at different stagger angles, DMEs and DFS, in the respective screw setup at defined liquid contents [143].

One of the main drawbacks of the approach is the estimation of η_v which lowers its practical realization [95]. It must be kept in mind that decisioning when the granulator works at its maximum capacity is rather subjective. This could have been avoided if the approach of Srivastava et al. [156] introduced for agricultural screw conveyors would have been considered to calculate the volumetric efficiency for screw setups made up of conveying elements only which is given in Eq. (29)

$$\eta_v = \frac{Q_a}{Q_t} = \frac{\frac{\dot{m}}{\rho_{bulk}}}{\frac{\pi}{4} \cdot \left({d_{element}}^2 - {d_{inner}}^2\right) \cdot l_{lead} \cdot n} \tag{29}$$

where Q_a is the actual volumetric capacity, Q_t is the theoretical volumetric capacity, $d_{element}$ is the outer diameter of the screw elements and d_{inner} is the inner diameter of the screws. The term $\pi/4 \cdot (d_{element}^2 - d_{inner}^2) \cdot l_{lead}$ reflects the volume of a cylinder which is moved per rotation.

However, when flow-resisting elements were incorporated, Eq. (29) would not easily be applicable as such particularities are not covered mathematically. However, the maximum screw capacity could have been determined more precisely. Based on this, if the term $\dot{m}_p \bar{\rho}_{bulk}^{-1}$ in Eq. (28) is assumed to reflect the actual volumetric capacity, Q_a, and (if we stick to the same terminology) $V_{free,element} \cdot n$ reflects the volume displaced per screw rotation, Q_t, the volumetric efficiency would have already been implemented by Gorringe et al. [143]. Thus, Eq. (28) could be rewritten as given in Eq. (30)

$$\varphi_{Gorringe} = \frac{Q_a}{Q_t} \cdot \frac{1}{\eta_v \cdot \left(\frac{l_{lead,screw}}{l_{screw}}\right)} = \eta_v \cdot \frac{1}{\eta_v \cdot \left(\frac{l_{lead,screw}}{l_{screw}}\right)} = \frac{1}{\left(\frac{l_{lead,screw}}{l_{screw}}\right)} \tag{30}$$

Therefore, the entire approach is distorted by the denominator of the second fraction, which makes it even less comprehensible and convincing.

The results of similar GSD curves obtained at similar φ values at different combinations of powder feed rates and screw speeds for different screw configurations investigated may emphasize the suitability of the proposed attempt, but the uncertainty in determining the volumetric efficiency makes the overall approach vague. The extent of uncertainty should be less decisive when all experiments are performed on the same granulator [94, 96, 143]. When the same fill level has been set by considering the same uncertainty, the GSDs should roughly be similar. However, this uncertainty would become dominant if a second granulator of different dimension is used to check the validity. Besides, it is recommended to put effort into the quantification of boundaries for flooded or starved barrel fill conditions [143], as these terms can otherwise easily be used arbitrarily. The attempt generally lacks validity, especially without the usage of another granulator. A similar conclusion has already been drawn by Mundozah et al. [95].

The mean residence time of a material inside the barrel was additionally estimated from material hold-up and actual mass throughput as shown in Eq. (31) [143]

$$t_{mean_{Gorringe}} = \frac{m_H}{\dot{m}_p} \tag{31}$$

where m_H is the material hold-up at given process conditions.

Unfortunately, the theoretically calculated t_{mean} and the measured ones were neither disclosed nor compared or critically discussed to evaluate the suitability of Eq. (31). However, the approach appears to be smart if the equation can accurately describe the process.

The next step in fill level prediction was provided by Mundozah et al. [95], who related the volumetric flow rate to the forward volumetric conveying rate of the screws as shown in Eq. (32)

$$\varphi_{Mundozah} = \frac{v_t}{v_a} = \frac{\frac{\dot{m}}{\rho_{bulk} \cdot A_m}}{\frac{l_{eff}}{t_1}} \tag{32}$$

where v_t is the theoretical velocity, v_a is the true velocity, A_m is the mean cross-sectional area and l_{eff} is the effective length. The bulk density was assumed to be constant for the sake of simplicity. The effective length was calculated as followed

$$l_{eff} = l_{total} - 2 \cdot l_{SPCE} = d_{element} \cdot \frac{l_{barrel}}{d_{barrel}} - 2 \cdot l_{SPCE} \tag{33}$$

where l_{total} is the total length of the granulator and l_{SPCE} is the length of a conveying element with short pitch.

The manner of calculating l_{eff} has to be criticised as the multiplication of the outer screw diameter ($d_{element}$) with the L/D ratio of the barrel leads to a smaller value, which does not correspond to the overall length. Confusion might increase when looking at the table of the parameter compilation (Table 1 in [95]). The outer diameter of the screw elements is not considered anymore but probably replaced by the diameter of one circle of each screw, D_c, which presumably represents the outer diameter according to the schematic drawing of the screws geometry profile (see Figure 5 in [95]). Additionally, D_c is given with 16 mm. Provided that no custom-made barrel design was available, construction and design of the granulators Pharma 16 (as used in the thesis) and Euro lab 16 (as used in the study) are identical according to Thermo Fisher Scientific (Germany). Thus, element diameter should be less than 16 mm. However, the given 16 mm for D_c (in Table 1 in [95]) indicated that the barrel diameter, d_{barrel}, was probably meant instead of $d_{element}$ which would prove that the total barrel length in mm was the real aim of Eq. (33). This confusion could have been avoided if it was clearly stated.

The granulation zone is of particular interest as granulation takes place once the liquid binder has wetted the powder and nuclei are formed. The screw setups used always started with two SPCEs followed by two LPCEs (long pitch conveying elements) but powder infeed occurred onto the LPCEs and liquid infeed after the two LPCEs in the area of another SPCE section. Therefore, the initial SPCEs do not contribute to granulation. However, since liquid addition occurred after the LPCE area, granule formation starts from there on. Although the attempt focused on the granulation zone, it is less plausible why only the lengths of the SPCEs were subtracted.

The free volumes of the given screw configurations were incorrectly depicted as the units of the volumes of the screw elements, determined by liquid displacement measurements, were incorrect (mm^3 instead of cm^3). However, the incorrect volumes were probably not decisive as these were not used subsequently but using the free volumes would be advisable, as the approach could thus better represent the real conditions.

The theoretical velocity, v_t (see Eq. (32)), gives the impression that it might reflect a real velocity that could be verified by experiments and used for model improvements. However, except for the units it does not reflect a velocity but rather a volumetric flow rate coincidentally related to the mean cross-sectional area. Thus, v_t is influenced by material throughput and screw geometry. The ineffectiveness of v_t was proven by the values given in Table 2-4 in [95], which were constant at given powder feed rates and screw configurations, despite the fact that different screw speeds (100, 300, 500 and 900 rpm) were applied.

Nevertheless, characterising the extent of granulation by relating x_{50} of the granules to that of the starting material was a smart idea as it may help to define boundaries for granule growth based on the size of the starting material. It would additionally be helpful if the extent of granule growth would be extended by including the respective ratios of x_{10} and x_{90}. Furthermore, filling conditions, e.g. starved, intermediate and flooded, were used in the discussion. The determination of boundaries would be helpful to better differentiate observations and results.

The attempt created during this thesis and introduced in section 3.4 aimed at considering the transportation velocity of the wet mass as well as screw elements that lower the velocity and led to more material inside the barrel. Based on the experiments and validation with literature data together with the insights of the other approaches discussed above, improvements were made to increase model predictability. The final version of the model is depicted in Eq. (34)

$$\varphi = \frac{\dot{m}_{tot}}{\bar{\rho}_{tapped}} \cdot \frac{l_{barrel}}{\bar{v}_{harmonic}} \cdot 1.50 \cdot x \cdot \frac{1}{V_{free}} = \frac{\dot{m}_{tot}}{\bar{\rho}_{tapped}} \cdot \frac{l_{barrel}}{\bar{v}_{harmonic}} \cdot f_{new} \cdot \frac{1}{V_{free}} \qquad (34)$$

It was decided to consider the mean tapped density instead of the true density as this might coincide best with reality. In addition, the tapped density was assumed to remain constant in the barrel, although it is likely to change when passing particular screw elements that cause breakage, consolidation, coalescence and growth [95]. However, a simplification at the current level of knowledge was necessary.

Prediction of mass hold-ups of the adjusted model were more accurate than of the very first version. A lack of predictability was still obtained for some process conditions, with an increasing deviation with increasing amount of MCC (see Figure 34). Nevertheless, when mass hold-ups were related to their respective dimensionless fill levels (calculated according to Eq. (34) and finalised f_{new} values used from Table 19, a positive trend was revealed for all formulations (Figure 37). The slope was the steepest for 20 % MCC content and lowest for pure MCC. Since the mean tapped densities of the compositions were responsible for this steepness effect (20 % MCC: 1.336 g/cm^3, 40 % MCC: 0.786 g/cm^3, 100 % MCC: 0.564 g/cm^3), the slopes themselves had no additional value. Even th ough the linearity was good, a slightly curved shape was still implied. Since barrel fill conditions are commonly denoted as starved or flooded, initial hope was to be able to delineate such different filling states based on the curve appearance, but boundaries probably have to be set on the basis of granule properties and their changes with changing barrel fill levels. In its latest version, the model has provided reliable predictions that encourage its use in twin-screw

granulation. However, similarly to the other attempts described above [95, 143], model validity must be tested on further granulators of different dimensions.

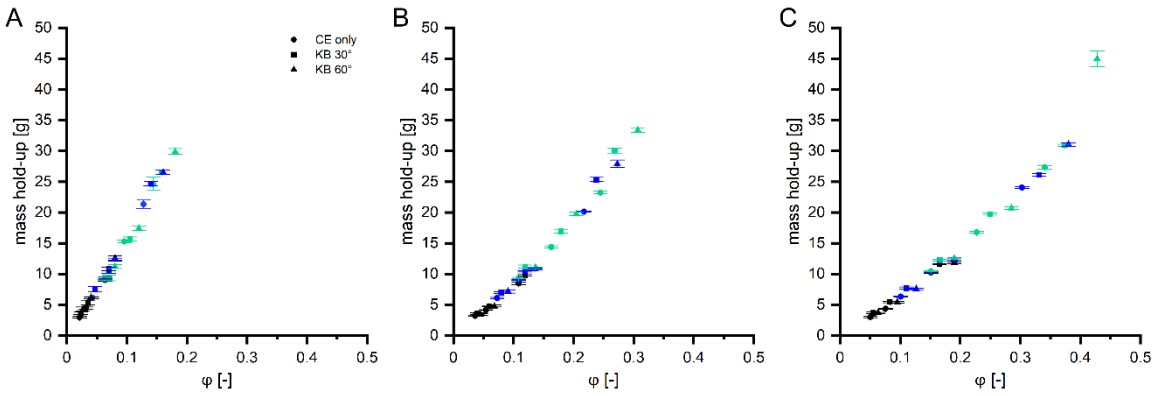

Figure 37. Mass hold-ups of the different compositions at different throughputs (black: 1.5 kg/h, blue: 3 kg/h, green: 4.5 kg/h) related to the respective dimensionless barrel fill: A) MCC-DCP 20-80, B) 60-40 and C) 100-0 (n=5, mean ± s).

In contrast, prediction of t_1 values using the general factor of 1.50 not only revealed very good fits among all process conditions, screw configurations and formulations investigated, the inclusion of the QbCon®25 and Leistritz Micro 27 GL-28D for verification also proved its applicability, reliability and utility of the model in general.

Independent of the findings described above, t_{mean} might generally be a better choice for assessing a granulation process than t_1. Despite the fact that the model is not being able to predict mean residence times, the overall prediction could be expanded by additionally applying Eq. (31). It was decided to use predicted mass hold-ups for calculation instead of the determined ones as it may ease the overall process. An exemplary depiction of predicted times according to Gorringe et al. [143] compared to the measured ones in the study for the MCC-DCP composition 20-80 can be found in Table 22. Interestingly, the results showed that although the calculation of t_{mean} was intended, the prediction of t_{peak} rather than t_{mean} was made, which could be shown for all formulations, screw configurations and process settings, with only a few exceptions. The measured values of t_{peak} matched the predictions well.

Table 22. Exemplary data of predicted times using Eq. (31) for formulation containing 20 % MCC in comparison to t_{peak} and t_{mean} obtained from RTD measurements (n=5, mean ± s).

Screw configuration	PFR [kg/h]	n [min^{-1}]	$t_{predicted}$ [s]	t_{peak} measured [s]	t_{mean} measured [s]
Only CE	1.5	150	25.1	26.0 ± 1.5	32.7 ± 1.5
		300	12.5	12.5 ± 1.2	20.0 ± 0.9
		450	8.4	9.2 ± 1.2	14.8 ± 1.3
	3.0	150	25.1	25.2 ± 0.7	27.3 ± 0.3
		300	12.5	11.8 ± 0.7	15.2 ± 0.4
		450	8.4	9.0 ± 0.4	12.5 ± 1.0
	4.5	200	18.8	18.1 ± 0.3	21.6 ± 0.3
		300	12.5	11.9 ± 0.3	14.4 ± 0.9
		450	8.4	7.6 ± 0.3	10.1 ± 0.8
KB 30°	1.5	150	27.5	26.7 ± 0.5	37.0 ± 0.9
		300	13.8	14.6 ± 0.7	25.3 ± 0.5
		450	9.2	10.9 ± 0.4	20.3 ± 1.3
	3.0	150	27.5	28.6 ± 0.4	40.6 ± 2.1
		300	13.8	14.0 ± 0.3	27.1 ± 1.1
		450	9.2	10.1 ± 0.5	16.7 ± 1.0
	4.5	200	20.6	21.3 ± 0.2	30.9 ± 0.4
		300	13.8	13.8 ± 0.2	22.2 ± 1.8
		450	9.2	9.4 ± 0.5	19.2 ± 1.2
KB 60°	1.5	150	31.6	29.6 ± 0.6	38.6 ± 1.5
		300	15.8	14.7 ± 0.6	21.4 ± 1.8
		450	10.5	10.6 ± 0.7	17.1 ± 1.3
	3.0	150	31.6	28.3 ± 1.1	39.8 ± 1.0
		300	15.8	15.9 ± 0.8	22.6 ± 1.0
		450	10.5	-	-
	4.5	200	23.7	20.8 ± 0.5	31.0 ± 2.6
		300	15.8	14.9 ± 0.4	24.7 ± 1.7
		450	10.5	9.6 ± 0.1	14.9 ± 0.6

It could be proven that the model headed into the right direction. The implementation of the materials conveying velocity throughout the barrel by considering the transport characteristics of the elements used in the screw setup was a good start. The newly created model enables the quantification of material remaining inside the barrel, which could improve the understanding of the actual fill level and is to my knowledge the first of its kind. The improvement by non-linear fitting and the verification with literature data enabled the development towards its current version and allowed good predictions of both mass hold-ups and times of first detections. It could be shown that there is a linear relationship of mass hold-ups with increasing number of kneading discs at the same stagger angles. However, although the attempt introduced in this section marks a step forward, numerous experiments are still needed to validate linear relationships for other stagger angles and to find a solution for screw setups with varying stagger angles or non-conveying elements. The current model might be a good start for upcoming experiments and improvements.

3.4.6 Summary

A new predictive model for the dimensionless quantification of barrel fill level was developed that considered the transportation velocity of the wet mass throughout the barrel for varying screw configurations at defined process conditions. For this, the geometries of the different elements and their axial conveying capability were determined. The flow hindering characteristic of kneading blocks and the resulting material hold-up was attempted to be described mathematically. Applying non-linear fitting with own and literature data improved model predictability considerably and led to accurate prediction of masses remaining in the barrel as well as their times of first detection during RTD measurement.

The calculated dimensionless fill levels showed a positive linear relationship to the mass hold-ups measured at the different process conditions for the varying compositions and screw setups. Its applicability was further successfully tested on several other granulation processes from other studies, including granulators of other dimension as well, and could convince with its predictive strength. Nevertheless, a classification in different fill conditions, e.g. flooded or starved, could not be done based on the results. It can be assumed that granule characteristics and their changes at different fill levels might encourage differentiation.

In comparison to the attempts that have already been proposed, a major a step forward was done with the creation of the new model, as it provided a comprehensive strategy, logical setup and considered the screw elements used in the configuration as well as their dimensions. Despite everything, numerous experiments are still needed to get further insights and to broaden its validity by using other granulators, screw setups, process settings and formulations.

3.5 Theoretical considerations on a regime map setup for twin-screw granulation[2]

3.5.1 Introduction

Once a new formulation is developed at the lab scale, different upscaling approaches onto the manufacturing level can be applied [87, 94] which facilitates the determination of suitable operation windows at different scales: DoE, regime map and full predictive model. Despite the highest workload, DoEs are the method of choice if sufficient mechanistic process knowledge is absent. Numerous experiments provide statistically relevant or irrelevant effects of single variables or interactions on the product characteristics and enable better process understanding [157, 158]. To use regime maps, extensive understanding about granule mechanism, its process-, formulation and equipment-related impacts and their respective extents on the formation of granules is required [12]. The main controlling input parameters are correlated with characteristics of final granules and allow for the formation of dimensionless groups and by this the setup of a scale-independent process windows [157-159]. Since the controlling variables influence the granulation process to different extents, different granule formation regimes can be observed and defined in the operation window [160]. When the regime map has been successfully and broadly validated, it can support the design of formulations and upscaling attempts as well as the operation of granulators [160], requiring few experiments only for verification of the determined process window [157]. The procedure for setting up a regime is depicted in Figure 38. The lowest effort must be made with the fully predictive approach resulting in the least number of experiments at the different scales [157, 158].

One of the first regime maps in general was proposed for high shear granulation and dealt with the granule formation behaviour based on material properties, liquid content and the consolidation and deformation of the wet mass during the process [13]. Discoveries on the elasticity and plasticity of surface-wet and surface-dry granules were additionally taken into consideration. It could be found amongst others that granulation was improper when the strength of the solid-liquid mixture was beneath a crucial threshold which produced weak and rather crumbly product and that higher liquid contents facilitates granule growth. The granule growth regimes were identified as dry, nucleation only, steady growth, induction time, rapid growth, crumb and slurry/over-wetted [13]. Although a prediction of the expected formation behaviour was possible, the approach lacked the ability to predict the extent of granule growth. Nevertheless, a very important first step towards process design had been made. Until today, numerous further approaches have been proposed for a broad range of wet granulation techniques [8, 18, 87, 161].

[2] Some of the dimensionless groups presented and discussed in this section were used in the setups of other regime maps and have already been assessed critically in "*A review of regime maps for granulation*" [160].

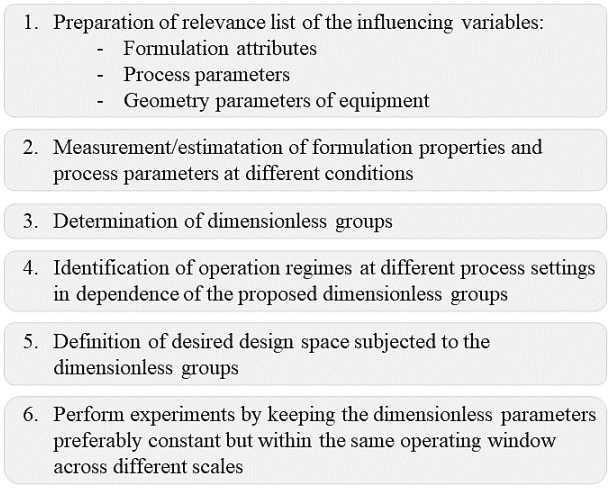

Figure 38. Procedure for creating a regime map [87, 157].

3.5.2 Current developments of regime maps for twin-screw granulation

In 2012 and 2013, the first regime maps for twin-screw granulation were proposed, one for a screw configuration made up of conveying elements only [85] and another one for a standard configuration containing two kneading blocks of 60° stagger angle [99]. The setups were inspired by Iveson and Litster [13] and took the deformability and pore saturation into account. Deformability of a system was indicated as shown in Eq. (35)

$$\beta = \frac{\sigma}{\tau} = \frac{T}{V \cdot \tau} \tag{35}$$

where β is the deformation value, τ is the granule strength, σ is the stress acting on the wet mass, e.g. due to screw configuration, mirrored by the motor torque, T, and the volume of the material, V, inside the barrel as a reflection of barrel fill [85, 99]. In contrast to σ and its relation to the wet mass, the granule strength, τ, was determined with the dried granules according to Adams et al. [162].

The pore saturation was assumed to be a function of the L/S ratio and viscosity of the granulation fluid. Therefore, the product of L/S and viscosity was used to reflect their combined influence on granulation behaviour [85, 99].

An exemplary depiction of a proposed regime map for TSG can be found in Figure 39. Granule formation regimes identified for TSG were under-wetted (dry), nuclei, crumb, granules and over-wetted/paste. Since the material does not enter the liquid addition area multiple times, the powder is commonly wetted only once and nucleation, consolidation and coalescence as well as breakage occurred separated from each other along the screw length. As it can derived from Eq. (35), the system is supposed to be more resistant against external forces the lower the value β is. In addition, if the system is in the dry regime on the left side of the regime map, an increase in liquid content and/or viscosity caused a shift towards over-wetting on the right side of the map, passing the crumb and granular regimes. This can be influenced with screw design, as it affects regime transition and growth of the agglomerates to different extents. The dry regime was referred to

the powder fed into the barrel or mixed with very little granulation liquid, resulting in ungranulated or poorly agglomerated material, while slightly higher liquid contents led to the production of poorly granulated material and small-sized granules, also called crumbs (high β). Depending on the screw setup, their strengths differ greatly. At moderate liquid levels, big, loosely bound and mechanically weak initial granules (nuclei) were formed, which may survive with little deformation when the screw setup contains only CE, while the application of shear forces can transfer the nuclei into consolidated and resistant granules (low β) if the screw contained kneading discs. Independently of screw design, further increase of liquid content can over-wet the system. In addition to that, it could be revealed that, independently of liquid content, the largest agglomerates could be obtained with high fluid viscosities. The system remained under-wetted at low viscosities. The few granules manufactured were weak and porous and broke easily (high β). At high viscosities, the granules appeared stronger, bigger and denser. The liquid provided stronger bridges with higher resistance against deformation, attrition and breakage (low β) [85, 99].

Although the regime maps mark an important and good first step, further research with different screw setups and dimensions together with their impacts on granule characteristics are needed to scale the axes and assess boundaries for the different growth regimes on the maps. More effort should be put into this topic as TSG receives increased attention by the pharmaceutical industry. Besides, in a next version, the product of L/S ratio and liquid viscosity should be replaced by a dimensionless term. The integration of the strength of dried granules into the determination of system deformability could cause trouble since the granule strength could be influenced by the drying temperature and period. However, it can be doubted that the granule strength of dried granules might reflect the granule strength of wet material appropriately.

Two further attempts proposed by Kumar et al. [87] and Tu et al. [161] are only in the early stages of creating a regime map. Kumar et al. [87] developed a process map for TSG based on a full-factorial DoE and investigated the impact of PFR, L/S ratio, screw configuration (one or two kneading blocks at 60° stagger angle) and screw speed. The screw torque was used to assess the energy required to turn the screws as well as to determine the energy imparted into each unit material (SME). Although the results enabled valuable insights, the approach has not yet exceeded the DoE stage. The status of validation is low as a single formulation had been investigated on one granulator only. The attempt of Tu et al. [161] proposed different growth regime maps for different screw setups used for TSG, but only little information could be extracted from their data representation as log(x) and f(log(x)).

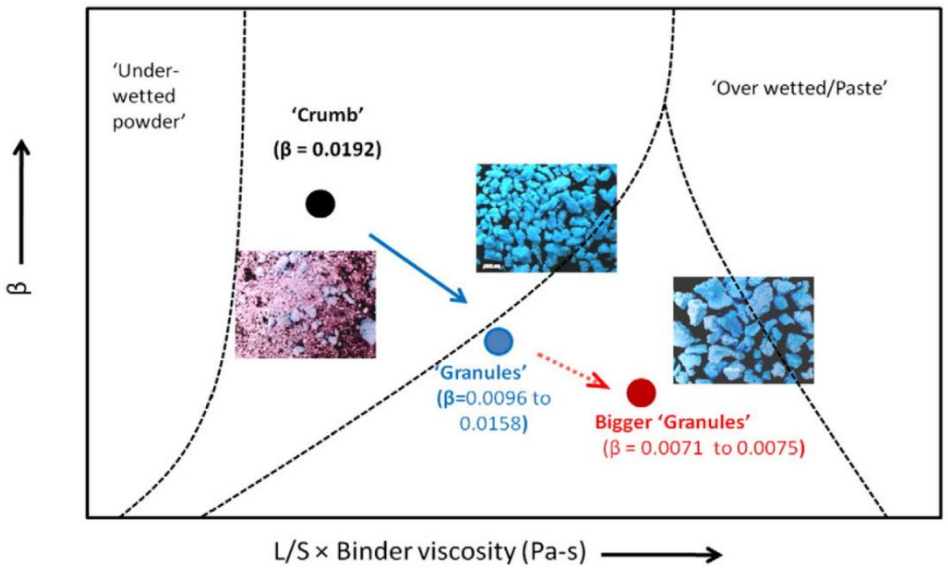

Figure 39. Regime map for TSG with screw setup with two kneading blocks [99]. (Reprinted with permission of Elsevier).

3.5.3 Promising parameters for regime map setup for twin-screw granulation

Twin-screw granulation is influenced by liquid content, barrel fill, screw configuration, diameter of screws and barrel, residence times and characteristics of the starting material (solid and granulation liquid) which should be covered in the regime map setup at best. It can be assumed that the ideal regime map is least three-dimensional or even multi-dimensional. However, especially the latter could lower clarity and, by this, comprehension and acceptance. A balance between the consideration of as many influencing parameters as possible and clarity must be found. The aim of this section is therefore to compile parameters that might be suitable for a regime map setup for TSG from the experience and knowledge gained during the PhD. Of course, the list (Table 23) does not claim to be complete, especially since no convincing attempt for predicting mean residence times has been proposed so far, which is a major gap in the research field of TSG. Although dimensionless values enable the definition of scale-independent operation windows and guarantee easy process transfers and upscalings, dimensional groups may provide initial assumptions or developments to new dimensionless groups, which is why all variables and groups that could be of interest are considered, independently of their dimension.

Table 23. Promising parameters for regime map setup for TSG.

Type	Eq.	Term	Legend		Evaluation	Usage in
Deformation	(36)	$St_{def} = \frac{\rho_p a^2 \dot{\gamma}^2}{2\tau_y} = \frac{\rho_p U^2}{2\tau_y} = \frac{\rho_p U^2}{2Y}$	ρ_p a $\dot{\gamma}$ τ_y Y U	particle/granule density granule radius shear rate flow stress of particle-binder mixture granule dynamic yield stress granule collision velocity	- Stokes deformation number - ratio of externally applied kinetic energy to energy required for deformation - mathematical relationship between deformation and breakage of granules - dimensionless - well validated and often used in regime map setups - the higher St_{def}, the weaker the system - initially developed for high shear granulation, why adaptions should be made for TSG	[10, 163]
	(35)	$\beta = \frac{\sigma}{\tau} = \frac{T}{V \cdot \tau}$	β τ σ T V	deformation value granule strength of dry granules stress acting on the wet mass motor torque volume of the material	- first adaption to TSG so far - scale-independent - usage of net torque recommended to compare different screw setups and granulators - insufficient so far, replacement of granule strength of dry granules strongly recommended	[85, 99]
Liquid content	(37)	$s_{max} = \frac{w\rho_s(1-\epsilon_{min})}{\rho_l \epsilon_{min}}$	w ρ_s ρ_l ϵ_{min}	mass ratio of liquid to solid particles density liquid density minimum porosity of the formulation under the experimental conditions	- maximum pore saturation as common indicator for liquid content and degree of saturation of granules - scale-independent - not easy to determine (mercury porosimetry needed), expensive, not every research groups can measure it causing trouble in comparability - mercury possess danger for environment, careful handling necessary - new determination methods should be invented to avoid drawbacks and to enable widely spread application	[13, 163]
	(38)	$\frac{L}{S} = \frac{\dot{m}_{liquid}}{\dot{m}_p}$	$\dot{m}_{liquid}$ $\dot{m}_p$	liquid infeed rate powder infeed rate	- liquid-to-solid-ratio - often used dimensionless depiction of liquid content during TSG - easy to determine and set on other granulators - scale-independent - often set equally to pore saturation for the sake of simplicity [99]	common usage
	(39)	$Ca^* = \frac{\eta_L u_r}{W_a} = \frac{\eta_L u_r}{\gamma_L(1+cos\theta)}$	η_L u_r W_a γ_L Θ	liquid/binder viscosity relative velocity work of adhesion surface tension contact angle	- modified Capillary number used as alternative to s_{max} - shifts focus to contact areas between particles where liquid bridges are formed, and the force needed to separate these particles from each other - the higher Ca*, the weaker the system, the less force needed to induce breakage - considers important parameters of binder fluid - developed for high shear granulation, why adaption to TSG is needed - sensitive to temperature changes (effect of friction and shearing) driven by local changes, solubility and viscosity might change along the screw which might impact W_a	[118]
Screw configuration	(1)	see section 3.2	-	-	- first attempt for quantification screw configuration as single value - not scale-independent, needs to be transferred into dimensionless term - not final yet, - further improvements needed	introduced in section 3.2

Type	Eq.	Term	Legend		Evaluation	Usage in
Barrel fill level	(34)	see section 3.4	-	-	- fill level determined by considering the transportation velocity of the material throughout the barrel - dimensionless - successful in prediction mass hold-up and times of first detections - further validation needed	introduced in section 3.4
	(13)	$BFD = \frac{SFL}{V_{free}} = \frac{\dot{m}_{tot}}{n \cdot V_{free}}$	$\dot{m}_{tot}$ n V_{free}	total material throughput screw speed free, available volumes	- barrel fill density - not dimensionless, but suitable indicator to estimate fill degree, even on different granulators as study results above showed	introduced in section 3.2
Other	(42)	$SME = \frac{2 \cdot \pi \cdot T \cdot n}{\dot{m}_p}$	T n $\dot{m}_p$	net screw torque screw speed powder infeed rate	- specific mechanical energy as indicator for process similarity and energy input into a defined unit of mass to be granulated - not dimensionless, but when using net torque of the screws, comparability is enabled	[96]
	(14)	$Fr = \frac{n^2 \cdot d_{element}}{g}$	n $d_{element}$ g	screw speed screw element diameter gravitational force	- Froude number as common indicator for dynamic similarity of granulation processes - dimensionless - ratio of centrifugal force to gravitational force - describes the force with pushing the materials against the barrel wall	[65, 66, 148-150]
	(40)	$\frac{L}{D} = \frac{l_{barrel}}{d_{barrel}}$	l_{barrel} d_{barrel}	barrel length barrel diameter	- length-to-diameter ratio as indicator for geometrical similarity of granulators - dimensionless - barrel length usually can be adapted by adjusting infeed port locations to generate a similar L/D ratio - focus on granulation length could also work (length from liquid infeed position till barrel outlet)	common usage

4 Summary and Outlook

Despite long-standing experience in continuous manufacturing (CM) in the food and chemical industry, pharmaceutical goods are still predominantly produced according to the traditional batch-concept where the various unit operations are performed one after the other. Batch-wise manufacturing is mainly driven by a regulatory framework that conserves this manner of production, while consciously accepting that the overall production may take a long time due to the storage of intermediate products and depending on the number and type of unit operations to be carried out. Nevertheless, rising healthcare costs and repeated recalls of medicinal products due to quality issues has started a mind change in the pharmaceutical industry about its production strategies. It should be eased by the provision of guidance of regulatory authorities and the International Council for Harmonization of Technical Requirements for Pharmaceuticals for Human Use (ICH). CM was found as a suitable alternative to the current state as CM offers several advantages, such as less equipment footprint, increased product quality ensured by close monitoring and control of both process and critical quality attributes (CQAs) of starting material, intermediates and final products in real time applying process analytical technologies (PAT) or the flexibility to react to market needs.

The overall aim of the thesis was the prediction of important influencing variables (liquid content, barrel fill) on twin-screw granulation (TSG) as well as suitable process parameters for continuous TSG.

To predict optimal liquid contents, formulations were examined on a mixer torque rheometer (MTR) first and the recorded torque curves subsequently mathematically analysed by determining their first and second derivatives. The usage of mixer torque rheometry seemed reasonable as the interaction between solid and liquid influences the systems behaviour in the kneading chamber and thus its recorded torque curve. Since the liquid content at the inflection point of the torque curve was described as suitable for high-shear granulation processes, the same working hypothesis was used for TSG. Results in subsequently performed granulation processes revealed no superiority of any L/S ratio that had been investigated, but extensive granule growth was obtained when exceeding a critical liquid content. It was assumed that lower L/S ratios would better suit for TSG as the screws are likely to exert stronger external forces onto the wet material and thus cause a more rapid shift towards capillary state than on the MTR. It was concluded that the MTR is suitable for gaining knowledge about the formulation and its behaviour at various liquid contents, but further research on the prediction of optimal liquid levels for TSG would be needed.

Since it has not yet been possible to represent screw configurations numerically, apart from the details of how many kneading elements, kneading blocks and other elements were used for the screw setup, a new approach was developed that also considers actual process parameters and

expresses them all as a single shear stress value. Several studies were conducted to transfer a TSG process from one twin-screw granulator to another by including different granulators of different dimensions. The experiments were mainly performed based on similar tip speeds and barrel fill levels, depicted as barrel fill density (BFD), but the newly developed approach was simultaneously checked regarding its usefulness. During preliminary transfer studies, barrel fill was found to be more decisive than the tip speed itself. Granule and tablet characteristics obtained on the different granulators were comparable when both BFD and tip speed were kept constant. As the calculated shear stresses on the granulators on which the comparative experiments were performed indicated essentially higher stresses, which should, however, have been reflected in differences in the properties of the final product, it was assumed that the new approach failed. Nevertheless, since there is a need to quantify the screw configurations as single values to make the results of different research groups more comparable, further considerations should be made.

Additional studies were performed that focused on the impact of KB setup and screw length on GSDs. The investigation of the KB design was again based on the same tip speeds and BFD values, while BFD values and shear stresses were kept constant when examining different screw lengths. The investigation of the KB setup comprised experiments using one, two or three KBs in the screw setup while the total number of kneading discs incorporated in the entire screw design were kept constant. Since the GSD curves were found almost identical among the different barrel fills, the KB setup seemed less decisive, provided that the number of discs were kept the same. The examination of varying screw lengths also found no difference in GSDs if the screw length and thus the length in which granule formation can take place is not too short. Despite the shortening of the screw length, liquid distribution behaviour seemed comparable and similar GSDs were obtained at the different barrel fill levels. Nevertheless, a distinctive right shift and broadening of the GSD curves resulted once a critical length was achieved. Although the shear stresses were kept similar in this study, the constant BFD values were more likely to result in similar GSDs.

In the last experimental part of the thesis, a new predictive model for barrel fill levels during TSG was developed as it has been reported to be one of the main key factors in TSG. The model considers the materials transportation velocity along the screw axis at defined process settings and flow obstacles of screw particularities such as KBs with defined offset angles. An improvement in the accuracy of model prediction was achieved by applying non-linear fits with own data and literature data. An accurate prediction of the masses remaining in the barrel, times of their first detection during RTD measurement and a positive linear relationship of the dimensionless fill level with the mass hold-ups determined for the varying compositions and screw setups could thus be achieved. Compared to attempts on defining the barrel fill non-dimensionally, a step forward could be made. To the best of my knowledge, the newly developed approach is comprehensive and comprehensible and considered the different screw elements used in the screw setup, but further experiments are still needed to get additional insight. For this, other

granulators, screw setups, process settings and formulations should be used. Once a sound understanding has been gained, different fill conditions can probably be defined in which more specific research could be done to investigate the impact on growth mechanism and granule characteristics.

At the end of the thesis, suitable parameters for a potential regime map setup for twin-screw granulation were compiled and critically evaluated. In a regime map, dimensionless groups are formed by correlating the main influencing input parameters to the output parameters, e.g. granule characteristics, and used to set up a process window. Once a regime map is sufficiently validated, it helps to design appropriate formulations and processes as well as the upscaling as the values of the dimensionless numbers only have to be kept constant. However, creating a regime map necessitates a deep understanding about growth mechanisms as well as process-, formulation- and equipment-specific parameters which mainly impact granule growth.

5 Experimental Part

5.1 Materials

5.1.1 Active pharmaceutical ingredients

Theophylline monohydrate (Theophylline Hydrous Powder Ph. Eur.; USP, JP, IP, batch no. 287031AX20, BASF, Germany) and paracetamol (Paracetamol Ph. Eur., USP, extra fine powder, batch no. 21701049, Atabay, Turkey) were chosen as the APIs in some working packages.

5.1.2 Binders and fillers

Several solid excipients were used as binders and fillers for the granulation processes within the different working packages of this thesis, which are listed in Table 24.

Table 24. Binding and filling excipients used.

Excipient	Trade name	Batch No.	Manufacturer
α-Lactose monohydrate	Granulac 200	L101854217, L101855018, L101850119, L101852020, L101852618, L101853318, L101851619, L101855013, L101854819	Meggle, Germany
Dicalcium phosphate anhydrous	DI-CAFOS A150	C58309A, C64947A, C73911A	Chemische Fabrik Budenheim, Germany
	DI-CAFOS A12	C72806A, C85805A, C85722A	Chemische Fabrik Budenheim, Germany
Mannitol	Parteck M 200	M680719	Merck, Germany
	Pearlitol 200SD	E430G	Roquette, France
Povidone	Kollidon 25	62205524U0	BASF, Germany
	Kollidon 30	17933256P0, 29448656P0, 93084568E0, 93084563E0, 97530536W0	BASF, Germany
	Polyvinylpyrrolidon K 30	178269607	Carl Roth, Germany
Microcrystalline cellulose	Vivapur 101	66101175748, 66101187948, 66101197047, 66101197349	JRS Pharma, Germany
	Vivapur 102	56102196937, 56102202818	JRS Pharma, Germany

5.1.3 Other substances

Table 25. Other substances used.

Excipient	Trade name	Batch No.	Manufacturer
Iron(III) oxide, red	Eisen(III)-oxid, rot	12058008	Caesar & Loretz, Germany
		299286293	Carl Roth, Germany
Fumed silica	Aerosil® 200 VV Pharma	157032716, 157031016	Evonik Industries, Germany
Demineralised water	-	-	produced by ion exchanger
Magnesium stearate	Parteck LUB MST	K42017563	Merck, Germany
Sodium croscarmellose	Disolcel GF	SIS02490	MINGTAI CHEMICAL, Taiwan

5.2 Methods

5.2.1 General Methods

5.2.1.1 Loss on drying of starting material

If not stated otherwise, the starting moisture content of the powder blend was measured six times using a halogen moisture analyser (HR73 Halogen Moisture Analyzer, Mettler Toledo, Ohio, USA) at L.B. Bohle Maschinen + Verfahren (Germany) or an infrared (IR) balance (MA100, Sartorius, Germany) at the university. Drying temperatures were always set to 105 °C. The termination criterion at L.B. Bohle Bohle Maschinen + Verfahren was < 1 mg in 60 s (default setting), whereas the process was stopped at the university if < 1 mg mass loss in 150 s was reached. The termination criterion at the university has been found to be appropriate in preliminary investigations.

Loss on drying (LOD) was automatically calculated by the software of the moisture analyser according to Eq. (41)

$$LOD = \frac{m_{start} - m_{dry}}{m_{start}} \cdot 100\ \% \tag{41}$$

where m_{start} is the sample mass at the beginning and m_{dry} is the dry mass after the system reached mass consistency.

The single content values were used to calculate the mean and standard deviations, which were taken into consideration for the calculation of the necessary granulation liquid infeed to achieve defined L/S ratios.

5.2.1.2 Sample preparation

For the purpose of proper characterisation of granules, samples taken during the experiments were representatively divided using a rotary sample divider (PT, Retsch, Germany). Sample sizes are specifically mentioned in the respective characterisation methods.

5.2.1.3 Residence time measurements

Determination of residence times and its distributions (RTD) were measured using an ExtruVis®3 software (ExtruVis, MeltPrep, Austria) with corresponding camera (USB-CAM-052H, Phytec, Germany) and LED ring light (VZ-001-X4, Phytec, Germany). Red iron(III) oxide, a non-soluble pigment, was used as a tracer and added at once into the powder infeed funnel. The amount of tracer needed was calculated by the software (~1 % of the actual throughput). The camera was located so that the barrel outlet was optimally focussed. While RTD measurements were performed, light conditions were kept as constant as possible by applying the ring light. The ring light ensured uniform light without reflections and shadows which could have impacted the actual measurements. The region of interest, an enlarged detail of the camera image, where the

measurement occurred was chosen by focusing on regions containing only material to avoid light reflections by any metal surfaces.

Five measurements were performed inline at each process setting after steady state was achieved. The results of each measurement were used to calculate the mean and standard deviation. The measurement principle is based on reflections and the change of colour intensity. The first 10 s of each measurement were dedicated to recording a baseline intensity value.

The red colour ratio was used for the analysis which was also done with the ExtruVis®3 software. First, a baseline correction was performed. The obtained curve over time was then smoothed and normalised to the area under the curve by the software leading to the exit age function E(t). Depending on the working package different residence time characteristics were of interest: The first onset (first change in colour intensity), t_1, the time of highest tracer concentration, t_{peak}, the mean residence time, t_{mean}, and the time when the tracer was completely washed out of the barrel, t_{out}.

5.2.2 Mixer torque rheometry

5.2.2.1 Sieving and blending of powder mixtures

As a first step, the materials were sieved through a 355 µm sieve. If powder blends were examined the components were weighed (16000D, Precisa Gravimetrics, Switzerland) and blended for 10 min at 49 min^{-1} using a Turbula mixer (T2F, Willy A. Bachofen, Switzerland).

5.2.2.2 Investigation on the Brabender mixer torque rheometer

Investigations of 35 g of powder blends or raw materials (16000D, Precisa Gravimetrics, Switzerland) were conducted three times on a MTR (Plastograph EC Plus, Brabender, Germany) equipped with two counter-rotating kneaders (N50, Brabender, Germany) at 100 min^{-1} at 25 °C kneading chamber temperature.

The operating principle of the MTR is the measurement and recording of the torque required to mix the material at given rotation speed.

After process start the material was kneaded for one minute. Afterwards, a multiple addition method was applied by adding a defined amount of demineralised water every 60 s into the kneading chamber using a precision pipette (Eppendorf, Germany). The process was stopped when the torque curve displayed a steady but unambiguous decrease or if it reached zero.

Monitoring and recording of torque development and kneading chamber shell temperature occurred by a WinMix application (Version 4.2.10, Brabender, Germany) at 0.5 Hz.

Starting moisture of the materials was examined on the day the tests were conducted as described in section 5.2.1.1.

5.2.2.3 Verification of precision and pipetting volumes of used pipettes

Due to the fact that different water addition schemes were applied, the precision and pipetting volumes of the Eppendorf pipettes had to be examined. For this, pipetting was conducted ten times by applying 10 pipetting steps (n=10x10) to be able to calculate the mean volume per pipetting throughout the process on the MTR.

5.2.3 Manufacturing methods

5.2.3.1 Preparation of powder mixtures

APIs, fumed silica and magnesium stearate were, if used, sieved through a 355 µm sieve before they were weighed. After weighing (16000D, Precisa Gravimetrics, Switzerland), all components were given into a lab-scale blender (LM 40, L.B. Bohle Maschinen + Verfahren, Germany) and blended for 20 min at 25 min^{-1}.

5.2.3.2 Granulation on twin-screw granulators

Depending on the working package and its respective aim, granulation was performed on different twin-screw granulators.

The Pharma 16 twin-screw granulator (Thermo Fisher Scientific, Massachusetts, USA) was mainly used in this thesis. The Pharma 16 consisted of a barrel of 640 mm length (barrel L/D of 40:1), which in turn composed of ten sections of 64 mm each that could be individually tempered. The barrel shell itself was temperature controlled using a liquid cooling system (STL 1-0-B5/10-TK6, Single Temperiertechnik, Germany) to achieve targeted barrel shell temperatures. If not stated differently, the screw shafts used had a L/D of 41:1 to avoid material adhesions and unintended densification at the barrel exit since screw shafts exceeded the barrel. The screw bearing was on one side only. A loss-in-weight feeder (K-SFS-24, K-Tron, Coperion, Switzerland) was used for the infeed of the powder blend while a micro annular gear pump (MZR 7205, HNP-Mikrosysteme, Germany) pumped the granulation liquid through a nozzle with an capillary inside (inner diameter 0.75 mm) directly into the barrel onto the top of one screw in front of the first kneading block, unless something else is specified in a respective section. The pump and its performance was controlled using the software Motion Manager 4 (Dr. Fritz Faulhaber, Germany). The working principle of the micro annular gear pump is based on the generation of differential pressures due to high rotational speeds of the internal and external rotor with a tooth ratio of 6/7. Since the liquid conveying chambers are both filled on the suction side and simultaneously emptied on the delivery side, a low-pulsating and homogeneous liquid flow can be obtained [164]. Liquid feed rates were displayed on a Coriolis mass flow meter (Proline Promass 80A, Endress+Hauser, Switzerland) and could be easily adjusted during the process to guarantee the targeted value. Monitoring and recording of the process parameters of the granulator, feeder and pump occurred with a Labview 2015 application (National Instruments, USA) at a sampling rate of 1 Hz.

Other granulators utilised intensively were the QbCon®1 and QbCon®25 (both L.B. Bohle Maschinen + Verfahren, Germany). Denotation of QbCon® always implies the combination of a granulation and drying unit directly linked to each other that can be run continuously without process interruptions for batch-wise product transfer from one unit towards the other. Whereas no separation of both process units was possible on the QbCon®1, the granulation unit of the QbCon®25 could also be used as stand-alone system (BCG 25; i.e.: Bohle Continuous Granulation), disjointed from the drying unit (BCD 25; i.e.: Bohle Continuous Drying). It must be emphasized that the QbCon®1 currently no longer exists in this form. At the time of usage, the QbCon®1 and QbCon®25 were identical regarding their design (barrel length and diameter, screw elements, maximum rotational speed) but scale and capacity of the respective dryers were different. The QbCon®1 possessed a throughput maximum of 4 kg/h, whereas the throughput could be increased up to 25 kg/h on the QbCon®25. In the meantime, the barrel diameter of the QbCon®1 has now been reduced from 25.5 mm to 16 mm. The granulators had barrel lengths of 500 mm (L/D 20:1) consisting of three barrel sections. The shells of the barrel were cooled by a liquid cooling system (CH-6-6-L, Single Temperiertechnik, Germany). The screw shafts exceeded from the barrel because screw bearing occurred on both sides. The screw elements also exceeded the barrel with the same objectives as described for Pharma 16. The powder blends were directly fed into the barrel using a gravimetric loss-in-weight feeder (GZD150.12, Gericke, Switzerland). An incorporated micro annular gear pump was used to pump the liquid through a nozzle (0.12 mm inner diameter) into the barrel on the top of one screw in front of the first kneading block. Process parameters of the granulator, feeder and pump were recorded at a rate of 1 Hz by an in-house written software (L.B. Bohle Maschinen + Verfahren, Germany). Actual parameters were displayed on a monitor on the granulator itself.

The Leistritz Micro 27 GL-28D (Leistritz Extrusionstechnik, Germany) was also used. The granulator had a barrel length of 756 mm (L/D 28:1) composed of seven barrel segments. A 54 mm-extension for mounting of pressure sensor for the extrusion processes led to a final barrel length of 810 mm (L/D 30:1). The screw bearing was on one side only and the shafts did not exceed the barrel. A liquid cooling system (STW 1-1.5-15-M2I/E/M4, Single Temperiertechnik, Germany) was used to cool the barrel shell. The powder blend was dosed using a gravimetric loss-in-weight feeder (K-CL-KT 20, K-Tron, Coperion, Switzerland). The granulation liquid was pumped by a piston diaphragm pump (Cerex EP-31, Bran + Luebbe, Germany) in combination with a flow through meter (Corimass MFC 081/K, Krohne, Germany). The liquid was pumped into the intermeshing zone between the screws in front of the first kneading block. Process parameters of the granulator, feeder and pump were recorded at 1 Hz by a Labview 2009 application (National Instruments, USA).

All experiments were performed at 25 °C barrel temperature and by using the total length of the barrel, unless otherwise specified. Before the process was started, the loss-in-weight feeders were tared and calibrated. The infeed of powder into the barrel occurred always in an upward barrel segment before liquid was added. Demineralised water was used as granulation liquid. Each setup

of the screw configuration started with conveying elements with long pitches (LPCE) to facilitate transport from the powder infeed area. Samples were always taken after the processes had achieved equilibrium/steady state, which was recognised based on the screw torque curves. All experiments within an experimental plan were conducted in random order.

5.2.3.3 Determination of net torque and specific mechanical energy

Being able to compare granulation processes on different twin-screw granulators at varying settings, the net screw torques were determined. For this, the screws of defined configurational setups were started on the different twin-screw granulator (see section 5.2.3.2) without any infeed of powder or liquid. The idle screw torques were determined after the process had reached its equilibrium at given screw speeds. In each case, 120 s (= 120 data points) were taken to calculate the mean idle torque which was finally used to subtract from the torque values recorded during sampling (gross torque).

Different screw speeds were set on BCG 25 and Pharma 16 to cover a broad range and to create a calibration line. The idle screw torques on BCG 25 and Pharma 16 at defined screw speeds were calculated by interpolation. Opponent, the screw speeds used on the Leistritz Micro 27 GL-28D were the same as in the respective experiments.

The specific mechanical energy (SME) as a scale-independent measure of energy input into the material was calculated according to Eq. (42) [96]

$$SME = \frac{2 \cdot \pi \cdot T \cdot n}{\dot{m}_p} \tag{42}$$

where T is the net torque.

5.2.3.4 Drying and storage of granules

If not stated otherwise, samples taken during the processes were spread on a tray and dried for several hours at 40 °C in a drying oven (Heraeus ET 6130, Kendro, Germany). After it was turned off the doors were opened for equilibration of the product with the surrounding conditions. The samples were stored in closed plastic bags at room temperature until representative division and further characterisation.

When experiments were performed on the granulators at L.B. Bohle Maschinen + Verfahren (Germany), a continuous dryer directly linked to the granulators as downstream unit was used. After the granules had passed the barrel exit they entered the dryer through the product inlet and landed on a vibrating meshed bottom plate. They moved forward while passing the drying chamber and left the dryer through a rotary valve. The dryers working principle (Figure 40) is based on a fluid-bed dryer. While a stream of hot, dry air flew from the air inlet through the meshed bottom plate and product zone towards the air outlet on the ceiling of the dryer, the granules were concurrently lightly fluidised and dried. A negative pressure caused the air stream

finding its way towards the air outlet and not towards the product inlet that, in turn, enabled also a stable powder feeding process. Vibrations of the bottom plate caused the forward movement of the materials. The vibration amplitudes (also vibration acceleration) determined their speed of motion through the dryer and could be set independently of the airflow rate that, in turn, strongly affected the materials residence time within the drying chamber and, thus, the drying time of the granules. The vibration loosened the granule bed density on the meshed bottom and eased air perfusion and the drying process. Implemented filters prevented fine material to be removed by the airflow, which also limited the product zone upwards to the exhaust air zone. Generally, the drying process could be influenced by the vibration acceleration, the amount of air flowing through the product zone (inlet airflow) and its temperature, T [165]. The material bed height was another important impact on the drying efficiency that was indirectly settable by the vibration acceleration and the inlet airflow. A powder bed height of 2 mm was recommended. Before sampling occurred, the actual drying settings were checked by measuring the residual moisture. The target values for the residual moisture contents were set in consideration of the moisture content of the starting material (powder blend). If the starting moisture was below 2 %, sampling was started when the achieved residual moisture content of the granules was ≤ 2 %. If the starting moisture was above 2 %, the aim was for the residual moisture to be less than or equal to the initial moisture of the blend. If the granules moisture content was still too high, adjustments of the drying conditions were carried out. Storage of samples occurred in closed plastic bags for the granule batches sampled in section 5.2.3.8 at room temperature and in plastic buckets at constant temperature and relative humidity (21 °C, 45% relative humidity) for the granule batches sampled in section 5.2.3.7 before representative sample division and further characterisation occurred. Drying settings are specifically mentioned in the respective manufacturing methods as they had to be adopted for each process setting.

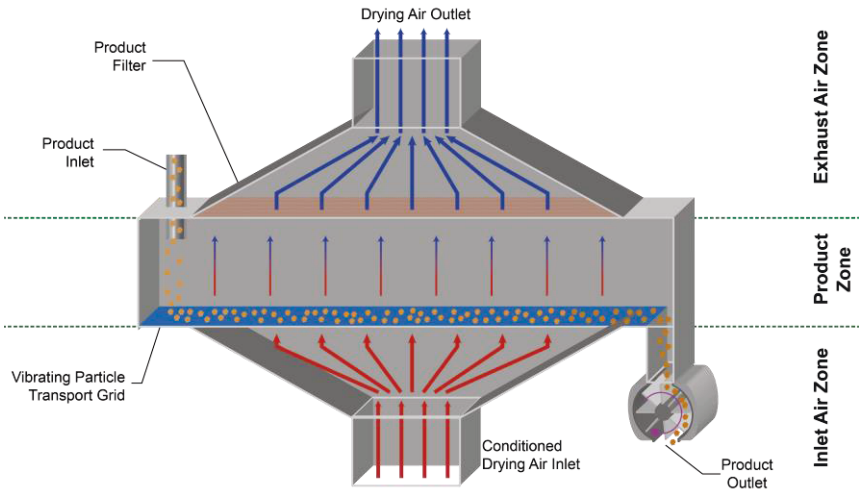

Figure 40. Basic setup and working principle of the continuous dryer [165]. (Reprinted with permission of TechnoPharm and with courtesy of L.B. Bohle Maschinen + Verfahren).

Another drying procedure was applied to the granule samples taken during the process transfer (section 5.2.3.7) at the university using a fluidised bed dryer (GCPG 1.1, Glatt, Switzerland). The wet granules collected were given into the drying chamber. The air flow was initially set to 70 m^3/h and to 60 m^3/h after fluidisation of the granules. The inlet air temperature was set to 65 °C. The drying process was stopped when a product temperature of 38-40 °C was reached. The residual moisture content of a sample was measured once using an IR balance. Drying temperature and termination criterion were the same as stated in section 5.2.1.1. Target moisture contents were ≤ 2 % or, if starting moistures were above 2 %, the residual moistures should be less or equal to the initial moisture of the blend. The product was stored in plastic buckets under climate conditions (21 °C, 45% relative humidity) before representative sample division and further characterisation were conducted.

5.2.3.5 Measurement and volume determination of screw elements and barrels of the different twin-screw granulators

The screw elements of each granulator were measured regarding their volumes and other parameters.

Volume determination of the screw elements of the Pharma 16 twin-screw granulator occurred by displacement measurements according to Archimedes' principle. The measurements were performed six times in total with each kind of element. The mean values and standard deviations were calculated.

Determination of the screw elements volume of the Leistritz Micro 27 GL-28D twin-screw granulator were performed ten times for each screw element type. These measurements were conducted within the frame of the Master's thesis of Katharina Kiricenko [166].

Additionally, the barrel, screw shafts, where the screw elements were assembled on, and the elements themselves of the Pharma 16, Leistritz Micro 27 GL-28D and QbCon®1/QbCon®25 granulators were measured ten times with regard to the required variables.

Parameters of conveying elements (Figure 11A, page 32) considered: $d_{element}$ as the element diameter, $l_{element}$ as the element length, d_{inner} as the inner diameter of a CE, w_{pitch} as the width of each pitch, w_{crest} as the threads crest width and l_{crest} as the crest length. In Figure 11B important parameters of kneading discs are depicted where $d_{element}$ is the element diameter, $l_{element}$ is the kneading disc breadth and w_{tip} is the length of the tip area. All parameters were measured six times utilising a calliper (at L.B. Bohle Maschinen + Verfahren: Absolute Digimatic CD-15 CPR, Mitutoyo, Kawasaki, Japan; at the university: Garant digital DC2, Hoffmann Group, Germany) or a ruler in case of the pitch lengths of the conveying elements of the Leistritz Micro 27 GL-28D.

The screw shafts of the granulator for the comparative experiments were hexagonal prisms; their volumes, V_{shaft}, were calculated according to Eq. (43)

$$V_{shaft} = \left(\frac{3 \cdot a^2 \cdot \sqrt{3}}{2}\right) \cdot l_{shaft} \quad (43)$$

where a is the side length of the hexagonal prism and l_{shaft} is the screw shaft length. Side lengths were measured six times.

The total horizontal width (w_{barrel} in Figure 10) of the two barrel cylinders as well as the diameter of one cylinder (d_{barrel} in Figure 10) of the Pharma 16 granulator were measured to calculate the empty barrel volume as specified in section 3.2.2.2. The measurements and calculations of the (empty) barrel and screw shafts of the Leistritz Micro 27 GL-28D twin-screw granulator were conducted by Katharina Kiricenko during her Master's thesis [166].

The volumes of the empty barrel, screw shafts and screw elements of the QbCon®1 and QbCon®25 twin-screw granulators were kindly provided by L.B. Bohle Maschinen + Verfahren (Germany).

A compiling overview of the different screw elements can be found in Table 3.

5.2.3.6 Verification of previously determined optimal L/S ratios

The L/S ratios identified for the systems investigated on the Brabender MTR (see section 5.2.2 and Table 1) and other L/S ratios were verified on the Pharma 16 twin-screw granulator (see section 5.2.3.2); all equidistant to each other. The equidistant steps based primarily on the distances between the L/S ratios at the inflection point and maxima on the torque curves of the respective formulations. These distances were divided into three equal sections and then used to define the target L/S ratios. The mean distance of the three runs on the MTR were used for the determinations. The obtained sub-distance for each system was used to determine two additional L/S ratios below the L/S ratio at the inflection point, between the L/S ratios at the inflection point and maximum as well as above the L/S ratio at the maximum of the torque curve. 0.2% (w/w) fumed silica were added to the systems to facilitate powder feeding.

Initially, the accuracy of liquid infeed was tested to ascertain the realisation of targeted L/S ratios. The theophylline monohydrate-fumed silica system (99.8-0.2 % w/w) was used as model. Bottles with snap-on caps were prepared and their respective tare weights determined (analytical balance, 1507 004, Sartorius, Germany). During the process, samples of wet material were taken directly at the barrel outlet every 30 s for approximately 20 s, hermetically sealed and the corresponding gross weight determined. 23 samples were taken in total at each L/S ratio. At the end of the experiment, samples were unsealed and dried at 50 °C in a drying oven (Heraeus ET 6130, Kendro, Germany) until mass consistency was reached according to the demands of the Ph.Eur. monograph 2.2.32 [167].

During the verification of defined L/S ratios of theophylline monohydrate, samples of about 250 g, based on dry mass, were gathered when the process had achieved its steady state. The granules were tray-dried at 50 °C in a drying oven (Heraeus ET 6130, Kendro, Germany). The further procedure (drying period and balance adjustments) was as described in section 5.2.3.4.

The screw shafts used for both testing the liquid feeding accuracy and the verification of defined L/S ratios had a L/D of 40:1, deviating from the specification given in section 5.2.3.2. The respective configuration consisted of 1x (0.25D) KE as spacer >> 4D LPCE >> 4D SPCE >> 5x (1.25D) KE 60° >> 10D SPCE >> 6x (1.5D) KE 60° >> 19D SPCE. Powder and liquid infeed occurred at the LPCE section and the adjacent SPCE section, respectively. The greater-than signs indicate the materials flow direction.

When Parteck M200 (mannitol) as well as DI-CAFOS A150 (dicalcium phosphate anhydrous), each with PVP K30 and fumed silica (96.8-3-0.2 % w/w) was investigated, the screw length was extended to L/D of 41:1 as described in section 5.2.3.2 because material adhesions were noticed at the barrel outlet when shorter screw shafts were used. The screw configuration utilised consisted of 4D LPCE >> 4D SPCE >> 5x (1.25D) KE 60° >> 10D SPCE >> 6x (1.5D) KE 60° >> 20D SPCE. The infeed locations of powder blend and granulation liquid remained the same as described above. Samples of about 400 g were taken and tray-dried as stated conditions in section 5.2.3.4.

The overall process settings of the tests carried out in present working package can be found in Table 26. The L/S ratios below the L/S ratio at the inflection point (IP), the L/S ratios in between the L/S ratios at the IP and maximum (Max) as well as the L/S ratios above the L/S ratio at the Max on the torque curves are herein abbreviated as IP -2, IP -1, IP +1, Max -1, Max +1 and Max +2, respectively. The results related to these investigations are described and discussed in section 3.1.

Table 26. Process settings for the granulation experiments at defined L/S ratios (*n=6, mean ± s).

Material	PFR [kg/h]	n [min^{-1}]	Starting moisture* [%]	L/S ratio at							
				IP -2 [-]	IP -1 [-]	IP [-]	IP +1 [-]	Max -1 [-]	Max [-]	Max +1 [-]	Max +2 [-]
TM, 0.2 % fumed silica	2	300	0.59 ± 0.02	0.289	0.324	0.359	0.394	0.429	0.464	0.499	0.534
PM200, 3 % PVP K30, 0.2 % fumed silica	3.3	350	0.25 ± 0.04	0.159	0.171	0.184	0.197	0.209	0.222	0.235	0.247
DCP A150, 3 % PVP K30, 0.2 % fumed silica	3.3	350	0.85 ± 0.08	0.198	0.222	0.246	0.270	0.294	0.318	0.342	0.366

Legend:
TM: theophylline monohydrate, PM: Parteck M (mannitol), PVP: polyvinylpyrrolidone, DCP: DI-CAFOS (dicalcium phosphate anhydrous), IP: inflection point, Max: Maximum, n: screw speed, PFR: powder feed rate

5.2.3.7 Investigation of process transfer with critical evaluation of a new approach for the quantitative description of screw configurations

Due to numerous and time-consuming trial and error approaches of transferring or upscaling twin-screw granulation processes to granulators of different dimensions, as well as the infinite options of a screw configuration, a quantitative description of screw configurations was developed in which the shear stress, τ, was the target variable (see Eq. (1)).

Preliminary experiments with a powder mixture of Granulac 200, MCC 101, PVP K30 (80-17-3% w/w) and demineralised water were performed on the QbCon®1 first with subsequent transfer onto Pharma 16 and Leistritz Micro 27 GL-28D.

Screw configurations used on the different granulators are given in Table 27. On Pharma 16, two configurations were used for the transfer approach, referred to as A and B. Powder and liquid were added at the LPCE and the adjacent MPCE (QbCon®1), SPCE (Pharma 16) or MPCE long (Leistritz Micro 27 GL-28D) parts, respectively.

Table 27. Screw configurations used for the transfer studies. The greater-than signs display the flow direction of the wet material.

Granulator	Screw configuration
QbCon®1	3.75D LPCE >> 4D MPCE >> 6x (0.875D) KE 67.5° >> 5D MPCE >> 6x (0.875D) KE 67.5° >> 4D MPCE >> 1.5D SPCE
Pharma 16	A: 4D LPCE >> 4D SPCE >> 7x (1.75D) KE 60° >> 10D SPCE >> 7x (1.75D) KE 60° >> 19D SPCE B: 4D LPCE >> 4.5D SPCE >> 5.5x (1.375D) KE 60° >> 10D SPCE >> 6x (1.5D) KE 60° >> 19D SPCE
Leistritz Micro 27 GL-28D	6.7D LPCE >> 3.35D MPCE long >> 1.1D KB 60 >> 1.12D MPCE short >> 6.7D MPCE long >> 1.1D KB 60 >> 2.23D MPCE inter >> 1.12D MPCE short >> 3.35D MPCE long >> 3.34D SPCE

To ensure similar process dynamics on the different granulators of different dimensions, the tip speeds were kept similar. Tip speeds were calculated as given in Eq. (44)

$$v_{tip} = n \cdot d_{element} \cdot \pi \tag{44}$$

where v_{tip} is the tip speed and $d_{element}$ is the outer diameter of the screw elements.

The tip speeds obtained on the QbCon®1 were considered as the target values to be achieved on Pharma 16 and the Leistritz Micro 27 GL-28D. Thus, the screw speeds, n, were initially set by intention on the other granulators in order to keep v_{tip} similar. PFRs were adjusted afterwards to achieve defined barrel fill levels.

Experiments in the different studies were mainly conducted at three barrel fill levels (low, intermediate and high), quantified as BFD according to Eq. (13), at L/S ratio of 0.191 (L/S ratio at the shoulder, determined on the Brabender MTR as described in section 5.2.2, see Table 34 in appendix) The L/S ratios kept constant in the studies on the granulators used and are further specified in the respective sections of this thesis.

When the process at low fill level was transferred onto Pharma 16, liquid feed rates below 2 g/min could not be displayed by the Coriolis mass flow meter. A gravimetric calibration on the micro annular gear pump was performed obtaining a functional equation ($y=0.0118x-1.7312$, $R^2=0.9950$), which was used for the calculation of the liquid flow rates needed and which outcome was checked three times for 3 minutes each. If necessary, adjustments were made.

Before process transfers were performed, a Design of Experiment (DoE) was conducted on the QbCon®1 to examine the operation window, determined from the torque curve obtained on the Brabender MTR, in order to discover the systems vulnerability with regard to liquid influences. A 3^2-full factorial Central Composite Face (CCF) design (star distance of 1) with BFD (at 0.45, 1.87 and 3.29 kg/m^3) and L/S ratios (at 0.177, 0.191 and 0.205) as factors on 3 levels each was performed using the screw configuration described above. Responses of interest were x-values (x_{10}, x_{25}, x_{50}, x_{75} and x_{90}), span (see section 5.2.4.3, Eq. (45)), percentage proportions of fine (< 125 µm), yield (125-1250 µm) and oversized granules (> 1250 µm), net torque and SME. The centre points were performed three times to evaluate process reproducibility, resulting in 11 runs in total. Experimental order was randomised. Data evaluation was performed by the statistical software MODDE 12.1 Pro (Umetrics, Umeå, Sweden). Process settings and experimental plan of the DoE is displayed in Table 28.

Results and process data of the experiments at different BFD performed during the DoE at L/S 0.191 were taken for preliminary transfer tests and used for comparison. Firstly, only the respective tip speeds were targeted with slight adjustments of respective BFDs (#0_i and #0_{iii} of configuration A and B, respectively). An additional approach (#0_{ii} of configuration A) aimed to investigate the influence of barrel fill level on the transfer of a TSG process. Thus, transfer experiments were conducted with intermediate barrel fill levels (BFD values close to those on the QbCon®1), but tip speeds were set lower or higher on Pharma 16 than on the QbCon®1. Process settings and further information on the preliminary investigations on the different granulators are given in Table 29.

Robustness and reproducibility of process transfer were checked three times on Pharma 16 at L/S 0.191 at three BFD values using both configurations (see Table 29, #1-3). Experiments were conducted on three different days. Powder blends were freshly produced each time.

Experiments on the Leistritz Micro 27 GL-28D were conducted only once (see Table 29, #1) at L/S 0.191 at the three BFD values as on Pharma 16 and the QbCon®1 to include a third granulator of different dimension and to broaden the assessment of the newly developed attempt.

Starting moistures of the powder blends were considered for the experiments on QbCon®1 and Pharma 16, but not for those on the Leistritz Micro 27 GL-28D. Samples of about 180-200 g were taken and dried by the drying unit on the QbCon®1 or tray-dried for those samples taken on Pharma 16 and Leistritz Micro 27 GL-28D according to the specifications in section 5.2.3.4.

In a second step, a formulation containing paracetamol, Granulac 200, MCC 101 and PVP K25 (20.51-58.97-17.44-3.08 % w/w) was twin-screw granulated with demineralised water and used for an in-depth investigation of the process transfer and its effect on granule and tablet qualities.

Process transfer occurred from the QbCon®25 onto Pharma 16 by utilising the same screw configuration on QbCon®25 as on QbCon®1 as well as configuration B on Pharma 16. Tip speeds and BFD values were again set as similar as possible on the two granulators during process transfer. In addition, two negative experiments were conducted in which the BFDs were kept similar to the process on the QbCon®25, but the tip speeds were set differently by intention. A L/S ratio of 19.5 % was applied throughout the study (L/S ratio at the shoulder, determined on the Brabender MTR as described in section 5.2.2, see Table 34 in appendix).

Starting moistures of the powder blends were measured three times but had only informative character with regard to the performance of the drying process. Three samples were taken per process setting on the QbCon®25 at the outlet of the drying unit– two times of approximately 650 g for thorough characterisation of unmilled (original) and milled granules and one time of approximately 1200 g for tableting and tablet characterisation. On Pharma 16, four samples had been taken at the barrel outlet of the granulator - twice of about 650 g for characterisation of original and milled granules, respectively, and twice of about 600 g for tableting and tablet characterisation. After finishing each sampling, the wet mass was transferred into the drying chamber of the fluidised bed dryer (recommended capacity of 700 g per drying) and dried according to the description in section 5.2.3.4. The processes were not stopped during drying and continued to run in steady state. The two samples for tableting and tablet characterisation were merged into one sample after they had been dried. An overview of the settings for the experiments on process transfer can be found in Table 30. More specific information on milling and tableting of granules are given in section 5.2.3.11.

The results related to this working package are depicted and discussed in section 3.2.

Table 28. Experimental plan of the DoE performed on the QbCon®1 (starting moisture: 1.15 ± 0.29%, n=6, mean ± s; *residual moisture: n=1, mean)

Screw configuration properties	No.	Run order	granulation process settings								drying process settings			
			n [min^{-1}]	PFR [kg/h]	L/S [-]	SFL [g]	BFD [kg/m^3]	v_{tip} [m/s]	τ [N/m^2]	BFL [-]	Vibration acceleration [m/s^2]	Inlet air flow [Nm^3/h]	Air T [°C]	Residual moisture* [%]
$l_{KB,tot}$: 45 mm	1	1	121	0.5	0.177	0.080	0.45	0.159	13.62	l	6.0	17.0	70	0.9
$\%_{KB}$: 8.98 %	2	5	123	0.5	0.191	0.080	0.45	0.161	12.92	l	5.0	15.0	70	0.9
V_{free}: 176.03 cm^3	3	3	124	0.5	0.205	0.080	0.45	0.163	12.32	l	5.0	15.0	75	0.9
	4	11	74	1.25	0.177	0.330	1.87	0.097	20.96	i	6.0	15.0	75	1.5
	5^{CP}	2	74	1.25	0.191	0.330	1.87	0.097	19.57	i	6.0	15.0	75	1.9
	6^{CP}	4	74	1.25	0.191	0.330	1.87	0.097	19.57	i	6.0	15.0	75	2.0
	7^{CP}	10	74	1.25	0.191	0.330	1.87	0.097	19.57	i	6.0	15.0	75	2.0
	8	7	75	1.25	0.205	0.330	1.87	0.098	18.38	i	6.0	15.0	75	2.4[a]
	9	6	84	2.5	0.177	0.580	3.29	0.111	47.70	h	5.0	17.0	87	2.4[a]
	10	9	85	2.5	0.191	0.580	3.29	0.111	44.55	h	5.0	17.0	87	2.4[a]
	11	8	85	2.5	0.205	0.580	3.29	0.111	41.83	h	5.0	17.0	87	3.0[a]

Legend:
$l_{KB,tot}$: total kneading block length, $\%_{KB}$: percentage of kneading blocks in screw configuration, KB: kneading block, KE: kneading element, CE: conveying element, PFR: powder feed rate, BFL: barrel fill level (low (l), intermediate (i), high (h)), Air T: drying air temperature, [a]: value exceeds target value (excess critically discussed in section 3.2.4.1), CP: centre point

Table 29. Process settings of preliminary transfer approaches. Experiments on the QbCon®1 were the basic ones and used for comparison. All experiments performed at L/S 0.191 (*n=6, mean ± s; **n=1, mean).

Granulator type	Screw configuration properties		Starting moisture* [%]	Granulation process settings						Drying process settings			
				n [min^{-1}]	PFR [kg/h]	BFD [kg/m^3]	v_{tip} [m/s]	τ [N/m^2]	BFL -	Vibration acceleration [m/s^2]	Inlet air flow [Nm^3/h]	Air T [°C]	Residual moisture** [%]
QbCon®1	basic[ax]	$l_{KB,tot}$: 45 mm $\%_{KB}$: 8.98 % V_{free}: 176.03 cm^3	1.15 ± 0.29	123	0.50	0.45	0.161	12.92	l	6.0	15.0	70	0.9
				74	1.25	1.88	0.097	19.57	i	6.0	15.0	75	1.9
				74	1.25	1.88	0.097	19.57	i	6.0	15.0	75	2.0
				74	1.25	1.88	0.097	19.57	i	6.0	15.0	75	2.0
				85	2.50	3.30	0.111	44.55	h	5.0	17.0	87	2.4[c]
Pharma 16	#0$_i$	A: $l_{KB,tot}$: 56 mm $\%_{KB}$: 8.72 % V_{free}: 122.80 cm^3	1.68 ± 0.20	200	0.55	0.44	0.163	17.16	l	tray-tried at 40°C			n.d.
				128	1.30	1.61	0.104	25.96	i				
				152	2.49	2.60	0.124	59.04	h				
	#0$_{ii}$			100	1.10	1.75	0.081	17.16	i[b]				n.d.
				172	2.20	2.03	0.140	59.02	i[b]				
	#1		1.26 ± 0.26	196	0.56	0.46	0.159	17.19	l	tray-tried at 40°C			n.d.
				118	1.40	1.89	0.096	25.88	i				
				135	2.79	3.30	0110	59.00	h				
	#2		1.07 ± 0.14	195	0.56	0.46	0.158	17.13	l	tray-tried at 40°C			n.d.
				119	1.39	1.87	0.097	25.96	i				
				135	2.79	3.31	0.110	59.12	h				
	#3		1.06 ± 0.10	195	0.56	0.46	0.158	17.13	l	tray-tried at 40°C			n.d.
				119	1.39	1.87	0.097	25.96	i				
				135	2.79	3.31	0.110	59.12	h				
	#0$_{iii}$	B: $l_{KB,tot}$: 46 mm $\%_{KB}$:7.17 % V_{free}: 122.42 cm^3	1.68 ± 0.20	208	0.53	0.41	0.169	17.29	l	tray-tried at 40°C			n.d.
				128	1.31	1.63	0.104	26.29	i				
				152	2.50	2.62	0.124	59.60	h				
	#1		1.26 ± 0.26	196	0.56	0.46	0.159	17.28	l	tray-tried at 40°C			n.d.
				119	1.40	1.88	0.097	26.24	i				
				136	2.79	3.28	0.111	59.76	h				
	#2		1.07 ± 0.14	196	0.56	0.46	0.159	17.31	l	tray-tried at 40°C			n.d.
				119	1.40	1.89	0.097	26.29	i				
				136	2.79	3.29	0.111	59.88	h				
	#3		1.06 ± 0.10	196	0.56	0.46	0.159	17.31	l	tray-tried at 40°C			n.d.
				119	1.40	1.89	0.097	26.29	i				
				136	2.79	3.29	0.111	59.88	h				

Granulator type	Screw configuration properties		Starting moisture* [%]	Granulation process settings						Drying process settings			
				n [min^{-1}]	PFR [kg/h]	BFD [kg/m^3]	v_{tip} [m/s]	τ [N/m^2]	BFL -	Vibration acceleration [m/s^2]	Inlet air flow [Nm^3/h]	Air T [°C]	Residual moisture** [%]
Leistritz Micro 27 GL-28D	#1	$l_{KB,tot}$: 60 mm $\%_{KB}$: 7.41 % V_{free}: 330.13 cm^3	n.d.	106 64 73	0.80 2.00 4.00	0.45 1.88 3.29	0.149 0.090 0.103	21.14 31.92 72.81	l i h	tray-tried at 40°C			n.d.
Legend: #: number of the transfer with the respective configuration, #0: first evaluation of screw configuration appropriate for transfer, [a]: basic data belong to the process data from the DoE depicted in Table 28, [b]: BFD mirrors an intermediate one, but tip speeds lower/higher than on the QbCon®1, [c]: value exceeds target value, n.d.: not determined (the product was stored open until it reached equilibrium with the ambient conditions), the other abbreviations and symbols are explained in Table 27													

Table 30. Process transfer from the QbCon®25 onto the Pharma 16 (*n=3, mean ± s; **n=1, mean). Experiments were performed at L/S 0.195.

Granulator type	Screw configuration	Starting moisture* [%]	Granulation process settings					Drying process settings			
			n [min^{-1}]	PFR [kg/h]	BFD [kg/m^3]	v_{tip} [m/s]	τ [N/m^2]	Vibration acceleration [m/s^2]	Inlet air flow [Nm^3/h]	Air T [°C]	Residual moisture** [%]
QbCon®25	see QbCon®1 in Table 29	2.43 ± 0.08	200 300	4.0 6.0	2.23 2.23	0.262 0.394	165.48 372.33	4.5 4.5	125 125	55 60	1.8 2.0
Pharma 16	see configuration B in Table 29	1.52 ± 0.42	321 482	4.4 6.6	2.23 2.23	0.261 0.392	219.52 495.99	as described in section 5.2.3.4			1.8 1.6
negative experiments:											
Pharma 16	see configuration B in Table 29	1.72 ± 0.20	291	4.0	2.24	0.237 (~90.5 %)[d]	182.47	as described in section 5.2.3.4			1.42
		1.77 ± 0.14	349	4.8	2.24	0.284 (~108.4 %)[d]	262.60				0.91
Legend: see Table 28 and Table 29, [d]: percentage value compared to original tip speed on QbCon®25 for 4 kg/h powder throughput											

5.2.3.8 Assessment of the impact of the kneading block configuration

The impact of one, two or three kneading blocks within a screw configuration of a powder blend of Granulac 200, MCC 101 and PVP K30 (80-17-3 % w/w) with otherwise the same screw elements (type and respective number) was investigated with demineralised water on the QbCon 1 at L.B. Bohle Maschinen + Verfahren (Germany).

The first screw configuration (hereinafter denoted as configuration I) used consisted of 3.75D LPCE >> 4D MPCE >> 6x (0.875D) KE 67.5° >> 5D MPCE >> 6x (0.875D) KE 67.5° >> 4D MPCE >> 1.5D SPCE, the second (configuration II) comprised 3.75D LPCE >> 4D MPCE >> 12x (1.75D) KE 67.5° >> 9D MPCE >> 1.5D SPCE and the third (configuration III) was composed of 3.75D LPCE >> 4D MPCE >> 4x (0.583D) KE 67.5° >> 3D MPCE >> 4x (0.583D) KE 67.5° >> 3D MPCE >> 4x (0.583D) KE 67.5° >> 3D MPCE >> 1.5D SPCE. The greater-than signs indicate the flow direction. Powder blend and demineralised water were added at the LPCE and the adjacent MPCE screw sections, respectively.

Experiments were performed at three barrel fill levels (low, intermediate, high) quantified as BFD according to Eq. (13) at L/S ratio of 0.191. Results and process data of the experiments applying screw configuration I were taken from the DoE mentioned in section 5.2.3.7.

Samples of about 180-200 g, based on dry mass, were taken at the outlet of the dryer unit. Process and specific drying settings on the QbCon®1 can be found in Table 31. Results are described and discussed in section 3.3.

Table 31. Process settings for the assessment of the impact of kneading block configuration on the QbCon®1 at L/S 0.191 (*n=6, mean ± s; **n=1, mean).

Granulator type	Screw configuration properties	Starting moisture* [%]	granulation process settings					drying process settings			
			n [min^{-1}]	PFR [kg/h]	BFD [kg/m^3]	v_{tip} [m/s]	BFL [-]	Vibration acceleration [m/s^2]	Inlet air flow [Nm^3/h]	air T [°C]	Residual moisture** [%]
QbCon®1	I[a], II, III: $l_{KB,tot}$: 45 mm $\%_{KB}$: 8.98 % V_{free}: 176.03 cm^3	I: 1.15 ± 0.29	123	0.5	0.45	0.161	l	6.0	15.0	70	0.9
			74	1.25	1.88	0.097	i	6.0	15.0	75	1.9
			85	2.5	3.30	0.111	h	5.0	17.0	87	2.4
		II: 0.98 ± 0.07	123	0.5	0.45	0.161	l	5.0	15.0	70	0.9
			74	1.25	1.88	0.097	i	6.0	15.0	75	2.1[b]
			85	2.5	3.30	0.111	h	5.0	17.0	87	4.3[b]
		III: 1.00 ± 0.07	123	0.5	0.45	0.161	l	5.0	15.0	70	1.0
			74	1.25	1.88	0.097	i	6.0	15.0	75	2.4[b]
			85	2.5	3.30	0.111	h	5.0	17.0	87	2.9[b]

Legend:
[a]: basic data belong to the process data from the DoE depicted in Table 28, [b]: value exceeds target value, the others: see Table 28 and Table 29

5.2.3.9 Assessment of the impact of screw lengths

Next to process transfer and assessment of the impact of kneading block configuration, the impact of varying screw lengths was examined on the Pharma 16 granulator of Granulac 200, MCC 101 and PVP K30 (80-17-3 % w/w) as powder blend and demineralised water as granulation liquid.

Three screw lengths and therefore four screw configurations (of different free, available volumes) were investigated. All contained two kneading blocks. The first screw configuration was 4D LPCE >> 4D SPCE >> 7x (1.75D) KE 60° >> 10D SPCE >> 7x (1.75D) KE 60° >> 19D SPCE and was the same configurational setup as described in section 5.2.3.7 for configuration A. The total barrel length of 640 mm was used. The second and third configurations were each shorter by 8D SPCE taken from the conveying part at the end of the configuration. The conveying end section consisted of 11D SPCE and 3D SPCE for the second and third configurations, respectively. The respective barrel lengths were 512 mm and 384 mm. The area in front of the LPCEs was fitted with cylindrical blind elements that only served as spacers. The powder feeder and liquid infeed port were moved towards the barrel outlet to adjust the used barrel lengths. The flow direction is displayed by the greater-than signs and the infeed of powder demineralised water occurred at the LPCE and the adjacent SPCE sections.

The experiments were performed at two barrel fill levels given as BFD (Eq. (13)), at L/S ratio of 0.191 with each configuration. Contrarily to the transfer approach, the powder feed rates were kept constant. The aim was to keep both the shear stresses (Eq. (1)) and BFD values similar throughout the investigations. Since the screw speeds had to be adjusted when the screw lengths were shortened, the tips speeds were different.

The starting moisture of the powder blend was neither determined nor considered in any way. Samples of about 180-200 g were taken at the barrel outlet and tray-dried (see section 5.2.3.4). Process settings are depcited in Table 32. Results are discussed in section 3.3, together with the examination of kneading block configuration.

Table 32. Process settings for the assessment of the impact of screw lengths on the Pharma 16 at L/S 0.191.

Screw information	PFR [kg/h]	n [min^{-1}]	SFL [g]	BFD [kg/m^3]	v_{tip} [m/s]	τ [N/m^2]
l_{barrel}: 640 mm (40D) V_{free}: 122.80 cm^3	1.5 3.0	150 150	0.199 0.397	1.62 3.23	0.122 0.122	35.69 71.39
l_{barrel}:512 mm (32D) V_{free}: 98.38 cm^3	1.5 3.0	185 185	0.161 0.322	1.64 3.27	0.150 0.150	35.49 70.98
l_{barrel}: 384 mm (24D) V_{free}: 73.96 cm^3	1.5 3.0	240 240	0.124 0.248	1.68 3.35	0.195 0.195	34.97 69.94

5.2.3.10 Evaluation of dimensionless description of the barrel fill level

A newly developed equation quantifying a barrel fill level during twin-screw granulation was tested regarding its validity of mass prediction inside the barrel as well as t_1-times during residence time measurements.

Examination occurred with three formulations containing MCC 102 and dicalcium phosphate anhydrous (DCP) A12 (DI-CAFOS A12) of varying percentages (20:80, 60:40, 100:0 % w/w) on Pharma 16. Three screw setups were tested, where the first one (hereinafter denoted as configuration CE only) consisted of conveying elements only, the second and third setups had kneading block (KB) of nine kneading discs each at either 30° (second configuration, denoted as KB 30°) or 60° (third configuration, denoted as KB 60°) stagger angles. Screw setup was 4D LPCE >> 36.5D SPCE for configuration CE only, 4D LPCE >> 10D SPCE >> 9x (2.25D) KE 30° >> 24D SPCE and 4D LPCE >> 10D SPCE >> 9x (2.25D) KE 60° >> 24D SPCE for configuration KB 30° and KB 60°, respectively. The greater-than signs indicate flow direction, powder infeed occurred at the LPCE part and liquid infeed at the adjacent SPCE screw sections. Free volumes of the screw configurations were 122.26 cm^3 when only CEs had been used and 122.76 cm^3 for the other two setups.

Experiments were carried out at three powder feed rates (1.5-3.0-4.5 kg/h) at L/S ratio of 0.150 with each configuration. At each powder feed rate, three screw speeds were applied (150-300-450 min^{-1} for 1.5 as well as 3.0 kg/h and 200-300-450 min^{-1} for 4.5 kg/h). After steady state was reached, the process (screws, powder feeder, pump) was stopped simultaneously. The barrel outlet was cleaned from material remains, the screws were started, the material exiting the barrel was collected in a vessel and weighed on a precision balance (1507 004, Sartorius, Germany). Afterwards, the process was started again and the determination procedure repeated. Five measurements were performed at each process setting being able to calculate mean and standard deviation.

The starting moisture was not considered in this working package. Results are discussed in section 3.4.

5.2.3.11 Milling and tableting of granules

Granule batches which were further processed into tablets were, after storage, first milled using a high speed cone mill (1 mm rasp sieve, BTS 100, L.B. Bohle Maschinen + Verfahren, Germany). For the preparation of the final tablet formulation, 1.5 % (w/w) sodium croscarmellose was added to 97.5 % (w/w) of granules (produced as specified in section 5.2.3.7; comprising paracetamol, Granulac 200, MCC 101 and PVP K25 (20.51-58.97-17.44-3.08 % w/w)) and blended for 10 min at 49 min^{-1} on a Turbula blender (T2F, Willy A. Bachofen, Switzerland). After blending, 1 % (w/w) magnesium stearate was added and blended for further 2 min on the same Turbula blender.

Approximately 150 tablets of 300 mg mass were compressed on a single punch tablet press (STYL'One Evolution, Medelpharm, France) using a flat-faced Euro B punch of 11.28 mm diameter (A=1.00 cm^2). Compaction was performed in the force mode at 25 % compression speed. Five compaction pressures (50, 100, 150, 200, 250 MPa) were applied. Tablets were produced in "1 compression cycle" mode. A feed shoe was utilised at 10 % speed. Acquisition frequency of the tableting process was set to 1000 Hz.

Tablets were stored in closed plastic bags at constant temperature and relative humidity (21 °C, 45 % relative humidity) for at least 72 h before further characterisation was conducted.

Results of the tablet batches are shown and discussed in section 3.2.

5.2.4 Characterisation methods

5.2.4.1 Loss on drying of granules

Analogous to the LOD determination of starting material (powder blends) (see section 5.2.1.1), the LOD determinations of granules were carried out and calculated according to Eq. (41).

Depending on the number of repetitions, which is specified in the respective sections, the means and standard deviations were calculated.

5.2.4.2 Determination of particle size distribution of starting material

To measure powder particle sizes and their distributions (PSD), a dynamic image analysis (Camsizer XT, Retsch, Germany) was used. A dispersion pressure of 0.8 bar was applied to de-agglomerate the primary particles from loosely-bound agglomerates while their sizes were determined in x-jet mode.

Sample amounts of approximately 10 g of starting material were measured. Measurements were performed only once for each starting material.

5.2.4.3 Determination of granule size distribution

The size distributions of granules were determined by utilising dynamic image analysis (x-fall mode, Camsizer XT, Retsch or CPA 2-1, Haver & Boecker, both Germany).

After representative division of sample batches (see section 5.2.1.2), sub-samples of about 20-30 g were measured. Measurements were performed three times.

Derived parameters from the size distribution were x_{10}, x_{50} and x_{90}, where the subscripted numbers mirror a granule size, where a percentage proportion of granules of the total amount of granules were below. The span indicates the width of a size distribution and can be calculated according to Eq. (45)

$$span = \frac{x_{90} - x_{10}}{x_{50}} \tag{45}$$

5.2.4.4 Earth Mover's Distance for comparing size distributions

To evaluate the similarity between granule size distributions (q3), the Earth Mover's Distance (EMD), also known as Wasserstein distance, was applied as statistical metric by using an in-house written Python script (version 1.4, written by Stefan Klinken) based on the description of Hu et

al. [144]. The assessment of the similarity of a test distribution profile with a reference distribution profile is enabled by comparing these distribution profiles by measuring the distance between them. Profile comparison is done by first calculating the mean reference of all individual reference curves and then calculating the distances between mean reference and all single reference curves to assess the variability. If only one reference distribution profile is available, this single curve is also the mean reference and no variability can be determined. In a next step, the distances between the individual test distribution profiles and the mean reference curve are calculated allowing for the assessment of the variability between the individual test profiles and the mean reference.

For the calculation of the EMD, the distribution profiles are considered as histograms, which can mathematically be represented as $P = \{(x_1, p_1),\ (x_2, p_2), \dots, (x_m, p_m)\}$ and $Q = \{(y_1, q_1),\ (y_2, q_2), \dots, (y_n, q_n)\}$, where P and Q reflect the histograms of the distribution profiles to be compared with each other, x_i and y_j are the information on the location of each column within the histogram profile and p_i and q_j are the respective heights, which can also be considered as weights in the context of the EMD. In a next step, the distances d between the columns at locations x_i and y_j of the two histograms are determined, where the distance is meant to be the distance along the x-axis and depicted as d_{ij}. Since the EMD measures the work necessary to transfer one distribution profile into the other, the optimal work flow (least amount of work), F, needed to move the weight, f_{ij}, present at the different locations within a distribution from distribution profile P to profile Q will be determined according to Eq. (46) [144, 168]

$$WORK(F, P, Q) = \sum_{i=1}^{m} \sum_{j=1}^{n} f_{ij} d_{ij} \tag{46}$$

by considering the following restriction for f_{ij} that must be fulfilled:

1) $f_{ij} \geq 0,\ i = 1, \dots, m\ 1, j = 1, \dots, n$
2) $\sum_{j=1}^{n} f_{ij} \leq p_i,\ i = 1, \dots, m$
3) $\sum_{i=1}^{m} f_{ij} \leq q_j,\ j = 1, \dots, n$
4) $\sum_{i=1}^{m} \sum_{j=1}^{n} f_{ij} = \min(\sum_{i=1}^{m} p_i, \sum_{j=1}^{n} q_i)$

where 1) states that f_{ij} must be nonnegative, 2) ensures that the amount of weight moved from P to Q does not exceed the weight available in P, 3) ensures that the amount of weight moved from P to Q does not exceed the maximum weight that can be unloaded in Q and 4) indicates that all weight moved from P to Q must be the entire amount of weight that was available in P and that no remains left.

When the lowest amount of work was identified, the EMD between the distributions profiles are determined as given in Eq. (47) [144, 168]

$$EMD(P, Q) = \frac{\sum_{i=1}^{m} \sum_{j=1}^{n} f_{ij} d_{ij}}{\sum_{i=1}^{m} \sum_{j}^{n} f_{ij}} \tag{47}$$

When the EMD approaches to zero, the size distributions can be considered very similar, or even identical at an EMD of zero, while higher EMDs indicate dissimilarity. Since there are no limits where similarity is defined, the individual EMDs between different test samples to the reference must therefore be used as comparative values.

The respective reference to which the tests are assessed is clarified in the respective sub-sections of section 3.

5.2.4.5 Bulk density and tapped density of powders and granules

Bulk and tapped density of powder blends and granules were determined three times in accordance with the Ph.Eur. monograph 2.9.34 [128].

The results of every single determination were used for a rough approximation of flowability, displayed as Hausner factor and calculated according to Ph.Eur. 2.9.36 [128] by Eq. (48)

$$Hausner\ factor = \frac{V_0}{V_f} = \frac{\rho_{tapped}}{\rho_{bulk}} \tag{48}$$

where V_0 is the unsettled apparent volume, V_f is the final tapped volume, ρ_{tapped} is the tapped density and ρ_{bulk} is the bulk density.

The three Hausner factor values were used to calculate the mean and standard deviation.

5.2.4.6 Helium density of powders and granules

Particle density was determined six times at 25 ± 0.2 °C at 1.6 bar from raw materials, powder blends and granules applying helium pycnometry (AccuPyc 1330, Micromeritics, Georgia, USA). Almost three-quarter of the sample vessel with 3.5 cm^3 volume was filled and the net quantity weighed (analytical balance, MC210P, Sartorius, Germany). Five measurement cycles were done after ten purging cycles had been performed. The filling pressure of the helium was set to 137.90 kPa. Each mean density of the five single measurements was considered as one determination cycle. For the final calculation of the mean particle density and its standard deviation, the six mean densities of the respective determination cycles were used.

5.2.4.7 Envelope density of granules

Sub-samples of 2-3 g (analytical balance, CP224S, Sartorius, Germany) containing the total spectrum of granular material were examined for their granule densities using an envelope density analyser (GeoPyc 1360, Micromeritics, Georgia, USA). Firstly, a blank measurement was performed using a solid medium with good flowability (quasi-fluid, DryFlo®), which was filled into a precision cylinder. A piston compacted the medium and determined a starting volume. The sub-sample was added afterwards and thoroughly incorporated into the medium. The medium-sample-mixture was compacted again. The final volume was determined and the envelope density

was automatically calculated [169, 170]. Targeted volume proportion of the sub-sample in the total volume was approximately 15 %. Six sub-samples of each batch were measured and cumulated to a mean (representing n=1).

The means of the sub-samples were used to calculate the overall mean and its standard deviation.

5.2.4.8 Granule porosity

Granule porosities were calculated according to Eq. (49)

$$\varepsilon_{granule} = \left(1 - \frac{\rho_{env}}{\rho_{He}}\right) \cdot 100\% \tag{49}$$

where $\varepsilon_{granule}$ is the granule porosity, ρ_{env} is the envelope density and ρ_{He} is the particle density of the blend.

5.2.4.9 Granule friability

Friability of granules was determined using an air jet sieve (LS-N 200, Hosokawa Alpine, Germany) with 125 µm sieve insert based on the description in Djuric et al. [75].

A sample mass of about 12 g (precision balance, ED 2201-CW, Sartorius, Germany) was given onto the sieve. Fine and loosely-bound particles were removed first by applying a negative pressure of 600 Pa for one minute. After that, the remaining mass was determined and used for the measurement of granule friability where 2000 Pa negative pressure was applied for ten minutes. Friability was finally defined as mass loss in percent [75].

Three measurements were conducted. The mean and standard deviation were calculated.

5.2.4.10 Granule strength and failure load

Granule strength, also failure load, was measured based on an uniaxial confined compression analysis [162] using the entire spectrum of the milled granules intended to be used in the tableting process (see section 5.2.3.11). A single punch tablet press (STYL'One Evolution, Medelpharm, France) with a flat-faced Euro B punch of 11.28 mm diameter and a punch surface area of 1.00 cm^2 was used for this characterisation method. The speed of the upper punch was set to 3.5 mm/min. Filling was conducted by hand into the die of 10 mm dosage height. During the measurement, the granule bed was steadily compressed uniaxially until a final height of 5 mm was reached. The frequency of data acquisition was set to 500 Hz.

Analysis was conducted according to Arndt et al. [141] and is based on Eq. (50) [162]

$$\ln P = \ln\left[\frac{\tau}{\alpha}\right] + \alpha\epsilon + \ln(1 - e^{-\alpha\epsilon}) \tag{50}$$

where P is the applied compaction pressure, τ is the cohesive strength, α is the friction coefficient and ϵ is the natural strain. P was calculated from the force applied on the granules and the cross-

sectional surface area of the punch, while the ϵ was obtained by referring the initial distance between the two punches to the actual distance. At large values of the ϵ, the plot revealed to linear, which slope corresponded to α and its y-axis-intercept to the $ln\ (\tau/\alpha)$-term, from which, in turn, τ was calculated.

The failure load was determined using Eq. (51) [162]

$$F_{calc} = \frac{\pi d_a^2}{4} \cdot \tau \tag{51}$$

where F_{calc} is the average failure load of a granule (force needed for disaggregation) and d_a is the mean granule diameter (x_{50}) of the milled granule batch obtained from GSD measurements (see section 5.2.4.3).

Eight replicate measurements were conducted with each granule batch.

5.2.4.11 Ring shear cell tester

Characterisation of flowability of granules and powder blend occurred on a ring shear cell tester RST-01.pc with an RST-CONTROL 95 application (Schulze Schüttgutmesstechnik, Germany) by determining the flow function coefficient (ff_c). Flowability of a bulk is defined as given in Eq. (52)

$$ff_c = \frac{\sigma_1}{\sigma_c} \tag{52}$$

where σ_1 is the unconfined yield strength and σ_c is the consolidation stress.

A normal load of 5000 Pa was applied as pre-shearing at first to ensure similar working conditions in all measurements. Secondly, samples were sheared at four normal stresses of 1000, 2000, 3000 and 4000 Pa in order to calculate a yield locus, which depicts the strength of the respective bulk. Each batch was examined in duplicate; the mean was calculated and used for interpretation.

The classification of bulk flowability [147, 171] can be found in Table 33.

Table 33. Classification of flowability of solids.

ff_c-value	**Flow behaviour**
$ff_c < 1$	Not flowing
$1 < ff_c < 2$	Very cohesive
$2 < ff_c < 4$	Cohesive
$4 < ff_c < 10$	Easy flowing
$10 < ff_c$	Free flowing

5.2.4.12 Resistance to crushing and tensile strength of tablets

The force necessary to crush tablets was determined according to Ph.Eur. 2.9.8 [128] with 20 tablets (instead of 10 tablets as stated in the monograph) of each compaction pressure using a tablet hardness tester (TBH 210, Erweka, Germany). The tablets were chosen randomly.

Height and diameter of each tablet were measured (*out-of-die method*) with a calliper (Garant digital DC2, Hoffmann Group, Germany) to be able to calculate the tablets tensile strengths by applying Eq. (53) [172]

$$TS = \frac{2 \cdot F}{\pi \cdot h_{tablet} \cdot d_{tablet}} \tag{53}$$

where *TS* is the tensile strength (in MPa), *F* is the force at which the tablet disrupted (breaking force) (in N), h_{tablet} is the tablet height and d_{tablet} is the tablet diameter.

5.2.4.13 Tablet porosity and solid fraction

The porosity of the tablets compressed at different compression pressures were calculated by determining the apparent tablet density based on the tablets cylindrical geometry according to Eq. (54)

$$\rho_{tablet} = \frac{m_{tablet}}{\pi \cdot \left(\frac{d_{tablet}}{2}\right)^2 \cdot h_{tablet}} = \frac{m_{tablet}}{V_{tablet}} \tag{54}$$

where ρ_{tablet} is the apparent density of a tablet, $d_{tablet/2}$ is the tablet radius, m_{tablet} is the respective mass and V_{tablet} is the tablet volume.

In a second step, tablet porosity was calculated using Eq. (55)

$$\varepsilon_{tablet} = 1 - \left(\frac{\rho_{tablet}}{\rho_{He}}\right) \tag{55}$$

where ε_{tablet} is the tablet porosity.

5.2.4.14 Friability of tablets

Friability was determined as specified in Ph.Eur. 2.9.7 [128] by applying 100 rotations in total. Dust on tablets was removed using compressed air before and after determination.

5.2.4.15 Disintegration of tablets

Test of disintegration was executed in compliance with Ph.Eur. 2.9.1 [128] with tablets manufactured at 50, 150 and 250 MPa compaction pressure utilising a disintegration tester (ZT 32, Erweka, Germany). Tablets were tested in approximately 650 mL demineralised water of 37 ± 0.5 °C.

5.2.4.16 Uniformity of tablet mass

Uniformity of mass was examined and evaluated in accordance with Ph.Eur. 2.9.5 (± 5 % deviation) [128] with the same 20 tablets taken for the investigation of resistance to crushing (see

section 5.2.4.12). Tablets had been weighed (analytical balance, FA 210-4iCE, Faust Labscience, Germany) before they underwent the procedure in section 5.2.4.12.

6 Appendix

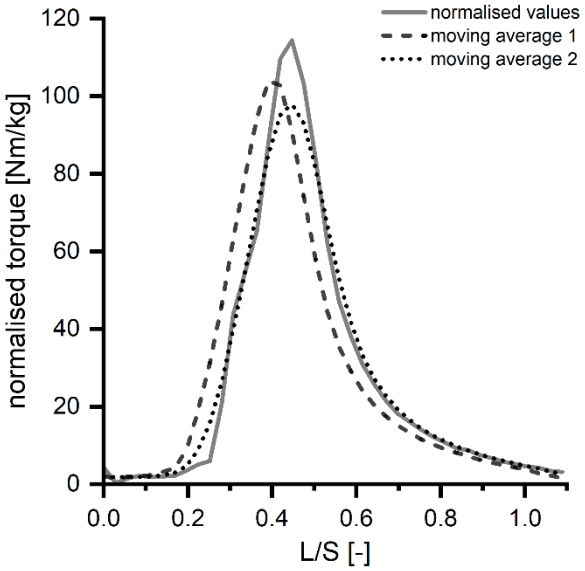

Figure 41. Smoothed approach of the normalised torque curve with the first application of the moving average and its resulting curve-shift to the left and with the position correction by applying the moving average second time.

Table 34. Further investigated materials and calculated L/S ratios using the MTR (*n=10x10, **n=6, ***n=3, mean ± s). Water addition scheme was kept constant throughout the experiments with the respective formulations.

Material [% w/w]	Water addition [µL]	Mean volume* [µL]	Starting Moisture** [%]	L/S ratio at		
				IP*** [-]	Max*** [-]	Min*** [-]
Granulac 200, 17 % MCC 101, 3 % PVP K30	500	0.4858	1.09 ± 0.07	0.211 ± 0.008 0.293 ± 0.008	0.191 ± 0.007# 0.329 ± 0.001	0.224 ± 0.017
Granulac 200, 20.51 % PCM, 17.44 % MCC 101, 3.08 % PVP K25	500	0.4886	1.31 ± 0.07	0.195 ± 0.009	0.314 ± 0.003	-
DCP A12, 20 % Pearl 200SD, 3 % PVP 30	200	0.1883	0.32 ± 0.04	0.127 ± 0.007 0.153 ± 0.006	0.099 ± 0.007 0.165 ± 0.003	0.139 ± 0.006

Legend:
PCM: paracetamol, PVP: polyvinylpyrrolidone, MCC: microcrystalline cellulose, DCP: dicalcium phosphate anhydrous, Pearl: Pearlitol (mannitol), IP: inflection point, Max: maximum, Min: minimum, #: L/S ratio at shoulder "maximum" on the torque curve

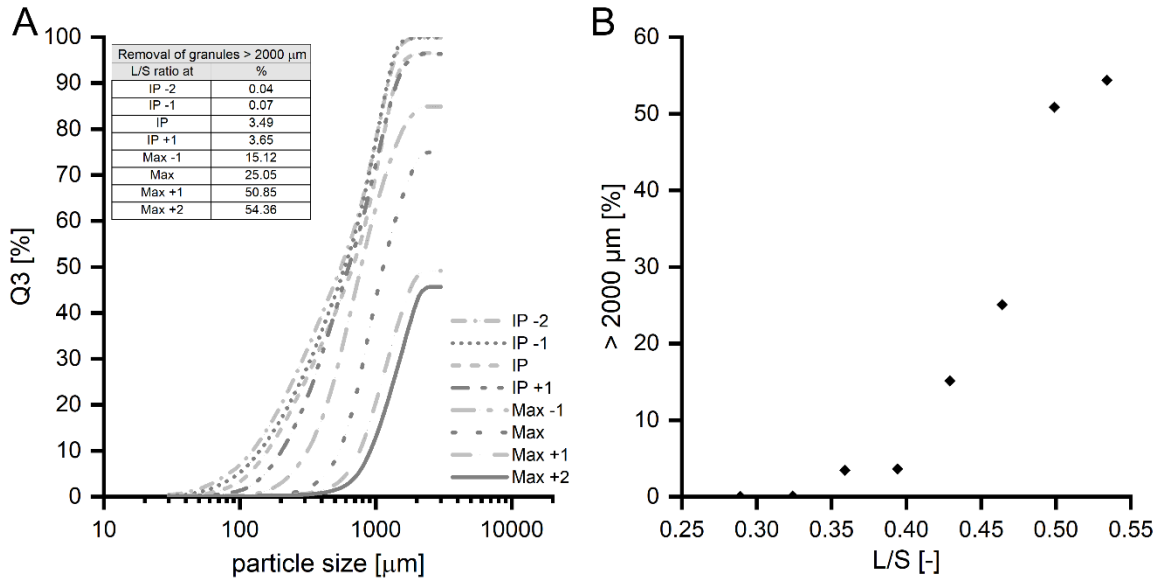

Figure 42. Original GSD of TM: A) after removal of granules greater 2000 µm; percentage proportions of removed granules are depicted in the inserted table and B) the removed proportions at the different L/S ratios (removal step: with the total sample; GSD: n=3, mean).

Table 35. Percentage proportion of defined volume fractions calculated from Q3 curves obtained during the DoE (n=1).

Barrel fill level	PFR [kg/h]	L/S [-]	BFD [kg/m³]	Fine fraction [%]	Yield fraction [%]	Oversized fraction [%]
low	0.5	0.177	0.45	0.4	66.8	32.8
	0.5	0.191	0.45	0.5	61.2	38.3
	0.5	0.205	0.45	0.5	59.5	40.0
intermediate	1.25	0.177	1.87	0.7	74.2	25.1
	1.25	0.191	1.87	0.7	75.4	23.8
	1.25	0.191	1.87	0.7	75.1	24.2
	1.25	0.191	1.87	0.7	74.8	24.5
	1.25	0.205	1.87	0.6	74.4	25.0
high	2.5	0.177	3.29	0.5	68.9	30.6
	2.5	0.191	3.29	0.3	68.3	31.4
	2.5	0.205	3.29	0.3	70.3	29.4

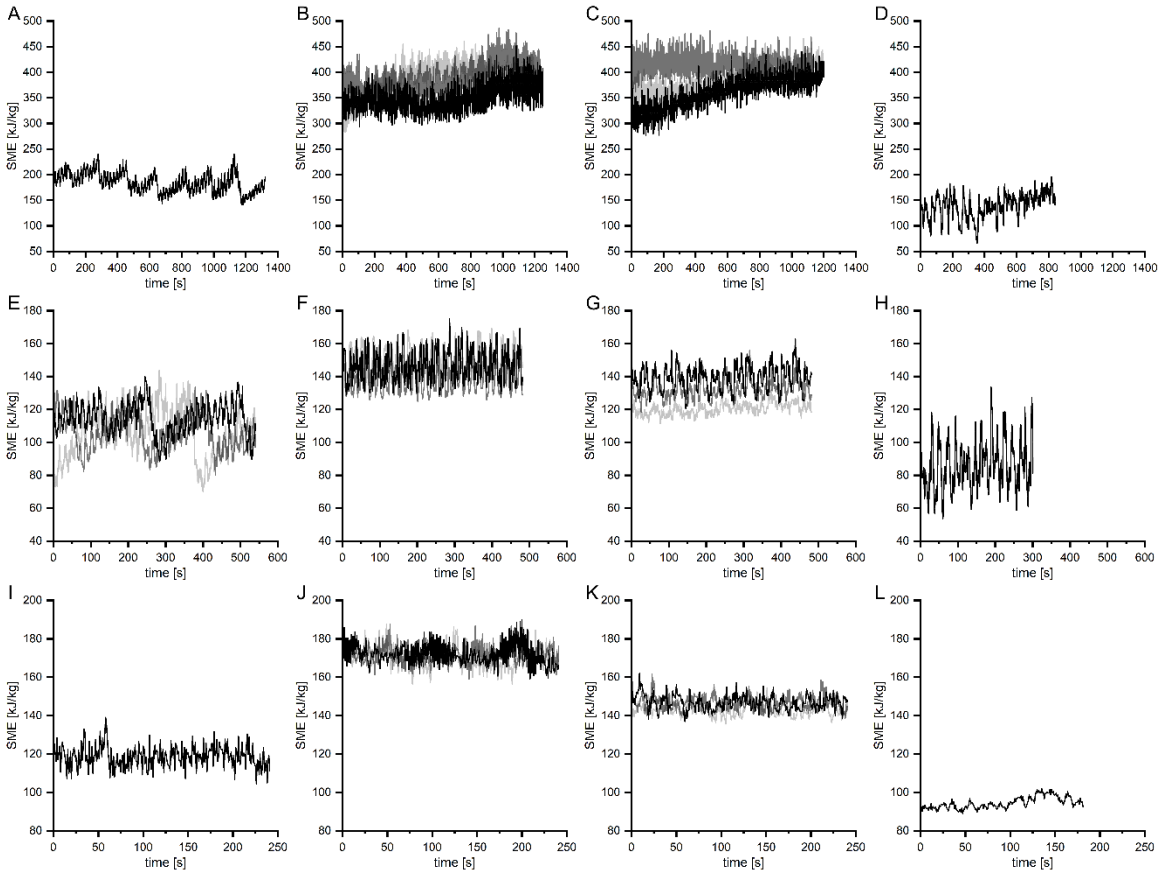

Figure 43. SME for each run during sampling period on the different twin-screw granulators using screw configuration: A, E, I) on the QbCon®1, B, F, J) A on Pharma 16 and C, G, K) B on Pharma 16 and D, H, L) on the Leistritz Micro 27 GL-28D at the different fill levels: A-D) low, E-H) intermediate and I-L) high BFD (n=1).

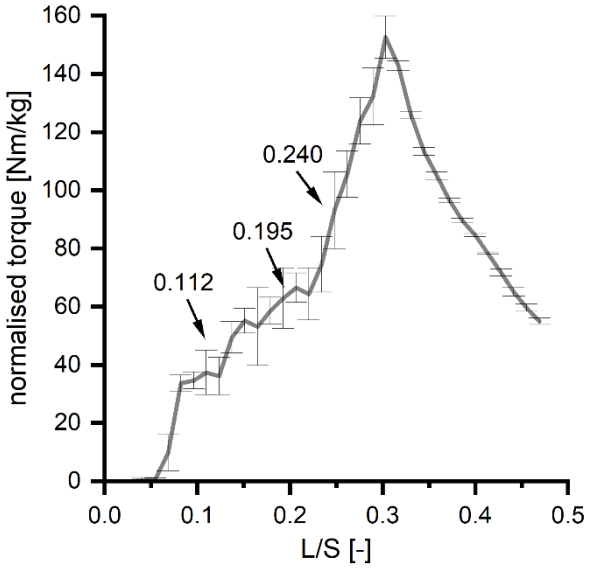

Figure 44. Normalised torque curve for formulation composed of paracetamol, lactose monohydrate, MCC and PVP obtained on the Brabender MTR (n=3, mean ± s). Arrows show the target liquid contents for the transfer study.

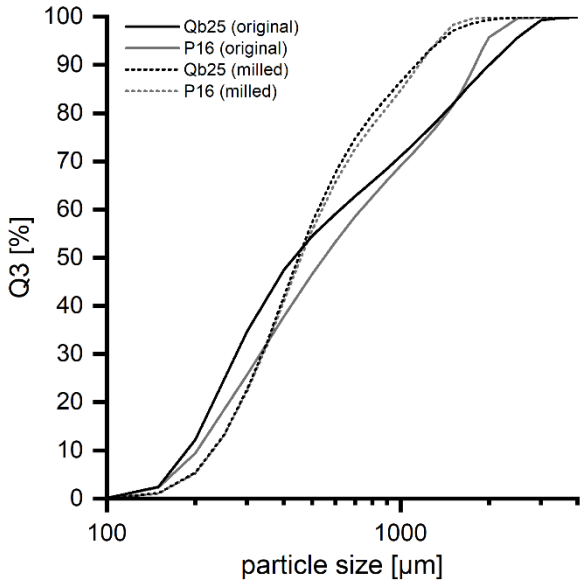

Figure 45. GSDs obtained during process transfer with initial PFR of 6 kg/h on the QbCon®25 and its counterpart on Pharma 16 applying similar tip speeds (n=3, mean).

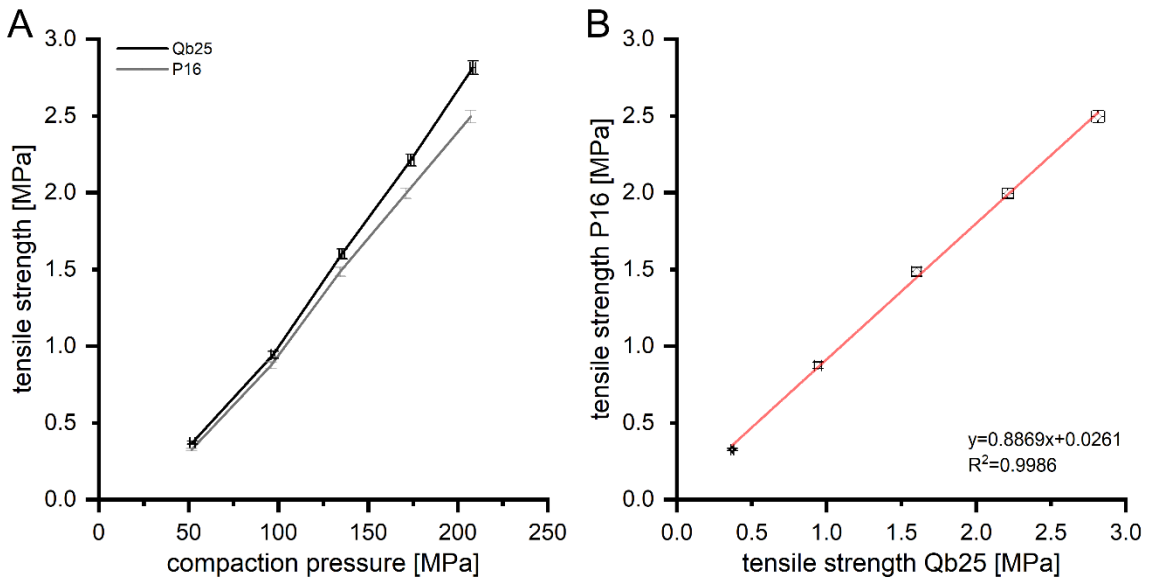

Figure 46. Examination of tablets made up of granules produced at 6 kg/h powder throughput on the QbCon®25 and its counterpart on Pharma 16: (A) tabletability plot and (B) correlation plot (n=20, mean ± CI).

Table 36. p-values of statistical analysis (F- and two-sided t-test, $\alpha = 0.05$) of tablet tensile strengths depicted in Figure 46A manufactured with the granule batches obtained at different process settings. Asterisks show a significant difference.

Compression pressure [MPa]	Qb25 <-> P16	
	F-test	t-test
50	0.398	$^{*}2.282 \cdot 10^{-8}$
100	0.676	$^{*}1.028 \cdot 10^{-4}$
150	0.596	$^{*}4.488 \cdot 10^{-6}$
200	0.534	$^{*}2.716 \cdot 10^{-10}$
250	0.669	$^{*}8.702 \cdot 10^{-13}$

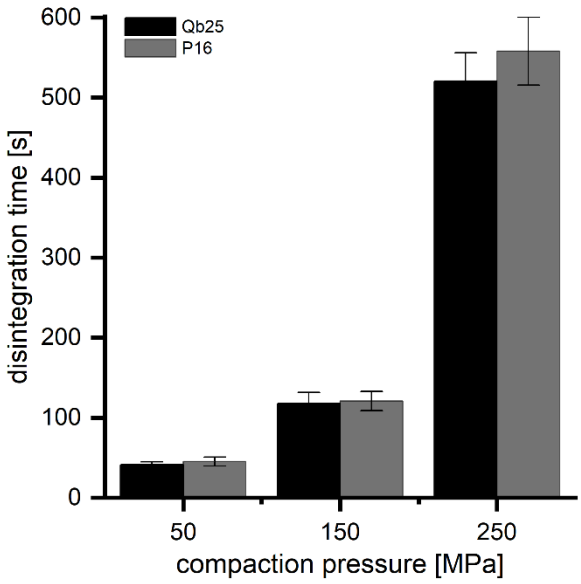

Figure 47. Disintegration times of tablets made up of granules produced at 6 kg/h mass throughput on the QbCon®25 and its counterpart on Pharma 16 (n=6, mean ± s).

Table 37. Variable x determined with non-linear curve fit for the given material compositions and total material throughputs. The new factor f was the product of the actual factor f and the determined variable x (*n=1).

Formulation MCC 102 : DCP A12 [% w/w]	Screw configuration	PFR [kg/h]	$\dot{m}_{tot}$ [kg/h]	n [min^{-1}]	$\overline{v}_{harmonic}$ [mm/s]	Actual factor f [-]	Determined variable x^* [-]	New factor $f_{new}{}^*$ [-]
20:80	Only CE	1.5	1.73	150 300 450	41.1 82.3 123.4	1.5	0.8014	**1.20**
		3.0	3.45	150 300 450	41.1 82.3 123.4	1.5	0.9192	**1.38**
		4.5	5.18	200 300 450	54.8 82.3 123.4	1.5	0.9403	**1.41**
	KB 30°	1.5	1.73	150 300 450	42.8 85.6 128.4	1.5	1.0016	**1.50**
		3.0	3.45	150 300 450	42.8 85.6 128.4	1.5	1.1070	**1.66**
		4.5	5.18	200 300 450	57.1 85.6 128.4	1.5	1.0330	**1.55**
	KB 60°	1.5	1.73	150 300 450	41.9 83.9 125.8	1.5	1.1393	**1.71**
		3.0	3.45	150 300 450	41.9 83.9 125.8	1.5	1.1907	**1.79**
		4.5	5.18	200 300 450	55.9 83.9 125.8	1.5	1.1453	**1.72**
60:40	Only CE	1.5	1.73	150 300 450	41.1 82.3 123.4	1.5	0.7615	**1.14**
		3.0	3.45	150 300 450	41.1 82.3 123.4	1.5	0.8746	**1.31**

Formulation MCC 102 : DCP A12 [% w/w]	Screw configuration	PFR [kg/h]	$\dot{m}_{tot}$ [kg/h]	n [min^{-1}]	$\overline{v}_{harmonic}$ [mm/s]	Actual factor f [-]	Determined variable x^* [-]	New factor $f_{new}{}^*$ [-]
		4.5	5.18	200 300 450	54.8 82.3 123.4	1.5	0.8929	**1.34**
	KB 30°	1.5	1.73	150 300 450	42.8 85.6 128.4	1.5	0.9135	**1.37**
		3.0	3.45	150 300 450	42.8 85.6 128.4	1.5	1.1209	**1.68**
		4.5	5.18	200 300 450	57.1 85.6 128.4	1.5	1.1640	**1.75**
	KB 60°	1.5	1.73	150 300 450	41.9 83.9 125.8	1.5	0.9744	**1.46**
		3.0	3.45	150 300 450	41.9 83.9 125.8	1.5	1.1927	**1.79**
		4.5	5.18	200 300 450	55.9 83.9 125.8	1.5	1.2670	**1.90**
100:0	Only CE	1.5	1.73	150 300 450	41.1 82.3 123.4	1.5	0.8790	**1.32**
		3.0	3.45	150 300 450	41.1 82.3 123.4	1.5	1.0268	**1.54**
		4.5	5.18	200 300 450	54.8 82.3 123.4	1.5	1.0427	**1.56**
	KB 30°	1.5	1.73	150 300 450	42.8 85.6 128.4	1.5	1.0598	**1.59**
		3.0	3.45	150 300 450	42.8 85.6 128.4	1.5	1.1870	**1.78**

Formulation MCC 102 : DCP A12 [% w/w]	Screw configuration	PFR [kg/h]	$\dot{m}_{tot}$ [kg/h]	n [min^{-1}]	$\overline{v}_{harmonic}$ [mm/s]	Actual factor f [-]	Determined variable x^* [-]	New factor $f_{new}{}^*$ [-]
		4.5	5.18	200 300 450	57.1 85.6 128.4	1.5	1.2446	**1.87**
	KB 60°	1.5	1.73	150 300 450	41.9 83.9 125.8	1.5	1.0522	**1.58**
		3.0	3.45	150 300 450	41.9 83.9 125.8	1.5	1.3298	**1.99**
		4.5	5.18	200 300 450	55.9 83.9 125.8	1.5	1.5862	**2.38**

Table 38. Mass hold-ups from literature data at defined process conditions and screw configurations (estimated values from Figures in respective sources). Theoretical mass hold-ups according to the improved equation (Eq. (24)) with application of factor f of 1.5. The underlined screw speeds were examined in the respective publication, but mass hold-up data were not revealed.

Source		Formulation	Screw configuration	PFR [kg/h]	n [min^{-1}]	$\overline{v}_{harmonic}$ [mm/s]	Mass hold-up theory [g]	Mass hold-up given [g]
Gorringe et al. [143]	in Figure 1a	Lactose monohydrate, MCC 101, hypromellose, croscarmellose sodium	Screw A	1.5	60 150 300 500	17.6 44.0 88.1 146.8	16.68 6.67 3.34 2.00	25 13 10 7.5
				3.0	110 200 500	32.3 58.7 146.8	18.19 10.01 4.00	29 18 11
				6.0	300 500	88.1 146.8	13.34 8.01	21 16
	in Figure 1b		Screw B	1.5	55 100 <u>250</u> 300 500	16.6 30.2 75.4 90.5 150.8	18.51 10.18 - 3.39 2.04	25.5 16.5 - 10 7.5
				3.0	<u>130</u> 200 500	39.2 60.3 150.8	- 10.18 4.07	- 21 14

Source		Formulation	Screw configuration	PFR [kg/h]	n [min^{-1}]	$\overline{v}_{harmonic}$ [mm/s]	Mass hold-up theory [g]	Mass hold-up given [g]
				6.0	300	90.5	13.58	22
					400	120.7	-	-
					500	150.8	8.15	15.5
Mundozah et al. [95]	in Figure 6	Polymethyl methacrylate (PMMA)	Screw A	1.0	100	29.6	6.20	11.5
					300	88.7	2.07	7.5
					500	147.9	1.24	6
					900	266.1	0.69	5.5
				2.0	100	29.6	12.40	16
					300	88.7	4.13	10.5
					500	147.9	2.48	8
					900	266.1	1.38	6.5
				3.0	100	29.6	18.60	22
					300	88.7	6.20	12.5
					500	147.9	3.72	9
					900	266.1	2.07	7
	in Figure 8		Screw B	1.0	100	28.3	6.47	8.5
					300	84.9	2.16	3.8
					500	141.6	1.29	2.1
					900	254.8	0.72	2
			Screw C	1.0	100	28.0	6.55	5.2
					300	83.9	2.18	2.5
					500	139.9	1.31	1.8
					900	251.8	0.73	1.1
	in Figure 9	Lactose monohydrate	Screw A	1.0	100	29.6	6.20	15
					300	88.7	2.07	7.5
					500	147.9	1.24	5.5
					900	266.1	0.69	2.8
			Screw B	1.0	100	28.3	6.47	11.5
					300	84.9	2.16	3.1
					500	141.6	1.29	3
					900	254.8	0.72	2.2
			Screw C	1.0	100	28.0	6.55	6
					300	83.9	2.18	2.5
					500	139.9	1.31	2
					900	251.8	0.73	1.5

7 References

[1] S. Sacher, J.G. Khinast, An overview of pharmaceutical manufacturing for solid dosage forms, in: M.G. Ierapetritou, R. Ramachandran (Eds.) Process Simulation and Data Modeling in Solid Oral Drug Development and Manufacture, Springer New York, New York, NY, 2016, pp. 311-383.

[2] A. Fahr, Voigt's Pharmaceutical Technology, John Wiley & Sons Ltd., Hoboken, NJ, 2018.

[3] Council of Europe, "Tablets", European Pharmacopoeia, 10th ed., Strasbourg, 2020

[4] M. Leane, K. Pitt, G. Reynolds, A proposal for a drug product Manufacturing Classification System (MCS) for oral solid dosage forms, Pharmaceutical Development and Technology, 20 (2015) 12-21.

[5] K.H. Bauer, K.-H. Frömming, C. Führer, Lehrbuch der Pharmazeutischen Technologie, 9. Auflage, Wissenschaftliche Verlagsgesellschaft Stuttgart, 2012.

[6] S.L. Lee, T.F. O'Connor, X. Yang, C.N. Cruz, S. Chatterjee, R.D. Madurawe, C.M.V. Moore, L.X. Yu, J. Woodcock, Modernizing pharmaceutical manufacturing: from batch to continuous production, Journal of Pharmaceutical Innovation, 10 (2015) 191-199.

[7] B.J. Ennis, J.D. Litster, T. Allen, R.H. Snow, Size reduction and size enlargement, in: R.H. Perry (Ed.) Perry's Chemical Engineer's Handbook, McGraw-Hill, New York, 1997, pp. 1748-1836.

[8] R. Boerefijn, P.-R. Dontula, R. Kohlus, Chapter 14: Detergent granulation, in: A.D. Salman, M.J. Hounslow, J.P.K. Seville (Eds.) Handbook of Powder Technology, Elsevier Science B.V., 2007, pp. 673-703.

[9] D.E. Parikh, Handbook of Pharmaceutical Granulation Technology, 2nd ed., Taylor & Francis Group, CRC Press, Boca Raton, 2005.

[10] G.I. Tardos, M.I. Khan, P.R. Mort, Critical parameters and limiting conditions in binder granulation of fine powders, Powder Technology, 94 (1997) 245-258.

[11] L. Fries, J. Dupas, M. Bellamy-Descamps, J. Osborne, A.D. Salman, S. Palzer, Bonding regime map for roller compaction of amorphous particles, Powder Technology, 341 (2019) 51-58.

[12] G.M. Walker, Chapter 4: Drum Granulation Processes, in: A.D. Salman, M.J. Hounslow, J.P.K. Seville (Eds.) Handbook of Powder Technology, Elsevier Science B.V., 2007, pp. 219-254.

[13] S.M. Iveson, J.D. Litster, Growth regime map for liquid-bound granules, AIChE Journal, 44 (1998) 1510-1518.

[14] M. Khorasani, J.M. Amigo, C.C. Sun, P. Bertelsen, J. Rantanen, Near-infrared chemical imaging (NIR-CI) as a process monitoring solution for a production line of roll compaction and tableting, European Journal of Pharmaceutics and Biopharmaceutics, 93 (2015) 293-302.

[15] S.L. Rough, D.I. Wilson, D.W. York, Effect of solids formulation on the manufacture of high shear mixer agglomerates, Advanced Powder Technology, 16 (2005) 145-169.

[16] M. Butensky, D. Hyman, Rotary drum granulation. An experimental study of the factors affecting granule size, Industrial & Engineering Chemistry Fundamentals, 10 (1971) 212-219.

[17] G.M. Walker, C.R. Holland, M.M.N. Ahmad, D.Q.M. Craig, Influence of process parameters on fluidised hot-melt granulation and tablet pressing of pharmaceutical powders, Chemical Engineering Science, 60 (2005) 3867-3877.

[18] K.P. Hapgood, J.D. Litster, R. Smith, Nucleation regime map for liquid bound granules, AIChE Journal, 49 (2003) 350-361.

[19] R.M. Dhenge, J.J. Cartwright, M.J. Hounslow, A.D. Salman, Twin screw granulation: Steps in granule growth, International Journal of Pharmaceutics, 438 (2012) 20-32.

[20] M. Leane, K. Pitt, G. K. Reynolds, N. Dawson, I. Ziegler, A. Szepes, A. Crean, R. Dall Agnol, Manufacturing Classification System in the real world: factors influencing manufacturing process choices for filed commercial oral solid dosage formulations, case studies from industry and considerations for continuous processing, Pharmaceutical Development and Technology 23 (2018) 1-59.

[21] S.M. Iveson, J.D. Litster, K. Hapgood, B.J. Ennis, Nucleation, growth and breakage phenomena in agitated wet granulation processes: a review, Powder Technology, 117 (2001) 3-39.

[22] S. Shanmugam, Granulation techniques and technologies: recent progresses, Bioimpacts, 5 (2015) 55-63.

[23] P. Serno, P. Kleinebudde, K. Knop, Granulieren - Grundlagen, Verfahren, Formulierungen (apv-basics), 2. ed., ECV Editio Cantor Verlag, Aulendorf, 2016.

[24] D.M. Newitt, J.M. Conway-Jones, A contribution to the theory and practice of granulation, Transactions of the Institution of Chemical Engineers, 36 (1958) 422-442.

[25] T.M. Chitu, D. Oulahna, M. Hemati, Rheology, granule growth and granule strength: Application to the wet granulation of lactose–MCC mixtures, Powder Technology, 208 (2011) 441-453.

[26] J. Rantanen, J. Khinast, The future of pharmaceutical manufacturing sciences, Journal of Pharmaceutical Sciences, 104 (2015) 3612-3638.

[27] H. Leuenberger, New trends in the production of pharmaceutical granules: batch versus continuous processing, European Journal of Pharmaceutics and Biopharmaceutics, 52 (2001) 289-296.

[28] C. Vervaet, J.P. Remon, Continuous granulation in the pharmaceutical industry, Chemical Engineering Science, 60 (2005) 3949-3957.

[29] K. Nepveux, J.-P. Sherlock, M. Futran, M. Thien, M. Krumme, How development and manufacturing will need to be structured - heads of development/manufacturing May 20–21, 2014, Continuous Manufacturing Symposium, Journal of Pharmaceutical Sciences, 104 (2015) 850-864.

[30] U.S. Department of Health and Human Services - Food and Drug Administration (FDA), Guidance for Industry - PAT - A framework for innovative pharmaceutical development, manufacturing, and quality assurance, https://www.fda.gov/media/71012/download (last accessed: 09.11.2021)

[31] G.V. Reklaitis, J. Khinast, F. Muzzio, Pharmaceutical engineering science - New approaches to pharmaceutical development and manufacturing, Chemical Engineering Science, 65 (2010) iv-vii.

[32] P. Basu, G. Joglekar, S. Rai, P. Suresh, J. Vernon, Analysis of manufacturing costs in pharmaceutical companies, Journal of Pharmaceutical Innovation, 3 (2008) 30-40.

[33] International Council for Harmonisation of Technical Requirements for Pharmaceuticals for Human Use (ICH), Pharmaceutical development Q8(R2), https://database.ich.org/sites/default/files/Q8%28R2%29%20Guideline.pdf (last accessed: 09.11.2021)

[34] International Council for Harmonisation of Technical Requirements for Pharmaceuticals for Human Use (ICH), Quality risk management Q9, https://database.ich.org/sites/default/files/Q9%20Guideline.pdf (last accessed: 09.11.2021)

[35] International Council for Harmonisation of Technical Requirements for Pharmaceuticals for Human Use (ICH), Pharmaceutical quality system Q10, https://database.ich.org/sites/default/files/Q10%20Guideline.pdf (last accessed: 09.11.2021)

[36] P. Poechlauer, J. Manley, R. Broxterman, B. Gregertsen, M. Ridemark, Continuous processing in the manufacture of active pharmaceutical ingredients and finished dosage forms: An industry perspective, Organic Process Research & Development, 16 (2012) 1586-1590.

[37] U.S. Department of Health and Human Services - Food and Drug Administration (FDA), Guidance for industry - cGMP for Phase 1 Investigational Drugs https://www.fda.gov/media/70975/download (last accessed: 11.11.2021)

[38] U.S. Department of Health and Human Services - Food and Drug Administration (FDA), Quality considerations for continuous manufacturing - Guidance for industry (draft guidance),

https://www.fda.gov/regulatory-information/search-fda-guidance-documents/quality-considerations-continuous-manufacturing (last accessed: 11.11.2021)

[39] International Council for Harmonisation of Technical Requirements for Pharmaceuticals for Human Use (ICH), Continuous manufacturing of drug substances and drug products Q13 EWG (under public consultation), https://database.ich.org/sites/default/files/ICH_Q13_Step2_DraftGuideline_%202021_0727.pdf (last accessed: 09.11.2021)

[40] International Council for Harmonisation of Technical Requirements for Pharmaceuticals for Human Use (ICH), Final concept paper - ICH Q13: Continuous manufacturing of drug substances and drug products, https://database.ich.org/sites/default/files/Q13%20Concept%20Paper.pdf (last accessed: 08.01.2022)

[41] C. Badman, C.L. Cooney, F. Alaistair, K. Konstantinov , M. Krumme, S. Mascia, M. Nasr, B.L. Trout, Why we need continuous pharmaceutical manufacturing and how to make it happen, Journal of Pharmaceutical Sciences, 108 (2019) 3521-3523.

[42] D.M. Roberge, L. Ducry, N. Bieler, P. Cretton, B. Zimmermann, Microreactor technology: A revolution for the fine chemical and pharmaceutical industries?, Chemical Engineering & Technology, 28 (2005) 318-323.

[43] S. Byrn, M. Futran, H. Thomas, E. Jayjock, N. Maron, R.F. Meyer, A.S. Myerson, M.P. Thien, B.L. Trout, Achieving continuous manufacturing for final dosage formation: Challenges and how to meet them May 20–21, 2014, Continuous Manufacturing Symposium, Journal of Pharmaceutical Sciences, 104 (2015) 792-802.

[44] K. Plumb, Continuous processing in the pharmaceutical industry: Changing the mind set, Chemical Engineering Research and Design, 83 (2005) 730-738.

[45] M. Ierapetritou, F. Muzzio, G. Reklaitis, Perspectives on the continuous manufacturing of powder-based pharmaceutical processes, AIChE Journal, 62 (2016) 1846-1862.

[46] T. Page, H. Dubina, G. Fillipi, R. Guidat, S. Patnaik, P. Poechlauer, P. Shering, M. Guinn, P. McDonnell, C. Johnston, Equipment and analytical companies meeting continuous challenges May 20–21, 2014, Continuous Manufacturing Symposium, Journal of Pharmaceutical Sciences, 104 (2015) 821-831.

[47] V.S. Dave, S.D. Saoji, N.A. Raut, R.V. Haware, Excipient variability and its impact on dosage form functionality, Journal of Pharmaceutical Sciences, 104 (2015) 906-915.

[48] J. Kushner, B.A. Langdon, J.I. Hiller, G.T. Carlson, Examining the impact of excipient material property variation on drug product quality attributes: A Quality-by-Design study for a roller compacted, immediate release tablet, Journal of Pharmaceutical Sciences, 100 (2011) 2222-2239.

[49] M. Fonteyne, A. Correia, S. De Plecker, J. Vercruysse, I. Ilić, Q. Zhou, C. Vervaet, J.P. Remon, F. Onofre, V. Bulone, T. De Beer, Impact of microcrystalline cellulose material attributes: A case study on continuous twin screw granulation, International Journal of Pharmaceutics, 478 (2015) 705-717.

[50] R.C. Moreton, Functionality and performance of excipients in a Quality-by-Design world: Part II Excipient variability, QbD, and robust formulations, in: A Supplement to American Pharmaceutical Review, Russel Publishing, Indianapolis, IN, 2010, pp. 10-13.

[51] M. Glodek, S. Liebowitz, R. McCarthy, G. McNally, C. Oksanen, T. Schultz, M. Sundararajan, R. Vorkapich, K. Vukovinsky, C. Watts, G. Millili, Process robustness - A PQRI white paper, Pharmaceutical Engineering, 26 (2006) 1-11.

[52] A.S. Myerson, M. Krumme, M. Nasr, H. Thomas, R.D. Braatz, Control systems engineering in continuous pharmaceutical manufacturing May 20–21, 2014, Continuous Manufacturing Symposium, Journal of Pharmaceutical Sciences, 104 (2015) 832-839.

[53] B. Kvarnström, P. Oghazi, Methods for traceability in continuous processes–Experience from an iron ore refinement process, Minerals Engineering, 21 (2008) 720-730.

[54] A. El Hagrasy, L.G. Wang, J. Litster, Chapter 8: Continuous wet granulation, in: AAPS Advances in the Pharmaceutical Sciences Series (Volume 42), Silver Spring, MD, 2020, pp. 269-300.

[55] G. Dahlgren, P. Tajarobi, E. Simone, B. Ricart, J. Melnick, V. Puri, C. Stanton, G. Bajwa, Continuous twin screw wet granulation and drying - Control strategy for drug product manufacturing, Journal of Pharmaceutical Sciences, 108 (2019) 3502-3514.

[56] W. Thiele, Twin-screw extrusion and screw design, in: I. Ghebre-Sellasie, C. Martin (Eds.) Pharmaceutical Extrusion Technology, Marcel Dekker, New York, 2003, pp. 69–98.

[57] M. Maniruzzaman, J.S. Boateng, M.J. Snowden, D. Douroumis, A review of hot-melt extrusion: process technology to pharmaceutical products, ISRN Pharm, 2012 (2012) 1-9.

[58] S. Bandari, D. Nyavanandi, V.R. Kallakunta, K.Y. Janga, S. Sarabu, A. Butreddy, M.A. Repka, Continuous twin screw granulation – an advanced alternative granulation technology for use in the pharmaceutical industry, International Journal of Pharmaceutics, 580 (2020) 119215.

[59] M.R. Thompson, Twin screw granulation – review of current progress, Drug Development and Industrial Pharmacy, 41 (2015) 1223-1231.

[60] M.J. Gamlen, C. Eardley, Continuous extrusion using a Raker Perkins MP50 (Multipurpose) extruder, Drug Development and Industrial Pharmacy, 12 (1986) 1701-1713.

[61] N.O. Lindberg, C. Tufvesson, L. Olbjer, Extrusion of an effervescent granulation with a twin screw extruder, Baker Perkins MPF 50 D, Drug Development and Industrial Pharmacy, 13 (1987) 1891-1913.

[62] N.O. Lindberg, C. Tufvesson, P. Holm, L. Olbjer, Extrusion of an effervescent granulation with a twin screw extruder, Baker Perkins MPF 50 D. Influence on intragranular porosity and liquid saturation, Drug Development and Industrial Pharmacy, 14 (1988) 1791-1798.

[63] N.O. Lindberg, M. Myrenas, C. Tufvesson, L. Olbjer, Extrusion of an effervescent granulation with a twin screw extruder, Baker Perkins MPF 50D. Determination of mean residence time, Drug Development and Industrial Pharmacy, 14 (1988) 649-655.

[64] T.C. Seem, N.A. Rowson, A. Ingram, Z. Huang, S. Yu, M. de Matas, I. Gabbott, G.K. Reynolds, Twin screw granulation — A literature review, Powder Technology, 276 (2015) 89-102.

[65] D. Djuric, B. Van Melkebeke, P. Kleinebudde, J.P. Remon, C. Vervaet, Comparison of two twin-screw extruders for continuous granulation, European Journal of Pharmaceutics and Biopharmaceutics, 71 (2009) 155-160.

[66] J.G. Osorio, R. Sayin, A.V. Kalbag, J.D. Litster, L. Martinez-Marcos, D.A. Lamprou, G.W. Halbert, Scaling of continuous twin screw wet granulation, AIChE Journal, 63 (2017) 921-932.

[67] U. Shah, Use of a modified twin-screw extruder to develop a high-strength tablet dosage form, Pharmaceutical Technology, 29 (2005) 52-66.

[68] E.I. Keleb, A. Vermeire, C. Vervaet, J.P. Remon, Extrusion granulation and high shear granulation of different grades of lactose and highly dosed drugs: A comparative study, Drug Development and Industrial Pharmacy, 30 (2004) 679-691.

[69] C. Köster, S. Pohl, P. Kleinebudde, Evaluation of binders in twin-screw wet granulation, Pharmaceutics, 13 (2021) 241.

[70] M.R. Thompson, S.J. Wu, W. Xu, K.P. O'Donnell, Heat activated dry granulation within the twin screw granulator, SPE Antec, (2016) 766-771.

[71] B. Van Melkebeke, B. Vermeulen, C. Vervaet, J.P. Remon, Melt granulation using a twin-screw extruder: A case study, International Journal of Pharmaceutics, 326 (2006) 89-93.

[72] E.I. Keleb, A. Vermeire, C. Vervaet, J.P. Remon, Cold extrusion as a continuous single-step granulation and tabletting process, European Journal of Pharmaceutics and Biopharmaceutics, 52 (2001) 359-368.

[73] E.I. Keleb, A. Vermeire, C. Vervaet, J.P. Remon, Continuous twin screw extrusion for the wet granulation of lactose, International Journal of Pharmaceutics, 239 (2002) 69-80.

[74] K.T. Lee, A. Ingram, N.A. Rowson, Twin screw wet granulation: The study of a continuous twin screw granulator using Positron Emission Particle Tracking (PEPT) technique, European Journal of Pharmaceutics and Biopharmaceutics, 81 (2012) 666-673.

[75] D. Djuric, P. Kleinebudde, Impact of screw elements on continuous granulation with a twin-screw extruder, Journal of Pharmaceutical Sciences, 97 (2008) 4934-4942.

[76] M.R. Thompson, J. Sun, Wet Granulation in a twin-screw extruder: Implications of screw design, Journal of Pharmaceutical Sciences, 99 (2010) 2090-2103.

[77] Y. Liu, M.R. Thompson, K.P. O'Donnell, Function of upstream and downstream conveying elements in wet granulation processes within a twin screw extruder, Powder Technology, 284 (2015) 551-559.

[78] S.V. Lute, R.M. Dhenge, M.J. Hounslow, A.D. Salman, Twin screw granulation: Understanding the mechanism of granule formation along the barrel length, Chemical Engineering Research and Design, 110 (2016) 43-53.

[79] S. Lee, K.L. McCarthy, Effect of screw configuration and speed on RTD and expansion of rice extrudate, Journal of Food Process Engineering, 19 (1996) 18.

[80] K. Kohlgrüber, Co-Rotating Twin-screw extruders: Fundamentals, 2nd ed., Carl Hanser Verlag GmbH & Co. KG, Munich, 2020.

[81] A. Kumar, M. Alakarjula, V. Vanhoorne, M. Toiviainen, F. De Leersnyder, J. Vercruysse, M. Juuti, J. Ketolainen, C. Vervaet, J.P. Remon, K.V. Gernaey, T. De Beer, I. Nopens, Linking granulation performance with residence time and granulation liquid distributions in twin-screw granulation: An experimental investigation, European Journal of Pharmaceutical Sciences, 90 (2016) 25-37.

[82] A.S. El Hagrasy, J.D. Litster, Granulation rate processes in the kneading elements of a twin screw granulator, AIChE Journal, 59 (2013) 4100-4115.

[83] J. Vercruysse, D. Córdoba Díaz, E. Peeters, M. Fonteyne, U. Delaet, I. Van Assche, T. De Beer, J.P. Remon, C. Vervaet, Continuous twin screw granulation: Influence of process variables on granule and tablet quality, European Journal of Pharmaceutics and Biopharmaceutics, 82 (2012) 205-211.

[84] J. Vercruysse, A. Burggraeve, M. Fonteyne, P. Cappuyns, U. Delaet, I. Van Assche, T. De Beer, J.P. Remon, C. Vervaet, Impact of screw configuration on the particle size distribution of granules produced by twin screw granulation, International Journal of Pharmaceutics, 479 (2015) 171-180.

[85] R.M. Dhenge, K. Washino, J.J. Cartwright, M.J. Hounslow, A.D. Salman, Twin screw granulation using conveying screws: Effects of viscosity of granulation liquids and flow of powders, Powder Technology, 238 (2013) 77-90.

[86] D. Djuric, P. Kleinebudde, Continuous granulation with a twin-screw extruder: Impact of material throughput, Pharmaceutical Development and Technology, 15 (2010) 518-525.

[87] A. Kumar, J. Dhondt, J. Vercruysse, F. De Leersnyder, V. Vanhoorne, C. Vervaet, J.P. Remon, K.V. Gernaey, T. De Beer, I. Nopens, Development of a process map: A step towards a regime map for steady-state high shear wet twin screw granulation, Powder Technology, 300 (2016) 73-82.

[88] B. Van Melkebeke, C. Vervaet, J.P. Remon, Validation of a continuous granulation process using a twin-screw extruder, International Journal of Pharmaceutics, 356 (2008) 224-230.

[89] A. Kumar, J. Vercruysse, M. Toiviainen, P.-E. Panouillot, M. Juuti, V. Vanhoorne, C. Vervaet, J.P. Remon, K.V. Gernaey, T. De Beer, I. Nopens, Mixing and transport during pharmaceutical twin-screw wet granulation: Experimental analysis via chemical imaging, European Journal of Pharmaceutics and Biopharmaceutics, 87 (2014) 279-289.

[90] R. Sayin, L. Martinez-Marcos, J.G. Osorio, P. Cruise, I. Jones, G.W. Halbert, D.A. Lamprou, J.D. Litster, Investigation of an 11 mm diameter twin screw granulator: Screw element performance and in-line monitoring via image analysis, International Journal of Pharmaceutics, 496 (2015) 24-32.

[91] J. Vercruysse, M. Toiviainen, M. Fonteyne, N. Helkimo, J. Ketolainen, M. Juuti, U. Delaet, I. Van Assche, J.P. Remon, C. Vervaet, T. De Beer, Visualization and understanding of the granulation liquid mixing and distribution during continuous twin screw granulation using NIR chemical imaging, European Journal of Pharmaceutics and Biopharmaceutics, 86 (2014) 383-392.

[92] A. Kumar, J. Vercruysse, G. Bellandi, K.V. Gernaey, C. Vervaet, J.P.l. Remon, T. De Beer, I. Nopens, Experimental investigation of granule size and shape dynamics in twin-screw granulation, International Journal of Pharmaceutics, 475 (2014) 485-495.

[93] R. Meier, K.-P. Moll, M. Krumme, P. Kleinebudde, Impact of fill-level in twin-screw granulation on critical quality attributes of granules and tablets, European Journal of Pharmaceutics and Biopharmaceutics, 115 (2017) 102-112.

[94] P. Pawar, D. Clancy, L. Gorringe, S. Barlow, A. Hesketh, R. Elkes, Development and scale-up of diversion strategy for twin screw granulation in continuous manufacturing, Journal of Pharmaceutical Sciences, 109 (2020) 3439-3450.

[95] A.L. Mundozah, J. Yang, C. Omar, O. Mahmah, A.D. Salman, Twin screw granulation: A simpler re-derivation of quantifying fill level, International Journal of Pharmaceutics, 591 (2020) 119959.

[96] C. Mendez Torrecillas, L.J. Gorringe, N. Rajoub, J. Robertson, R.G. Elkes, D.A. Lamprou, G.W. Halbert, The impact of channel fill level on internal forces during continuous twin screw wet granulation, International Journal of Pharmaceutics, 558 (2019) 91-100.

[97] E.I. Keleb, A. Vermeire, C. Vervaet, J.P. Remon, Twin screw granulation as a simple and efficient tool for continuous wet granulation, International Journal of Pharmaceutics, 273 (2004) 183-194.

[98] R.M. Dhenge, J.J. Cartwright, D.G. Doughty, M.J. Hounslow, A.D. Salman, Twin screw wet granulation: Effect of powder feed rate, Advanced Powder Technology, 22 (2011) 162-166.

[99] R.M. Dhenge, J.J. Cartwright, M.J. Hounslow, A.D. Salman, Twin screw wet granulation: Effects of properties of granulation liquid, Powder Technology, 229 (2012) 126-136.

[100] F.T. Fayose, Z. Huan, Specific mechanical energy requirement of a locally developed extruder for selected starchy crops, Food Science and Technology Research, 20 (2014) 793-798.

[101] K. Kolter, M. Karl, A. Gryczke, Hot-melt extrusion with BASF pharma polymers extrusion compendium, 2nd ed., BASF SE, 2012.

[102] M. Zlokarnik, Scale-up of processes using material systems with variable physical properties, Chemical and Biochemical Engineering Quarterly, 15 (2001) 47.

[103] M. Zlokarnik, Scale-up in chemical engineering, 2nd ed., Wiley-VCH Verlag GmbH & Co. KGaA, Weinheim, 2006.

[104] Y. Gao, F.J. Muzzio, M.G. Ierapetritou, A review of the residence time distribution (RTD) applications in solid unit operations, Powder Technology, 228 (2012) 416-423.

[105] A.S. El Hagrasy, J.R. Hennenkamp, M.D. Burke, J.J. Cartwright, J.D. Litster, Twin screw wet granulation: Influence of formulation parameters on granule properties and growth behavior, Powder Technology, 238 (2013) 108-115.

[106] R.M. Dhenge, R.S. Fyles, J.J. Cartwright, D.G. Doughty, M.J. Hounslow, A.D. Salman, Twin screw wet granulation: Granule properties, Chemical Engineering Journal, 164 (2010) 322-329.

[107] S.K. Rahimi, S. Paul, C.C. Sun, F. Zhang, The role of the screw profile on granular structure and mixing efficiency of a high-dose hydrophobic drug formulation during twin screw wet granulation, International Journal of Pharmaceutics, 575 (2020) 118958.

[108] A. Kumar, G.M. Ganjyal, D.D. Jones, M.A. Hanna, Digital image processing for measurement of residence time distribution in a laboratory extruder, Journal of Food Engineering, 75 (2006) 237-244.

[109] A. Gautam, G.S. Choudhury, Screw configuration effects on residence time distribution and mixing in twin-screw extruders during extrusion of rice flour, Journal of Food Process Engineering, 22 (1999) 263-285.

[110] A. Megarry, A. Taylor, A. Gholami, H. Wikström, P. Tajarobi, Twin-screw granulation and high-shear granulation: The influence of mannitol grade on granule and tablet properties, International Journal of Pharmaceutics, 590 (2020) 119890.

[111] C. Portier, K. Pandelaere, U. Delaet, T. Vigh, A. Kumar, G. Di Pretoro, T. De Beer, C. Vervaet, V. Vanhoorne, Continuous twin screw granulation: Influence of process and formulation variables on granule quality attributes of model formulations, International Journal of Pharmaceutics, 576 (2020) 118981.

[112] J.L.P. Soh, C.V. Liew, P.W.S. Heng, Torque rheological parameters to predict pellet quality in extrusion–spheronization, International Journal of Pharmaceutics, 315 (2006) 99-109.

[113] P. Luukkonen, T. Schæfer, L. Hellén, A.M. Juppo, J. Yliruusi, Rheological characterization of microcrystalline cellulose and silicified microcrystalline cellulose wet masses using a mixer torque rheometer, International Journal of Pharmaceutics, 188 (1999) 181-192.

[114] R.C. Rowe, G.R. Sadeghnejad, The rheology of microcrystalline cellulose powder/water mixes — measurement using a mixer torque rheometer, International Journal of Pharmaceutics, 38 (1987) 227-229.

[115] B.C. Hancock, P. York, R.C. Rowe, Characterization of wet masses using a mixer torque rheometer: 2. Mixing kinetics, International Journal of Pharmaceutics, 83 (1992) 147-153.

[116] M. Cavinato, E. Andreato, M. Bresciani, I. Pignatone, G. Bellazzi, E. Franceschinis, N. Realdon, P. Canu, A.C. Santomaso, Combining formulation and process aspects for optimizing the high-shear wet granulation of common drugs, International Journal of Pharmaceutics, 416 (2011) 229-241.

[117] G.A. Campbell, D.J. Clancy, J.X. Zhang, M.K. Gupta, C.K. Oh, Closing the gap in series scale up of high shear wet granulation process using impeller power and blade design, Powder Technology, 205 (2011) 184-192.

[118] A.C. Santomaso, R. Baggio, F. Zorzi, G. Salviulo, N. Realdon, E. Franceschinis, Sugars with different thickening power in high shear granulation, Powder Technology, 317 (2017) 391-399.

[119] M. Kuhs, J. Moore, G. Kollamaram, G. Walker, D. Croker, Predicting optimal wet granulation parameters for extrusion-spheronisation of pharmaceutical pellets using a mixer torque rheometer, International Journal of Pharmaceutics, 517 (2017) 19-24.

[120] H. Leuenberger, H.P. Bier, H. Sucker, Theorie und Praxis der Bestimmung des Granulierflüssigkeitsbedarfes beim konventionellen Granulieren, Chemie Ingenieur Technik, 52 (1980) 609-609.

[121] B.C. Hancock, P. York, R.C. Rowe, An assessment of substrate-binder interactions in model wet masses. 1: Mixer torque rheometry, International Journal of Pharmaceutics, 102 (1994) 167-176.

[122] T.M. Chitu, D. Oulahna, M. Hemati, Wet granulation in laboratory scale high shear mixers: Effect of binder properties, Powder Technology, 206 (2011) 25-33.

[123] R. Meier, M. Thommes, N. Rasenack, K.P. Moll, M. Krumme, P. Kleinebudde, Granule size distributions after twin-screw granulation - Do not forget the feeding systems, European Journal of Pharmaceutics and Biopharmaceutics, 106 (2016) 59-69.

[124] J.J. Cartwright, J. Robertson, D. D'Haene, M.D. Burke, J.R. Hennenkamp, Twin screw wet granulation: Loss in weight feeding of a poorly flowing active pharmaceutical ingredient, Powder Technology, 238 (2013) 116-121.

[125] S. Paul, P. Tajarobi, C. Boissier, C.C. Sun, Tableting performance of various mannitol and lactose grades assessed by compaction simulation and chemometrical analysis, International Journal of Pharmaceutics, 566 (2019) 24-31.

[126] C.M. Wagner, M. Pein, J. Breitkreutz, Roll compaction of mannitol: Compactability study of crystalline and spray-dried grades, International Journal of Pharmaceutics, 453 (2013) 416-422.

[127] A. Kosugi, K.H. Leong, E. Urata, Y. Hayashi, S. Kumada, K. Okada, Y. Onuki, Effect of different direct compaction grades of mannitol on the storage stability of tablet properties investigated using a Kohonen Self-Organizing Map and Elastic Net Regression Model, Pharmaceutics, 12 (2020) 886.

[128] Council of Europe, European Pharmacopoeia, 10th ed., Strasbourg, 2020

[129] R.C. Rowe, P.J. Sheskey, M.E. Quinn, Handbook of pharmaceutical excipients, 6th ed., RPS Publisher, London: Pharmaceutical Press, Washington, DC: American Pharmaceutical Association, 2009.

[130] S. Paul, C.C. Sun, The suitability of common compressibility equations for characterizing plasticity of diverse powders, International Journal of Pharmaceutics, 532 (2017) 124-130.

[131] W.D. Tu, A. Ingram, J. Seville, S.S. Hsiau, Exploring the regime map for high-shear mixer granulation, Chemical Engineering Journal, 145 (2009) 505-513.

[132] A. Goldszal, J. Bousquet, Wet agglomeration of powders: from physics toward process optimization, Powder Technology, 117 (2001) 221-231.

[133] K.M. Kyttä, S. Lakio, H. Wikström, A. Sulemanji, M. Fransson, J. Ketolainen, P. Tajarobi, Comparison between twin-screw and high-shear granulation - The effect of filler and active pharmaceutical ingredient on the granule and tablet properties, Powder Technology, 376 (2020) 187-198.

[134] J. Vercruysse, E. Peeters, M. Fonteyne, P. Cappuyns, U. Delaet, I. Van Assche, T. De Beer, J.P. Remon, C. Vervaet, Use of a continuous twin screw granulation and drying system during formulation development and process optimization, European Journal of Pharmaceutics and Biopharmaceutics, 89 (2015) 239-247.

[135] A. Kumar, J. Vercruysse, V. Vanhoorne, M. Toiviainen, P.-E. Panouillot, M. Juuti, C. Vervaet, J.P. Remon, K.V. Gernaey, T.D. Beer, I. Nopens, Conceptual framework for model-based analysis of residence time distribution in twin-screw granulation, European Journal of Pharmaceutical Sciences, 71 (2015) 25-34.

[136] D.M. Kalyon, H.N. Sangani, An experimental study of distributive mixing in fully intermeshing, co-rotating twin screw extruders, Polymer Engineering & Science, 29 (1989) 1018-1026.

[137] D. Zimmermann, M. Steffens, E. Roos, Screw design for co-rotating twin-screw extruders, Plastics, Additives and Compounding, 6 (2004) 38-41.

[138] G.S. Rekhi, R. Caricofe, D. Parikh, L. Augsburger, A new approach to scale-up of a high-shear granulation process, Pharmaceutical Technology, 20 (1996) 1-10.

[139] J. Tao, P. Pandey, D.S. Bindra, J.Z. Gao, A.S. Narang, Evaluating scale-up rules of a high-shear wet granulation process, Journal of Pharmaceutical Sciences, 104 (2015) 2323-2333.

[140] Thermo Fisher Scientific, 16 mm screw elements portfolio, https://assets.thermofisher.com/TFS-Assets/CAD/Specification-Sheets/PP016-e-16-mm-Screw-elements.pdf (last accessed: 28.11.2021)

[141] O.-R. Arndt, R. Baggio, A.K. Adam, J. Harting, E. Franceschinis, P. Kleinebudde, Impact of different dry and wet granulation techniques on granule and tablet properties: A comparative study, Journal of Pharmaceutical Sciences, 107 (2018) 3143-3152.

[142] H.G. Kristensen, T. Schaefer, Granulation: A review on pharmaceutical wet-granulation, Drug Development and Industrial Pharmacy, 13 (1987) 803-872.

[143] L.J. Gorringe, G.S. Kee, M.F. Saleh, N.H. Fa, R.G. Elkes, Use of the channel fill level in defining a design space for twin screw wet granulation, International Journal of Pharmaceutics, 519 (2017) 165-177.

[144] M. Hu, X. Jiang, M. Absar, S. Choi, D. Kozak, M. Shen, Y.-T. Weng, L. Zhao, R. Lionberger, Equivalence testing of complex particle size distribution profiles based on Earth Mover's Distance, The AAPS Journal, 20 (2018) 62.

[145] C. Köster, Evaluation of binders in continuous twin-screw wet granulation, in: Institute of Pharmacy, Martin-Luther-University Halle-Wittenberg, 2020, pp. 1-77.

[146] J. Vercruysse, U. Delaet, I. Van Assche, P. Cappuyns, F. Arata, G. Caporicci, T. De Beer, J.P. Remon, C. Vervaet, Stability and repeatability of a continuous twin screw granulation and drying system, European Journal of Pharmaceutics and Biopharmaceutics, 85 (2013) 1031-1038.

[147] A.W. Jenike, Storage and flow of solids, 1st ed., Engineering Experiment Station, University of Utah: Salt Lake City, 1964.

[148] G.J.B. Horsthuis, J.A.H. van Laarhoven, R.C.B.M. van Rooij, H. Vromans, Studies on upscaling parameters of the Gral high shear granulation process, International Journal of Pharmaceutics, 92 (1993) 143-150.

[149] J.S. Ramaker, M.A. Jelgersma, P. Vonk, N.W.F. Kossen, Scale-down of a high-shear pelletisation process: Flow profile and growth kinetics, International Journal of Pharmaceutics, 166 (1998) 89-97.

[150] E.H. Jang, Y.S. Park, M.-S. Kim, D.H. Choi, Model-based scale-up methodologies for pharmaceutical granulation, Pharmaceutics, 12 (2020) 1-51.

[151] K.G. Pitt, M.G. Heasley, Determination of the tensile strength of elongated tablets, Powder Technology, 238 (2013) 169-175.

[152] C.C. Sun, H. Hou, P. Gao, C. Ma, C. Medina, F.J. Alvarez, H. Hou, P. Gao, Development of a high drug load tablet formulation based on assessment of powder manufacturability: Moving towards quality by design, Journal of Pharmaceutical Sciences, 98 (2009) 239-247.

[153] H. Li, M.R. Thompson, K.P. O'Donnell, Progression of wet granulation in a twin screw extruder comparing two binder delivery methods, AIChE Journal, 61 (2015) 780-791.

[154] C. Portier, C. De Vriendt, T. Vigh, G. Di Pretoro, T. De Beer, C. Vervaet, V. Vanhoorne, Continuous twin screw granulation: Robustness of lactose/MCC-based formulations, International Journal of Pharmaceutics, 588 (2020) 119756.

[155] C. Portier, K. Pandelaere, U. Delaet, T. Vigh, G. Di Pretoro, T. De Beer, C. Vervaet, V. Vanhoorne, Continuous twin screw granulation: A complex interplay between formulation properties, process settings and screw design, International Journal of Pharmaceutics, 576 (2020) 119004.

[156] A.K. Srivastava, C.E. Goering, R.P. Rohrbach, D.R. Buckmaster, Chapter 14: Conveying of Agricultural Materials, ASABE, St. Joseph, MI, 2006.

[157] D. Kayrak-Talay, S. Dale, C. Wassgren, J. Litster, Quality by design for wet granulation in pharmaceutical processing: Assessing models for a priori design and scaling, Powder Technology, 240 (2013) 7-18.

[158] D. Kayrak-Talay, J.D. Litster, A priori performance prediction in pharmaceutical wet granulation: Testing the applicability of the nucleation regime map to a formulation with a broad size distribution and dry binder addition, International Journal of Pharmaceutics, 418 (2011) 254-264.

[159] M. Pishnamazi, S. Casilagan, C. Clancy, S. Shirazian, J. Iqbal, D. Egan, C. Edlin, D.M. Croker, G.M. Walker, M.N. Collins, Microcrystalline cellulose, lactose and lignin blends: Process mapping of dry granulation via roll compaction, Powder Technology, 341 (2019) 38-50.

[160] S. Pohl, P. Kleinebudde, A review of regime maps for granulation, International Journal of Pharmaceutics, 587 (2020) 119660.

[161] W.D. Tu, A. Ingram, J. Seville, Regime map development for continuous twin screw granulation, Chemical Engineering Science, 87 (2013) 315-326.

[162] M.J. Adams, M.A. Mullier, J.P.K. Seville, Agglomerate strength measurement using a uniaxial confined compression test, Powder Technology, 78 (1994) 5-13.

[163] S.M. Iveson, P.A.L. Wauters, S. Forrest, J.D. Litster, G.M.H. Meesters, B. Scarlett, Growth regime map for liquid-bound granules: Further development and experimental validation, Powder Technology, 117 (2001) 83-97.

[164] HNP Mikrosysteme, Operation Principle, https://www.hnp-mikrosysteme.de/en/products/technical-information/operation-principle/ (last accessed: 16.02.2021)

[165] R. Meier, D. Emanuele, P.B. Harbaum, Important elements in continuous granule drying processes, TechnoPharm, 10 (2020) 92-101.

[166] K. Kiricenko, Scaling of twin-screw granulation process, in: Institute of Pharmaceutics and Biopharmaceutics, Heinrich Heine University, Düsseldorf, 2020, pp. 1-75.

[167] Council of Europe, European Pharmacopoeia, 9th ed., Strasbourg, 2017

[168] S. Cohen, Finding color and shape patterns in images, in: Department of Computer Science, Stanford University, 1999, pp. 274.

[169] Micromeritics, https://www.micromeritics.com/Product-Showcase/GeoPyc-1365.aspx (last accessed: 05.10.2020)

[170] Micromeritics, https://www.micromeritics.com/pressroom/press-release-list/geopyc-1360-press-release.aspx (last accessed: 05.10.2020)

[171] D. Schulze, Pulver und Schüttgüter: Fließeigenschaften und Handhabung, Springer-Verlag, Berlin Heidelberg, 2006.

[172] J.T. Fell, J.M. Newton, Determination of tablet strength by the diametral-compression test, Journal of Pharmaceutical Sciences, 59 (1970) 688-691.

Danksagung

Zuvorderst möchte ich meinem Doktorvater, Prof. Dr. Dr. h. c. Peter Kleinebudde, dafür danken, dass er mich in seinem Arbeitskreis aufgenommen und mir die Möglichkeit eingeräumt hat, diese Promotionsarbeit anzufertigen. Ungeachtet seiner Aufgaben im Universitätsbetrieb und seines vollen Terminkalenders hat er sich stets Zeit für das Beantworten von Fragen sowie das Besprechen von Ergebnissen und Problemen genommen. Diese Art der Betreuung habe ich nicht als selbstverständlich erachtet. Besonders hervorzuheben ist seine ehrliche und konstruktive Kritik, die mich wachsen lassen und diese Arbeit ungemein bereichert hat.

Prof. Dr. Jörg Breitkreutz danke ich für die Übernahme des Koreferats, sowie für seine kritischen Fragen in Fokusgruppen und nach diversen Doktorandenvorträgen. Für die herzliche Aufnahme in seinen Verantwortungsbereich mit Antritt meiner Funktion als Koordinator des M. Sc. Industrial Pharmacy-Studienganges möchte ich ihm an dieser Stelle ebenfalls danken.

Der INVITE GmbH möchte ich für meine Anstellung danken, welche mir die Promotion überhaupt erst ermöglicht hat. Besonderer Dank gilt an dieser Stelle Dr. Werner Hoheisel, meinem Betreuer und Vorgesetzten bei INVITE, für seine Empathie und Hilfsbereitschaft. Dem DDIC (Drug Delivery Innovation Center) wünsche ich für die Zukunft alles Gute.

Dr. Klaus Knop danke ich für das nochmalige Korrekturlesen der Arbeit, bevor es „ernst“ wurde. Ich danke ihm darüber hinaus für die wertvollen Ratschläge bei fachlichen Fragen während meiner gesamten Promotionszeit. Seine Antworten haben mir geholfen, experimentelle wie hypothetische Ansätze zu reflektieren und zu überdenken.

Dr. Robin Meier danke ich für seine stete und unkomplizierte Erreichbarkeit bei spezifischen Fragestellungen, seine Hinweise und Ratschläge zu Versuchen und Ansätzen in meiner Arbeit sowie das problemlose Ermöglichen von Versuchen bei L.B. Bohle. Mit seiner motivierenden Art und seinem sonnigen Gemüt hat er jeden Aufenthalt in Ennigerloh bereichert und dazu beigetragen, dass ich mich auf den nächsten Aufenthalt freuen konnte.

Zusätzlicher Dank gilt Daniel Emmanuele, Andreas Teske, Philipp Harbaum, Sven Kämmering, Damian Mika und allen hier nicht namentlich genannten Mitarbeitern bei L.B. Bohle für ihr Engagement, ihre Herzlichkeit und ihre Hilfsbereitschaft bei Problemen während meiner Aufenthalte in Ennigerloh.

Dr. Julian Quodbach und Dr. Raphael Wiedey danke ich für den fachlichen Austausch und die vielen hilfreichen Ratschläge, sowie die tolle Aufnahme in den Mittelbau. Mir haben die ehrlichen Gespräche immer gefallen und ich habe beide bereits am Tag nach deren Weggängen vermisst. Ich wünsche ihnen nur das Beste – privat wie beruflich. Großer Dank gilt auch Dr. Tanja Knaab, deren Art ich im DAB-Praktikum kennen und schätzen gelernt habe. Sie hatte von Anfang volles Vertrauen in mich als ihren Elternzeitersatz als Studiengangskoordinator. Ich erachte es nicht als selbstverständlich, dass sie sich auch während ihrer Abwesenheit Zeit für Telefonate und die Beantwortung von den vielen Fragen zu organisatorischen und verwaltungstechnischen Besonderheiten genommen hat.

Meinen Bürokollegen Hanna Ponsar und Sebastian Bollmann danke ich besonders für die produktiven, persönlichen und ehrlichen Gespräche, die das gesamte Spektrum von tiefernst bis absolut absurd abdecken konnten. Ihre kritischen Rückmeldungen haben diese Arbeit erheblich mit geformt. Die gemeinsame Zeit auch fernab der Uni hat meine Promotionszeit ungemein bereichert und ich hätte mir keine bessere Zusammensetzung des Büros 00.30 vorstellen können! Besonders gern werde ich mich an die liebevollen Umgestaltungen der Arbeitsplätze bei Geburtstagen zurückerinnern. Die entstandenen Freundschaften möchte ich nicht mehr missen.

Jerome Hansen möchte ich für die vielen kulinarischen Erlebnisse sowie den gemeinsamen Austausch bei dem einen oder anderen (Alt-)Bier oder Wein außerhalb der Uni danken. Auch waren sein Blickwinkel und seine Ansichten bei fachlichen Fragestellungen sehr wertvoll. Besonders danke ich ihm, dass er sich neben seiner eigenen Promotion die Zeit dafür genommen hat, die Erstversion dieser Arbeit Korrektur zu lesen. Er hat damit die Arbeit auf dem Weg zur abgabefähigen Version erheblich vorangebracht. Besonders hoffe ich, dass es ihm als *native speaker* nicht allzu sehr die Haare zu Berge hat stehen lassen. Ihm, sowie Sabrina Berkenkemper und Hanna Plappert, danke ich außerdem für all die schönen Abende, den Gesprächen, die im herzhaften Lachen endeten und den Spaß, den wir zusammen hatten. Ich habe die gemeinsame Zeit stets genossen.

Dr. Annika Wilms danke ich für die Freundschaft, die sich von der ersten Minute unseres gemeinsamen Promotionsstarts entwickelt hat. Unsere Aufenthalte in Ennigerloh bleiben unvergessen, allen voran die Autofahrten und Gespräche. Aber auch an die gemeinsamen Abendessen, die Nintendo Switch-Stunden und das Vermessen der Schneckenelemente werde ich mich noch lange erinnern. Ich hätte zudem bei niemandem lieber Beifahrer sein wollen – auch wenn ich letztlich daran denken musste, die Autoschlüssel mitzunehmen …

Dr. Vincent Lenhart danke ich für seine unverkennbare und von mir sehr geschätzte Art, Dinge zu sagen, ohne dabei ein Blatt vor den Mund zu nehmen. Die vielen hilfreichen Kommentare während meiner Arbeit sowie die gemeinsamen (außer-)universitären Erlebnisse waren eine Bereicherung meiner Promotionszeit.

Dr. Dina Kottke danke ich für die zahlreichen gemeinsamen Stunden sowie Abende auf dem Balkon in der Schützenstraße. Unvergessen bleibt definitiv auch der Toblerone-Abend in Köln.

Stefan Klinken danke ich für das kurzfristige Schreiben des Python-Skriptes zur EMD-Auswertung sowie die Zeit und Engelsgeduld, um mit mir über Statistik und DoEs zu sprechen.

Mein Dank geht auch an Claudia Köster und Katharina Kiricenko, die ich während meiner Promotionszeit in ihren Diplom- und Masterarbeiten fachlich betreuen durfte. Neben dem Gewinn an neuen fachlichen Erkenntnissen, habe ich mich vor allem persönlich weiterentwickeln dürfen, was mir im Umgang mit Studierenden sowie in meiner Lehrtätigkeit zugutekam. Ich danke beiden für ihre Neugier an den jeweiligen Themen, ihre kritischen Fragen und die fachlichen Diskussionen.

Meinen WPP-Studierenden Elisabeth Yek, Fatma Yilmaz, Luna Maschke und Leah Schlüsener danke ich für ihren Einsatz und den Erkenntnisgewinn, den ich daraus ziehen konnte.

Dorothee Eikeler möchte ich besonders für ihre Unterstützung, praktischer wie mentaler Natur, danken. Über die Zeit haben wir uns zu einem gut abgestimmten Team entwickelt – das hat sich auch außeruniversitär gezeigt. Sie hat erheblich dazu beigetragen, mehr Aufgaben in kürzer Zeit zu bewerkstelligen. Die Gespräche nebenbei haben die ansonsten stressigen Tage abgerundet. Genauso wertvoll war die Unterstützung durch Andrea Michel, die für mich zahlreiche Messungen am AccuPyk gemacht und mir somit die Gelegenheit gegeben hat, mich auf andere Aufgaben zu konzentrieren. Bei beiden Kolleginnen hatte ich nie Sorge über die Qualität der Arbeit und der Daten, weshalb ein einfaches Dankeschön fast unzureichend erscheint. Beide haben mit ihrer Hilfe erheblich zum Gelingen dieser Arbeit beigetragen.

Stefan Stich möchte ich dafür danken, dass er immer zur Stelle war, wenn etwas repariert oder für die Feinmechanik eine technische Zeichnung angefertigt werden musste.

Allen nicht namentlich genannten Mitgliedern des Instituts danke ich ebenso für die gemeinsame Zeit sowie die Unterstützung bei meinen Lehrtätigkeiten. Es gab fast niemanden, mit dem ich nicht lachen und tolle Gespräche führen konnte.

Meiner Familie danke ich für ihre Unterstützung sowie den häufigen Ermahnungen, auch mal abzuschalten und „an die frische Luft“ zu gehen. GLB danke ich für die grenzenlose Unterstützung und dafür, dass ich so sein kann wie ich bin. Auch, dass ich überall hingehen kann, solange es eine direkte Flugverbindung von Berlin aus gibt.

Eidesstattliche Erklärung

Ich versichere an Eides Statt, dass die Dissertation von mir selbständig und ohne unzulässige fremde Hilfe unter Beachtung der „Grundsätze zur Sicherung guter wissenschaftlicher Praxis an der Heinrich-Heine-Universität Düsseldorf“ erstellt worden ist.

Die Dissertation wurde noch bei keiner anderen Fakultät vorgelegt.

Sebastian Pohl